ABSTRACT

This thesis describes the development, fundamental extension and extensive testing (validation and verification) of mathematical models for predicting outflow following the failure of pressurised pipelines containing incompressible liquids. The models, for the first time, account for all the important sequential flow regimes taking place during the discharge process. These include full pipe flow, bubble formation and propagation, followed by open channel flow. The system configurations modelled include a draining pipeline connected to a storage tank and pipe with one closed-end.

In the first part of this thesis, the development of outflow models to simulate the full-bore rupture of horizontal pipelines is presented. In order to model the full pipe flow in a pipe fed from an upstream tank, the published model by Joye & Barrett (2003) is employed in this study. Bubble propagation and open channel flow for both configurations (in the presence of upstream tank and pipe with one closed-end) are modelled by assuming critical flow condition throughout the pipe and in the tank (where applicable). Bubble propagation velocity is calculated based on Benjamin's (1968) and Bendiksen's (1984) proposed equations.

The second part of this study focuses on the extension of the developed models to account for pipe inclination angle. Bubble propagation and open channel flow are modelled by replacing the critical flow equation with Darcy-Weisbach equation, applicable to downward-inclined pipes. The bubble propagation pattern in the pipe is determined based on the drift velocity method through the results obtained from parametric studies.

The developed models are validated by comparing the predicted values against experimental measurements recorded using laboratory scale setups. Through sensitivity analysis based on comparing the results of the models to case studies representative of real events, the importance of accounting for post-full pipe flow on the total amount of inventory discharged is demonstrated.

ACKNOWLEDGEMENTS

I wish to thank the following people and organisations who have contributed so much in many ways to facilitate the completion of this thesis.

My husband, Mr Matthew Pegg, for bearing with my non-stop complaints and long hours of work.

My parents, Mr and Mrs Rafigh, my sister Shideh and my brother Shahab for their unconditional love and moral support.

A big thank you to Dr Jan Stene from DNV Software for his invaluable advice and support throughout my PhD as well as the writing-up. Thank you ever so much.

My advisors, Prof. Haroun Mahgerefteh from UCL and Mr Henk Witlox from DNV software, for their support throughout my PhD.

Special thanks to Mr Alberto Barral for his help with the experiments.

The technical and admin. staff of the Department of Chemical engineering, UCL.

تقدیم به پدر و مادر عزیز تر از جانم

TABLE OF CONTENTS

ABSTRACT 1
ACKNOWLEDGEMENTS 2
TABLE OF CONTENTS 4
CHAPTER 1: INTRODUCTION 8
CHAPTER 2: FUNDAMENTAL EQUATIONS AND BACKGROUND THEORY 14
2.1 Introduction 14
2.2 Full Pipe Flow 15
2.2.1 Conservation of Mass (Continuity) (Coulson & Richardson, 1999) 15
2.2.2 Conservation of Energy (Coulson & Richardson, 1999) 16
2.2.3 Frictional Loss 17
2.3 Open Channel Flow 22
2.3.1 Conservation of Mass (Continuity) (Sturm, 2001) 23
2.3.2 Specific Energy (Akan, 2006) 24
2.3.3 Subcritical, Critical and Supercritical Flow (French, 1994; Akan, 2006) 25
2.3.4 Uniform Flow 26
2.3.5 Steep and Mild/Horizontal Channels 28
2.3.6 Frictional loss 30
2.4 Conclusion 30
CHAPTER 3: LITERATURE REVIEW 32
3.1 Introduction 32
3.2 Full Pipe Flow 33
3.3 Bubble Formation and Propagation 38
3.3.1 Bubble Propagation in Stagnant Liquid 39
3.3.2 Bubble Propagation in Co-current Liquid 41
3.4 Open Channel Flow 42
3.4.1 Horizontal Channels 42
3.4.2 Downward-inclined Channels 45
3.5 Conclusion 47

CHAPTER 4: OUTFLOW SIMULATION UPON FULL-BORE RUPTURE IN HORIZONTAL PIPELINES 49
4.1. Introduction 49
4.2. Key Models Assumptions 50
4.2.1. One-dimensional flow anywhere in the pipeline 50
4.2.2. Incompressible flow, i.e. constant fluid density 50
4.2.3. Constant cross sectional area of the pipe, much smaller than tank cross sectional area (where applicable) 51
4.2.4. No friction between the fluid and tank 51
4.2.5. Isothermal conditions in the pipe 51
4.2.6. No inlet flow to the feed tank 51
4.2.7. No hammer effect upon valve closure 51
4.2.8. Negligible impact of surface tension and viscosity during bubble formation and propagation regime 52
4.3. Transient Hydraulic Flow Modelling Following Full-bore Rupture of a Horizontal Pipeline Fed from an Upstream Tank 52
4.3.1. Introduction 52
4.3.2. Model Theory 52
4.3.2.1. Full Pipe Flow 52
4.3.2.2. Bubble Formation and Propagation 55
4.3.2.3. Open Channel Flow 62
4.3.3. Parametric Studies 67
4.3.3.1. Discharge Velocity and Wetted Area 67
4.3.3.2. Normalised Cumulative Discharged Mass 74
4.3.4. Experiments 79
4.3.4.1. Upstream Bubble Propagation Velocity u_{ub} and Liquid Depth $\boldsymbol{d_c^{bf}}$ 79
4.3.4.2. Normalised Cumulative Discharged Mass and Discharge Rate 86
4.4. Transient Hydraulic Flow Modelling Following Full-bore Rupture of an Isolated Horizontal Pipeline 93
4.4.1. Introduction 93
4.4.2. Model Theory 93
4.4.2.1. Bubble Formation and Propagation 93
4.4.2.2. Open Channel Flow 96
4.4.3. Parametric Studies 97

4.4.3.1. Discharge Velocity and Wetted Area 97
4.4.3.2. Released Mass during Individual Flow Regimes 103
4.4.4. Error Analysis and Dependence of Convergence on $\Delta\phi_c$ 104
4.4.5. Experiments 107
4.5. Conclusion 112
CHAPTER 5: IMPACT OF PIPELINE INCLINATION ANGLE ON THE OUTFLOW FROM PIPELINES 116
5.1. Introduction 116
5.2. Key Models Assumptions 117
5.3. Transient Hydraulic Flow Modelling Following Full-bore Rupture of Downward-inclined Pipelines 117
5.3.1. Introduction 117
5.3.2. Model Theory 118
5.3.2.1. Full Pipe Flow 118
5.3.2.2. Bubble Formation & Propagation 119
5.3.2.2.1. Bubble Propagation from Both Ends 120
5.3.2.2.2. Bubble Propagation Only from the Upstream End of the Pipe 124
5.3.2.3. Open Channel Flow 125
5.3.3. Parametric Studies 127
5.3.3.1. Comparison of the Two Models for Bubble Propagation 128
5.3.3.2. Discharge Velocity and Wetted Area 130
5.3.3.3. Normalised Cumulative Discharged Mass 139
5.3.3.4. Variation of Liquid Depth Angle (ϕ_n^{bf}) with θ 144
5.3.4. Experiments 148
5.3.4.1. Upstream Bubble Propagation Velocity u_{ub} and Liquid Depth d_n^{bf} 148
5.3.4.2. Normalised Cumulative Discharged Mass and Discharge Rate 157
5.4. Transient Hydraulic Flow Modelling Following Full-bore Rupture of an Isolated Downward-inclined Pipeline 162
5.4.1. Introduction 162
5.4.2. Model Theory 162
5.4.2.1. Bubble Formation and Propagation 162
5.4.2.2. Open Channel Flow 164
5.4.3. Parametric Studies 165
5.4.3.1. Discharge Velocity and Wetted Area 166

5.4.3.2. Variation of Liquid Depth Angle (ϕ_n^{bf}) with θ 173
5.4.3.3. Released Mass during Individual Regimes 176
5.4.4. Error Analysis and Dependence of Convergence on $\Delta\phi_n$ 177
5.4.5. Experiments 180
5.5. Conclusion 185
CHAPTER 6: CONCLUSION AND FUTURE WORK 189
6.1. Conclusion 189
6.2. Suggested Future Work 193
NOMENCLATURE 195
REFERENCES 198
WEB REFERENCES 204

CHAPTER 1: INTRODUCTION

Global oil demand is set to grow by 14% by 2035 (The Economic Times, 2011) due to economic growth and expanding populations in the world's developing countries such as India and China. The International Energy Agency has estimated that such demand for oil will reach 99mbd in 2035; 12mbd more than in 2010 (The Economic Times, 2011). This growing demand is expected to be met with increased oil production, resulting in a significant increase in the use of pressurised pipelines, already by far the most widely used method for transporting oil and gas across the globe. According to the research conducted by London-based steel business consultancy CRU, the demand for pipelines was said to go up by 78% in Eastern Europe and by over 100% in the Middle East and Asia between 2007 and 2011 (Energy Global, 2010).

Given that such pipelines can be several hundreds of kilometres long conveying millions of tonnes of highly pressurised inventory, their accidental rupture may lead to catastrophic consequences, including injuries, fatalities, significant environmental damage and financial loss. According to data published by the US Department of Transport (1982-1997), short pipelines will have a reportable accident during a 20-year lifetime. Operators of long pipeline networks (1000 km or over) can expect a reportable accident at a frequency of one per year.

There are numerous examples of such incidents. According to the US Department of Transportation Pipeline and Hazardous Materials Safety Administration (2011), over 5000 hazardous liquid pipeline accidents were reported during 1991 – 2010, representing a total property damage of over US$2 billion. The rupture of an Enbridge pipeline near Cohasset, Minnesota, USA in 2002 resulted in the release of approximately 6,000 barrels of crude oil, representing a financial loss of approximately US$5.6 million (Pipeline Accident Report, 2002). The cost of the clean-up operation was estimated to be significantly higher. In 2010, a ruptured crude oil pipeline sent at least 800,000 gallons of crude oil pouring into the Kalamazoo

River, Michigan, USA. The spill is believed to be the largest in the history of the Midwest (Green Technology, 2010). The clean-up cost is estimated to exceed US$650 million (Klug, 2011). In Nigeria, the puncture and rupture of a crude oil pipeline in Abule Egba and Lagos in 2006 and 2008 respectively resulted in more than 260 (International Business Times, 2006) and 100 (The Seattle Times, 2008) fatalities. More recently in Alberta, Canada, approximately 28,000 barrels of crude oil was released as a result of a crude oil pipeline rupture in 2011. The accident is believed to be the biggest spill from a crude oil pipeline in Alberta since 1975 (CBC News, 2011).

In many developing countries it is now a statutory requirement to evaluate the risks for all the major safety hazards associated with pressurised pipelines prior to their commissioning. In the United Kingdom, the Offshore Installations (Safety Case) Regulations 2005 (Health and Safety Executive, 2006) require quantitative assessment of major accident risks and the measures employed to control and mitigate them. This is to ensure that the relevant statutory provisions will be complied with. The above procedure industry is normally referred to as "Quantitative Risk assessment", or in short form QRA.

By definition Risk is the likelihood (frequency) of a specific consequence of a specific accident. The event frequency can normally be obtained from the available historical data. On the other hand, the consequence of a specific accident needs to be determined before performing QRA.

Following an accident involving hazardous materials, first the inventory is released to the atmosphere. This phase is normally referred to as "Discharge". In the absence of an immediate ignition of the released flow, depending on the fluid phase there will be either "Dispersion" (cloud formation) for gas/two phase flow or "Pool Formation" for liquid releases. The resulting consequences can then be fire, explosion, toxic release and environmental pollution. The Discharge phase, which involves the calculation of release rate, provides the source conditions for quantifying all these major consequences.

On the other hand, pipeline failure may be in the form of full-bore rupture where the pipe splits into two, a simple puncture or longitudinal tear. Among these, full-bore rupture is considered to be the most catastrophic scenario.

Numerous studies with various degrees of sophistication have been conducted to model the transient outflow following the failure of pressurised pipelines (see for example Bendiksen et al. (1991), Richardson & Saville (1991, 1996a, 1996b) and Mahgerefteh et al. (1997, 1999, 2000)). Although important, these studies are confined to gas or flashing liquid pipelines.

On the other hand, the available models for failure of pipelines containing liquids ignore the drainage once the pipeline pressure has reached the ambient pressure. In other words, the pipe is assumed to remain full throughout the discharge process (see for example Loiacono (1987), Schwarzhoff & Sommerfeld (1988), Sommerfeld & Stallybrass (1992), Kossik (2000), Joye & Barrett (2003)). This regime, which is normally referred to as full pipe flow, can only happen if the feed tank never drains dry. Therefore, the subsequent flow regimes involving bubble formation followed by open channel flow (Wallis et al., 1977) are not considered.

As a result, the remaining mass in the pipe with ambient pressure is ignored. While this might be a valid assumption for short/small diameter pipes, for long/large diameter pipelines, which are commonly used for transporting petroleum products, may result in significant underestimation of released mass. In addition, if the pipe is isolated following the closure of an ESD valve, it will reach the ambient pressure instantaneously due to the absence of feed tank.

As the flow rate decreases over time, air ingress will result in the formation and propagation of a bubble in the pipe. Bubble formation in the pipe is of significant interest since the formation of air pockets can reduce the effective pipe cross sectional area thus reducing pipe capacity. Also the transported air will be released at the discharge location, which can raise environmental concerns due to foaming (Launchlan et al., 2005).

Based on a force balance, Benjamin (1968) calculated the liquid velocity required to keep a bubble stagnant at the downstream end of a horizontal pipe. The author determined that the calculated liquid velocity is the same as the velocity of the propagating bubble into a stationary liquid. Bendiksen (1984) experimentally predicted the bubble propagation velocity in non-stationary liquids in small diameter pipes with various inclinations. Inogamov & Oparin (2003) developed an analytical model for the bubble propagation velocity in a stationary liquid in downward-inclined pipes. Their model for horizontal pipes produced close agreement with Benjamin's (1968) predictions. In all the above studies the pipe had either a closed-end (stationary liquids) or the bubble was introduced from the bottom of the pipe into the flow (non-stationary liquids). The impact of an upstream storage tank on the flow regime and bubble propagation velocity was not considered.

Following further decrease in the flow rate, the bubble will elongate forming a free surface on top of the liquid. This regime is called open channel flow. Modelling such flows is of particular interest in civil engineering projects involving water distribution networks. The so called California Pipe Method (Water measurement manual, 2001) for example predicts the discharge rate from a horizontal pipe based on the liquid depth at the free fall. The model is however limited to when the pipe runs less than half full. Since then, a number of authors have studied the relation between the discharge rate and liquid depth at the pipe exit (see for example Dey (2001) and Sterling & Knight (2001)).

This thesis describes the development, verification and validation of analytical models for simulating the transient discharge rate following the full-bore rupture of incompressible liquid transporting pipelines with various inclinations. The models, for the first time, account for all the important flow regimes taking place during discharge, focusing specifically on bubble formation and propagation, and open channel flow. Two configurations including pipe fed from an upstream storage tank and with a closed-end due to ESD valve closure are considered. For the pipe fed from an upstream tank the importance of accounting for post-full pipe flow on the total amount of inventory discharged is demonstrated based on the simulation data. In addition, the impact of upstream storage tank on the bubble propagation velocity is

investigated. The developed models for pipes with closed-end for the first time simulate the transient outflow throughout the drainage process. The relation between the liquid depth and pipeline characteristics during open channel flow is also determined for both horizontal and downward-inclined pipes. The new equations provide an alternative to the measured liquid depth data from the experiments, not always available, required for the calculation of the discharge rate. The developed models are validated against laboratory based experiments.

This thesis is divided into 6 chapters.

In Chapter 2, the theoretical basis for the pipeline outflow model with its assumptions and justifications are presented. The chapter presents the basic equations governing the flow of incompressible liquids in pipes, including the conservation equation for mass and the Bernoulli equation.

Chapter 3 presents a review of the mathematical models available in the open literature for simulating failures of pipelines containing incompressible (non-flashing) liquids. This includes models for full pipe flow, bubble formation and propagation, and open channel flow.

Chapter 4 describes the development, verification and validation of hydraulic transient models to simulate the outflow following full-bore rupture in horizontal pipes. First, the pipe is assumed to be fed from an upstream storage tank. The overall model for this configuration includes the published model for full pipe flow (Joye & Barret, 2003) and the reported models for bubble formation and propagation, and open channel flow. Then the pipe is assumed to be isolated instantaneously upon rupture following emergency shut down. Due to the absence of an upstream tank, the model developed for this configuration only includes bubble formation and propagation, and open channel flow. Ultimately the models are verified through sensitivity analysis.

In addition, for the configuration with upstream tank, a series of experiments investigates the applicability of Bendiksen's (1984) proposed value for the empirical coefficient C_0 for the upstream bubble propagation velocity in the presence of upstream storage tank and downstream bubble. The accuracy of the two models in predicting the discharge rate is also examined through series of experiments.

Chapter 5 focuses on the extension of the developed models in Chapter 4 to account for the pipe inclination for both isolated pipes and those fed from an upstream tank. The validity of Bendiksen's (1984) proposed value for the empirical coefficient C_0 for the upstream bubble propagation velocity in the presence of upstream storage tank for downward-inclined pipes is tested through experiments. Once again the efficacies of the models are tested based on their application to the failure of a hypothetical pipeline system. The accuracy of the models predictions for the discharge rate is also assessed through series of experiments.

Chapter 6 deals with general conclusions and suggestions for future work.

CHAPTER 2: FUNDAMENTAL EQUATIONS AND BACKGROUND THEORY

2.1 Introduction

The development of an outflow fluid dynamics model entails three main steps. The first involves formulating the basic equations governing flow, thermodynamics and pertinent boundary conditions. The next stage is applying an efficient and accurate method to resolve or simplify these equations into easily solvable forms. The final step is concerned with the validation of the model against field or experimental data, and/or evaluation of its performance against case studies which are representative of realistic scenarios.

An important part of the first step mentioned above is the formulation of the conservation equations for mass, momentum and energy. The final form of these equations can be obtained through various assumptions and simplifications depending on the type of the flow and/or state of the fluid.

The flow of an incompressible liquid in a conduit with an open end may be either open channel or full pipe flow. The two flows are similar in many ways except in one important respect: in contrast to full pipe flow, open channel flow has a free surface (Chow, 1959) which is subjected to atmospheric pressure. Open channels may have an open top; for example in rivers, streams and estuaries. They also occur in conduits with a closed top. These include pipes and culverts; provided that the conduit is partly full (Akan, 2006).

The transition regime from full pipe flow to open channel flow is called bubble formation and propagation where depending on the pipe configuration, air bubbles are formed and propagate from the pipe inlet, outlet or both. The flow during this regime is a combination of the two flows: open channel flow where the bubbles exist, and full pipe flow throughout the rest of the pipe. The full description of this transition regime is presented in Chapter 3.

This chapter covers the pertinent theory and governing equations for full pipe flow and open channel flow. Description of flows, range of applications and the pertaining assumptions are also presented.

2.2 Full Pipe Flow

The flow is called full pipe flow as long as the pipe remains full of liquid at all times. Pressure difference and gravitational forces are the key drivers for the liquid flow during full pipe flow.

2.2.1 Conservation of Mass (Continuity) (Coulson & Richardson, 1999)

Considering one-dimensional flow in a straight pipe with a constant cross sectional area, the continuity equation is given by

$$\frac{\partial \rho}{\partial t} + \rho \frac{\partial u}{\partial x} = 0 \qquad \textbf{(2.1)}$$

where ρ, u, x, and t represent the liquid density, mean axial liquid velocity, position along the pipe and time, respectively.

The fluid is assumed to be incompressible; therefore $\frac{\partial \rho}{\partial t} = 0$. Consequently Equation (2.1) becomes:

$$\rho \frac{\partial u}{\partial x} = 0 \qquad \textbf{(2.2)}$$

or

$$u = \text{Constant} \qquad \textbf{(2.3)}$$

2.2.2 Conservation of Energy (Coulson & Richardson, 1999)

The total energy of a fluid in motion is made up of number of components including internal, pressure, potential and kinetic energy. Therefore, the total energy of unit mass of fluid, *e*, may be defined as:

$$e = i + P\upsilon + gZ + \frac{\dot{u}^2}{2} \qquad \textbf{(2.4)}$$

where *i*, *P* and υ are internal energy, pressure and volume per unit mass ($1/\rho$) respectively. Furthermore, *g*, *Z* and $\dot{u}$ are gravitational acceleration, elevation above the datum level and the velocity of a finite element of the fluid respectively. The above equation may be applied to the fluid as it flows from point 1 to 2 assuming *q* and W_s represent the net heat absorbed from the surroundings and net work done by the fluid on the surroundings respectively:

$$i_2 + P_2\upsilon_2 + gZ_2 + \frac{\dot{u}_2^2}{2} = i_1 + P_1\upsilon_1 + gZ_1 + \frac{\dot{u}_1^2}{2} + q - W_s \qquad \textbf{(2.5)}$$

or

$$\Delta i + \Delta(P\upsilon) + g\Delta Z + \Delta\frac{\dot{u}^2}{2} = q - W_s \qquad \textbf{(2.6)}$$

where Δ denotes a finite change in the quantities. Also specific enthalpy, *h*, may be defined by:

$$h = i + P\upsilon \qquad \textbf{(2.7)}$$

Replacing $i + P\upsilon$ in Equation (2.6) by *h* gives:

$$\Delta h + g\Delta Z + \Delta\frac{\dot{u}^2}{2} = q - W_s \qquad \textbf{(2.8)}$$

Also for an irreversible process enthalpy may be defined by:

$$dh = \delta q + \delta F + \nu dP \qquad \textbf{(2.9)}$$

where F represents the mechanical energy converted irreversibly into heat. Replacing h from the above equation into Equation (2.8):

$$\dot{u}\,d\dot{u} + g\,dZ + \upsilon dP + \delta W_s + \delta F = 0 \qquad \textbf{(2.10)}$$

When the above equation is applied over the whole cross sectional area of the pipe, allowance must be made for the fact that the mean square velocity is not equal to the square of the mean velocity. Therefore, a correction factor, α, is introduced into the kinetic term with a value of 0.5 and 1 for laminar and turbulent flow respectively. Thus, in the absence of external work and assuming the flow to be turbulent, for finite changes, Equation (2.10) is integrated for flow from point 1 to 2 and gives:

$$\Delta\left(\frac{u^2}{2}\right) + g\Delta Z + \upsilon\Delta P + F = 0 \qquad \textbf{(2.11)}$$

2.2.3 Frictional Loss

For the flow of a liquid through the pipe, the total frictional loss, F, can be expressed as (Perry, 1997; Mannan, 2005):

$$F = F_c + F_e + F_{ft} + F_f \qquad \textbf{(2.12)}$$

where F_c and F_e are the frictional loss due to sudden contraction and expansion respectively. On the other hand, F_{ft} and F_f are the frictional loss due to fittings and bends and the fluid/pipe wall loss respectively.

Loss due to sudden contraction (F_c)

For a sudden contraction at a sharp-edged entrance to the pipe, the entry loss can be approximated via the following equation (Crane, 1957; Evet et al., 1989):

$$F_c = 0.5(1 - \frac{A_2}{A_1})\frac{u^2}{2} \quad \textbf{(2.13)}$$

A_2 and A_1 are the smaller and larger areas of the pipe respectively. For the case of the pipe attached to an upstream vessel $\frac{A_2}{A_1} \approx 0$. Therefore Equation (2.13) is simplified to the following equation:

$$F_c = 0.5\frac{u^2}{2} \quad \textbf{(2.14)}$$

McCabe et al. (1956) proposed the following equation for the entry loss of a pipe attached to an upstream vessel:

$$F_c = 0.4\frac{u^2}{2} \quad \textbf{(2.15)}$$

Loss due to sudden expansion (F_e)

Friction loss due to sudden expansion of ducts of any cross section may be estimated by the Borda-Carnot equation (Perry, 1997):

$$F_e = (1 - \frac{A_1}{A_2})^2 \frac{u^2}{2} \quad \textbf{(2.16)}$$

For the case of a pipe attached to a downstream vessel, $\frac{A_1}{A_2} \approx 0$. Therefore Equation (2.16) is simplified to the following equation:

$$F_e = \frac{u^2}{2} \qquad \textbf{(2.17)}$$

Fittings, bends and valves friction loss (F_{ft})

The two most common methods for calculating the fittings, bends and valves losses are (Perry, 1997):

1. equivalent length method (L_e)
2. velocity head method (K)

In the equivalent length method, the losses are reported as the length of a straight pipe which has the same loss as the fittings, bends or valves. For turbulent flow the equivalent length is normally reported as a number of diameters of the pipe of the same size as the fitting connection with fixed quantity for L_e/D. For laminar flow L_e/D is dependent on Reynolds number (Perry, 1997).

In the velocity head method, the losses are reported as a number of velocity heads, i.e. $Ku^2/2g$. The values of K for different fittings, bends and valves may be found in references such as Crane (1957) and Perry (1997).

Fluid/Pipe Wall Frictional loss (F_f)

The fluid/pipe wall frictional loss for laminar flow may be calculated from the Hagen-Poiseuille equation (Bird et al., 2007):

$$F_f = \frac{32\mu L u}{\rho D^2} \qquad \textbf{(2.18)}$$

and in terms of head:

$$h_l = \frac{32\mu L u}{\rho g D^2} \qquad \textbf{(2.19)}$$

where h_l, L, μ and D are the head loss, pipe length, dynamic viscosity and pipe internal diameter respectively.

For turbulent flow, the fluid/pipe wall frictional loss may be calculated by Darcy-Weisbach equation (French, 1994):

$$F_f = \frac{2fLu^2}{D} \qquad \textbf{(2.20)}$$

and in terms of head:

$$h_l = \frac{2fLu^2}{gD} \qquad \textbf{(2.21)}$$

where f is the Fanning friction factor. The Fanning friction factor should not be confused with the Darcy friction factor which is 4 times greater. For turbulent flow in smooth pipes, the Blasius equation gives f for Reynolds number, Re, in the range of 4000-10^5 (Perry, 1997):

$$f = \frac{0.079}{\mathrm{Re}^{0.25}} \qquad \textbf{(2.22)}$$

where Re is defined via:

$$\mathrm{Re} = \frac{\rho u L}{\mu} \qquad \textbf{(2.23)}$$

The Colebrook formula is accepted as the most accurate for rough pipes as long as $Re > 4000$ (Perry, 1997):

$$\frac{1}{\sqrt{f}} = -2\log[\frac{\varepsilon}{3.7D} + \frac{2.51}{\mathrm{Re}\sqrt{f}}] \quad \textbf{(2.24)}$$

where ε is the pipe surface roughness. The disadvantage of the above equation lies in expressing f implicitly, requiring iterations for its evaluation.

Churchill (1977) (Perry, 1997) suggested the following explicit equation for f for both smooth and rough pipes for $Re > 4000$:

$$\frac{1}{\sqrt{f}} = -4\log[\frac{0.27\varepsilon}{D} + (\frac{7}{\mathrm{Re}})^{0.9}] \quad \textbf{(2.25)}$$

All the above equations are dependent on Reynolds number and consequently on velocity in the pipe which may be unknown. Coulson and Richardson (1999) proposed a simplistic expression for f as long as $\mathrm{Re}\frac{\varepsilon}{D} f^{0.5} >> 2.3$:

$$f = \frac{2}{[3.2 - 2.5\ln(\varepsilon / D)]^2} \quad \textbf{(2.26)}$$

Darcy-Weisbach equation for turbulent flow (Equation (2.21)) is equivalent to Hagen-Poiseuille equation (Equation (2.19)) for laminar flow with the exception of friction factor f. Equating the two equations for head loss gives an expression of f that allows the Darcy-Weisbach equation to be applied to laminar flow:

$$\frac{32\mu Lu}{\rho g D^2} = \frac{2fLu^2}{gD} \quad \textbf{(2.27)}$$

or

$$f = \frac{16}{\mathrm{Re}} \quad \textbf{(2.28)}$$

The above equation is called Poiseuille's equation (Rohsenow et al., 1998).

2.3 Open Channel Flow

In open channel flow, due to the presence of a free surface on top of the liquid, the pipe is not pressurised. Despite the similarities between open channel and full pipe flow, it is much more difficult to solve problems for open channel flow. This is due to variation of the free surface position with respect to time and space (Chow, 1959). In fact, although the basic principles of fluid mechanics are still applicable to open channel flow, such flow is significantly more complex than full pipe flow due to the presence of free surface on top of the liquid. In order to have a streamline with atmospheric pressure at the free surface, the forces causing and resisting the flow and the inertia must form a balance. Consequently, unlike full pipe flow, the flow boundaries are no longer fixed by the conduit geometry. Here the free surface adjusts itself to accommodate the given flow conditions (Sturm, 2001). Table 2.1 summarises the main differences between full pipe and open channel flow.

	Full pipe flow	**Open channel flow**
Flow driven mainly by	Pressure	Gravity
Flow cross sectional area	Fixed (pipe cross section)	Variable (reducing)
Specific boundary conditions	-	Ambient pressure at free surface

Table 2.1:Comparison between full pipe and open channel flow

As it can be observed from the above table, gravity is the main driver for the flow in open channel flow. The main dimensionless parameter for this type of flow is the ratio of inertia and gravity forces, defined as the Froude number:

$$Fr = \frac{u_{liquid}}{\sqrt{g\frac{A_{wet}}{T}}} \qquad \textbf{(2.29)}$$

where T , A_{wet} and u_{liquid} are the top width of the channel, channel wetted area and liquid film velocity respectively. The ratio A_{wet} /T is also called hydraulic depth. Figure 2.1 presents the cross section of a circular channel with the various characteristics dimensions.

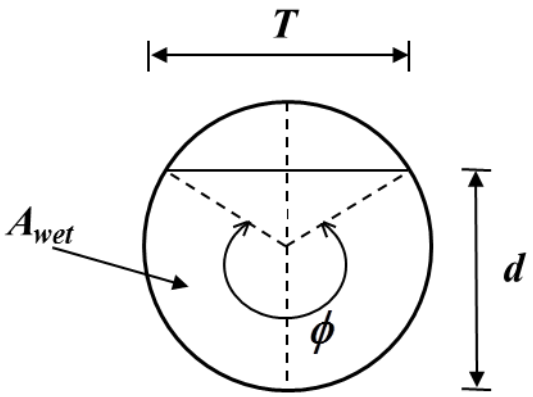

Figure 2.1: Cross section of a circular channel representing the various characteristic dimensions:

***d* = liquid depth**

ϕ = liquid depth angle

***T* = flow top width**

A_{wet} = Wetted area

2.3.1 Conservation of Mass (Continuity) (Sturm, 2001)

Once again considering one-dimensional flow in a channel, the continuity equation is given by:

$$\frac{\partial A_{wet}}{\partial t} + \frac{\partial Q_{liquid}}{\partial x} = 0 \qquad \textbf{(2.30)}$$

where Q_{liquid} is the liquid volumetric flow rate. Assuming A_{wet} remains unchanged with time and position along the channel, Equation (2.30) is simplified as:

$$\frac{\partial u_{liquid}}{\partial x} = 0 \qquad \textbf{(2.31)}$$

or

$$u_{liquid} = \text{Constant} \tag{2.32}$$

2.3.2 Specific Energy (Akan, 2006)

The principle for the energy conservation equation in open channel flow is the same as for full pipe flow. Assuming one-dimensional flow in a channel, the following equation describes energy conservation for open channel flow:

$$\frac{1}{g}\frac{\partial u_{liquid}}{\partial t} + \frac{u}{g}\frac{\partial u_{liquid}}{\partial x} + \frac{\partial d}{\partial x} + S_e - S_0 = 0 \tag{2.33}$$

where d, S_e and S_o are the liquid depth in the channel, energy slope and channel slope respectively. Energy slope is related to the work done by the friction forces.

In open channel flow problems, it is often desirable to consider the energy content with respect to the channel base. This is called the specific energy or specific head, $E_{specific}$, and is given by:

$$E_{specific} = d + \frac{u_{liquid}^2}{2g} \tag{2.34}$$

Another common term in open channel flow is the energy grade line which is defined as sum of the specific head and the elevation of the channel base above a selected datum, z:

$$E_{grade\ line} = z + d + \frac{u_{liquid}^2}{2g} \tag{2.35}$$

The slope (gradient) of the energy grade line, S_e in Equation (2.33), is the rate of energy head loss due to friction (h_l). Figure 2.2 shows the energy grade line and specific energy in a channel.

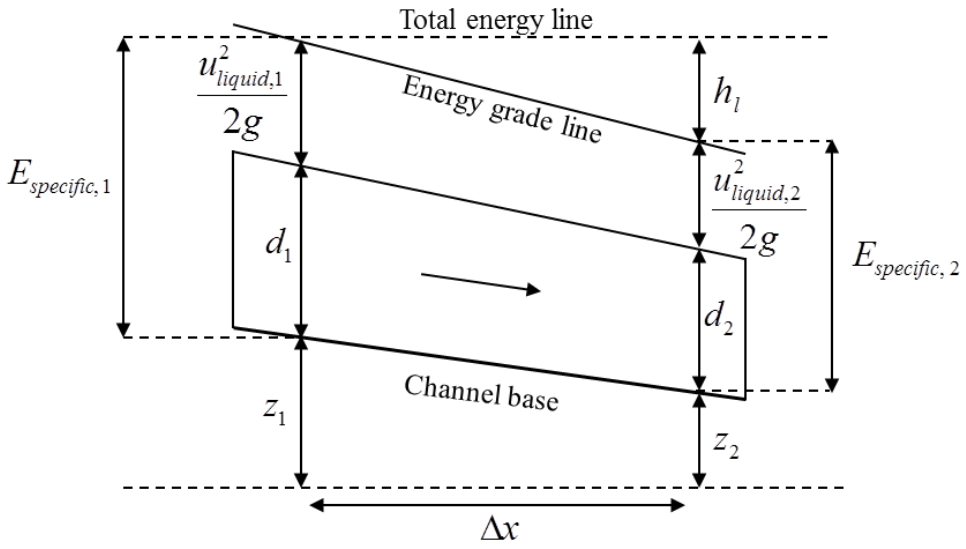

Figure 2.2: Total and specific energy lines in a channel

2.3.3 Subcritical, Critical and Supercritical Flow (French, 1994; Akan, 2006)

Figure 2.3 shows the plot of d versus $E_{specific}$ for a fixed discharge and channel section (French, 1994; Akan, 2006). The depth at which the specific energy is at its minimum is called critical depth, d_c, and the corresponding flow is referred to as critical flow. Flows with liquid depth higher and lower than critical depth are called subcritical and supercritical flow respectively.

The condition of minimum specific energy at critical depth implies that its derivative with respect to d must be zero:

$$\frac{d\left(E_{specific}\right)}{d(d)} = 1 + \frac{2u_{liquid}}{2g}\frac{du_{liquid}}{d(d)} = 0 \qquad \textbf{(2.36)}$$

Replacing u_{liquid} in the above equation by ($Q_{critical}$ / A_{wet}) produces:

$$1-\frac{2Q_{critical}^2}{2g}\frac{d\left(A_{wet}\right)/d(d)}{A_{wet}^3}=0 \qquad \textbf{(2.37)}$$

where $Q_{critical}$ is the critical liquid discharge rate. Noting T, the top width of the channel, is $d(A_{wet}) / d(d)$, the above equation may be rewritten as:

$$1-\frac{u_{critical}^2}{g}\frac{T}{A_{wet}}=0 \qquad \textbf{(2.38)}$$

or

$$u_{critical}=\sqrt{\frac{gA_{wet}}{T}} \qquad \textbf{(2.39)}$$

Based on the above equation, the Froude number (Equation (2.29)) is 1 for critical flow. Flows with Fr higher than 1 are supercritical, while in subcritical flows, Fr is less than 1.

2.3.4 Uniform Flow

A channel is said to have uniform flow if the flow depth and the velocity remain unchanged with time and space. The corresponding flow depth is called normal depth, d_n. This constitutes the fundamental type of the flow in an open channel. It occurs when gravity forces are in equilibrium with resistance forces.

The definition of uniform flow implies that S_e is the same as the channel slope, S_o. This type of flow only happens in prismatic channels and rarely occurs naturally. However, in very long channels and in the absence of flow controls such as hydraulic structures the flow becomes uniform (Akan, 2006).

Determining the discharge rate for uniform flow for a given depth or vice versa has been of particular interest for many researchers. Historically, such formulas have been presented for the flow velocity as a function of hydraulic radius and slope. The

famous Chezy equation empirically predicts the flow rate in a channel with uniform flow (White, 1999):

$$u_{liquid} = C_{Chezy}(R_h S_0)^{1/2} \quad \textbf{(2.40)}$$

where R_h and C_{Chezy} are the hydraulics radius and Chezy coefficient respectively. R_h is defined as:

$$R_h = \frac{1}{4} D_h = \frac{A_{wet}}{P_{wet}} \quad \textbf{(2.41)}$$

Here D_h and P_{wet} represent hydraulic diameter and wetted perimeter of the channel respectively. Despite what the name may suggest, the hydraulic diameter is not twice the hydraulic radius, but four times.

C_{chezy} is defined as (Sturm, 2001):

$$C_{Chezy} = (\frac{8g}{f})^{1/2} \quad \textbf{(2.42)}$$

f is the Fanning friction factor which will be described in Section 2.3.6. A good approximation of Equation (2.42) has been proposed by Robert Manning (White, 1999):

$$C_{Chezy} = (\frac{8g}{f})^{1/2} \approx c\frac{R_h^{1/6}}{n} \quad \textbf{(2.43)}$$

Here n is a roughness parameter which is presented in Table 2.2 for various materials, and c is a parameter = 1.0 $m^{2/6}s^{-1}$. n is a dimensionless parameter.

Replacing C_{Chezy} from Equation (2.43) into Equation (2.40) gives:

$$u_{liquid} = \frac{c}{n} R_h^{2/3} S_0^{1/2} \quad \textbf{(2.44)}$$

The use of Chezy coefficient for man-made channels seems to be somewhat controversial. Chanson (2004) stated that in open channels, the Darcy-Weisbach equation is the only sound method to estimate the friction loss. Therefore, recalling Equation (2.21) for full pipe flow and replacing D by D_h gives:

$$\frac{h_l}{L} = \frac{2 f u_{liquid}^2}{g D_h} \quad \textbf{(2.45)}$$

For uniform flow the head loss per unit length is the same as channel slope (S_0). Therefore, replacing the left side of the above equation by S_0 produces:

$$u_{liquid} = \sqrt{\frac{S_o g D_h}{2 f}} \quad \textbf{(2.46)}$$

For mainly historical reasons empirical resistance coefficients (e.g. Chezy coefficient) are still used. Chanson (2004) stated that their use is highly inaccurate for man-made channels. The Darcy-Weisbach equation is the only suitable method to predict the flow rate in open channel flow.

2.3.5 Steep and Mild/Horizontal Channels

Depending on the channel slope with a selected datum, a channel can be classified as mild or steep. When the inclination of the pipe is greater than 6^o, the pipe is called steep (Akan, 2006). French (1985) suggested a value of 10^o as the criteria for steep channels. In mild/horizontal channels, normal depth (d_n) is larger than critical depth (d_c), while for steep pipes critical depth has a larger value. Figure 2.4 and Figure 2.5

respectively show schematic sketches for mild/horizontal and steep channels both ending with free fall.

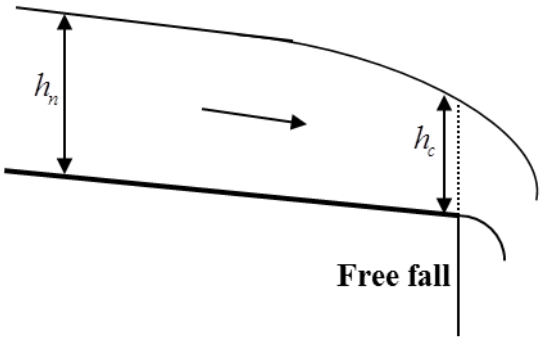

Figure 2.4: Flow in mild/horizontal channel ending with a free fall

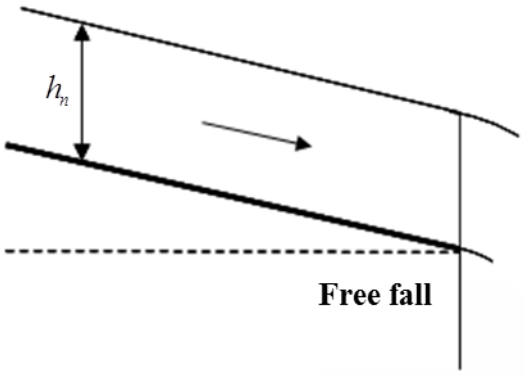

Figure 2.5: Flow in steep channel ending with a free fall

Normally in mild/horizontal channels due to low liquid velocity, the flow is subcritical. If the channel terminates at a free fall, the liquid depth at the free fall may be assumed to be the same as critical depth. In reality, when the flow is subcritical, the critical depth occurs a short distance, about $4d_c$, upstream of the free falls. The depth at the end of the pipe which is called brink depth, d_e, is less than critical depth. However, for sufficiently long channels, the assumption of critical depth is a reasonably good assumption (Wallis et al., 1977; Akan, 2006; Tiğrek et al., 2008). On the other hand, in steep pipes due to high liquid velocity the flow is supercritical and the free fall does not affect the liquid depth. As such, the liquid depth at the pipe outlet and along the pipe is the same as normal depth (d_n) (French, 1985; Akan, 2006).

2.3.6 Frictional loss

In open channels the flow is normally turbulent. Therefore the Fanning friction factor may be calculated from the Colebrook equation by replacing D with D_h:

$$\frac{1}{\sqrt{f}} = -2\log[\frac{\varepsilon}{3.7D_h} + \frac{2.51}{\mathrm{Re}\sqrt{f}}] \quad \textbf{(2.47)}$$

Also since typical channels are rough, for fully turbulent flow, f may be defined by (White, 1999):

$$f \approx \left(2\log\frac{14.8R_h}{\varepsilon}\right)^{-2} \quad \textbf{(2.48)}$$

Typically the equations used to calculate the Fanning friction factor in full pipes are also applicable to open channel flow, except that the pipe diameter needs to be replaced by the hydraulic diameter for open channel flow.

2.4 Conclusion

In this chapter, the two types of flows occurring in incompressible liquid pipelines, i.e. full pipe flow and open channel flow, were described. The equations describing mass and energy conservation were presented for both types of flow. The critical condition at the pipe exit in open channel flow was explained and the difference between subcritical and supercritical flow was highlighted. Also mild/horizontal and steep channels were described and the boundary conditions along with the corresponding discharge equations for each were explained.

This chapter concluded that the mass conservation and the Bernoulli equation would be applicable to both types of flow. In open channel flow, depending on the pipe inclination, the flow can be either subcritical (mild/horizontal channels) or supercritical (steep channels). In addition, in horizontal channels with free fall, critical condition prevails at the channel exit, i.e. the liquid depth is the same as

critical depth. In steep channels, on the other hand, the flow is uniform across the channel with the liquid depth being the same as the normal depth. These conclusions form the basis for developing hydraulic-based outflow models to simulate the failure of horizontal and downward-inclined pipelines in the following chapters.

CHAPTER 3: LITERATURE REVIEW

3.1 Introduction

Modelling of accidents involving the failure of pressurised pipelines has been the subject of significant interest since research carried out in the nuclear power industry (Offshore Technology Report, 1998) evaluating the critical scenarios of loss of coolant accidents (LOCAs) in Pressurised Water Reactors (PWRs). Since then, numerous studies with various degrees of sophistication have been conducted to model the transient outflow following the failure of pressurised pipelines (see for example Bendiksen et al.(1991); Richardson & Saville (1991, 1996a, 1996b) and Mahgerefteh et al.(1997, 1999, 2000)). However, these are confined to gas or flashing liquid pipelines. Although equally important, for pipelines containing incompressible liquids there is no unified model to simulate the outflow throughout the complete drainage of the pipeline.

Wallis et al. (1977), Montes (1997) and Hager (1999) identified three flow regimes which may be observed following the rupture of horizontal, permanent liquid transporting pipelines. These include full pipe flow, bubble formation and propagation, and finally open channel flow. Full pipe flow occurs during depressurisation for as long as the pipe remains full. Bubble propagation and open channel flow on the other hand take place sequentially following air ingress to the pipe after full pipe flow.

The three flow regimes occurring in horizontal pipe have also been observed in downward-inclined pipes (Yen & Pansic, 1980; Joy & Barrett, 2003; Pothof, 2011).

This chapter presents a review of the pertinent models for simulating the transient or steady-state discharge following the failure of pressurised pipelines containing incompressible liquids. The transient modelling includes the three regimes of full pipe flow, bubble formation and propagation, and open channel flow. For the bubble formation and propagation regime, researchers have mainly focused on the bubble

propagation velocity rather than the liquid discharge rate. However, since this forms the basis of the models developed in this study, the available equations for bubble propagation velocity are also presented in this chapter.

3.2 Full Pipe Flow

The most conventional method to calculate the discharge rate following incompressible liquid pipeline rupture is to assume the pipeline remains full throughout the discharge process. Loiacono (1987) developed a full pipe flow model to calculate the required time, t_f, to drain a vertical cylindrical tank through a vertical pipe connected to its base. First, Loiacono (1987) applied the Bernoulli equation between points 1 and 2, presented in Figure 3.1, which produced Equation (3.1). Then, Equation (3.1) was combined with the transient flow mass balance, Equation (3.2), to produce Equation (3.3) to calculate t_f:

$$\frac{u_d^2}{2} - gZ + \frac{2fL_e}{D}u_d^2 = 0 \qquad \textbf{(3.1)}$$

$$\frac{dM}{dt} = -\rho A u_d \qquad \textbf{(3.2)}$$

$$t_f = \left(\frac{D_{\tan k}}{D}\right)^2 \sqrt{\frac{2}{g}\left(\frac{4fL_e}{D}+1\right)}\left(\sqrt{Z_0} - \sqrt{Z_f}\right) \qquad \textbf{(3.3)}$$

where:

u_d = discharge velocity

Z = liquid level height

Z_0 = initial liquid level height at $t = 0$

Z_f = final liquid level height

H = liquid head in the tank

L_e = equivalent length of piping and fitting (see Section 2.2.3)

A = pipe cross sectional area

D_{tank} = tank diameter

D = Pipe inner diameter

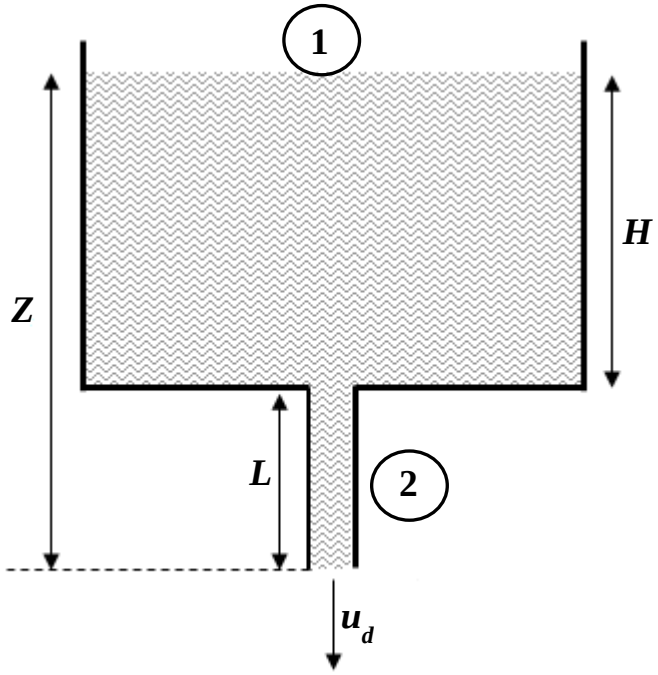

Figure 3.1: Tank drainage through a vertical pipe

Loiacono (1987) only considered tanks with flat base. Shoaei & Sommerfeld (1989) modified Loiacono's model to account for tanks with elliptical base which are more common in industry. The difference between a tank with flat base and one with elliptical base is the reduction in the tank cross sectional area for the later case when the liquid level approaches the pipe inlet. To account for this, Shoaei & Sommerfeld (1989) suggested the following equation to describe A_{tank} as a function of liquid head in the tank:

$$A_{\tan k} = \frac{\pi D_{\tan k}^2}{4b}\left(2H - \frac{H^2}{b}\right) \qquad \textbf{(3.4)}$$

where b is the depth of elliptical dished head. Defining $H = Z\text{-}L$ and replacing A_{tank} from the above equation into Equation (3.3) yields:

$$\left(Y^2 - 2BZ + Z^2\right)\frac{dZ}{dt} = \left(\frac{D}{D_{\tan k}}\right)^2 \sqrt{\frac{2gZ}{1+\frac{4fL_e}{D}}} \qquad \textbf{(3.5)}$$

where

$$B = L + b \qquad \textbf{(3.6)}$$

and

$$Y^2 = L^2 + 2bL \qquad \textbf{(3.7)}$$

Integrating Equation (3.5) between (0, Z_0) and (t_f, Z_f) yields:

$$t_f = C\left[\left(\frac{2}{5}Z_0^2 - \frac{4B}{3}Z_0 + 2Y^2\right)\sqrt{Z_0} - \left(\frac{2}{5}Z_f^2 - \frac{4B}{3}Z_f + 2Y^2\right)\sqrt{Z_f}\right] \qquad \textbf{(3.8)}$$

where

$$C = \left(\frac{D_{\tan k}}{D}\right)^2 \sqrt{\frac{1}{2g}\left(1+\frac{4fL_e}{D}\right)} \qquad \textbf{(3.9)}$$

Joye & Barrett (2003) modified Loiacono's model (1987) by replacing the equivalent length for the piping and fittings (minor losses) with the resistance coefficient due to wider availability of values for resistance coefficient than equivalent length. Assuming the tank never drained dry, they proposed the following equation for the transient discharge rate from pipes with any inclination:

$$t_f = \frac{D_{\tan k}^2}{D^2}\sqrt{\frac{2}{g}\left(\frac{4fL}{D}+\Sigma K\right)}\left(\sqrt{Z_0}-\sqrt{Z_f}\right) \quad \textbf{(3.10)}$$

where ΣK represent the minor losses including the exit kinetic loss and the pipe entrance loss. Here the flow was assumed to be turbulent, thus *f* remained constant. Joye & Barret (2003) validated the above equation through a series of experiments for tanks with diameters of 0.075m and 0.37m. The pipe fed from the small tank was smooth stainless steel with inner diameter ranging from 0.003m to 0.007m. The larger tank on the other hand was connected to a smooth hard-drawn copper pipe with the diameter of 0.019m. They also conducted some tests for a system of horizontal and vertical pipe segments. Figure 3.2 and Figure 3.3 respectively present their predicted efflux time (t_f) from Equation (3.10) for $\frac{L}{D} > 3$ and $\frac{L}{D} \leq 3$ for various pipe configurations. From the graphs, they concluded that Equation (3.10) predicted the efflux time with good accuracy with maximum deviation of about 15%.

For laminar flow, Bird et al. (2007) combined Hagen-Poiseuille equation (Equation 2.18) for steady state flow with transient flow mass balance (Equation (3.2)):

$$\frac{dz}{dt} = -\frac{\pi\rho g D^4 (H+L)}{128\mu L\left(\frac{\pi D_{\tan k}^2}{4}\right)} \quad \textbf{(3.11)}$$

or

$$\frac{dz}{dt} = -\frac{\rho g D^4 (H+L)}{32\mu L D_{\tan k}^2} \quad \textbf{(3.12)}$$

Although Hagen-Poiseuille equation was originally derived for steady-state flow, it could still be used here due to quasi-steady state nature of the flow (Bird et al., 2007).

By rearranging the above equation and subsequently integrating between (0, H_0) and (t_f, H_f), Bird et al. (2007) derived Equation (3.14) for the efflux time for laminar flow:

$$\frac{dH}{H+L} = -\frac{\rho g D^4}{32\mu L D_{\tan k}^2} dt \qquad \textbf{(3.13)}$$

$$t_f = \frac{32\mu L D_{\tan k}^2}{\rho g D^4} \ln\left(\frac{H_0 + L}{H_f + L}\right) \qquad \textbf{(3.14)}$$

The above equation assumes the exit kinetic energy and other friction losses are negligible. Joye & Barrett (2003) tested this assumption by conducting experiments for 98% glycerol/water. They compared the predicted efflux time from Equation (3.14) with those obtained from Equation (3.10) where exit kinetic energy and frictional loss were also included. Fanning friction factor in Equation (3.10) was calculated from Equation (2.28) for laminar flow. The values for minor losses were assumed to be the same as those for the turbulent flow. Figure 3.4 and Figure 3.5 show the results of their comparisons for $\frac{L}{D} > 3$ and $\frac{L}{D} \leq 3$ respectively. Based on the graphs, Joye & Barrett (2003) claimed that, overall, the predicted efflux time (t_f) from Equation (3.10) was in slightly better agreement with the experimental results than Equation (3.14). On the other hand, for $\frac{L}{D} \leq 1.5$ both equations underestimated t_f, with the deviation more than 50% for $\frac{L}{D} = 0$. They suggested the better agreement from Equation (3.10) for turbulent flow could be due to uncertainties for K values for laminar flow. The consequence of the uncertainty regarding K values was even more detrimental for shorter pipes where the minor losses dominated fluid/pipe wall loss.

The DISC model developed by DNV Software (2005) predicts the steady-state discharge from an orifice in the tank wall or from a horizontal pipe attached to the tank for all fluid states. In the special case of incompressible liquids, the DISC model is simplified to a model very similar to Joye & Barett's model (2003). Employing Equation (3.15) instead of Equation (2.14) for pipe entry loss (F_c), the model calculates the discharge velocity via Equation (3.16):

$$F_{fe} = 0.5\left(\frac{1}{C_v^2} - 1\right)u_d^2 \qquad \textbf{(3.15)}$$

where C_v is velocity coefficient and is assumed to be 0.6.

$$u_d = \sqrt{\frac{gz}{\frac{2fL}{D} + 0.89}} \qquad \textbf{(3.16)}$$

The above model was validated against Uchida and Nariai's experimental data (1966) for water for the upstream pressure in the range 2-8 bara. The pipe diameter was 0.004m and the pipe length varied in the range 0-2.5m. The maximum difference between the predicted and experimental discharge velocity was 28%.

3.3 Bubble Formation and Propagation

As the flow rate decreases in the pipe, air ingress will result in the formation and propagation of bubbles, either at the pipe upstream or downstream or even both, depending on the pipe inclination and configuration. Bubble formation is of significant practical importance since air pockets can reduce the effective pipe cross sectional area thus reducing pipe capacity. Also the transported air may be released at the discharge location, which can raise environmental concerns due to foaming (Lauchlan et al., 2005).

3.3.1 Bubble Propagation in Stagnant Liquid

The classical problem of determining the drift velocity, i.e. propagation velocity of a long bubble through a stagnant liquid, in vertical pipes has been of interest to numerous authors in recent years. As long as surface tension effects are negligible, the bubble velocity is proportional to $\sqrt{gD}$ (Wisner et al., 1975; Falvey, 1980; Bendiksen, 1984). Based on the assumption of potential flow, Dumitrescu (1943) obtained a value of 0.35 for the proportionality coefficient which was in excellent agreement with experimental measurements. Zukoski (1966) experimentally investigated the impact of viscosity and surface tension on the bubble propagation velocity for different pipe inclinations. The conclusion was that for small pipe diameters with any inclinations, the influence of surface tension was to reduce the bubble propagation velocity more than $\sqrt{gD}$.

Benjamin (1968) was the first to consider bubble propagation along a closed-end or isolated horizontal pipe. Ignoring viscosity and surface tension and based on a force balance between the approaching and receding sections of the stream, Benjamin (1968) calculated a value of 0.542 for the proportionality coefficient for a horizontal pipe with the corresponding liquid depth below the bubble, *d*:

$$u_{drift} = 0.542\sqrt{gD} \qquad \textbf{(3.17)}$$

$$d = 0.561D \qquad \textbf{(3.18)}$$

where u_{drift} is the drift velocity. The calculated bubble velocity is the same as the minimum required liquid velocity to keep a bubble stagnant (Benjamin, 1968; Lauchlan et al., 2005).

On the other hand, for downward-inclined pipes there has been considerable debate on the minimum required liquid velocity to transport air bubbles and pockets along the pipe. Majority of the available literature relate to the results of experimental

investigations (Lauchlan, 2005). Most researchers agree that the required velocity in a downward-inclined pipeline is a function of $\sqrt{gD}$ and pipe slope S_o (Kalinske & Bliss, 1943; Kent, 1952).

Kent (1952) conducted detailed experiments for a 0.102m diameter, 5.5m long pipe with pipe angle varying between 15° and 60° relative to a horizontal level. Based on the curve presented in Figure 3.6 showing $-\sqrt{\sin\theta}$ versus experimental drift velocity, the author proposed the following equation for the minimum required velocity to transport air bubbles and pockets upstream of the pipe:

$$u_{drift} = 1.23\sqrt{gD}\sqrt{\sin\theta} \qquad \textbf{(3.19)}$$

θ is the pipe inclination angle relative to a horizontal level.

However Kent (1962) made a crucial mistake by graphically fitting the obtained data to the functional relation in Equation (3.19) (Pothof, 2011). The straight line in Figure 3.6 is not the same as what predicted by Equation (3.19). By carefully studying Figure 3.6 and Equation (3.19), it is clear that Equation (3.19) includes the origin, while the linear extrapolation of the experimental data does not, and the dotted parabolic curve is also incorrect (Pothof, 2011).

Mosvell (1976) suggested the following equation as a clearly better curve fit on Kent's data (1952), which allows for a non-zero offset:

$$u_{drift} = \sqrt{gD}\left(0.55 + 0.5\sqrt{\sin\theta}\right) \qquad \textbf{(3.20)}$$

Bendiksen (1984) suggested an empirical equation based on the drift velocity for horizontal and vertical pipes:

$$u_{drift} = 0.542\sqrt{gD}\cos\theta + 0.35\sqrt{gD}\sin\theta \quad \textbf{(3.21)}$$

The above equation gives the same value for drift velocity as the predicted value by Benjamin (1968) and Dumitrescu (1943) for horizontal and vertical pipes respectively.

Inogamov & Oparin (2003) developed an equation for bubble propagation velocity in downward-inclined pipes by applying analytical methods of potential theory and complex analysis:

$$u_{drift} = \sqrt{\frac{\cos(\pi/6 - \theta)}{\pi}}\sqrt{gD} \quad \textbf{(3.22)}$$

For horizontal and vertical pipes, the above equation predicts very similar results to what Benjamin (1968) and Dumitrescu (1943) predicted for horizontal and vertical pipes respectively:

$$\theta = 0 \qquad u_{drift} = 0.525\sqrt{gD} \quad \textbf{(3.23)}$$

$$\theta = 90^{o} \qquad u_{drift} = 0.399\sqrt{gD} \quad \textbf{(3.24)}$$

3.3.2 Bubble Propagation in Co-current Liquid

Bubble propagation in a co-current moving liquid was first studied by Nicklin et al. (1962) for a 0.026m diameter, vertical tube for Reynolds numbers in the range (8-50) l0 [3]. Their proposed model involves adding an extra term to the drift velocity to account for the liquid movement:

$$u_{moving} = u_{drift} + C_0 u \quad \textbf{(3.25)}$$

Here u_{moving}, C_0 and u are the bubble rise velocity in a moving liquid, a parameter = 1.2 and the liquid velocity respectively.

By conducting experiments with various diameter pipes, Bendiksen (1984) showed that for horizontal pipe, C_0 varied in the range of 1.0-1.2. In addition, for downward-inclined pipes with the inclination angle less than 30^o, C_0 was found to be 0.98.

3.4 Open Channel Flow

Following further decrease in the flow rate, the bubble will elongate forming a free surface on top of the liquid. This regime is called open channel flow. Modelling such flows is of particular interest in civil engineering projects involving water distribution networks.

3.4.1 Horizontal Channels

The California Pipe Method developed by Van Leer (1922) (Water measurement manual, 2001) predicts the discharge rate of water from a horizontal pipe based on the liquid depth at the free fall, d_e, via:

$$Q_d = 8.69\left(\frac{d_e}{D}\right)^{1.88} D^{2.48} \qquad \textbf{(3.26)}$$

where Q_d, d_e and D are in ft^3/s, ft and ft respectively. The model is however limited to:

- when the pipe runs less than half full
- the liquid depth at the outlet (brink depth) is less than $0.56D$
- the pipe is longer than $6D$
- pipe diameter is in the range of 0.05-0.15m

When the brink depth (d_e) is greater than 0.56*D*, the more general Purdue pipe method developed at Purdue University by Greve (1928) is used (Water measurement manual, 2001). This model is applicable equally well to both partially and completely full water pipes. It consists of measuring two coordinates of the upper surface of the jet, *X* and *Y*, as presented in Figure 3.7.

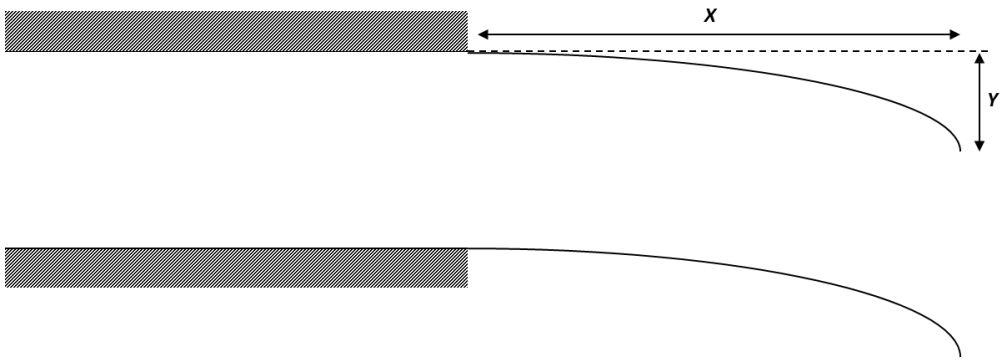

Figure 3.7: Purdue pipe method for measuring flow from a horizontal pipe

The model assumes that the horizontal velocity component of the flow is constant and the only force acting on the jet is gravity. In time *t*, a particle on the upper surface of the jet will travel a horizontal and vertical distance *X* and *Y* from the outlet of the pipe equal to:

$$X = u_0 t \qquad \textbf{(3.27)}$$

$$Y = 0.5gt^2 \qquad \textbf{(3.28)}$$

where u_0 is the velocity at $X = 0$. Combining the two equations and introducing a discharge coefficient = 1.1, the discharge rate is calculated via:

$$Q_d = 0.864D^2\sqrt{g\frac{X^2}{2Y}} \qquad \textbf{(3.29)}$$

Since then numerous authors carried out research to investigate the relationship between the discharge rate and the brink depth.

An alternative approach to calculate the discharge rate from a horizontal pipe is based on the assumption that the liquid depth at the exit to be the same as the critical depth, d_c (Smith, 1962; Wallis et al., 1977; Akan, 2006; Tiğrek et al., 2008). Recalling Equation (2.39) for critical velocity:

$$u_d = \sqrt{\frac{gA_{wet}}{T}} \tag{2.39}$$

A_{wet} and T may be defined via:

$$A_{wet} = \frac{D^2}{8}(\phi - \sin\phi) \tag{3.30}$$

$$T = D\sin\frac{\phi}{2} \tag{3.31}$$

where ϕ represents the liquid depth angle (radians) presented in Figure 2.1.

Replacing A_{wet} and T from Equation (3.30) and Equation (3.31) into Equation (2.39) produces:

$$u_d = 0.354\sqrt{\frac{gD(\phi - \sin\phi)}{\sin(\phi/2)}} \tag{3.32}$$

Therefore, the discharge rate is calculated via:

$$Q_d = A_{wet}u_d = 0.354\sqrt{\frac{gD(\phi - \sin\phi)}{\sin(\phi/2)}} \times \frac{D^2}{8}(\phi - \sin\phi) \tag{3.33}$$

or

$$Q_d = 0.044\rho D^2\sqrt{gD}(\phi - \sin\phi)\sqrt{\frac{\phi - \sin\phi}{\sin\frac{\phi}{2}}} \quad \textbf{(3.34)}$$

3.4.2 Downward-inclined Channels

For downward-inclined channels, there are two established methods to calculate the discharge rate and velocity, as described in Section 2.3.4 in Chapter 2. The first is applying the Manning equation. Recalling Equation (2.44) for Manning equation and Equation (2.41) for hydraulic radius:

$$u = \frac{k}{n} R_h^{2/3} S_0^{1/2} \quad \textbf{(2.44)}$$

$$R_h = \frac{1}{4} D_h = \frac{A_{wet}}{P_{wet}} \quad \textbf{(2.41)}$$

P_{wet} may also be defined via:

$$P_{wet} = \phi\frac{D}{2} \quad \textbf{(3.35)}$$

Replacing A_{wet} and P_{wet} from Equations (3.30) and (3.35) into Equation (2.44) gives:

$$R_h = \frac{\frac{D^2}{8}(\phi - \sin\phi)}{\phi\frac{D}{2}} \quad \textbf{(3.36)}$$

or

$$R_h = \frac{D}{4}\frac{(\phi - \sin\phi)}{\phi} \tag{3.37}$$

and

$$D_h = D\frac{(\phi - \sin\phi)}{\phi} \tag{3.38}$$

Now by substituting R_h from the Equation (3.37) into the Manning equation (Equation (2.44)), u_d may be calculated via:

$$u_d = \frac{c}{n}\left(\frac{D}{4}\frac{(\phi - \sin\phi)}{\phi}\right)^{2/3} S_0^{1/2} \tag{3.39}$$

or

$$u_d = 0.397\frac{c}{n}D^{2/3}\left(\frac{\phi - \sin\phi}{\phi}\right)^{2/3} S_0^{1/2} \tag{3.40}$$

Finally the volumetric discharge rate is calculated by substituting A_{wet} and u_d from Equation (3.30) and Equation (3.40) respectively:

$$Q_d = u_d A_{wet} = 0.397\frac{c}{n}D^{2/3}\left(\frac{\phi - \sin\phi}{\phi}\right)^{2/3} S_0^{1/2}\frac{D^2}{8}(\phi - \sin\phi) \tag{3.41}$$

or

$$Q_d = 0.050D^{2.667}\frac{c}{n}S_0^{1/2}(\phi - \sin\phi)\left(1 - \frac{Sin\phi}{\phi}\right)^{2/3} \tag{3.42}$$

However, as mentioned in Section 2.3.4, the Manning equation is an empirical formula and is only applicable for water pipes. An alternative approach to cover a

wider range of liquids is using the Darcy-Weisbach equation (Equation (2.46)) described in Section 2.3.4. Substituting D_h from Equation (3.38) into Equation (2.46) produces:

$$u_d = \sqrt{\frac{S_0 g D}{2f}\left(\frac{\phi - \sin\phi}{\phi}\right)} \tag{3.43}$$

Therefore, the volumetric discharge rate is calculated via:

$$Q_d = u_d A_{wet} = \sqrt{\frac{S_0 g D}{2f}\left(\frac{\phi - \sin\phi}{\phi}\right)}\frac{D^2}{8}\left(\phi - \sin\phi\right) \tag{3.44}$$

or

$$Q_d = \frac{D^2}{8}\sqrt{\frac{D S_0 g}{2f\phi}}\left(\phi - \sin\phi\right)^{1.5} \tag{3.45}$$

3.5 Conclusion

Based on the above review, it is clear that significant work has been done to calculate both steady-state and transient discharge during full pipe flow for various upstream tank configurations. On the other hand, the focus of the previous research on the bubble formation and propagation regime has been on the bubble propagation velocity rather than discharge rate. Several studies have been conducted to calculate the propagation velocity for horizontal and downward-inclined pipes with stagnant and moving liquids. For the open channel flow, numerous researches have studied the relationship between the discharge rate and brink depth, both theoretically and experimentally, assuming the information on the brink depth is available.

The review also showed that the models dealing with pipeline failure have only considered full pipe flow and ignored the subsequent regimes including bubble

formation and open channel flow. Neglecting these regimes specifically for long pipelines may lead to significant underestimation of total released inventory as will be shown in Chapter 4 and Chapter 5.

CHAPTER 4: OUTFLOW SIMULATION UPON FULL-BORE RUPTURE IN HORIZONTAL PIPELINES

4.1. Introduction

Crude oil and other hydrocarbon products must be transported from the storage tanks at the production site to refineries and then consumers. On-shore, this is done by means of pipelines. In order to stop the flow of a hazardous liquid following detection of a failure, Emergency Shut Down Valves (ESDV) are widely used in liquid transportation pipelines. These actuated valves ensure the safety of the operations by automatically closing in an emergency.

Many authors have focused on the failure of pipelines containing gas or two phase flow and developed numerous mathematical models with various degrees of sophistication to simulate the outflow. However, despite its importance, little has been done for incompressible liquids. As discussed in Section 3.2, researchers who have worked on this field have only considered full pipe flow regime where the feed tank never drains dry, thus the pipe remains full (see for example Loiacono (1987) and Joye & Barrett (2003)). In their studies, the subsequent regimes including bubble formation and propagation and open channel flow are not considered. On the other hand, studies available on bubble formation and propagation regime only focus on predicting bubble propagation velocity, rather than the liquid discharge rate (see for example Benjamin (1968) and Bendiksen (1984)). Finally, although for open channel flow, methods such as Purdue pipe method (Water measurement manual, 2001) focus on the liquid discharge rate, they are based on known liquid depth at the pipe exit. However, this data is not always available during the drainage process.

This chapter presents the development and testing of mathematical models to determine the discharge rate following full-bore rupture at the end of a horizontal pipeline containing an incompressible liquid.

In Section 4.2 the key models assumptions are summarised. In Section 4.3, the pipeline is assumed to be attached to an upstream storage tank. The associated model accounts for all subsequent regimes including full pipe flow, bubble formation and propagation, and open channel flow. Section 4.4 is concerned with pipes being isolated instantaneously using emergency shut down upon rupture. Due to the absence of upstream tank, the associated model only includes bubble formation and open channel flow. The efficacy and accuracy of the developed models are tested through parametric studies and series of experiments respectively. The results obtained from the application of the reported model for the system of pipe and upstream tank highlight the significance of post-full pipe flow regime on the total inventory loss.

In Section 4.5 the main conclusions are presented.

4.2. Key Models Assumptions

The key assumptions made in deriving the flow models are:

4.2.1. One-dimensional flow anywhere in the pipeline

In pipelines with large value of *L/D* the variation of velocity along the pipe radius is negligible. Therefore, for the liquid transport pipelines the flow can be easily assumed to be one-dimensional.

4.2.2. Incompressible flow, i.e. constant fluid density

The fluid considered in this study is liquid. As liquids are quite difficult to compress, they are normally treated as incompressible. Consequently the density can well be assumed to remain unchanged.

4.2.3. Constant cross sectional area of the pipe, much smaller than tank cross sectional area (where applicable)

Pipelines transporting liquids from a storage tank to the delivery point have diameter much smaller than the liquid storage tank diameter. Consequently, the pipe cross sectional area is much smaller than the tank cross sectional area.

4.2.4. No friction between the fluid and tank

Since the pipeline length is normally much larger than the liquid height in the tank, the frictional loss along the pipe is more significant than that of tank wall. Therefore, the latter is ignored in this study.

4.2.5. Isothermal conditions in the pipe

The liquid is incompressible and hence the density is invariant. Thus, the variation of temperature for the duration of the release is negligible.

4.2.6. No inlet flow to the feed tank

In normal operating conditions storage tanks are fed through a pump with constant inflow. However, in the event of an accident in a pipe charged from the tank the pump shuts down. As a result there will be no inflow to the tank. Since the time difference between the failure detection and emergency shut down is short (only a few minutes), the inlet flow in this study is assumed to be zero.

4.2.7. No hammer effect upon valve closure

Water hammer occurs when a valve is closed suddenly at the end of a pipeline. This will produce a pressure wave which propagates along the pipe. Due to the finite compressibility of the liquid the initial discharge as a result of this over pressure will occur in a very short period of time (more like a splash), comparing to the total release duration. As such, the over pressure due to water hammer is ignored here.

4.2.8. Negligible impact of surface tension and viscosity during bubble formation and propagation regime

Pipelines transporting liquids have normally large diameter (more than 50mm). Therefore, the impact of surface tension can be easily ignored. In addition, the impact of viscosity on the bubble propagation velocity for flows with the Reynolds Number higher than 20 is negligible (Zukoski (1966). Due to the high Reynolds number expected normally for liquid transport pipelines, in this study the impact of viscosity is also assumed to be negligible.

4.3. Transient Hydraulic Flow Modelling Following Full-bore Rupture of a Horizontal Pipeline Fed from an Upstream Tank

4.3.1. Introduction

The following presents the formulation of various flow equations for predicting the discharge rate following full-bore rupture in a horizontal pipe connected to the base of a storage tank containing an incompressible fluid. The modelling encompasses the three flow regimes namely full pipe flow, bubble formation and propagation, and open channel flow. The overall model is then tested through parametric studies in Section 4.3.3 to investigate the impact of pipeline inner diameter and length on the discharge velocity and wetted area of the pipe. Normalised cumulative discharged mass and the released mass during individual regimes are also calculated and compared against the theoretical values. Based on these results, the importance of post-full pipe flow is discussed for a range of pipeline inner diameters and lengths. Finally, the accuracy of the developed model is assessed through series of experiments, presented in Section 4.3.4.

4.3.2. Model Theory

4.3.2.1. Full Pipe Flow

Following a rupture in a horizontal pipe fed from an upstream tank, the pipe depressurises due to the reduction in the liquid head in the tank. During this phase,

the dominant regime is full pipe flow, i.e. the pipe remains full. Figure 4.1 presents a horizontal pipe with pipe attached to the base of an upstream storage tank.

Recalling Equation (3.10) developed by Joye & Barrett (2003) for the calculation of the required drainage time for a tank through a horizontal pipe and rearranging it for an arbitrary time *t* produces:

$$t_f = \frac{D_{\tan k}^2}{D^2}\sqrt{\frac{2}{g}\left(\frac{4fL}{D}+\Sigma K\right)}\left(\sqrt{Z_0}-\sqrt{Z_f}\right) \qquad \textbf{(3. 10)}$$

$$\sqrt{Z} = \sqrt{Z_0} - \frac{A}{A_{\tan k}}\sqrt{\frac{g}{2\left(\frac{4fL}{D}+\Sigma K\right)}}t \qquad \textbf{(4.1)}$$

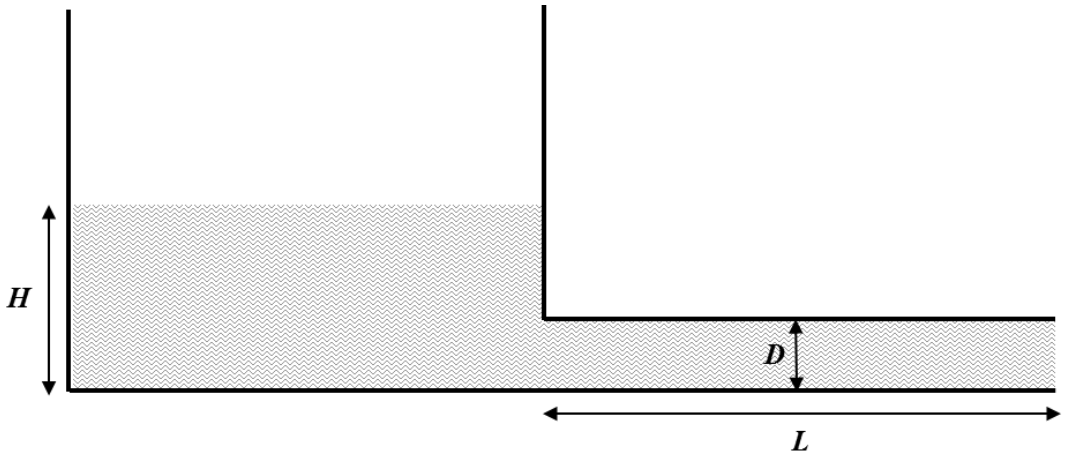

Figure 4.1: Full pipe flow following full-bore rupture in a horizontal pipe fed from an upstream storage tank

The term ΣK includes both kinetic energy and the pipe entrance losses. Joye & Barrett (2003) employed a value of 0.5 for *K* to account for the pipe entrance loss (see Equation 2.14):

$$F_c = 0.5\frac{u^2}{2} \tag{2.14}$$

By recalling Equation (3.1) and replacing L_e with K = 1 for the kinetic energy loss and 0.5 for pipe entrance loss, the discharge velocity may be calculated via:

$$(1)\frac{u_d^2}{2} + (0.5)\frac{u_d^2}{2} - gZ + \frac{2fL}{D}u_d^2 = 0 \tag{4.2}$$

or

$$u_d = \sqrt{\frac{gZ}{0.75 + \frac{2fL}{D}}} \tag{4.3}$$

Replacing Z from (4.1) into the above equation gives:

$$u_d = \frac{-g}{1.5 + \frac{4fL}{D}}\left(\frac{A}{A_{\tan k}}\right)t + \sqrt{\frac{gZ_0}{0.75 + \frac{2fL}{D}}} \tag{4.4}$$

For a horizontal pipe, $Z_0 = H_0$ (see Figure 3.1). Therefore:

$$u_d = \frac{-g}{1.5 + \frac{4fL}{D}}\left(\frac{A}{A_{\tan k}}\right)t + \sqrt{\frac{gH_0}{0.75 + \frac{2fL}{D}}} \tag{4.5}$$

and in terms of mass discharge rate, $\dot{m}_d$:

$$\dot{m}_d = \rho A \left[\frac{-g}{1.5 + \frac{4fL}{D}} \left(\frac{A}{A_{\tan k}} \right) t + \sqrt{\frac{gH_0}{0.75 + \frac{2fL}{D}}} \right] \quad \textbf{(4.6)}$$

Equation (4.6) is used to calculate the discharge rate until $H = d_c$ where d_c is the critical depth of the flow as introduced in Section 2.3.3.

McCabe et al. (1956) proposed the lower value of 0.4 instead of 0.5 to take into account the loss at the pipe entrance. Following Joye & Barrett (2003), in this work due to various citations the value of 0.5 is used to calculate the pipe entrance loss (see for example Crane (1957), Evett & Liu (1989) and Joye & Barrett (2003)). It should be noted that both values of 0.5 and 0.4 are only approximation and various publications are not always in agreement. In fact, some may even differ by 25% (Jones et al, 2008).

4.3.2.2. Bubble Formation and Propagation

In practice, as soon as the liquid level in the tank falls below the pipe diameter, a bubble will form at the upstream end of the pipe. This is followed by propagation of bubbles from both ends of the pipe towards one another (Kandasamy, 1999). As described in Section 2.3.5, the liquid depth at the free fall below the downstream bubble may be assumed to be equal to the critical depth (Tiğrek et al., 2008). Assuming a horizontal pipeline so that the upstream and downstream bubbles have the same height, the liquid depth below the upstream bubble and inside the tank will also be equal to the critical depth. This depth and consequently the discharge rate and velocity are assumed to remain constant during the bubble propagation regime.

Figure 4.2 shows a horizontal pipe attached to a tank with bubble formation and propagation from both ends.

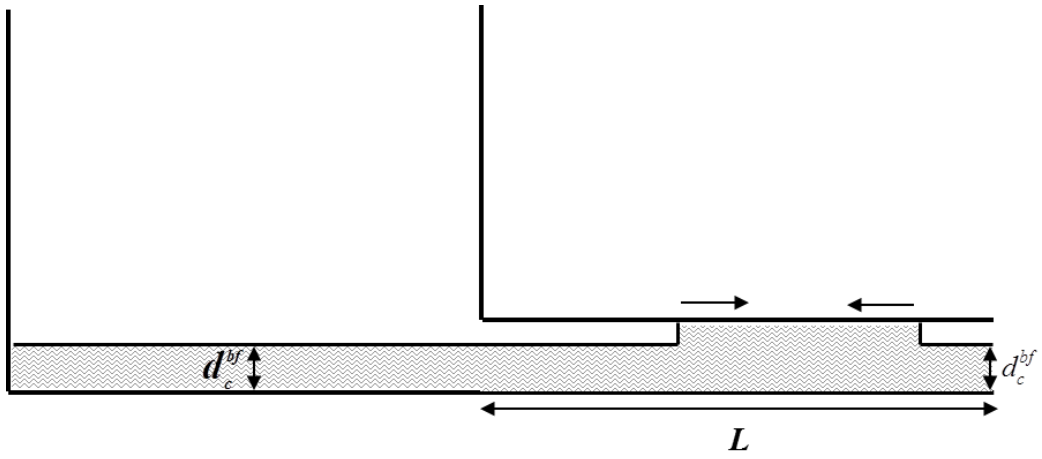

Figure 4.2: Bubble propagation from both ends of a horizontal pipe fed from an upstream storage tank

In this study it is assumed that the bubble formation at the pipe downstream does not occur during full pipe flow. Instead, the two bubbles start propagating towards each other simultaneously. As such, the discharge rate is calculated from Equation (4.6) for as long as the liquid level in the tank is higher than d_c^{bf}, the constant critical depth during bubble propagation regime. This is a conservative assumption as the full pipe flow equation produces higher discharge rate due to wetted area being the same as pipe cross sectional area.

Based on the assumption of negligible fluid/pipe wall friction and critical liquid depth below the bubbles, the critical discharge velocity (Equation (3.32)) during bubble formation and open channel flow is given by:

$$u_d = 0.354\sqrt{\frac{gD\left(\phi_c^{bf} - \sin\phi_c^{bf}\right)}{\sin(\phi_c^{bf}/2)}} \qquad \textbf{(4.7)}$$

where ϕ_c^{bf} denotes the constant, time-invariant, critical angle ϕ (see Figure 2.1) during this regime. Thus, the corresponding critical liquid depth below the bubbles (d_c^{bf}) is given by:

$$d_c^{bf} = \frac{D}{2}\left(1 - \cos\frac{\phi_c^{bf}}{2}\right) \qquad \textbf{(4.8)}$$

Figure 4.3 is a schematic representation of bubble formation and propagation regime showing the relevant flow parameters. For simplification, the bubble curvature is ignored by assuming a rectangular cross-section for the bubbles along the pipe axis. The application of the continuity equation between the rupture plane (section 1) and full cross section of the pipe (section 2) produces the following formula for the volumetric liquid flow rate Q_d:

$$Q_d = u_d A_{wet}^{bf} = Au \qquad \textbf{(4.9)}$$

or

$$u = \frac{u_d A_{wet}^{bf}}{A} \qquad \textbf{(4.10)}$$

where u and A_{wet}^{bf} are the liquid velocity in the full section of the pipe and the constant wetted area during bubble propagation regime respectively.

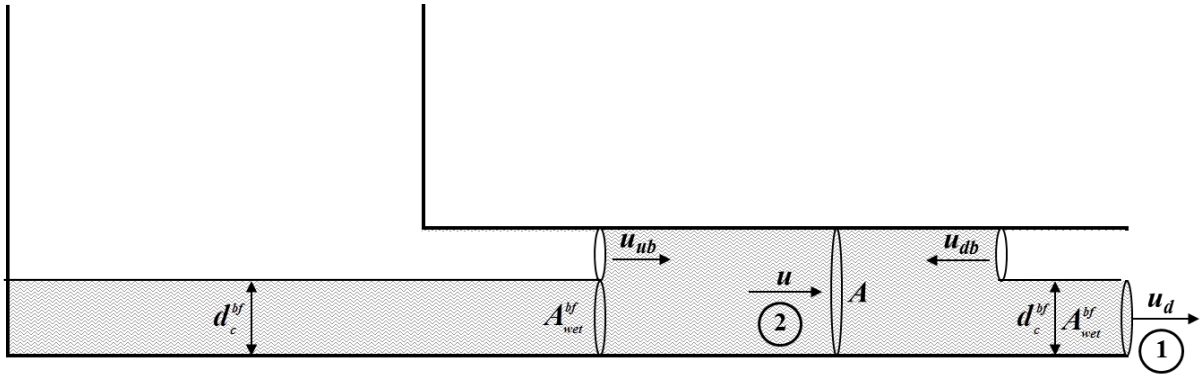

Figure 4.3: Schematic representation of bubble propagation regime showing the relevant flow parameters

Also at any given time the volumetric flow rate of the discharging liquid is equal to that of air entering the pipe. Therefore:

$$Q_d = u_d A_{wet}^{bf} = u_{ub} A_b + u_{db} A_b \quad \textbf{(4.11)}$$

u_{db} and u_{ub} are the downstream and upstream bubble propagation velocity respectively. Also A_b is the bubble cross sectional area and is given by:

$$A_b = A - A_{wet}^{bf} \quad \textbf{(4.12)}$$

Substituting A_b from the above equation into Equation (4.11) produces:

$$u_d = \frac{\left(A - A_{wet}^{bf}\right)\left(u_{ub} + u_{db}\right)}{A_{wet}^{bf}} \quad \textbf{(4.13)}$$

Recalling Equation (3.30), A_{wet}^{bf} may be calculated via:

$$A_{wet}^{bf} = \frac{D^2}{8}\left(\phi_c^{bf} - \sin\phi_c^{bf}\right) \quad \textbf{(4.14)}$$

Due to the absence of liquid head in the tank, the propagation of the downstream bubble is similar to the case of bubble propagation in an isolated pipe. Therefore, recalling Equation (3.17) developed by Benjamin (1968) for bubble propagation velocity in stationary liquid in the absence of fluid/pipe wall friction:

$$u_{db} = 0.542\sqrt{gD} \quad \textbf{(3.17)}$$

where u_{drift} is replaced by u_{db}. The above equation is used in this study as it has been referred to by various authors (see for example Bendiksen (1984), Hager (1999), Lauchlan et al. (2005) and Pothof (2011)).

For the upstream bubble Equation (3.25) is recalled for the co-current single bubble propagation in moving liquids, initially developed by Nicklin et al. (1962) for vertical pipes:

$$u_{ub} = u_{db} + C_0 u \qquad \textbf{(3.25)}$$

where u_{drift} and u_{moving} are replaced by u_{db} and u_{ub} respectively. By conducting experiments for various pipe diameters, Bendiksen (1984) showed that with C_0 being in the range of 1.0-1.2, Equation (3.25) may also be used for the case of single bubble propagation in a horizontal pipe.

In the present study C_0 is taken as the conservative value of 1.2 as it will produce the maximum u_{ub} and hence $\dot{m}_d$, thus representing the worst case scenario.

Bendiksen (1984) proposed the above value for C_0 by only considering the upstream bubble. Consequently, the impact of downstream bubble propagation on C_0 is ignored. The validity and accuracy of the above value of C_0 for a system with bubble propagation from both ends of the pipe is investigated experimentally in Section 4.3.4.

Replacing C_0 with 1.2 and u_{db} from Equation (3.17) in Equation (3.25) yields:

$$u_{ub} = 0.542\sqrt{gD} + 1.2u \qquad \textbf{(4.15)}$$

Therefore, replacing u from Equation (4.10) into Equation (4.15) gives:

$$u_{ub} = 0.542\sqrt{gD} + 1.2\left(\frac{u_d A_{wet}^{bf}}{A}\right) \quad \textbf{(4.16)}$$

Finally the discharge velocity (u_d) may be calculated by replacing u_{ub} and u_{db} from the above equation and Equation (3.17) respectively into Equation (4.13) :

$$u_d = \frac{\left(A - A_{wet}^{bf}\right)\left(1.084\sqrt{gD} + 1.2\left(\frac{u_d A_{wet}^{bf}}{A}\right)\right)}{A_{wet}^{bf}} \quad \textbf{(4.17)}$$

or

$$\left(\frac{A_{wet}^{bf}}{A - A_{wet}^{bf}} - 1.2\frac{A_{wet}^{bf}}{A}\right)u_d = 1.084\sqrt{gD} \quad \textbf{(4.18)}$$

or

$$u_d = \frac{1.084\sqrt{gD}}{\left(\frac{A_{wet}^{bf}}{A - A_{wet}^{bf}} - 1.2\frac{A_{wet}^{bf}}{A}\right)} \quad \textbf{(4.19)}$$

Substituting A_{wet}^{bf} from Equation (4.14) and $A = \pi\frac{D^2}{4}$ into the above equation produces:

$$u_d = \frac{1.084\sqrt{gD}}{\frac{\phi_c^{bf} - \sin\phi_c^{bf}}{\left(2\pi - (\phi_c^{bf} - \sin\phi_c^{bf})\right)} - 0.6\frac{(\phi_c^{bf} - \sin\phi_c^{bf})}{\pi}} \quad \textbf{(4.20)}$$

Finally by equating Equations (4.7) and (4.20) ϕ_c^{bf} is calculated iteratively producing 216^o as solution.

This is an important finding showing that during bubble propagation regime in a horizontal pipe where liquid/wall friction may be ignored (Pothof, 2011), the angle of depth remains uniquely constant for all pipe length and diameters. The validity of this prediction is tested through experiments in Section 4.3.4.1

By substituting ϕ_c^{bf} =216° into Equations (4.7) , (4.8), (4.14) , (4.10) and (4.15), u_d , d_c^{bf} , A_{wet}^{bf} , u and u_{ub} may be determined from:

$$u_d = 0.757\sqrt{gD} \quad \textbf{(4.21)}$$

$$d_c^{bf} = 0.654D \quad \textbf{(4.22)}$$

$$A_{wet}^{bf} = 0.544D^2 \quad \textbf{(4.23)}$$

$$u = 0.525\sqrt{gD} \quad \textbf{(4.24)}$$

$$u_{ub} = 1.172\sqrt{gD} \quad \textbf{(4.25)}$$

Finally recalling Equation (3.34) for critical volumetric discharge rate for $\phi = \phi_c^{bf}$, the mass discharge rate ($\dot{m}_d$) is calculated via:

$$\dot{m}_d = 0.044\rho D^2\sqrt{gD}\left(\phi_c^{bf} - \sin\phi_c^{bf}\right)\sqrt{\frac{\phi_c^{bf} - \sin\phi_c^{bf}}{\sin\frac{\phi_c^{bf}}{2}}} \quad \textbf{(4.26)}$$

Replacing ϕ_c^{bf} =216° in the above equation gives:

$$\dot{m}_d = 0.412\rho D^2\sqrt{gD} \quad \textbf{(4.27)}$$

d_c^{bf}, u_{ub} and u_{db} are assumed to be time invariant during bubble formation regime, thus producing a constant $\dot{m}_d$.

As described in Section 3.3.1, the downstream bubble velocity (u_{db}) is the same as the minimum required liquid velocity to keep a bubble stagnant (Benjamin, 1968; Lauchlan et al., 2005). In other words, the downstream bubble propagates along the pipe with a velocity equal to u_{db} only if u is less than the calculated u_{db} (see Equation 3.17).

Comparing Equations (4.24) and (3.17) for liquid velocity (u) in the full section of the pipe and the downstream bubble velocity (u_{db}), it may be observed that for the same pipe diameter, u is always smaller than u_{db}, confirming the propagation of downstream bubble upstream.

In addition, the time lapsed for the downstream and upstream bubbles to merge, t_{bubble}, is:

$$t_{bubble} = \frac{L}{u_{ub} + u_{db}} = \frac{L}{1.714\sqrt{gD}} \quad \textbf{(4.28)}$$

4.3.2.3. Open Channel Flow

The merging of the upstream and downstream bubbles marks the termination of bubble formation regime and start of open channel flow. Figure 4.4 presents a horizontal pipe with open channel flow attached to an upstream tank.

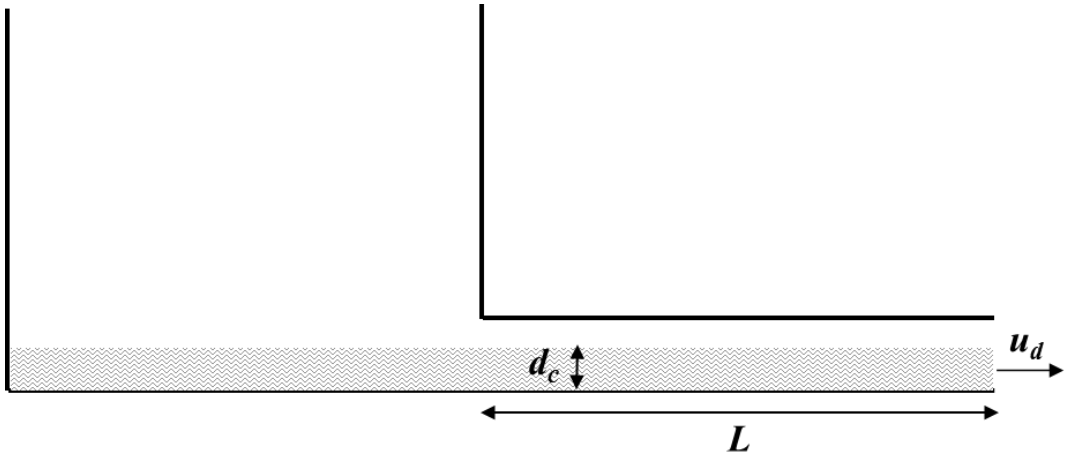

Figure 4.4: Open channel flow in a horizontal pipe fed from an upstream storage tank

Following the discussion for bubble propagation regime in Section 4.3.2.2, the liquid depth at the pipe exit is equal to the critical depth. However, during open channel flow this depth and consequently the corresponding ϕ_c is not constant and decreases over time. The starting value of ϕ_c for open channel flow is ϕ_c^{bf} = 216°, as calculated for the previous regime. For simplicity, it is assumed that the liquid depth is uniform across the pipe and tank and equal to the critical depth, d_c^{bf}. Therefore *M*, the total mass of liquid in the tank and the pipe is defined as:

$$M = \left(L + L_{eq}\right) A_{wet} \rho \qquad \textbf{(4.29)}$$

where L_{eq} is the length of an equivalent pipe of diameter *D* containing the remaining mass inside the tank at the commencement of open channel flow , M_r, and is given by:

$$L_{eq} = \left(\frac{M_r}{\rho}\right) \frac{1}{A_{wet}^{bf}} \qquad \textbf{(4.30)}$$

or

$$L_{eq} = \left(\frac{M_r}{\rho}\right)\frac{1}{0.544D^2} \tag{4.31}$$

Also assuming that full pipe flow terminates when the liquid level in the tank reaches d_c^{bf}, M_r is calculated via:

$$M_r = \rho d_c^{bf} A_{\tan k} \tag{4.32}$$

Replacing M_r from the above equation into Equation (4.31) and Equation (4.29) produces:

$$L_{eq} = \frac{d_c^{bf} A_{\tan k}}{0.544D^2} \tag{4.33}$$

$$M = \left(L + \frac{d_c^{bf} A_{\tan k}}{0.544D^2}\right) A_{wet}\rho \tag{4.34}$$

In order to account for the variation of M with time, the critical discharge rate equation (Equation (3.34)) is combined with the transient flow mass balance representing the rate of mass loss from the storage tank (Equation (3.2)):

$$\frac{dM}{dt} = -0.044\rho D^2\sqrt{gD}\left(\phi_c - \sin\phi_c\right)\sqrt{\frac{\phi_c - \sin\phi_c}{\sin\frac{\phi_c}{2}}} \tag{4.35}$$

Substituting M from Equation (4.34) into the above equation gives:

$$\frac{d\left((L + \frac{d_c^{bf} A_{\tan k}}{0.544D^2})A_{wet}\right)\rho}{dt} = -0.044\rho D^2\sqrt{gD}\left(\phi_c - \sin\phi_c\right)\sqrt{\frac{\phi_c - \sin\phi_c}{\sin\frac{\phi_c}{2}}} \tag{4.36}$$

or

$$\frac{dA_{wet}}{0.044\rho D^2\sqrt{gD}\left(\phi_c-\sin\phi_c\right)\sqrt{\dfrac{\phi_c-\sin\phi_c}{\sin\dfrac{\phi_c}{2}}}}=-\frac{dt}{\rho\left(L+\dfrac{d_c^{bf}A_{\tan k}}{0.544D^2}\right)} \qquad \textbf{(4.37)}$$

At the initial time t_0 = 0 at the onset of open channel flow, $A_{wet} = A_{wet}^{bf} = 0.544D^2$ from Equation (4.23). Based on this, integrating the above equation between t = 0 and an arbitrary time t produces:

$$\int_{0.544D^2}^{A_{wet}}\frac{dA_{wet}}{0.044\rho D^2\sqrt{gD}\left(\phi_c-\sin\phi_c\right)\sqrt{\dfrac{\phi_c-\sin\phi_c}{\sin\dfrac{\phi_c}{2}}}}=-\frac{t}{\rho\left(L+\dfrac{d_c^{bf}A_{\tan k}}{0.544D^2}\right)} \qquad \textbf{(4.38)}$$

Equation (4.38) is solved numerically by employing the trapezoidal rule where the region under the graph of the function *f(x)* is approximated as a trapezoid and its area is calculated via (Atkinson, 1989):

$$\int_b^a f(x)\,dx \approx \frac{1}{2}\sum_{i=1}^{N}\left(x_{i+1}-x_i\right)\left(f_{i+1}+f_i\right) \qquad b \le x_i \le a \qquad \textbf{(4.39)}$$

Comparing the left side of the above equation with that of Equation (4.38), *f(x)* and *x* represent $\frac{1}{\dot{m}_d}$ and A_{wet} respectively.

Figure **4.5** shows the flow diagram of the procedure used to estimate the above integral. Here $\dot{m}_{d,i}$, $A_{wet,i}$, $\phi_{c,i}$ and I_i are the mass discharge rate, wetted area, angle

ϕ_c and the value of the integral at time t_i respectively. Once I_i is determined, the corresponding time t_i is calculated via:

$$t_i = I_i \rho \left(L + \frac{d_c^{bf} A_{\tan k}}{0.544 D^2} \right) \qquad \textbf{(4.40)}$$

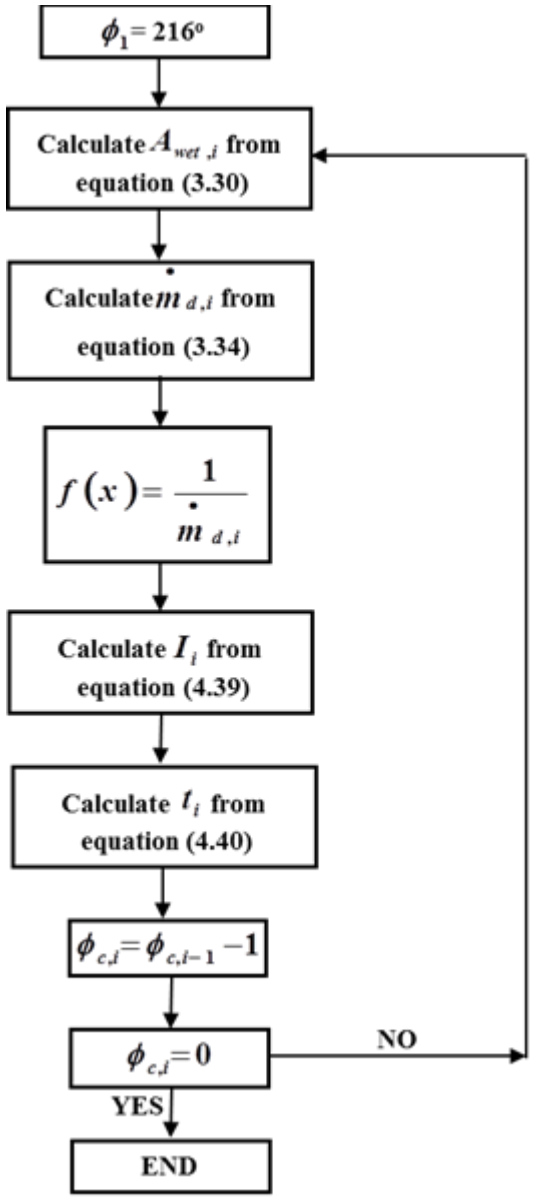

Figure 4.5: Calculation flow diagram for determining $\phi_{c,i}$ at t_i for a horizontal pipe attached to an upstream tank

4.3.3. Parametric Studies

In the previous section a detailed mathematical model was developed to simulate the outflow following a rupture in a horizontal pipe connected to an upstream storage tank containing incompressible liquid. The model accounted for all the subsequent regimes including full pipe flow, bubble formation and propagation, and open channel flow.

This section presents the results of a series of parametric studies based on the application of the above model. The study includes investigating changes in the pipeline length and inner diameter in order to investigate the significance of bubble propagation and open channel flow regimes on the total inventory loss.

Table 4.1 gives the test conditions employed for the base case in the current parameter studies.

Tank cross sectional area, A_{tank} (m^2)	5
Initial liquid head in the tank, H_o (m)	5
Inventory	Water
Pipeline inner diameter, D (m)	0.356
Pipeline length, L (m)	100
Pipe roughness, ε (mm)	0.05

Table 4.1: Outflow simulations test conditions for full-bore rupture scenario in a horizontal pipe fed from an upstream tank

The cylindrical storage tank is assumed to have a cross sectional area of $5m^2$ and is connected to a 100m long, 0.356m diameter pipe. The tank is filled with water up to a depth of 5m prior to pipe failure. A pipe roughness of 0.05mm is assumed during full pipe flow. The impact of friction during bubble propagation and open channel flows are ignored as it is assumed to be negligible. Unless otherwise specified, the characteristics given in the table are assumed to apply throughout the investigations.

4.3.3.1. Discharge Velocity and Wetted Area

In this section the impact of pipeline characteristics on the discharge velocity and wetted area (A_{wet}) is studied. The parametric studies are conducted for the pipeline

length and inner diameter in the ranges 50-200m and 0.305-0.406m respectively. Figure 4.6-4.7 and Figure 4.8-4.9 respectively show the variation of normalised wetted area and discharge velocity with time for various values of pipeline length and inner diameter. Normalised wetted area is defined as the ratio of the wetted area (A_{wet}) and the pipe cross sectional area (A). For discharge velocity all figures indicate three distinct ranges in behaviour. The first is a rapid and significant linear drop corresponding to the discharge during full pipe flow. This is then followed by a rapid and relatively small recovery in the discharge velocity prior to reaching a constant discharge rate. Finally there is a slow non-linear decline in the discharge velocity which corresponds to open channel flow.

It may be observed that the discharge velocity during bubble formation and propagation is the same for all pipeline lengths. This is because the critical discharge velocity is independent of pipeline length (see Equation (4.7)). This is believed to be due to ignoring fluid/wall friction in the pipe during this regime. The rapid increase in discharge velocity as the flow regime changes from full pipe to bubble formation and propagation is due to the impact of frictional loss (fluid/pipe wall and entry) during full pipe flow. There is no entry loss during bubble formation regime due to the absence of liquid head in the tank. Also Pothof (2011) claimed that water acceleration along the air bubble nose in a horizontal pipe is essentially frictionless. Thus, in the reported model the frictional loss is not considered during this regime (see Section 4.3.2.2). Consequently, the discharge velocity is lower at the end of full pipe flow compared to that during bubble formation and propagation regime.

Furthermore, the increase in the magnitude of the recovery in the discharge velocity with the pipeline length is the result of the direct proportionality of fluid/pipe wall loss with pipeline length (see Section 2.2.3). Therefore, the frictional loss is more significant in longer pipes, resulting in greater reduction in discharge velocity during full pipe flow.

The same trend may also be observed for the impact of pipeline inner diameter on the discharge velocity. However, here the magnitude of the recovery in the discharge

velocity decreases with pipe inner diameter. This is because the fluid/pipe wall loss is inversely proportional to the pipe inner diameter and thus, the impact of pipe wall loss on discharge velocity for large diameters is not as significant as for small diameters.

On the other hand, the normalised wetted area remains constant and equal to 1 during full pipe flow. This stems out from the definition of full pipe flow, i.e. $A_{wet} = A$. Then A_{wet} drops to 0.693, shown below, as the regime changes to bubble formation and propagation. As assumed in the model, A_{wet} remains unchanged throughout this regime. Upon initiation of open channel flow along the pipe, A_{wet} decreases slowly until reaching zero, marking the termination of the drainage process.

$$\frac{A_{wet}}{A} = \frac{A_{wet}^{bf}}{A} = \frac{0.544D^2}{\frac{\pi D^2}{4}} = 0.693 \qquad \textbf{(4.41)}$$

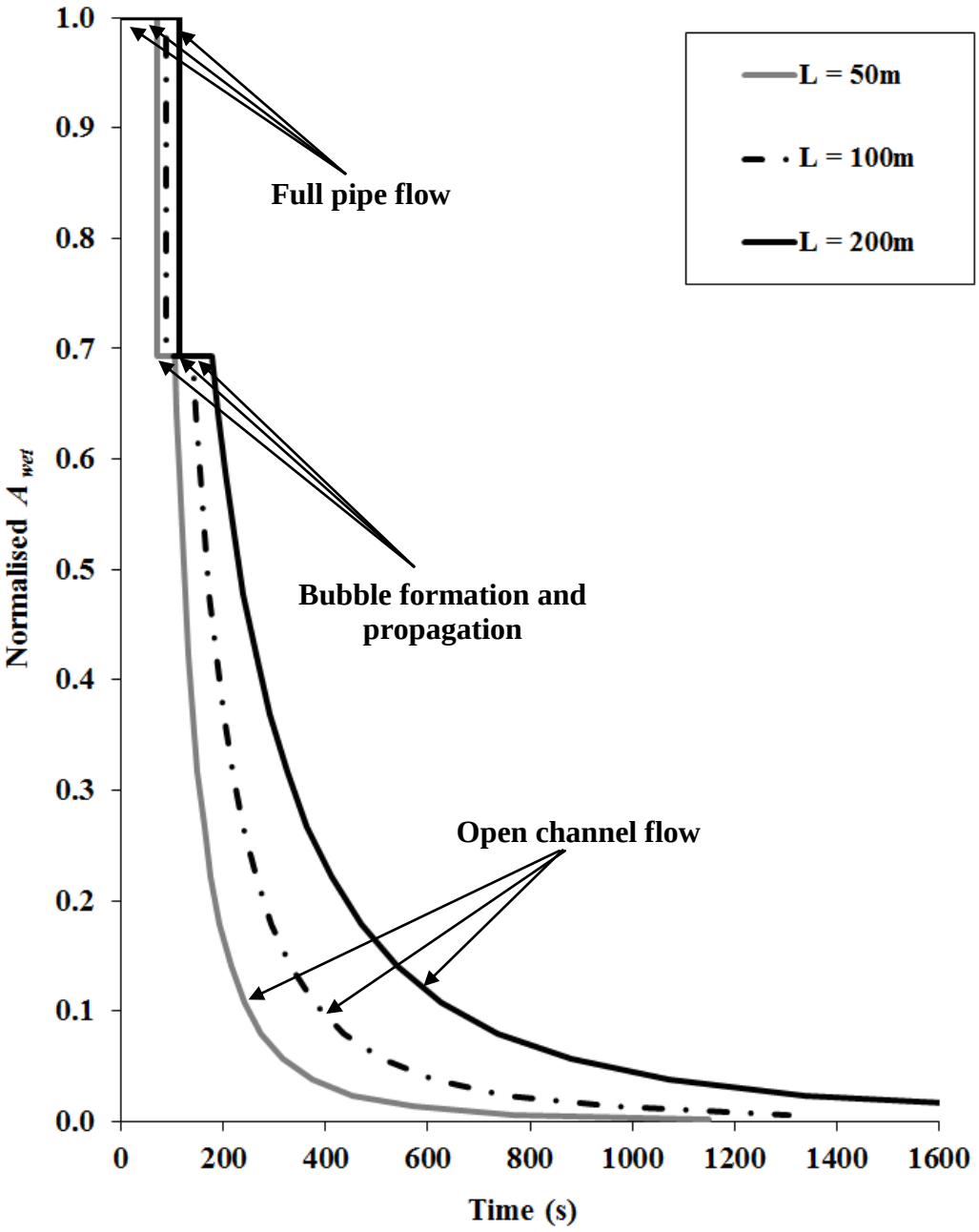

Figure 4.6: Impact of pipeline length on the variation of normalised A_{wet} with time following full-bore rupture in a 0.356m diameter, horizontal pipe fed from an upstream tank

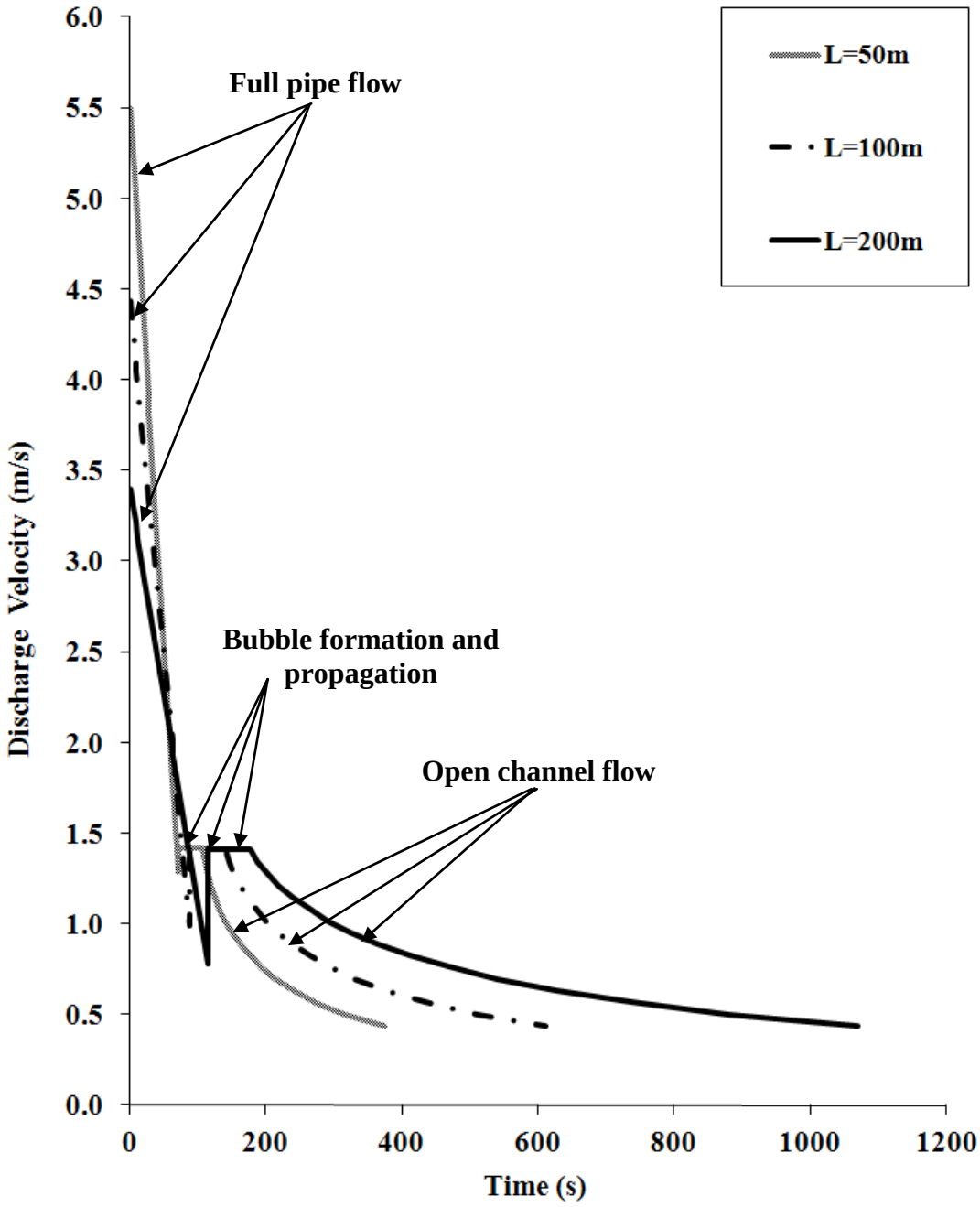

Figure 4.7: Impact of pipeline length on the variation of the discharge velocity with time following full-bore rupture in a 0.356m diameter, horizontal pipe fed from an upstream tank

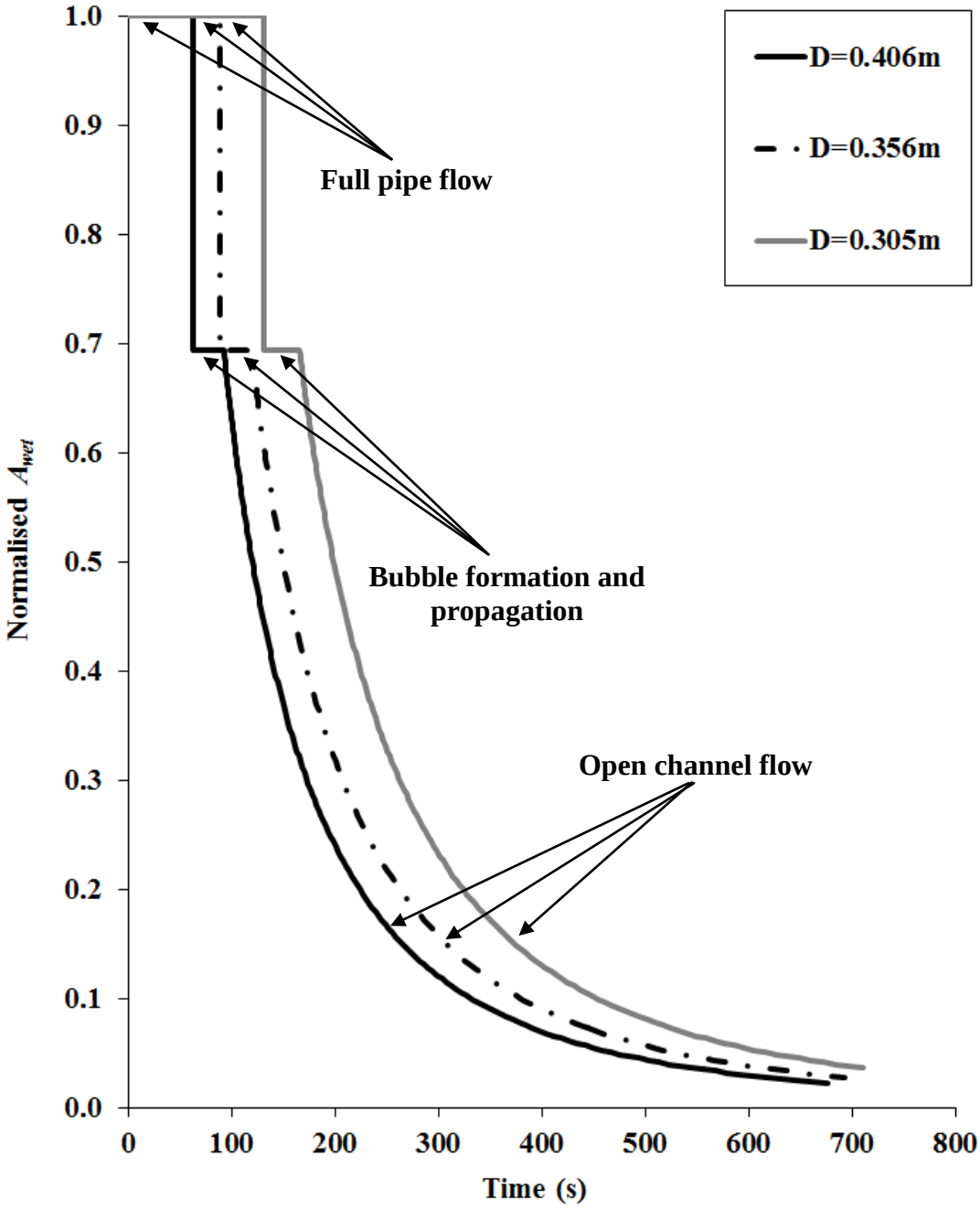

Figure 4.8: Impact of pipeline diameter on the variation of normalised A_{wet} with time following full-bore rupture in a 100m long, 0.305m diameter, horizontal pipe fed from an upstream tank

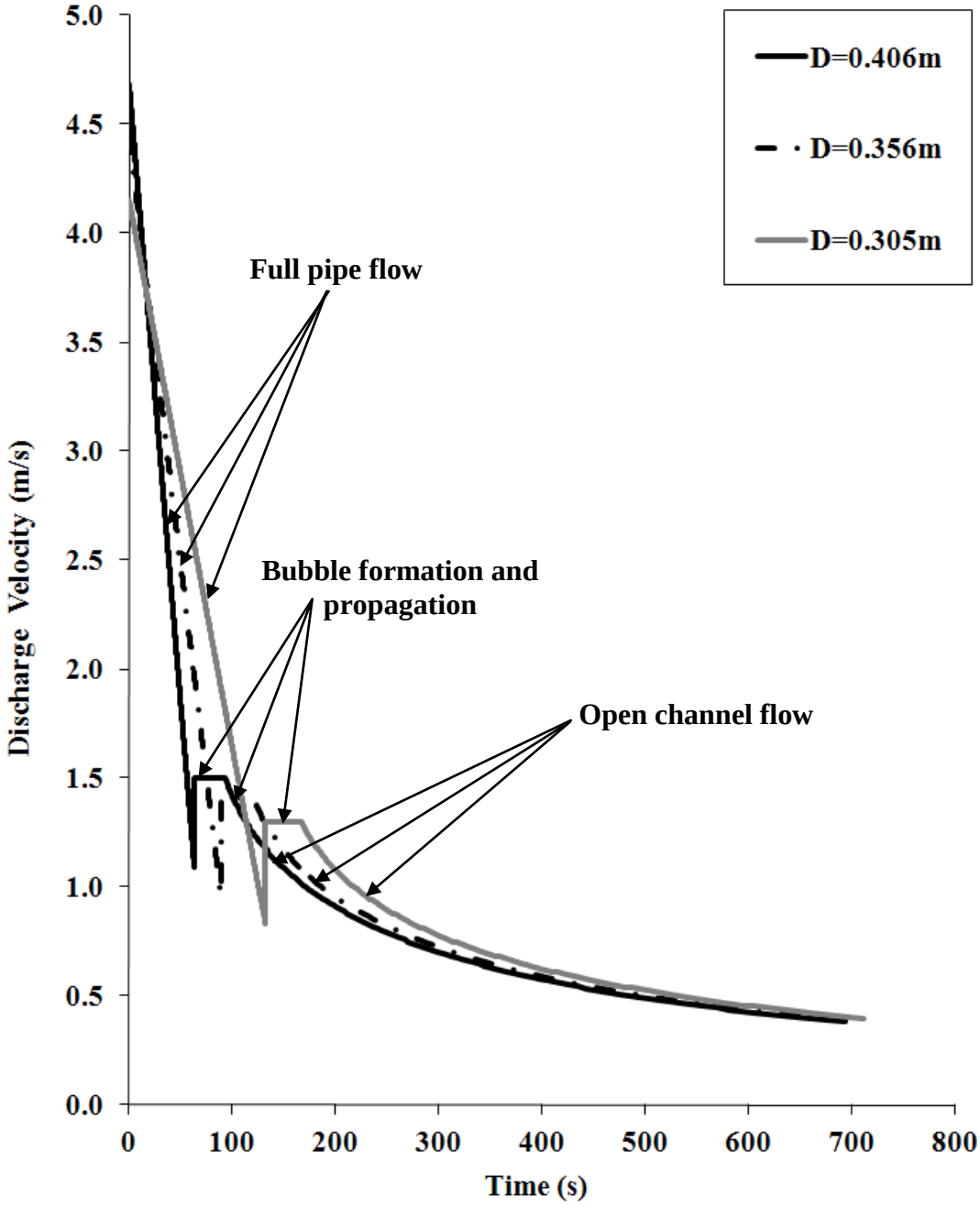

Figure 4.9: Impact of pipeline diameter on the variation of discharge velocity with time following full-bore rupture in a 100m long, horizontal pipe fed from an upstream tank

4.3.3.2. Normalised Cumulative Discharged Mass

Figure 4.10 shows the impact of the change in the pipe length in the range 100-300m on the variation of the normalised cumulative discharged mass (ratio between cumulative discharged mass and initial inventory in the system) with time. Figure 4.11 shows the corresponding data demonstrating the impact of the change in the pipe diameter in the range 0.305-0.508m.

In each figure, the transition from full pipe to bubble propagation, and from bubble propagation to open channel flow are marked by black circular and triangular dots respectively. It may be observed from Figure 4.10 that the released mass during post-full pipe flow increases with the pipeline length. For the longest pipeline (300m), more than half of the initial inventory is released during post-full pipe flow, whereas almost 70% of the mass is released during full pipe flow for the shortest pipeline (100m). The same trend can be seen in Figure 4.11 for the impact of pipeline inner diameter. For the pipe with the largest inner diameter (0.508m), almost half of the inventory is released during bubble formation and open channel flow. This study emphasises the significance of taking account of such flow regimes in long distance or large diameter pipelines. Ignoring these regimes can result in significant underestimation of the released mass.

Table 4.2 presents the comparison between the predicted and theoretical discharged mass during each regime. The theoretical mass released during each flow regime is calculated as follow:

- Full pipe flow

$$M_{full\ pipe\ flow} = \rho A_{\tan k}\left(H_0 - d_c^{bf}\right) \quad \textbf{(4.42)}$$

or

$$M_{full\ pipe\ flow} = \rho A_{\tan k}\left(H_0 - 0.654D\right) \quad \textbf{(4.43)}$$

where 0.654D is the critical depth, d_c^{bf} from Equation (4.22).

- Bubble formation and propagation

$$M_{bubble\ propagation} = \rho L\left(A - A_{wet}^{bf}\right) = \rho L\left[\frac{1}{4}\pi D^2 - 0.544D^2\right] = 0.241\rho L D^2 \quad \textbf{(4.44)}$$

- Open channel flow

$$M_{open\ channel\ flow} = \rho\left(0.544D^2\right)\left(L + \frac{0.654DA_{\tan k}}{0.544D^2}\right) \quad \textbf{(4.45)}$$

or

$$M_{open\ channel\ flow} = \rho\left(0.544D^2\right)\left(L + \frac{1.202A_{\tan k}}{D}\right) \quad \textbf{(4.46)}$$

where $0.544D^2$ and $\frac{0.654DA_{\tan k}}{0.544D^2}$ are A_{wet}^{bf} and L_{eq} from Equations (4.23) and (4.33) respectively.

On the other hand, the predicted released mass during each flow regime $M_{predicted}$ is calculated via:

$$M_{predicted} = \dot{m}_d\,\Delta t \quad \textbf{(4.47)}$$

where Δt is the duration of the flow regime.

It may be observed from Table 4.2 that for all scenarios, during each regime the predicted released mass is very close to the corresponding theoretical mass, with a maximum deviation of 1%.

Scenario		Full pipe flow		Bubble propagation		Open channel flow	
Length (m)	Diameter (m)	Theoretical (kg)	Predicted (kg)	Theoretical (kg)	Predicted (kg)	Theoretical (kg)	Predicted (kg)
100	0.305	23859	23856	2226	2209	6021	6026
100	0.406	23530	23533	3944	3919	10233	10171
100	0.508	23199	23185	6175	6136	15605	15642
100	0.356	23693	23682	3033	3013	8010	8033
200	0.356	23693	23682	6065	6027	14863	14897
300	0.356	23693	23682	9098	9040	21716	21761

Table 4.2: Comparison of the theoretical and predicted discharged mass during individual regimes following full-bore in a horizontal pipe fed from an upstream tank

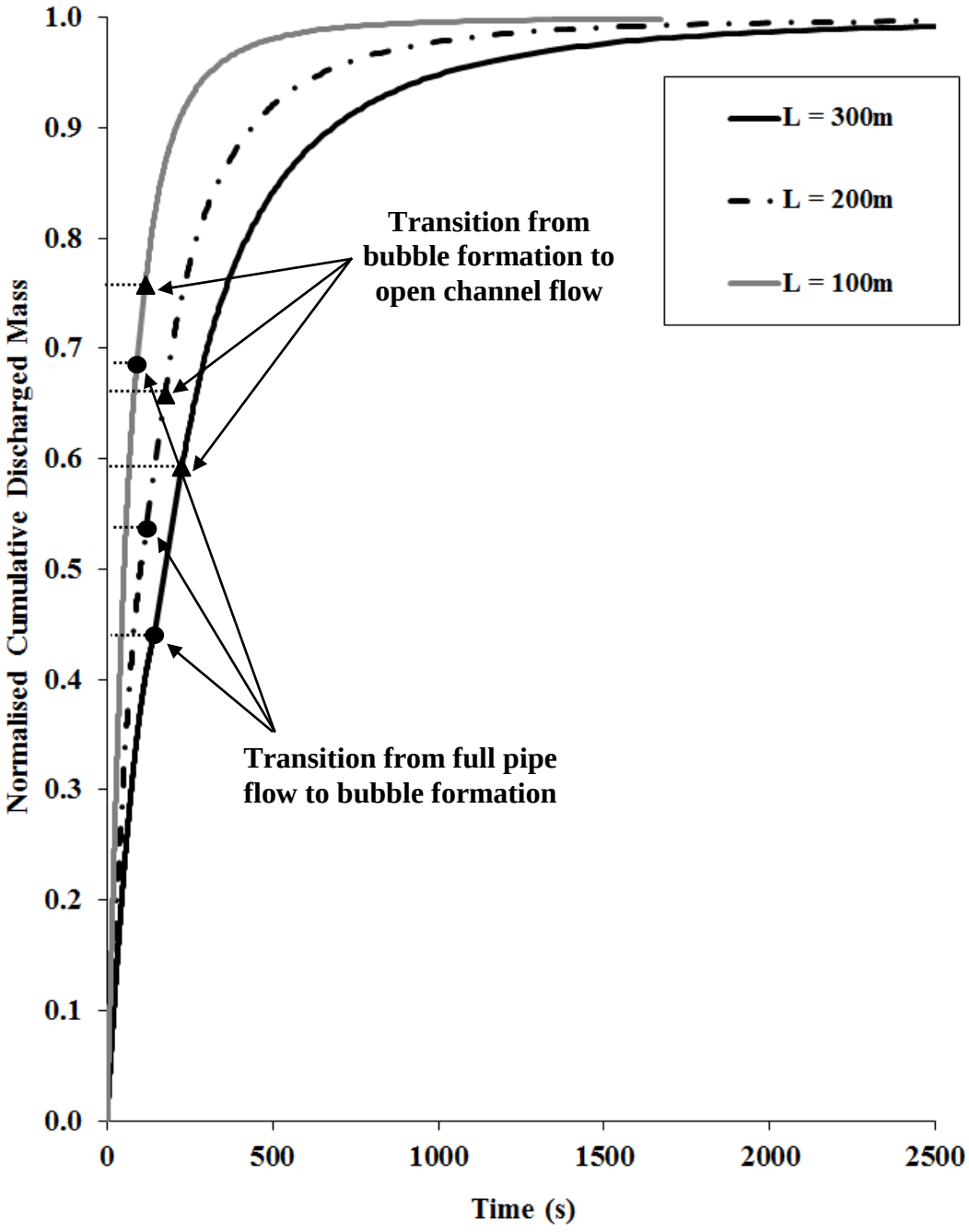

Figure 4.10: Impact of pipeline length on the normalised cumulative discharged mass following full-bore rupture in a 0.356m diameter, horizontal pipe fed from an upstream tank

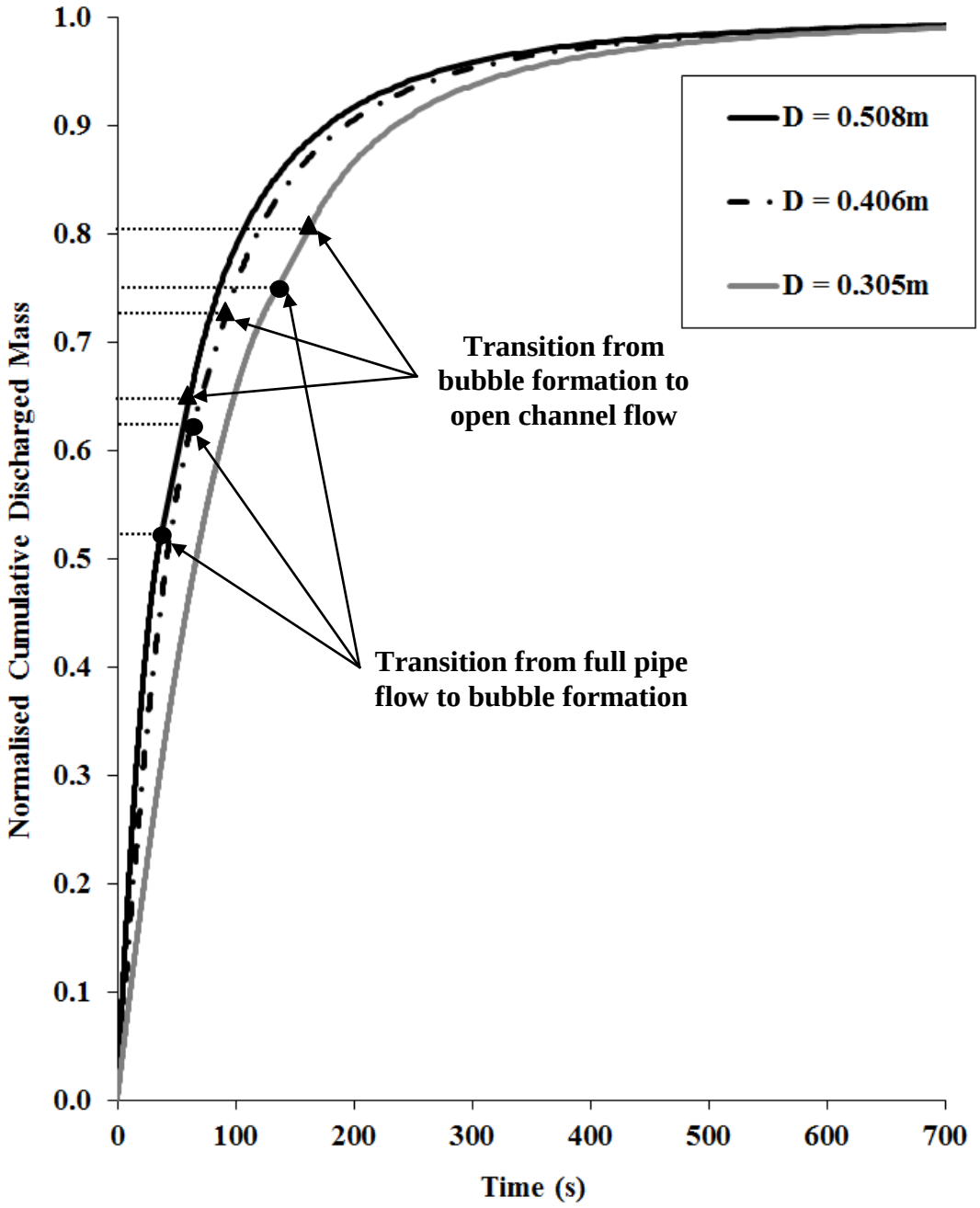

Figure 4.11: Impact of pipeline diameter on the normalised cumulative discharged mass following full-bore rupture in a 100m long, horizontal pipe fed from an upstream tank

4.3.4. Experiments

The following presents the results of a series of experiments conducted to validate the outflow model developed above. The first series of experiments are carried out to validate the developed equations for the liquid depth below the bubble, d_c^{bf} (see Equation (4.22)) and the upstream bubble propagation velocity, u_{ub} (see Equation (4.25)) for water in a pipe upon a simulated full-bore rupture. The validity of the proposed value of 1.2 for the empirical coefficient C_0 corresponding to bubble propagation velocity by Bendiksen (1984) for the case of bubble propagation from both ends of a horizontal pipe attached to an upstream tank is investigated.

Based on the second series of experiments, the accuracy of the model developed for predicting the transient discharge rate following full-bore rupture in a horizontal pipe fed from a storage tank containing water is examined through measuring the cumulative discharged mass and estimating the corresponding discharge rate. The measured values are compared against those obtained from the model.

4.3.4.1. Upstream Bubble Propagation Velocity u_{ub} and Liquid Depth d_c^{bf}

Figure 4.12 presents the experimental setup constructed to validate Equations (4.22) and (4.25) for the liquid depth below the bubble (d_c^{bf}) and the upstream bubble propagation velocity (u_{ub}) respectively.

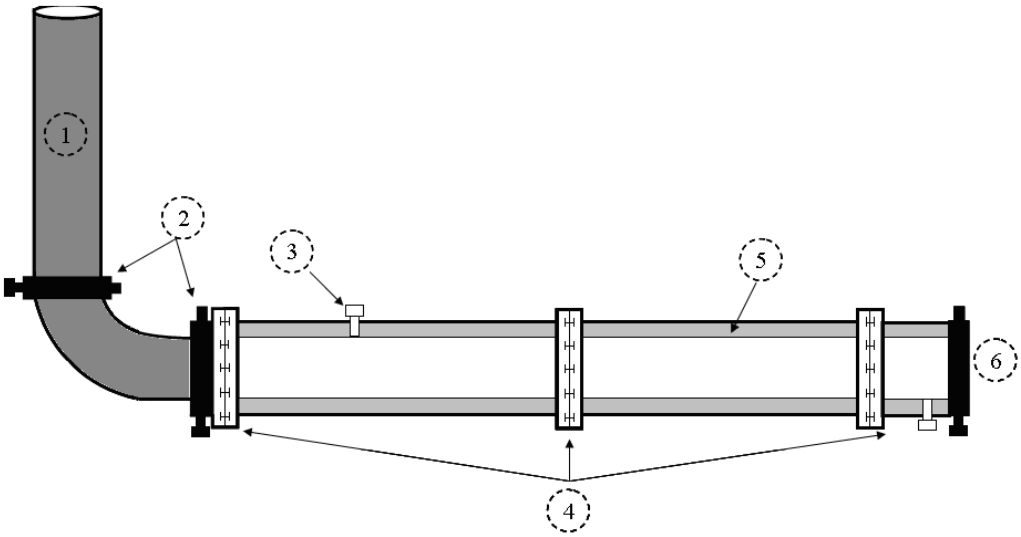

Figure 4.12: Experimental setup to measure the bubble propagation velocity (u_{ub}) and the liquid depth below the bubble (d_c^{bf}) following full-bore rupture in a horizontal pipe:

1) Stainless steel pipe
2) Connecting clamps
3) Deaerating orifice
4) Connecting flanges
5) Acrylic pipe
6) Plug with a screw

The acrylic pipe (5) is 2.5m long with 0.038m inner diameter. The fluid/wall friction is unlikely to be significant as a result of the pipe material and smooth inner wall. A stainless steel pipe (1), with the same inner diameter as the acrylic pipe represents the upstream tank. When filling the pipe, the deaerating orifice on top of the pipe is opened and closed frequently to release any trapped air bubbles in the system. Once the pipe is full, the plug at the end of the pipe (6) is rapidly unscrewed manually to simulate the full-bore rupture. In order to measure the bubble propagation velocity, Kodak Ektapro high speed motion analyser, model 4540 is used to record the bubble location at the speed of 500 frame/s.

In order to reduce the impact of reaction error, the Motion Analyser is switched on before the rubber plug is manually removed. Manually unscrewing the plug can potentially cause some error as it takes some time for the screw to be unfastened completely to simulate full-bore rupture. The mass released before the complete

removal of the plug can potentially have an impact on the discharge rate and cause an underestimation of the discharged mass.

Figure 4.13 presents a selection of the photographs taken at different time intervals following the simulated pipe rupture using the experimental setup shown in Figure 4.12. In order to calculate the upstream bubble velocity (u_{ub}), the distance travelled by the bubble from the photographs taken at a given time interval Δt is calibrated to obtain the actual distance Δx_{actual}. The following steps present the approach adopted for the distance calibration:

1. Measuring the pipe outer diameter from the photographs.
2. Finding the correction factor by dividing the real pipe outer diameter (in this case 0.056m) by the measured value from step 1.
3. Multiplying the measured distance travelled by the bubble by the correction factor from step 2 to calculate Δx_{actual}.

Once Δx_{actual} is determined, the bubble velocity may be calculated via:

$$u_{ub} = \frac{\Delta x_{actual}}{\Delta t} \tag{4.48}$$

In the above equation is also calculated from the following equation:

$$\Delta t = \frac{Frame2 - Frsme1}{500\ frame/s} \tag{4.49}$$

Here *Frame1* and *Frame2* are the frame numbers reported by the Motion Analyser for each photograph.

Figure 4.14 shows the results in the form of a ratio between the measured and predicted bubble velocity versus time. From the figure it may be observed that the predicted values for u_{ub} from Equation (4.25) are in relatively good agreement with

experimental data. The measured values range between 75%-99% of the predicted values, which implies that the model is conservative.

In addition, based on the photographs, the average measured liquid depth below the downstream and upstream bubbles (d_c^{bf}) is 0.024m. The corresponding liquid depth angle ϕ_c^{bf} = 210°. This is in remarkably close agreement with the predicted value of 216° based on simultaneous solution of Equations (4.7) and (4.20) (see Section 4.3.2.2).

These results confirm the validity of Bendiksen's (1984) suggested value for empirical coefficient C_0 for a system with upstream storage tank and two bubbles propagating towards each other.

Systematic and Experimental Errors

Uncertainty in an experiment is due to either experimental error or systematic error. Experimental errors are statistical fluctuations in the measured data as a result of the precision limitations of the measurement device. Experimental errors usually result from the experimenter's inability to take the same measurement in exactly the same way to get exact the same number. Systematic errors, on the other hand, are reproducible inaccuracies that are consistently in the same direction. Systematic errors are often due to a problem which persists throughout the entire experiment.

Based on the above definition, possible systematic and experimental error during measuring the bubble propagation velocity in horizontal pipes are:

Systematic Errors

1. As described previously, here FBR is simulated by manually unscrewing and removing the plug. As such, FBR does not occur instantaneously, resulting in releasing some mass prior to FBR. The liquid velocity during this transient phase is lower than that upon FBR. As a result, initially bubble propagates slower than the predicted value by the model (see Figure 4.14). The bubble propagation velocity increases once the plug is fully removed.

2. Manually unscrewing the plug also causes vibrations to the pipe and consequently to the contained water. This will have an impact on the bubble propagation velocity, producing scattered results for bubble propagation velocity initially. Once the plug is fully removed and the pipe is stable, the measured results for the bubble propagation velocity become closer, eventually reaching the predicted value by the model (see Figure 4.14).

Experimental Errors

1. In order to minimise the number of bubbles trapped along the pipe while filling the system with water, deaerating orifice is opened and closed frequently. However, sometimes there are still small bubbles trapped on top of the pipe. This will have an impact on the bubble propagation velocity as the presence of these bubbles introduces a new frictional loss between the bubbles and the water.
2. Since the process of removing the plus is not automatic and thus not instantaneous, the time taken to unscrew the plug can vary from one experiment to another. The longer it takes to manually unscrew the plug, the more mass is discharged prior to FBR, resulting in larger deviation of the measured bubble propagation velocity from the predicted value for FBR from the model.
3. In order to produce the upstream bubble, the liquid level in the stainless steel pipe representing the upstream tank has to be around the critical depth. If the liquid head is much higher than the critical depth, due to short length of the pipe and high initial liquid momentum, the downstream bubble will not fully propagate towards the upstream bubble. On the other hand, very small liquid head in the stainless still pipe causes the upstream bubble to form at the pipe inlet even before the plug is removed. Both cases will produce different results for bubble propagation velocity for the configuration considered in this study.

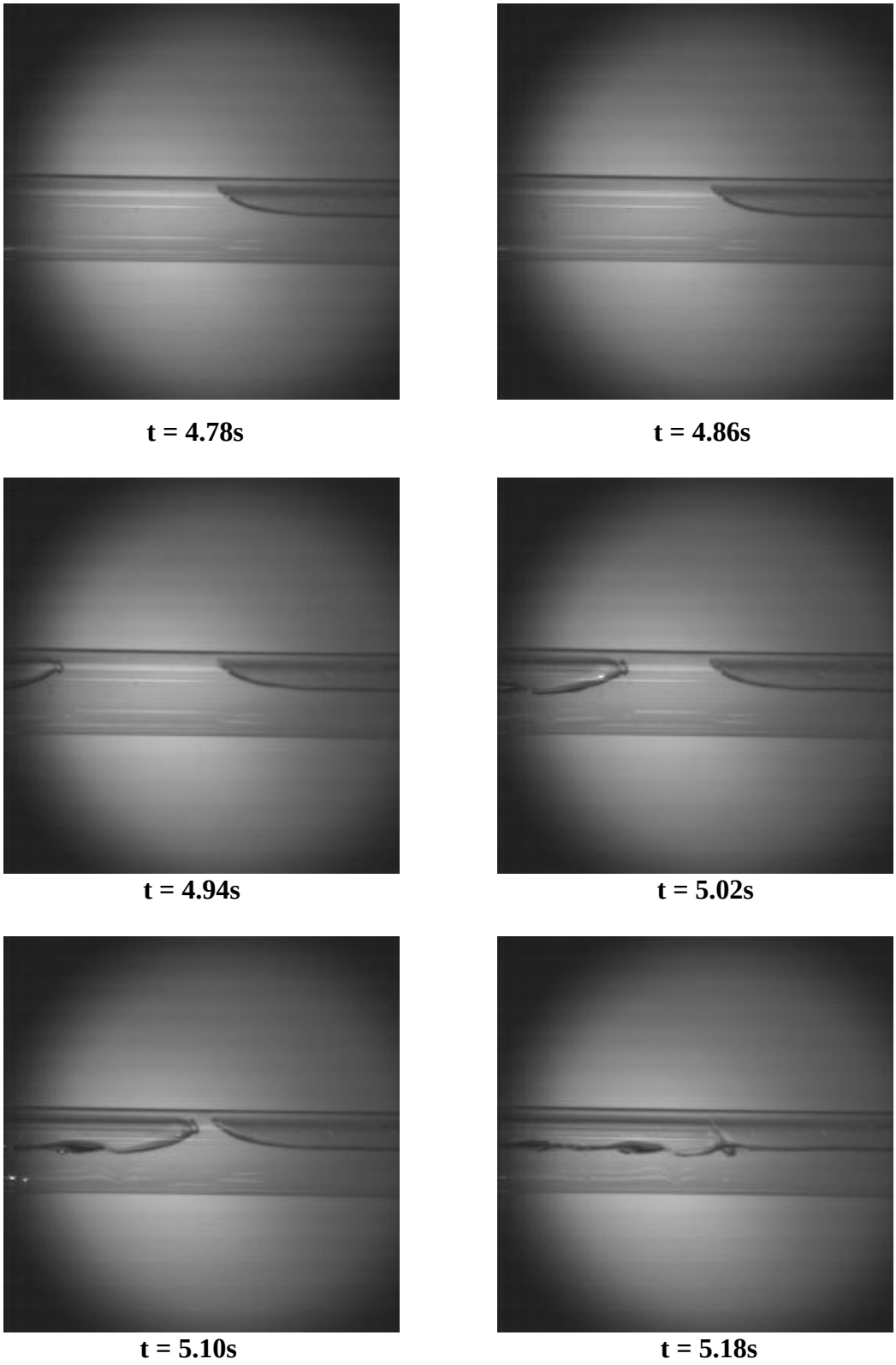

Figure 4.13: Snapshots taken at the speed of 500frame/s from bubble propagation in 0.038m inner diameter, 2.5m long, horizontal pipe

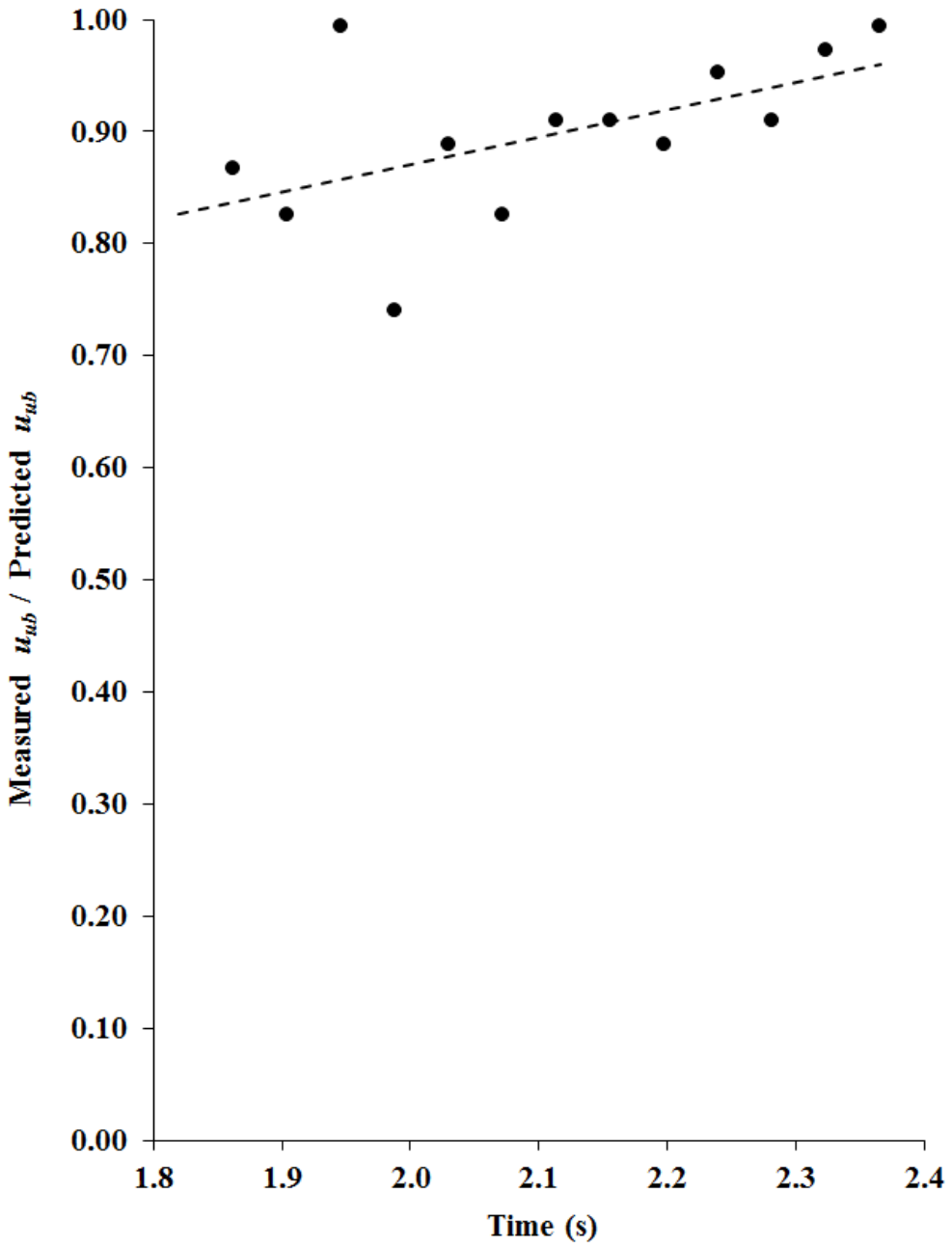

Figure 4.14: Variation of (measured u_{ub} / predicted u_{ub}) with time following full-bore rupture in a 0.038m inner diameter, 2.5m long, horizontal pipe

4.3.4.2. Normalised Cumulative Discharged Mass and Discharge Rate

This section presents the results from a series of experiments conducted to determine the accuracy of the outflow model developed in Section 4.3.2 in predicting the transient discharge rate. Figure 4.15 shows the experimental setup used to measure the cumulative discharged mass.

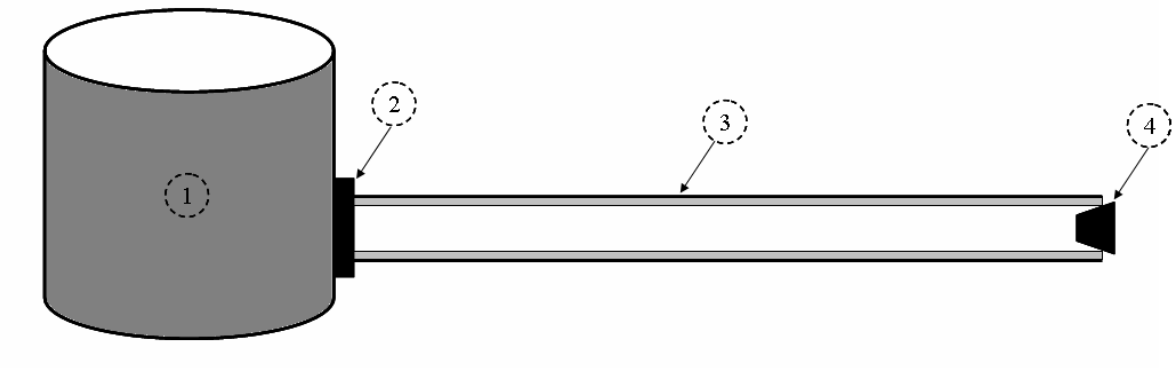

Figure 4.15: Experimental setup to measure the cumulative discharged mass following full-bore rupture in a horizontal pipe fed from a plastic container

1) Plastic container
2) Cable gland
3) Acrylic pipe
4) Rubber bung

A 0.034m inner diameter, 3m long, acrylic pipe (3) is connected to a 0.025m^3, cylindrical plastic container (1). Silicone sealant is used at the connection point between the pipe and the tank to avoid leakage. The open end of the pipe is initially closed by a rubber bung (4). Once the system is full, the rubber bung is removed to simulate the full-bore rupture. Similar to the setup used for measuring the bubble propagation velocity, the bung is removed manually. Although more accurate, still this can be a source of error as there will be some discharge before the complete removal of the runner bung. The discharged water is collected in another plastic container placed on top of a Mettler PM30K industrial balance whereby using a LabView – based software (National Instruments Company, 2011), the cumulative discharged mass is measured as a function of time throughout the drainage of the

system. In order to mitigate the error in measuring the discharged mass, the plastic container used here has a cross sectional area almost the same size as the scale surface area. However, due to high liquid velocity the discharged water creates vibrations once it hits the container. This can have an impact on the accuracy of the measured discharged mass. As such, the plastic container has a relatively large height not only to minimise this impact, but also to prevent the incoming water from splashing outside the container.

The LabView-based software reports the discharged mass in the form a curve as a function of time. In order to extract the data from the curve, Engauge Digitiser 4.1 (Mitch, 2007) is used. The software transfers the corresponding data from the curve, M_i the cumulative discharged mass at $t = t_i$, into an Excel spreadsheet. Then the discharge rate at $t = t_i$, $\dot{m}_{d,i}$, is calculated via:

$$\dot{m}_{d,i} = \frac{M_i - M_{i-1}}{t_i - t_{i-1}} \qquad \textbf{(4.50)}$$

Figure 4.16 shows the comparison between the predicted and measured normalised cumulative discharged mass with time. Normalised cumulative discharged mass is defined as the ratio of the measured cumulative discharged mass and system initial inventory. As mentioned in Section 4.3.2.1 (Equation (2.14)), the resistance coefficient for the entry loss (K) is assumed to be 0.5 in the discharge model. The end of full pipe flow for the model is indicated in the figure.

It may be observed from the figure that during full pipe flow, the model overestimates the cumulative discharged mass. As the regime changes from full pipe to bubble formation, the deviation of the predicted results from the measured values reduces to less than 14%.

The overestimation of the cumulative discharged mass by the model during full pipe flow can be due to the additional frictional loss caused by the silicone sealant used at

the pipe entrance inside the tank. In order to test the impact of this additional frictional loss on the discharge rate, the cumulative discharged mass is also calculated for K in the range of 0.5-3.5. The results are presented in Figure 4.17 for K = 2.5 which produces the closest results to the measured value. With this new value for K, the model predictions are very close to the measured data from the experiments. The maximum deviation between the predicted and measured values during full pipe flow and post-full pipe flow (bubble formation and open channel flow) are 20% and $\pm$ 2% respectively.

Figure 4.18 shows the comparison between the measured discharge rate with the predicted values from the models with K = 0.5 and K = 2.5. From the graph, it seems that upon initiation of full pipe flow the measured discharge rate is closer to the predicted values by the model with K = 0.5. However, towards the end of this regime and during the subsequent regimes, bubble formation and open channel flow, the model with K = 2.5 predicts more accurate results. One possible explanation for the initial agreement between the measured and predicted values for K = 0.5 could be the presence of large liquid head in the tank at the outset. As a result, there is negligible impact of additional frictional loss imposed by silicone sealant upon initiation of full pipe flow. Consequently, using K = 2.5 results in underestimation of discharge rate.

Systematic and Experimental Errors

Systematic Errors

The measured total discharged mass at the end of the drainage process is always slightly less than the system initial mass. Because:

1. Due to the manual removal of the rubber bung, there will be some release prior to FBR. Part of the released water during this phase will not be contained in the container as it is not a one dimensional flow.
2. Due to the pipe curvature, there will be some inventory left at the base of the pipe even after the drainage is complete.
3. Once the discharged water hits the container, it will partly bounce back and splash outside the container.

Experimental Errors

1. Due to the high liquid discharge velocity there will be some vibrations imposed on the container. In addition, part of discharge hits the container wall first, rather than the base. These two have an impact on the measured mass of the liquid by the scale, producing scattered results for the measured discharged mass. The LabView-based software takes the average of the measured results, producing a smooth curve as presented in Figure 4.16.

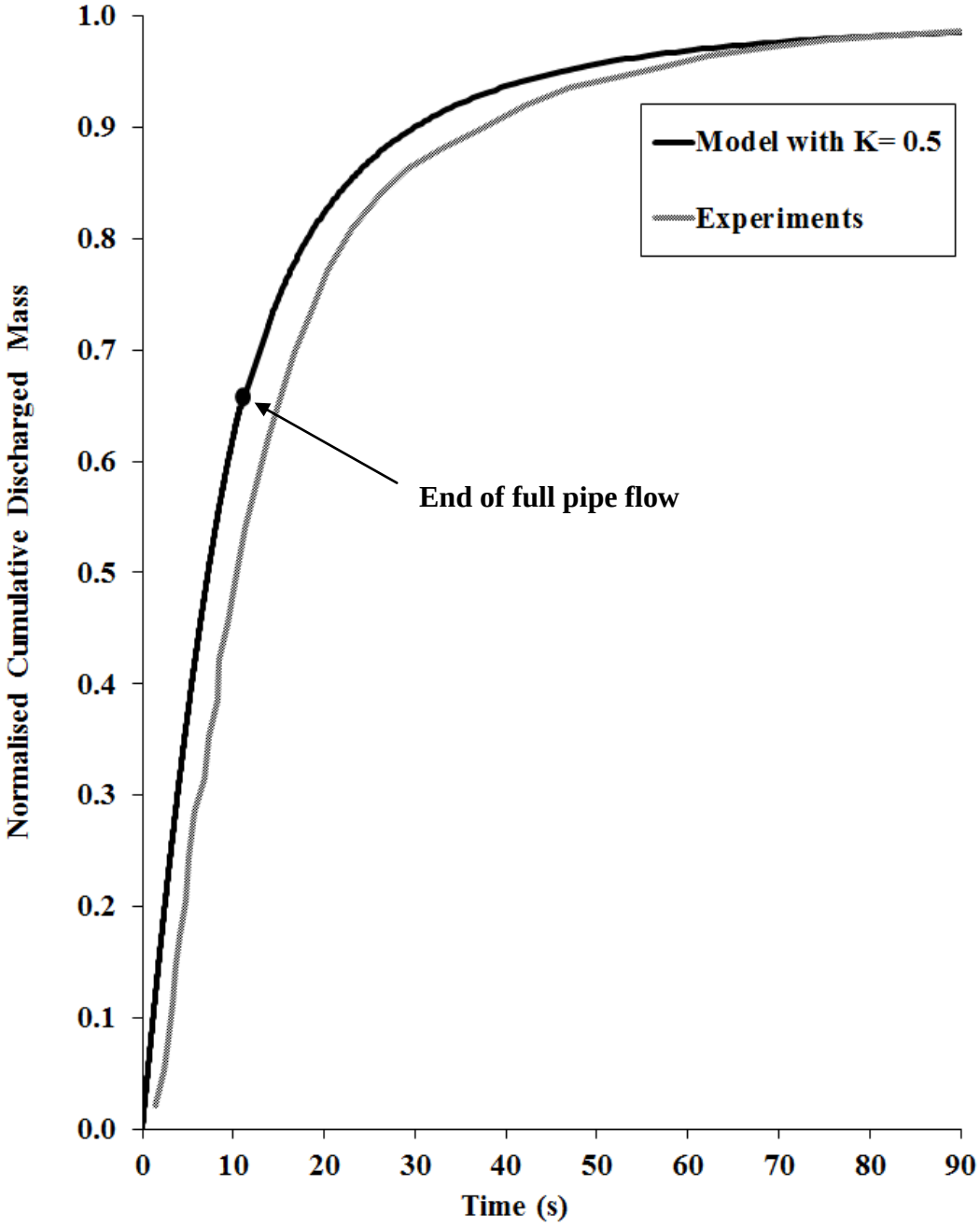

Figure 4.16: Comparison of the measured normalised cumulative discharged mass with the predicted values from the model with *K* = 0.5 following full-bore rupture in a horizontal pipe fed from a plastic container

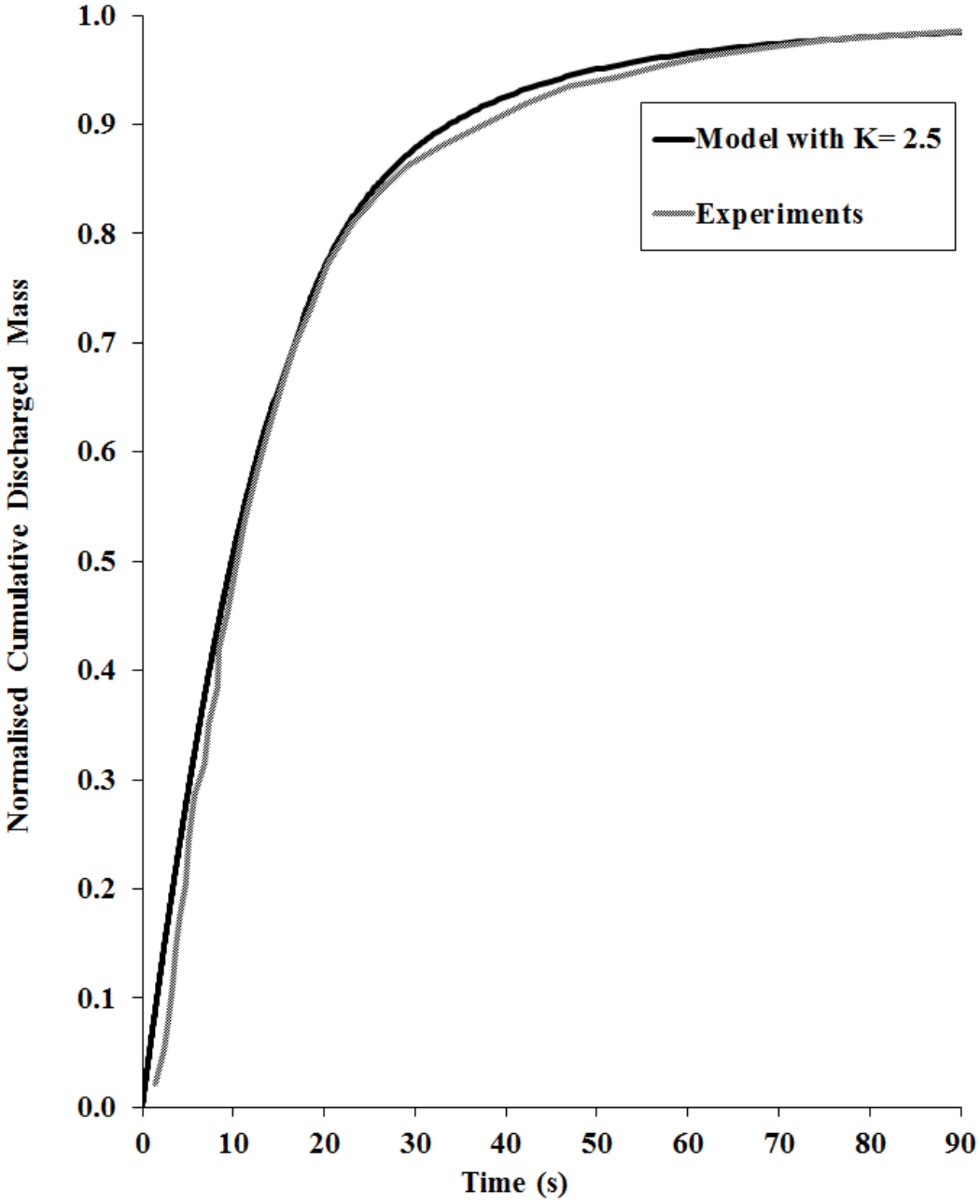

Figure 4.17: Comparison of the measured normalised cumulative discharged mass with the predicted values from the model with K = 2.5 following full-bore rupture in a horizontal pipe fed from a plastic container

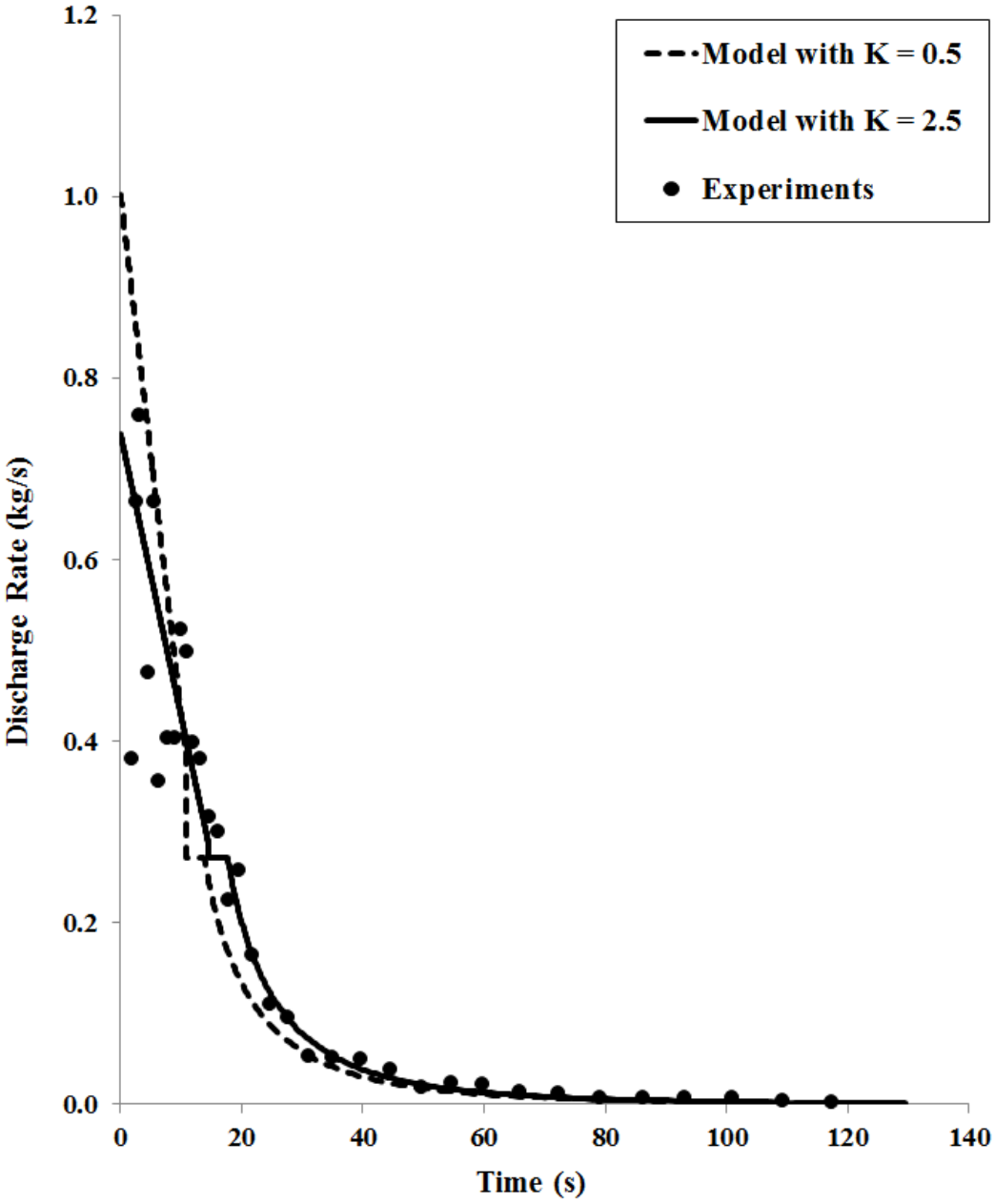

Figure 4.18: Comparison of the measured discharge rate with the predicted values from the models with K = 0.5 and K = 2.5 following full-bore rupture in a horizontal pipe fed from a plastic container

4.4. Transient Hydraulic Flow Modelling Following Full-bore Rupture of an Isolated Horizontal Pipeline

4.4.1. Introduction

This section is concerned with the formulation of various flow equations for predicting the discharge rate following full-bore rupture from the end of an isolated horizontal pipe containing an incompressible liquid. The pipe is assumed to be closed at one end due to emergency shut down, while the liquid releases from the rupture plane at the other end of the pipe.

Due to the absence of an upstream storage tank, the initial full pipe flow regime is not present. Also in practice, an initial discharge upon valve closure happens over a short period of time before the bubble formation regime starts. Given the liquid finite compressibility, the liquid mass released during this rapidly transient regime is negligible and thus ignored in this study. Therefore, only the flow regimes of bubble formation and open channel flow are considered here.

The associated theory is discussed in Section 4.4.2. In Section 4.4.3 the outflow model is tested through parametric studies by investigating the impact of pipeline inner diameter and length on the discharge velocity and wetted area. The released mass during individual regimes are also calculated and compared against the corresponding theoretical values. Finally, the accuracy of the developed model is assessed through a series of experiments, presented in Section 4.4.5.

4.4.2. Model Theory

4.4.2.1. Bubble Formation and Propagation

Upon rupture at the end of an isolated pipe, a bubble forms at the rupture plane and propagates along the pipe until it reaches the closed-end. Figure 4.19 presents the bubble propagation in a horizontal pipe with one closed-end.

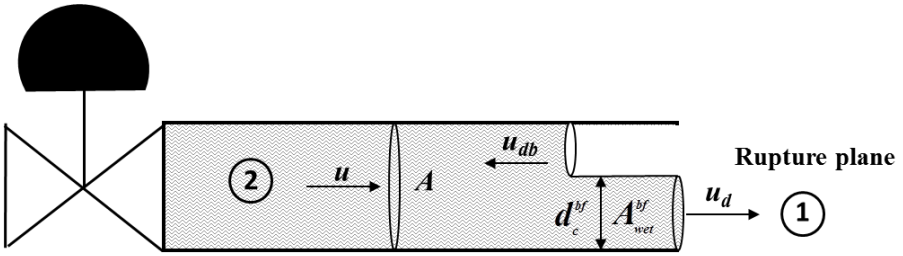

Figure 4.19: Bubble propagation in an isolated horizontal pipe

Given the incompressibility of the liquid, the volume of the released liquid is the same as the volume of the air entering the pipe. Therefore, the discharge velocity may be expressed as:

$$u_d = \frac{u_{db} A_b}{A_{wet}^{bf}} \tag{4.51}$$

or

$$u_d = \frac{u_{db}\left(A - A_{wet}^{bf}\right)}{A_{wet}^{bf}} \tag{4.52}$$

A_{wet}^{bf} may also be calculated from Equation (4.14) :

$$A_{wet}^{bf} = \frac{D^2}{8}\left(\phi_c^{bf} - \sin\phi_c^{bf}\right) \tag{4.14}$$

u_{db} is also determined by using Equation (3.17) proposed by Benjamin (1968):

$$u_{db} = 0.542\sqrt{gD} \tag{3.17}$$

On the other hand, as described in Section 2.3.5, the liquid depth at the pipe exit and below the bubble is the same as the critical depth. Therefore, Equation (4.7) is recalled for the discharge velocity:

$$u_d = 0.354\sqrt{\frac{gD\left(\phi_c^{bf} - \sin\phi_c^{bf}\right)}{\sin(\phi_c^{bf}/2)}} \qquad \textbf{(4.7)}$$

Substituting u_{db} and A_{wet}^{bf} from Equations (3.17) and (4.14) into Equation (4.52) gives the following equation for the discharge velocity:

$$u_d = \frac{2\pi - \phi_c^{bf} + \sin\phi_c^{bf}}{\phi_c^{bf} - \sin\phi_c^{bf}} 0.542\sqrt{gD} \qquad \textbf{(4.53)}$$

Finally equating Equations (4.7) and (4.53) and solving iteratively produces 175^o for ϕ_c^{bf}. Similar to the pipe attached to an upstream tank, in the absence of frictional loss, the above value is independent of pipe characteristics.

Inserting the value ϕ_c^{bf} = 175^o into Equations (4.26), (4.53) and (4.14) , $\dot{m}_d$, u_d and A_{wet}^{bf} can be respectively determined via:

$$\dot{m}_d = 0.225\rho D^2\sqrt{gD} \qquad \textbf{(4.54)}$$

$$u_d = 0.610\sqrt{gD} \qquad \textbf{(4.55)}$$

$$A_{wet}^{bf} = 0.371D^2 \qquad \textbf{(4.56)}$$

Consequently, the time required for the bubble to reach the closed-end may be calculated from the following equation:

$$t_{bubble} = \frac{L}{u_{db}} = \frac{L}{0.542\sqrt{gD}} \tag{4.57}$$

4.4.2.2. Open Channel Flow

As soon as the elongated bubble reaches the closed-end of the pipe, open channel flow prevails. Figure 4.20 shows an isolated horizontal pipeline with open channel flow.

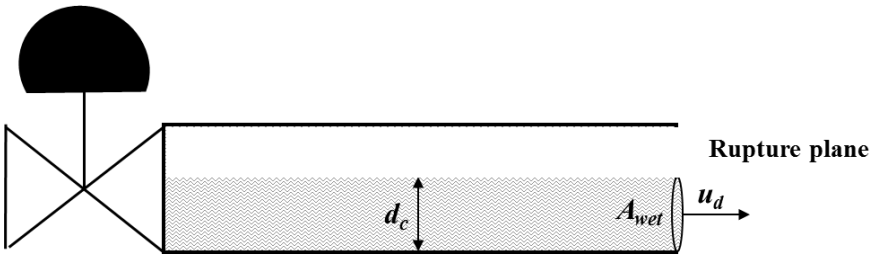

Figure 4.20: Open channel flow in an isolated horizontal pipe

The model for this regime is similar to the described model in the presence of upstream storage tank in Section 4.3.2.3, except that the equivalent length of the tank is not applicable here. Therefore, recalling Equation (4.37) with L_{eq} = 0 gives:

$$\frac{dA_{wet}}{0.044\rho D^2\sqrt{gD}\left(\phi_c - \sin\phi_c\right)\sqrt{\dfrac{\phi_c - \sin\phi_c}{\sin\dfrac{\phi_c}{2}}}} = -\frac{dt}{\rho L} \tag{4.58}$$

Here at $t = 0$, $\phi_c = \phi_c^{bf} = 175^o$ and thus $A_{wet} = A_{wet}^{bf}$ which is calculated from Equation (4.56). Based on this, the above equation is integrated to produce:

$$\int_{0.371D^2}^{A_{wet}} \frac{dA_{wet}}{0.044\rho D^2\sqrt{gD}\left(\phi_c - \sin\phi_c\right)\sqrt{\dfrac{\phi_c - \sin\phi_c}{\sin\dfrac{\phi_c}{2}}}} = -\frac{t}{\rho L} \tag{4.59}$$

Once again Equation (4.59) must be solved numerically. Once again the procedure presented in Figure 4.5 is used to evaluate the above integral, except that here instead of $\phi_c^{bf} = 216^o$, $\phi_c^{bf} = 175^o$ .Once the value of the integral I_i is determined, the corresponding time t_i is calculated via:

$$t_i = I_i \rho L \qquad \textbf{(4.60)}$$

4.4.3. Parametric Studies

In the previous section a detailed mathematical model was developed to simulate the outflow following a rupture at the end of an isolated horizontal pipe. Due to the absence of upstream storage tank, only bubble propagation and open channel flow were considered here.

This section presents the results of a series of parametric studies based on the application of the above model. Similar to the verification of the developed model with an upstream tank, the impact of the changes in the pipeline length and inner diameter on the discharge velocity and the normalised cumulative discharged mass during individual regimes are studied here.

The characteristics given in Table 4.1 for the verification of the model with an upstream storage tank are also applicable here except the initial liquid head. The impact of pipe friction is ignored here as it is assumed to be negligible during bubble formation and open channel flow.

4.4.3.1. Discharge Velocity and Wetted Area

In this section the impact of pipeline characteristics on the discharge velocity and wetted area (A_{wet}) is studied. The parametric studies are conducted for the pipeline length and inner diameter in the ranges 50-200m and 0.305-0.406m respectively.

Figure 4.21 and Figure 4.22 show the impact of pipeline length and diameter on the transient discharge velocity. On the other hand, the impacts of the above characteristics on A_{wet} are presented in Figure 4.23 and Figure 4.24.
In all the graphs, the initial horizontal line shows the discharge velocity and wetted area during bubble formation and propagation regime. This is then followed by a slow non-linear decline in the discharge velocity and wetted area corresponding to open channel flow.

As it may be observed from the figures, the discharge velocity during the bubble propagation regime increases with pipe inner diameter due to increase in bubble propagation velocity (Equation (3.17)). However, the discharge velocity during this regime is not dependent on pipe length. This can be seen from Figure 4.21 where for all pipe lengths, the discharge velocity remains unchanged. The time required for the bubble to reach the closed-end is shown to be proportional to the pipeline length L, in line with Equation (4.57).

On the other hand, the normalised wetted area during bubble propagation regime remains constant and equal to 0.473, given below, regardless of pipeline length and inner diameter. This stems out from a constant ϕ_c^{bf} obtained in Section 4.4.2.1 based on the assumption of negligible frictional loss for all pipeline characteristics.

$$\frac{A_{wet}}{A} = \frac{A_{wet}^{bf}}{A} = \frac{0.371D^2}{\frac{\pi D^2}{4}} = 0.473 \qquad \textbf{(4.61)}$$

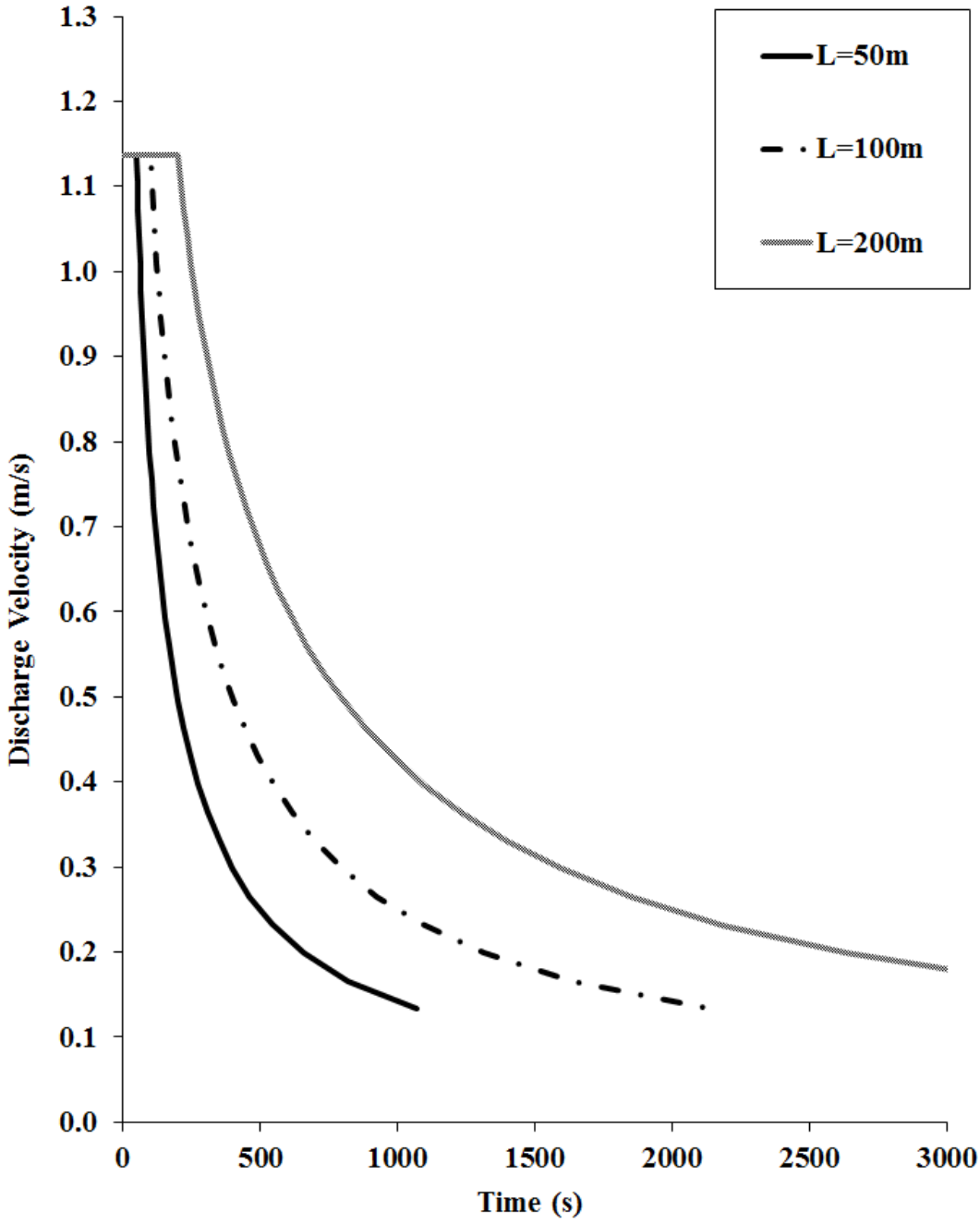

Figure 4.21: Impact of pipeline length on the variation of discharge velocity with time following full-bore rupture in a 0.356m diameter, isolated, horizontal pipe

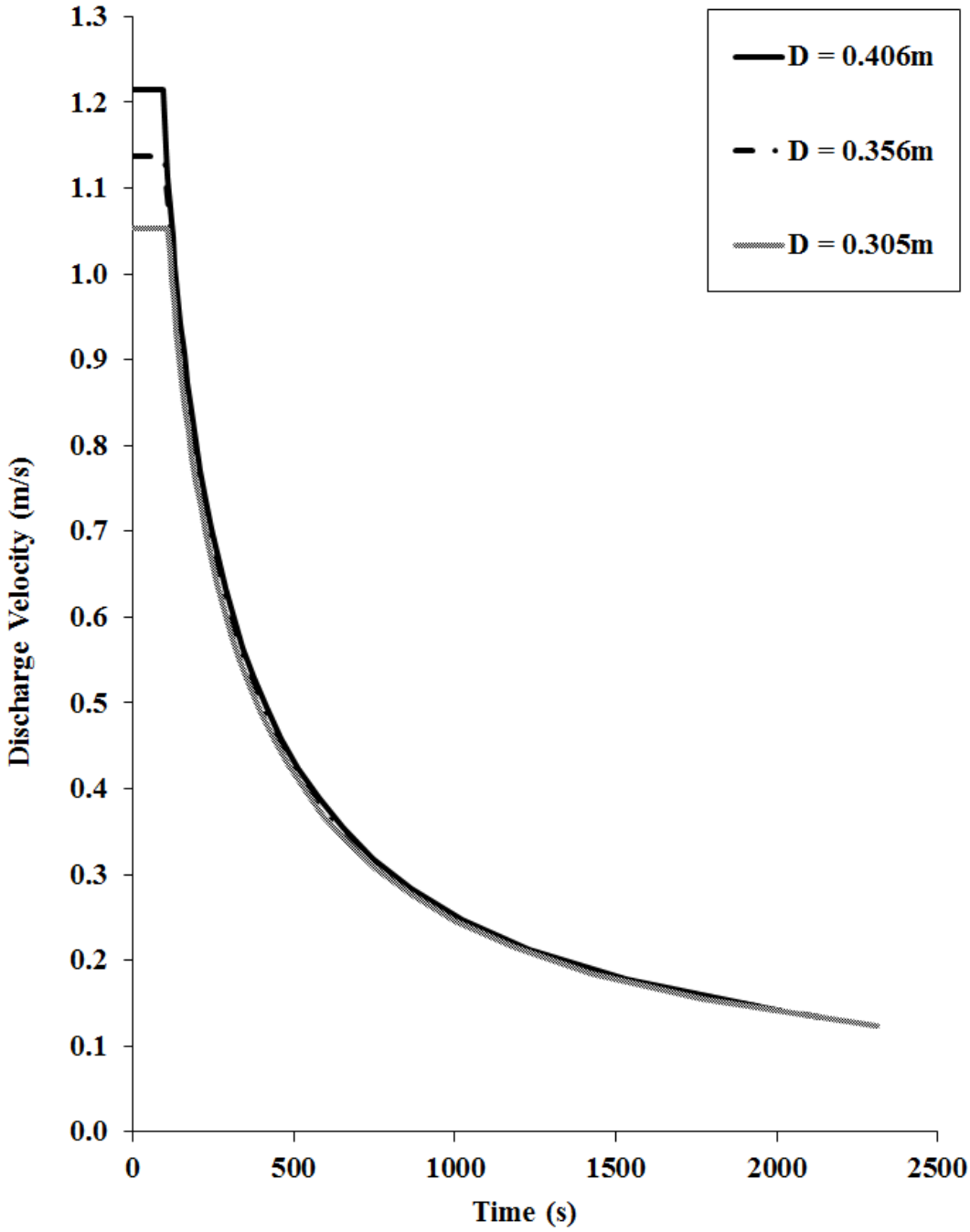

Figure 4.22: Impact of pipeline diameter on the variation of discharge velocity with time following full-bore rupture in a 100m long, isolated, horizontal pipe

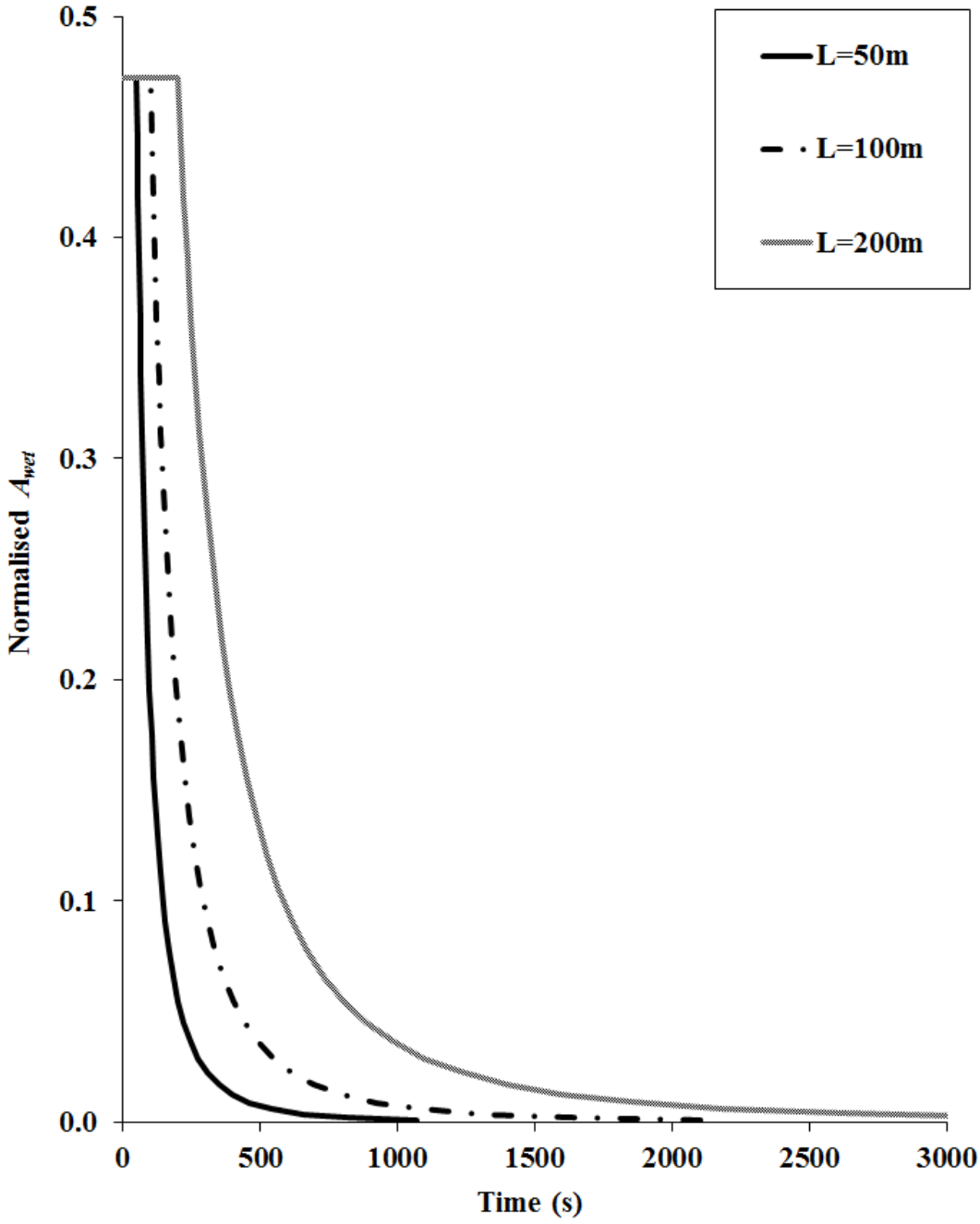

Figure 4.23: Impact of pipeline length on the variation of normalised A_{wet} with time following full-bore rupture in a 0.356m diameter, isolated, horizontal pipe

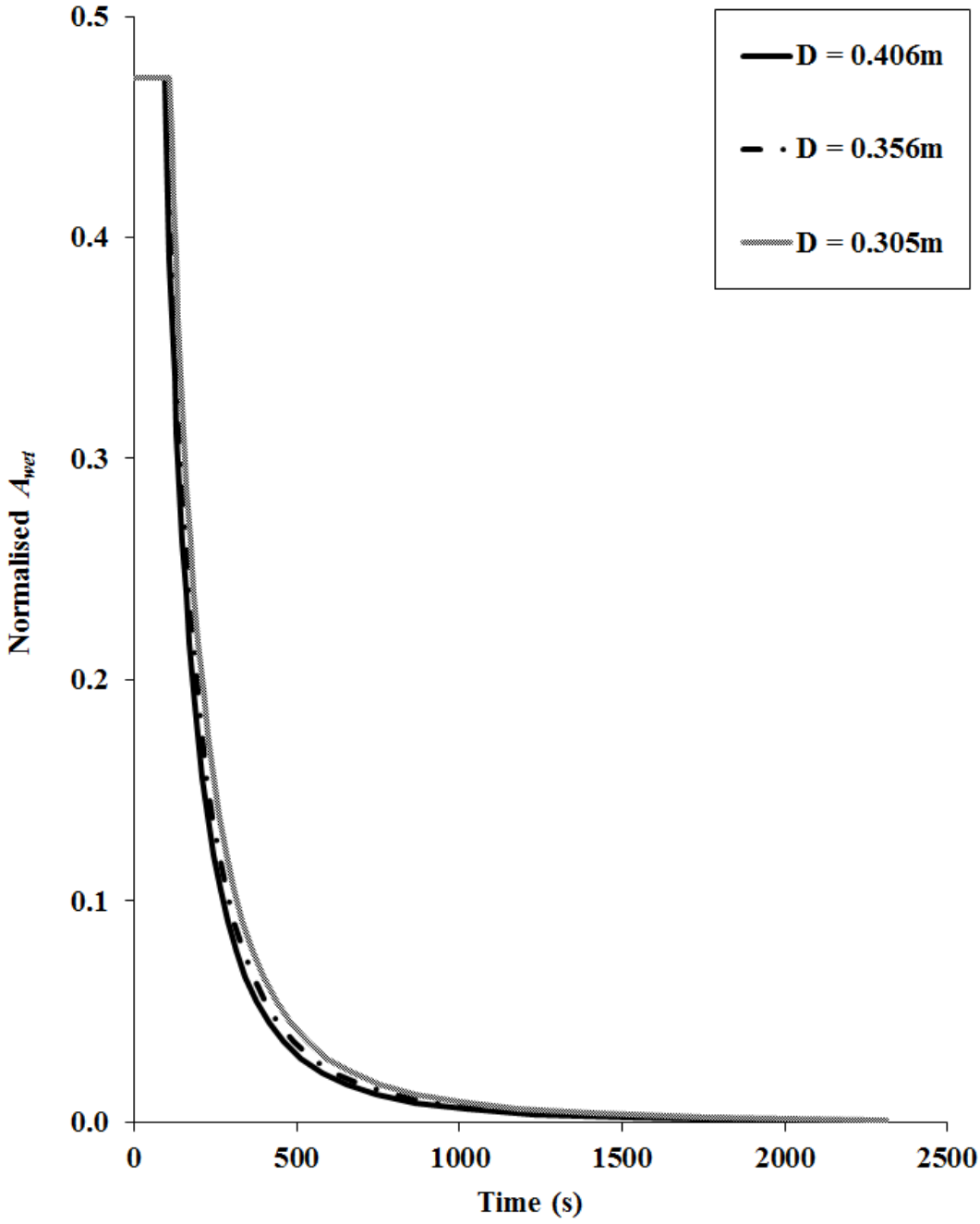

Figure 4.24: Impact of pipeline diameter on the variation of normalised A_{wet} with time following full-bore rupture in a 100m long, isolated, horizontal pipe

4.4.3.2. Released Mass during Individual Flow Regimes

Table 4.3 presents the comparison between the predicted and theoretical discharged mass during each regime for pipeline length and diameter in the ranges 100-300m and 0.305-0.508m respectively. The calculation for the theoretical released mass during each regime is similar to that described in Section 4.3.3.2 except that only bubble propagation and open channel flow are relevant here. In addition, due to the absence of upstream tank, equivalent length, L_{eq} (see Equation (4.31)) is also not applicable.

- Bubble formation and propagation

$$M_{bubble\ propagation} = \rho L\left[A - A_{wet}^{bf}\right] = \rho L\left[\frac{1}{4}\pi D^2 - 0.371D^2\right] = 0.414\rho L D^2 \quad \textbf{(4.62)}$$

- Open channel flow

$$M_{open\ channel\ flow} = \rho L\left(0.371D^2\right) \quad \textbf{(4.63)}$$

where $0.371D^2$ is A_{wet}^{bf} from equations (4.56).

The predicted released mass during each flow regime, $M_{predicted}$, is calculated from Equation (4.47):

$$M_{predicted} = \dot{m}_d\,\Delta t \quad \textbf{(4.47)}$$

Scenario		Bubble propagation		Open channel flow	
Length (m)	Diameter (m)	Theoretical (kg)	Predicted (kg)	Theoretical (kg)	Predicted (kg)
100	0.305	3823	3873	3426	3391
100	0.406	6791	6862	6071	6009
100	0.508	10632	10744	9504	9406
100	0.356	5222	5277	4668	4620
200	0.356	10443	10553	9335	9239
300	0.356	15665	15829	14003	13859

Table 4.3: Comparison of the theoretical and predicted discharged mass during individual regimes following full-bore in an isolated horizontal pipe

Once again it is clear from the table that the predicted and the expected mass to release are very close for all scenarios, less than 2% deviation.

4.4.4. Error Analysis and Dependence of Convergence on $\Delta\phi_c$

This section presents the error analysis for the drainage process including bubble formation and open channel flow in a horizontal pipe. In addition, the impact of the increment $\Delta\phi_c$ on the convergence in trapezoidal rule used to estimate Equation (4.59) is investigated. The default value is set to 1, as presented in Figure 4.5.

Figure 4. 25 shows the discharge rate versus time for various values of $\Delta\phi_c$. The pipe length and diameter are 100m and 0.356m respectively. As it may be observed from the graph, the convergence in the trapezoidal method used to estimate Equation (4.58) is not affected by the increment $\Delta\phi_c$.

On the other hand the impact of the increment $\Delta\phi_c$ on the accuracy of the developed model in calculating the total expelled mass is presented in Figure 4. 26. Axis *y* shows "Δ total expelled mass" where it is defined as **predicted** total expelled mass minus **theoretical** expelled mass. The theoretical values are calculated based on the approach described in Section 4.4.3.2. It may be observed from the figure that as expected, reduction of $\Delta\phi_c$ results in less deviation of the predicted total expelled mass from the theoretical values.

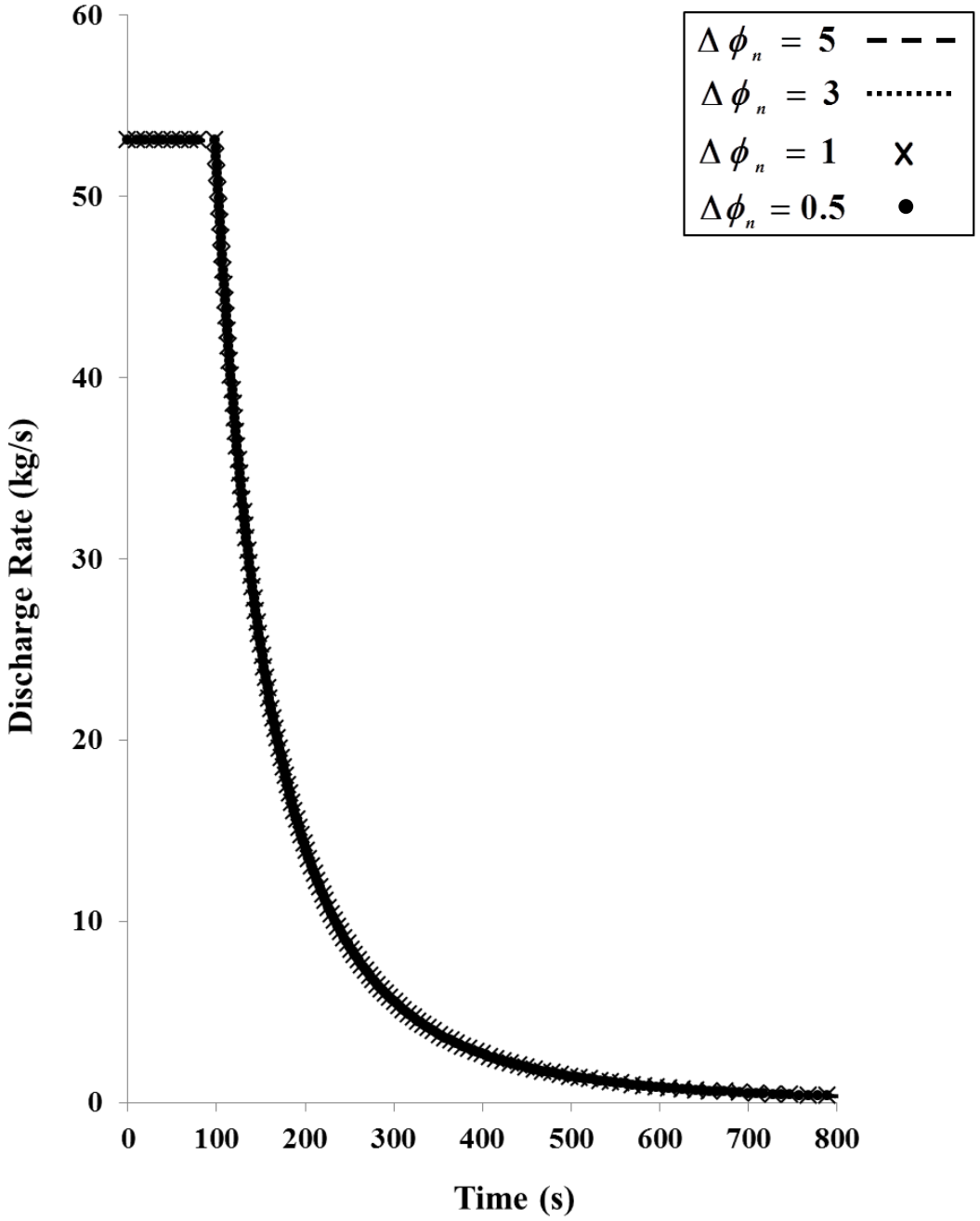

Figure 4. 25: Impact of $\Delta\phi_c$ on the convergence in trapezoidal method in a 100m long, 0.356m diameter, horizontal pipe

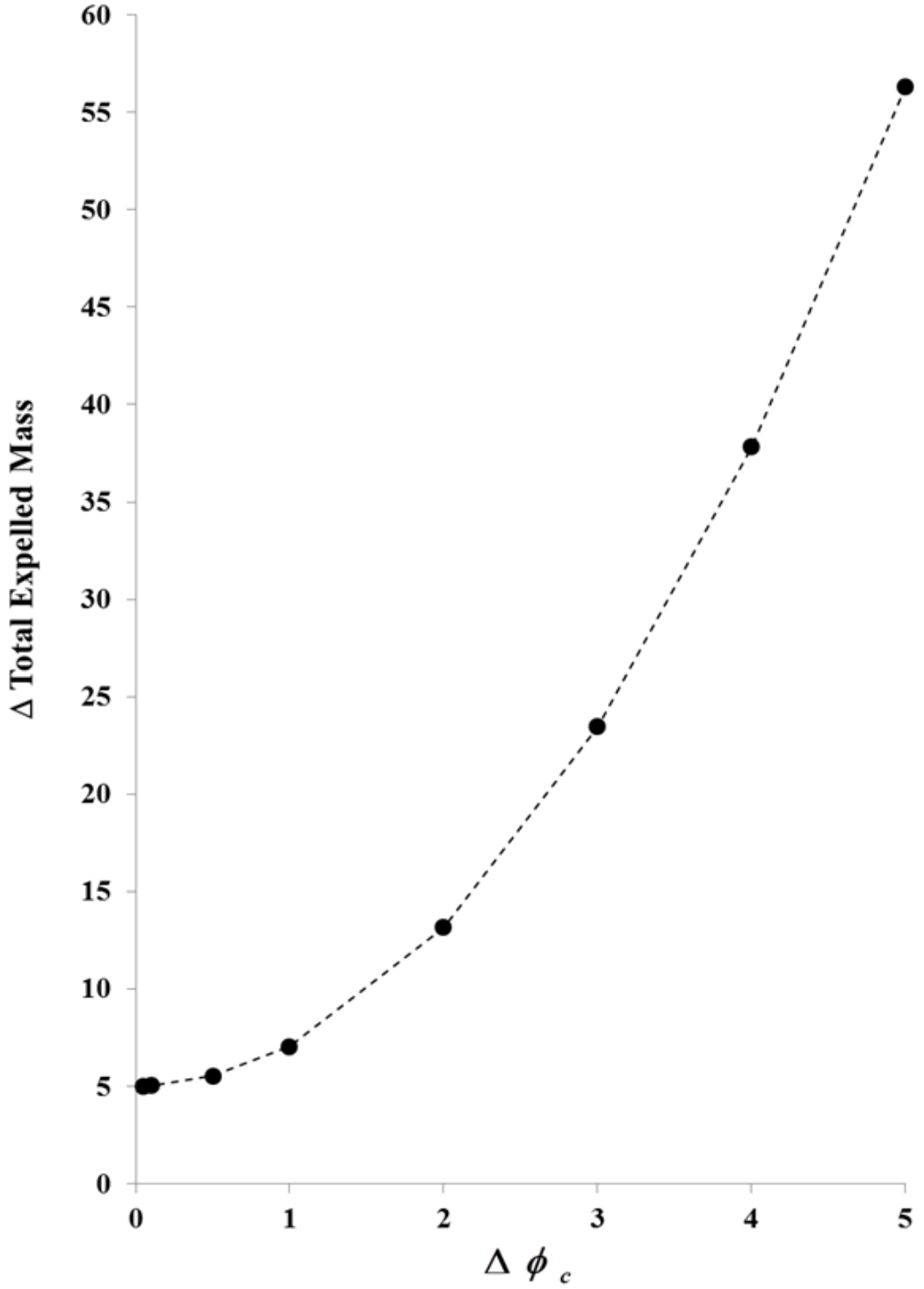

Figure 4. 26: Impact of $\Delta\phi_c$ on the accuracy of the developed model for a 100m long, 0.356m diameter, horizontal pipe in predicting the total expelled mass

4.4.5. Experiments

The following presents the results from a series of experiments conducted to determine the accuracy of the above model by comparison of its predictions for the cumulative discharged mass and transient discharge rate against measured data. The discharge rate from the experiments are calculated from Equation (4.50) based on the measured cumulative discharged mass.

Figure 4.27 shows the experimental setup constructed for the model validation. Here, the 0.034m inner diameter, 3m long, acrylic pipe (2) inlet is closed by using a rubber bung (1). Once the system is full, the rubber bung (3) is removed to simulate the full-bore rupture, while rubber bung (1) remains as the closed-end of the pipe. The discharged water is collected in a plastic container placed on top of a Mettler PM30K industrial balance whereby using a LabView – based software (National Instruments Company, 2011), the cumulative discharged mass is measured as a function of time throughout the drainage of the system.

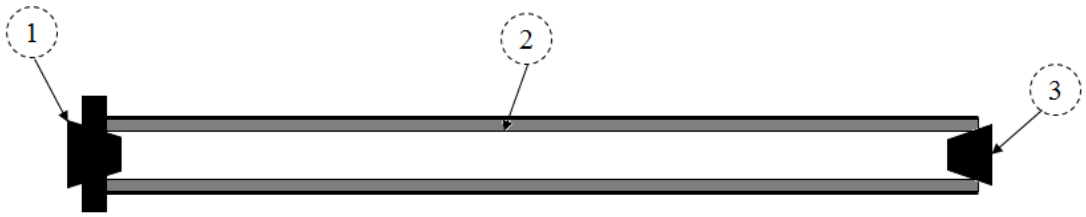

Figure 4.27: Experimental setup to measure the cumulative discharged mass following full-bore rupture in an isolated horizontal pipe

1 & 3) Rubber bung
2) Acrylic pipe

Figure 4.28, Figure 4.29 and Figure 4.30 respectively show the comparison between the predicted and measured discharge rate in linear and logarithmic scale, and measured normalised cumulative discharged mass respectively.

It may be observed from the figures that the measured discharge rate during bubble propagation regime marginally varies, in line with the assumption of constant

discharge during this regime in the model. Although the pipe is acrylic and thus very smooth, there might still be some frictional loss. The slight increase in the discharge can be due to the reduction of frictional loss as the full section of the pipe decrease towards the end of bubble propagation regime. This can potentially explain the over prediction of the discharge rate by the model as in developing the flow equations, the frictional loss is assumed to be negligible (see Section 4.4.2.1).

On the other hand, during open channel flow the measured discharge rate is slightly higher than the predicted values, showing the negligible impact of frictional loss during this regime.

Based on the above, as expected, the predicted cumulative discharged mass is higher than the measured values. The difference between the two reduces as the measured discharge rate during open channel flow becomes greater than the predicted vales.

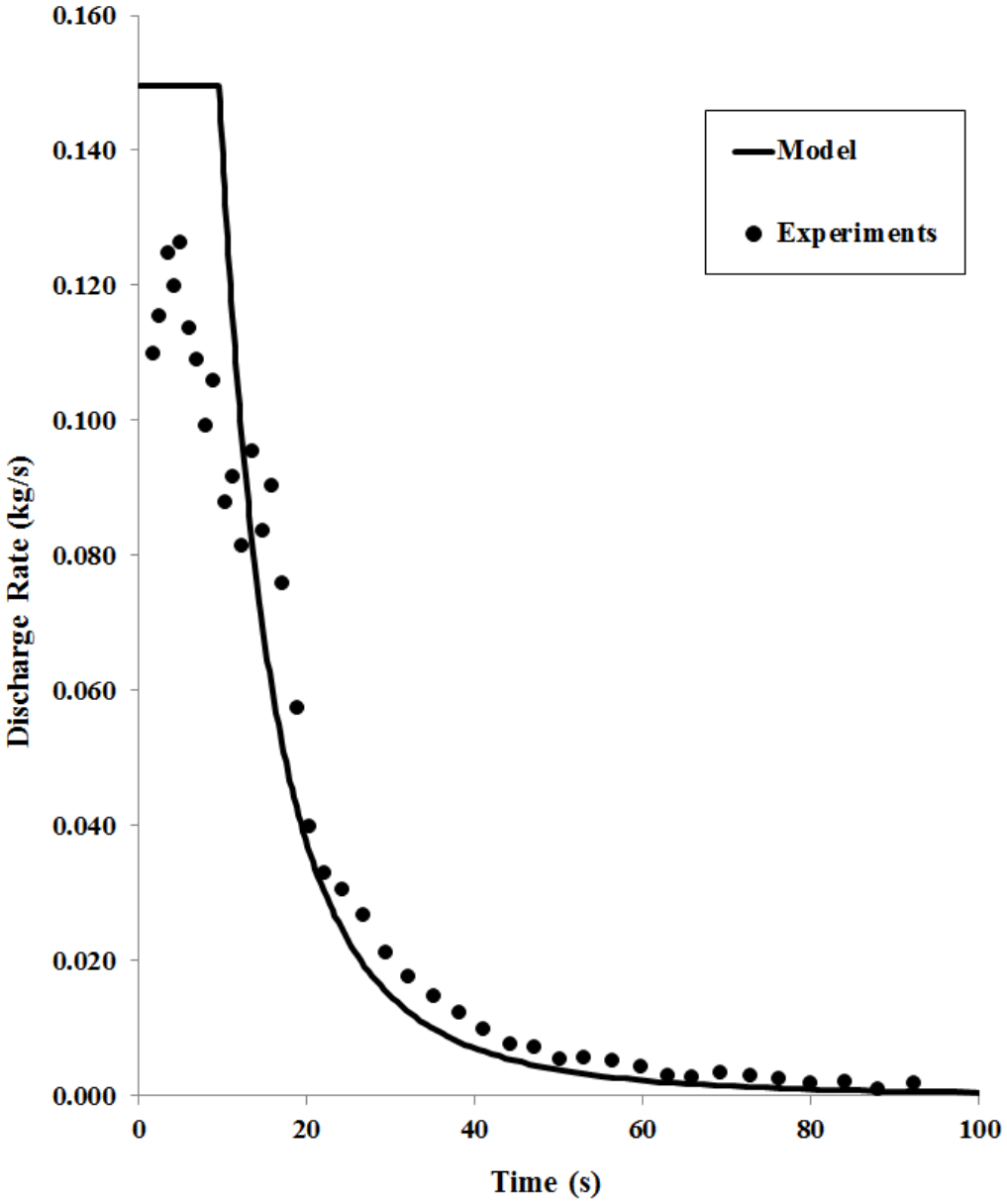

Figure 4.28: Comparison of the measured discharge rate with the predicted values from the model in linear scale following full-bore rupture in an isolated horizontal pipe

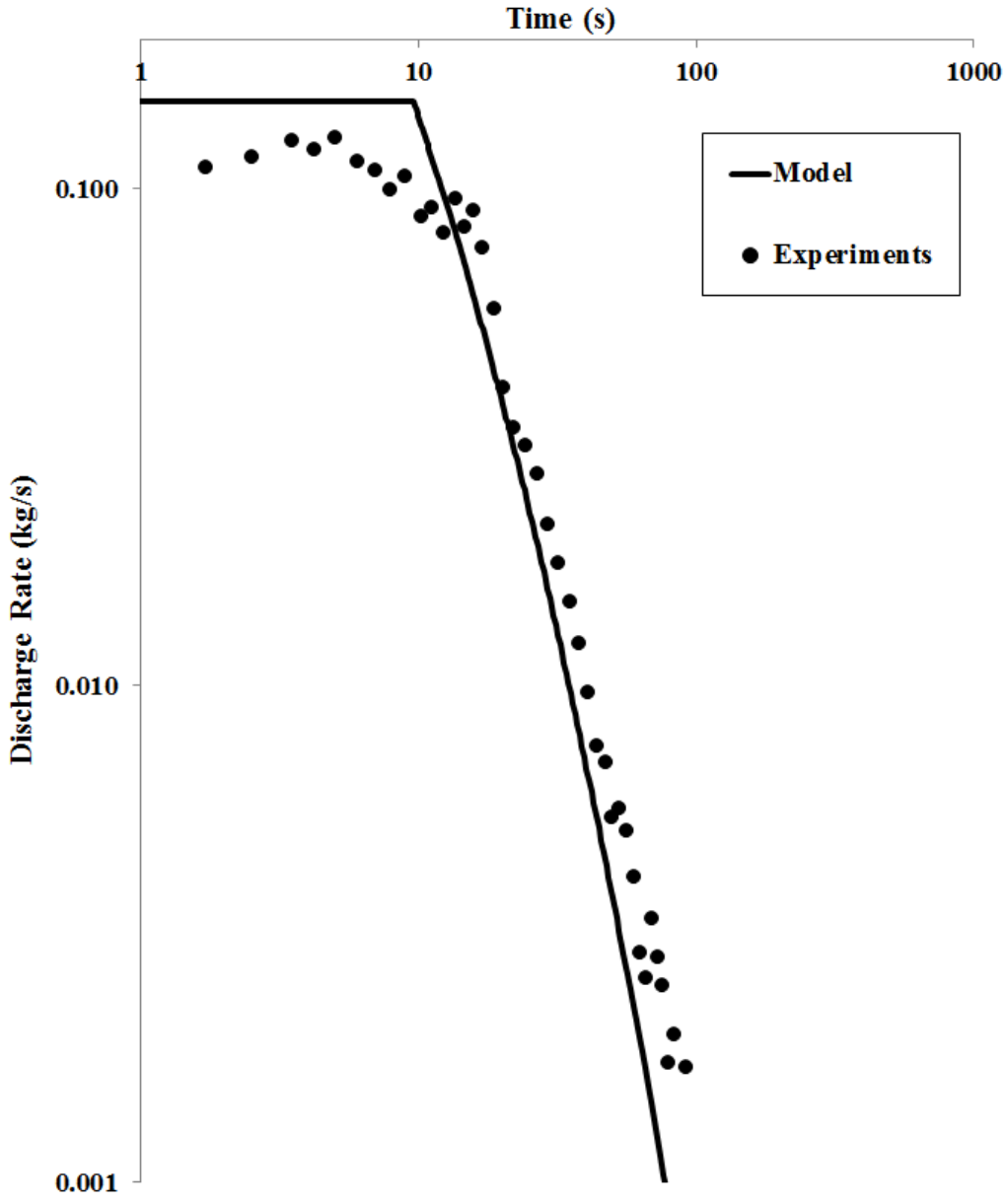

Figure 4.29: Comparison of the measured discharge rate with the predicted values from the model in logarithmic scale following full-bore rupture in an isolated horizontal pipe

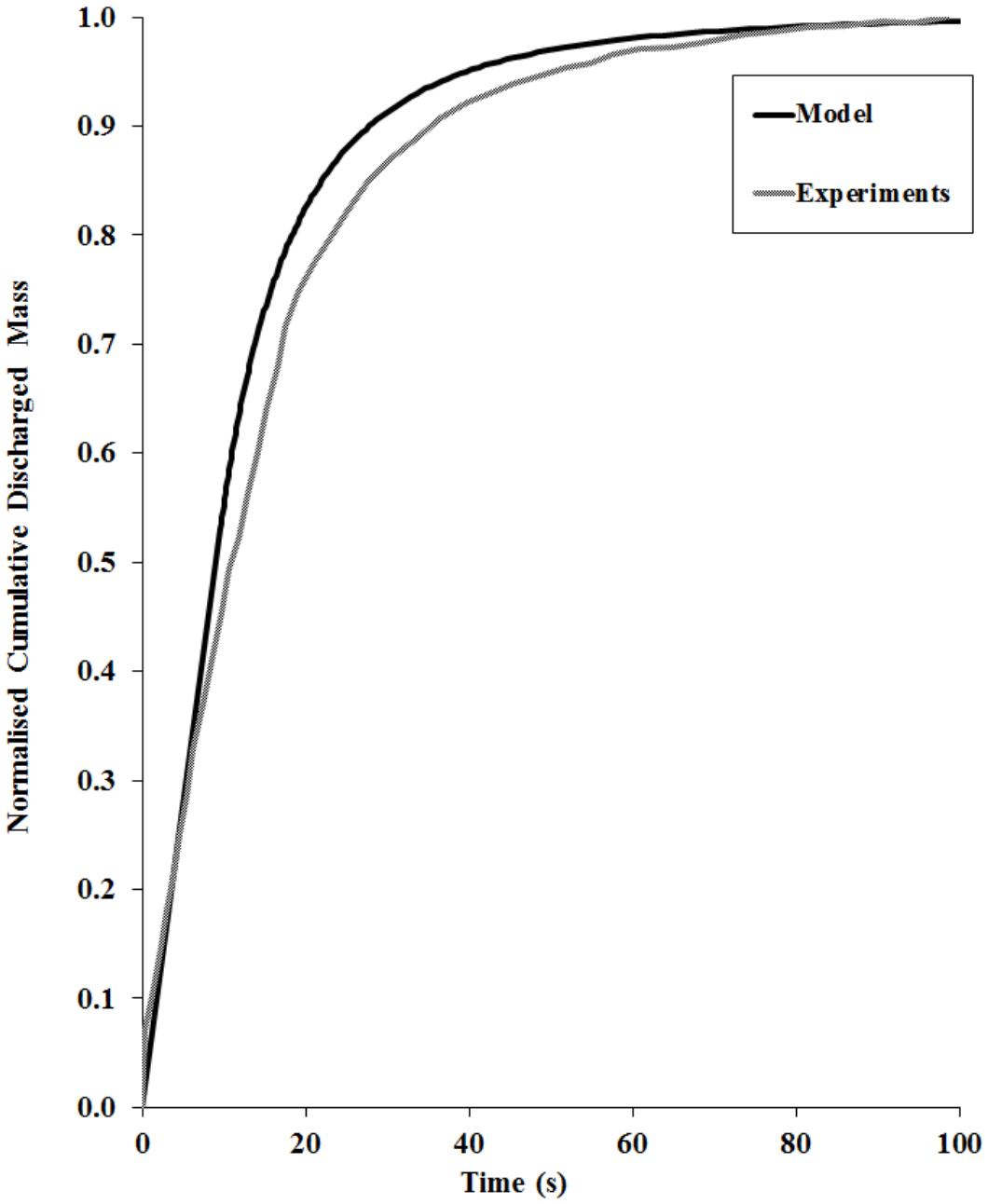

Figure 4.30: Comparison of the measured normalised cumulative discharged mass with the predicted values from the model following full-bore rupture in an isolated horizontal pipe

4.5. Conclusion

This chapter presented the formulation, verification and validation of mathematical models for simulating the transient outflow following full-bore rupture of a horizontal pipeline containing an incompressible liquid. Two configurations were considered for the system:

- Pipeline fed from an upstream storage tank
- Isolated pipeline where the pipe was closed at one end following emergency shut down

Historically, in order to model the transient discharge rate following full-bore rupture in a pipe attached to an upstream tank, the pipe was assumed to remain full throughout the discharge process. Based on this assumption, full pipe flow theory was then applied to simulate the outflow.

In this chapter, two additional flow regimes namely bubble formation and propagation, and open channel flow were modelled to simulate the complete drainage of the system.

In order to model the bubble formation and propagation along the pipe, Benjamin's (1968) proposed equation for bubble propagation velocity was used to calculate the velocity of the bubble formed at the pipe downstream. As suggested by Nicklin et al. (1962), the upstream bubble velocity was assumed to be a function of the downstream bubble velocity and the liquid velocity in the full section of the pipe. A value of 1.2 was employed for the empirical coefficient C_o as proposed experimentally by Bendiksen (1984) for the case of single, co-current bubble propagation in a horizontal pipe. By employing the above value for C_o and assuming critical flow throughout the pipe, a system of 6 equations was produced and solved simultaneously**,** giving 216° as solution for the liquid depth angle ϕ_c^{bf} .

Based on the assumption of negligible frictional loss during this regime, the calculated value for ϕ_c^{bf} was found to be independent of pipe characteristics such as pipe inner diameter and length. Based on this value and assuming a uniform, time-invariant liquid depth along the pipe, the discharge velocity and discharge rate during this regime were determined.

For the open channel flow, assuming a uniform critical depth along the pipe and negligible frictional loss, the transient flow mass balance equation was coupled with the critical discharge equation. The resulting integral was then solved numerically by employing trapezoidal rule. The final equation predicted the variation of ϕ_c^{bf} and consequently the discharge rate and velocity with time.

The overall model for the configuration with upstream tank was verified through parametric studies to investigate the impact of pipeline length and inner diameter on the discharge velocity, wetted area and cumulative discharged mass. It was observed that for all ranges of pipeline length and diameter, there was a small but rapid recovery in the discharge velocity at the transition from full pipe to bubble formation regime. The magnitude of this recovery increased with pipeline length, but decreased with pipe inner diameter due to impact of fluid/pipe wall frictional loss. This was believed to be the model artefacts and as a result of ignoring frictional loss during post-full pipe flow. Further investigations can clarify this matter.

In addition, it was shown that for long or large-diameter pipelines, majority of the mass was released during post-full pipe flow. Therefore, ignoring bubble propagation and open channel flow regimes would result in significant underestimation of released mass for such pipelines; sometimes by up to 50%.

Through series of experiments involving short pipes with low pipe roughness, the validity of the empirical coefficient $C_0 = 1.2$ suggested by Bendiksen (1984) for the case of single, co-current bubble propagation was tested for the case of upstream bubble propagation in the presence of downstream bubble and upstream storage tank. It was observed that the predicted results from the model by using the above value

for C_0 were in relatively good agreement with the experimental results, with less than 20% deviation on average. In addition, the angle ϕ_c^{bf} corresponding to the liquid depth below the bubble measured from the snapshots was 210°; remarkably close to the calculated value of 216° from the model.

In order to measure the accuracy of the model in predicting the discharge rate, the cumulative discharged mass was measured. The discharge rate was then calculated from the measured released mass. Based on the comparison with the experimental results it was observed that the proposed model significantly overestimated the discharge rate and consequently cumulative discharged mass during full pipe flow. It was found that the overestimation was due to additional entry loss (K) caused by the silicone sealant used at the pipe entrance to avoid leakage. The best fit to the experimental results was obtained for K = 2.5 instead of the original value of 0.5. With this value, apart from a short period of time at the beginning of discharge, the maximum deviation between the predicted and measured cumulative discharged mass reduced to 20% throughout the entire drainage.

The other flow configuration considered in this study was the full-bore rupture of an isolated horizontal pipeline with one closed-end. Given the absence of an upstream tank, only bubble formation and open channel flow were applicable here. The model based on the application of Benjamin's proposed bubble velocity equation along with the critical discharge equation produced 175° for ϕ_c^{bf} .

The model was also validated through a series of experiments by measuring the cumulative discharged mass and calculating the discharge rate. From the results it was observed that the discharge rate remained almost unchanged during the bubble propagation regime, in line with the assumption made in the model. The slight increase in the measured discharge rate towards the end of this regime was believed to be the result of the reduction in the frictional loss, although very small, as the bubble approached the closed-end.

Based on the validations results, it can be concluded that the developed models for a horizontal pipe with and without an upstream storage tank provide reasonably accurate results for sufficiently short pipes with a small value of pipe roughness. The applicability of the model for longer pipes with larger values of pipe roughness requires additional experimental work.

CHAPTER 5: IMPACT OF PIPELINE INCLINATION ANGLE ON THE OUTFLOW FROM PIPELINES

5.1. Introduction

Liquid transport pipelines are not always horizontal. A pipeline slope can vary from rather flat to almost vertical depending on the process specification or the pipe location terrain. Normally when the pipeline inclination is greater than 6^o, the pipe is called steep (Akan, 2006).

The full pipe flow model developed by Joye & Barrett (2003) is applicable to both horizontal and downward-inclined pipes and accounts for frictional losses for any inclination. However, as described in the previous chapter, in horizontal pipelines the fluid/pipe wall loss is negligible during post-full pipe flow due to low liquid velocity. However, in the case of downward-inclined pipelines, it needs to be taken into account.

This chapter first focuses on developing a mathematical model for bubble formation and open channel flow in downward-inclined pipelines fed from an upstream tank following full-bore rupture. The extension and modification of the model developed earlier for isolated horizontal pipelines to account for pipe inclination angle is presented next. For both configurations, the Darcy-Weisbach equation is employed instead of critical discharge formula to account for gravity and frictional losses. The above is followed by the main conclusions.

The overall models including full pipe flow (for the configuration with upstream tank), bubble formation and propagation, and open channel flow are tested through parametric studies and series of experiments.

5.2. Key Models Assumptions

The key assumptions listed in Section 4.2 for horizontal pipelines are also employed to the model for downward-inclined pipes.

5.3. Transient Hydraulic Flow Modelling Following Full-bore Rupture of Downward-inclined Pipelines

5.3.1. Introduction

This section is concerned with the development and testing of a mathematical model to simulate the outflow upon full-bore rupture in a downward-inclined pipeline fed from an upstream tank. Similar to the horizontal pipe, the model includes full pipe flow, bubble formation and propagation, and open channel flow.The full pipe flow model developed by Joye & Barrett (2003) is also used here to simulate the discharge during this regime.

During the bubble formation and propagation regime, two distinctive flow patterns can be assumed. The first pattern is similar to the flow behaviour in the horizontal pipe, i.e. bubbles propagating from both ends of the pipe. In the second pattern, due to the impact of pipe inclination angle, only the bubble formed at the pipe inlet will propagate along the pipe. At the pipe outlet, instead of a bubble, there will be a stagnant cavity which is washed away by the approaching upstream bubble at the end of this regime. In order to determine the prevailing pattern, the predicted drift velocity (u_{drift}), described in Section 3.3.1, is compared against the liquid velocity in the full section of the pipe (u). For pipes with u lower than u_{drift} the first pattern is applicable, whereas the second pattern is dominant in pipes with equal or higher u than u_{drift}.

Therefore, in this chapter first the previously developed model for the horizontal pipe is modified by introducing the inclination angle, based on the assumption of two bubbles propagating towards one another. This is then followed by an alternative model for the second pattern where the bubble only propagates from the upstream of the pipe. The two models are then tested through a sensitivity analysis by studying

the impact of pipeline length, inner diameter and pipe inclination angle on the liquid velocity in the full section of the pipe (u). Based on the results and by applying the drift velocity method, the dominant pattern is determined for various pipeline characteristics. The acuracy of the corresponding model is assessed through series of experiments.

In addition, the impact of the above pipeline characteristics on the discharge velocity, wetted area and cumulative discharged mass is studied. Ultimately, based on the results from the parametric studies, an approximate relationship between the starting angle for open channel flow, ϕ_n^{bf}, and the inclination angle, θ, is established.

5.3.2. Model Theory

5.3.2.1. Full Pipe Flow

Similar to model for the case of a horizontal pipeline, Equation (4.4) is used to calculate the transient discharge velocity for full pipe flow:

$$u_d = \frac{-g}{1.5+\frac{4fL}{D}}\left(\frac{A}{A_{\tan k}}\right)t + \sqrt{\frac{gZ_0}{0.75+\frac{2fL}{D}}} \qquad \textbf{(4.4)}$$

and in terms of discharge rate $\dot{m}_d$:

$$\dot{m}_d = \rho A\left[\frac{-g}{1.5+\frac{4fL}{D}}\left(\frac{A}{A_{\tan k}}\right)t + \sqrt{\frac{g(H_0+L\sin\theta)}{0.75+\frac{2fL}{D}}}\right] \qquad \textbf{(5.1)}$$

where Z_0 is replaced by $H_0+Lsin\theta$ with θ being the angle of the pipe exit with a horizontal level. Figure 5.1 presents a downward-inclined pipe with full pipe flow fed from an upstream tank.

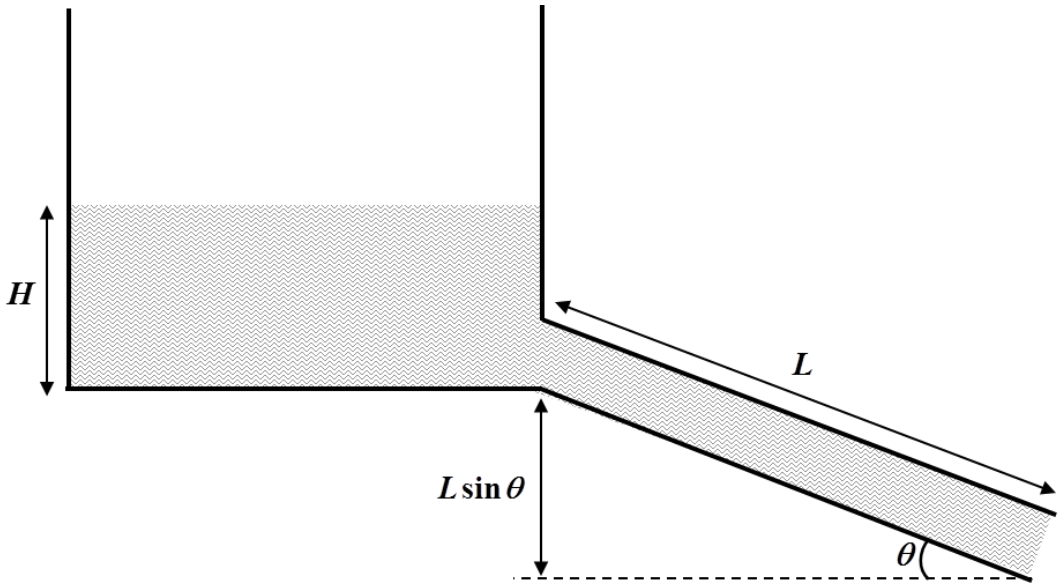

Figure 5.1: Full pipe flow in a downward-inclined pipe fed from an upstream storage tank

For the previously considered case of a horizontal pipe (see Section 4.3.2.1), it was assumed that the dominant regime in the pipe was full pipe flow until the liquid level in the tank H reduced to the critical depth d_c^{bf}. For the currently considered case of a downward-inclined pipe, it is assumed that the dominant regime in the pipe is full pipe flow throughout the drainage of the tank, i.e. until $H = 0$.

5.3.2.2. Bubble Formation & Propagation

Bubble formation and propagation regime commences after the tank drains dry. In a horizontal pipe, upon rupture there will be two bubbles propagating towards each other from the pipe inlet and outlet. In downward-inclined pipes, there are two possibilities for the bubble propagation pattern along the pipe:

1) Similar to the horizontal pipe, the upstream and downstream bubbles propagate towards each other along the pipe.

2) The bubble only propagates from the pipe inlet (upstream), while a stagnant cavity forms at the pipe outlet. This cavity will be washed away by the approaching upstream bubble at the end of this regime.

The models for the two flow patterns are described in the following sections. Based on the application of the drift velocity method the applicability of each pattern is investigated later in Section 5.3.3.1 for a range of pipeline characteristics. In both cases, for simplicity the bubble curvature is ignored.

5.3.2.2.1. Bubble Propagation from Both Ends

Figure 5.2 shows a downward-inclined pipe with bubble formation and propagation from both ends. Similar to the case of the horizontal pipe, the liquid depth below the bubbles and consequently the discharge rate are assumed to remain constant during this regime.

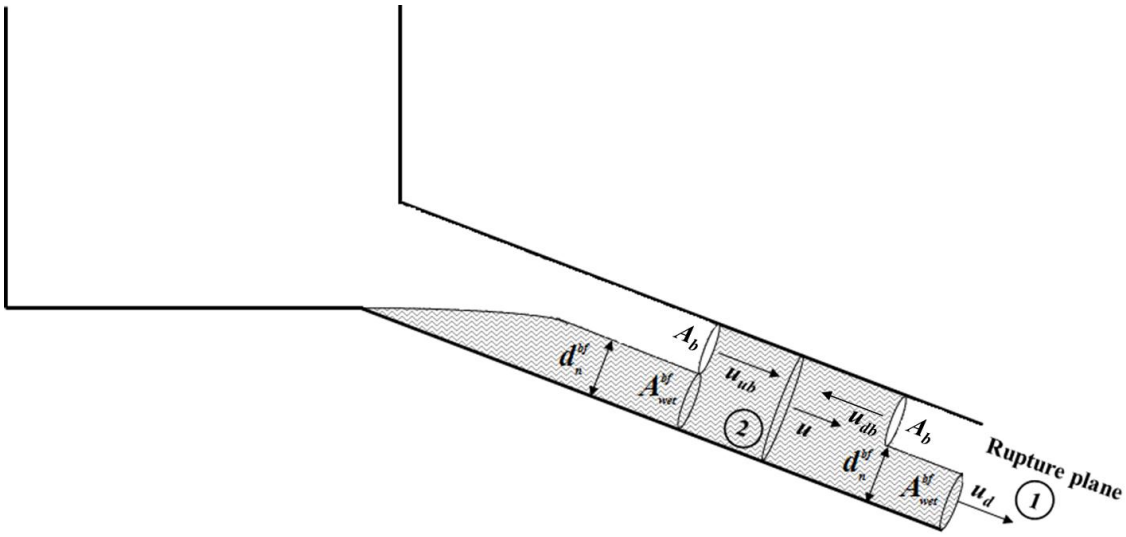

Figure 5.2: Bubble propagation from both ends of a downward-inclined pipe fed from an upstream storage tank

As described in Section 2.3.5, in downward-inclined pipes the liquid depth is the same as the normal depth d_n. Thus, the discharge velocity may be calculated from the

Darcy-Weisbach equation (Equation (3.43)) for $\phi = \phi_n^{bf}$ where ϕ_n^{bf} denotes the constant, time-invariant ϕ corresponding to normal depth during bubble propagation regime:

$$u_d = \sqrt{\frac{S_0 g D}{2f}\left(\frac{\phi_n^{bf} - \sin\phi_n^{bf}}{\phi_n^{bf}}\right)} \tag{5.2}$$

S_o, the pipe slope, is defined by the ratio of the vertical pipe elevation and the pipe length and is therefore equal to $\sin\theta$.

The discharge rate is calculated from $\dot{m}_d = Q_d \rho$ by replacing Q_d from Equation (3.45) for $\phi = \phi_n^{bf}$:

$$\dot{m}_d = \rho\sqrt{\frac{S_0 g D}{2f}\left(\frac{\phi_n^{bf} - \sin\phi_n^{bf}}{\phi_n^{bf}}\right)}\frac{D^2}{8}\left(\phi_n^{bf} - \sin\phi_n^{bf}\right) \tag{5.3}$$

or

$$\dot{m}_d = \rho\frac{D^{2.5}}{8}\sqrt{\frac{S_0 g}{2f\phi_n^{bf}}}\left(\phi_n^{bf} - \sin\phi_n^{bf}\right)^{1.5} \tag{5.4}$$

In addition, the corresponding liquid depth below the bubbles, d_n^{bf}, is given by:

$$d_n^{bf} = \frac{D}{2}\left(1 - \cos\frac{\phi_n^{bf}}{2}\right) \tag{5.5}$$

Recalling Equation (4.10) based on the application of continuity equation between sections 1 and 2 in Figure 5.2, the liquid velocity in the full section of the pipe is calculated via:

$$u = \frac{u_d A_{wet}^{bf}}{A} \tag{4.10}$$

In addition, similar to the horizontal pipe, at any given time the volumetric flow rate of the discharging liquid equals that of air entering the pipe. Therefore, the discharge velocity may also be calculated from Equation (4.13):

$$u_d = \frac{\left(A - A_{wet}^{bf}\right)\left(u_{ub} + u_{db}\right)}{A_{wet}^{bf}} \tag{4.13}$$

where A_{wet}^{bf} is calculated from Equation (3.30) for $\phi = \phi_n^{bf}$:

$$A_{wet}^{bf} = \frac{D^2}{8}\left(\phi_n^{bf} - \sin\phi_n^{bf}\right) \tag{5.6}$$

The downstream bubble propagation or the drift velocity (u_{db}) for inclined pipes has been correlated by Bendiksen (1984) as a weighted superposition of the drift velocity in vertical and horizontal flow (Equation (3.21)):

$$u_{drift} = u_{db} = 0.542\sqrt{gD}\cos\theta + 0.350\sqrt{gD}\sin\theta \tag{3.21}$$

Despite various studies on bubble propagation velocity, there is no universally accepted formula to calculate the downstream bubble propagation velocity in downward-inclined pipes (Little, 2002). The above equation is known as the most common formula for bubble propagation velocity in downward-inclined pipes and has been cited by many authors (see for example Little (2002), Inogamov & Oparin (2003) and Pothof (2011)). As such, in this study it is used to calculate the downstream bubble propagation velocity.

For upstream bubble velocity (u_{ub}) the equation proposed by Nicklin et al. (1962) (Equation (3.25)) is applicable to the downward-inclined pipes with the empirical coefficient C_0 = 0.98 for $\theta \leq 30^o$ (Bendiksen, 1984). In Bendiksen's setup, the pipe was open at one end, while the constant liquid inlet flow rate was achieved through presetting the pressure reduction and throttling valves (Bendiksen, 1984). The pressurised air was injected to the pipe to form a bubble. Despite the differences between Bendiksen's setup and the configuration considered in this study, due to lack of information, the same value for C_0 is used for all ranges of $0 < \theta < 90^o$. The validity of this assumption is investigated through experiments in Section 5.3.4.1.

Therefore, recalling Equation (3.25) and replacing C_0 and u_{moving} with 0.98 and u_{ub} produces:

$$u_{ub} = u_{drift} + 0.98u \tag{5.7}$$

u_{drift} is also the same as u_{db}. Replacing u, u_{db} and u_{ub} from equations (4.10), (3.21) and (5.7) into Equation (4.13) gives:

$$u_d = \frac{\left(A - A_{wet}^{bf}\right)\left(1.084\sqrt{gD}\cos\theta + 0.700\sqrt{gD}\sin\theta + 0.98\left(\frac{u_d A_{wet}^{bf}}{A}\right)\right)}{A_{wet}^{bf}} \tag{5.8}$$

or replacing A_{wet}^{bf} from Equation (5.6):

$$u_d = \frac{\sqrt{gD}\left(1.084\cos\theta + 0.700\sin\theta\right)\left(2\pi - \phi_n^{bf} + \sin\phi_n^{bf}\right)}{\left(\phi_n^{bf} - \sin\phi_n^{bf}\right)\left(1 - \frac{0.98\left(2\pi - \phi_n^{bf} + \sin\phi_n^{bf}\right)}{2\pi}\right)} \tag{5.9}$$

Finally equating equations (5.2) and (5.9) provides ϕ_n^{bf} as a function of θ:

$$\frac{\left(1.084\cos\theta+0.700\sin\theta\right)\left(2\pi-\phi_n^{bf}+\sin\phi_n^{bf}\right)}{\left(1-\frac{0.98\left(2\pi-\phi_n^{bf}+\sin\phi_n^{bf}\right)}{2\pi}\right)} - \sqrt{\frac{\sin\theta}{2f\phi_n^{bf}}}\left(\phi_n^{bf}-\sin\phi_n^{bf}\right)^{1.5}=0 \quad \textbf{(5.10)}$$

Knowing θ and *f*, the above equation needs to be solved iteratively for ϕ_n^{bf}.

5.3.2.2.2. Bubble Propagation Only from the Upstream End of the Pipe

In this case there is only the upstream bubble which propagates along the pipe, thus u_{db} = 0. The equations presented in Section 5.3.2.2.1 remain unchanged, except Equation (4.13). In this case, the volume of the discharging liquid is equal to the volume of upstream bubble only. Therefore, assuming a stagnant cavity at the pipe downstream (u_{db}=0) with the same area A_b as the upstream bubble, Equation (4.13) is modified as:

$$u_d=\frac{\left(A-A_{wet}^{bf}\right)\left(u_{ub}\right)}{A_{wet}^{bf}} \quad \textbf{(5.11)}$$

Thus, replacing u_{ub}, u_{db} and A_{wet}^{bf} from equations (5.7)**,** (3.21) and (5.6) respectively into Equation (5.11) gives:

$$u_d=\frac{\sqrt{gD}\left(0.542\cos\theta+0.350\sin\theta\right)\left(2\pi-\phi_n^{bf}+\sin\phi_n^{bf}\right)}{\left(\phi_n^{bf}-\sin\phi_n^{bf}\right)\left(1-\frac{0.98\left(2\pi-\phi_n^{bf}+\sin\phi_n^{bf}\right)}{2\pi}\right)} \quad \textbf{(5.12)}$$

The discharge rate is then calculated using the above equation and Equation (5.6):

$$\dot{m}_d = \rho A_{wet}^{bf} u_d = \frac{\rho D^2 \sqrt{gD}\left(0.542\cos\theta + 0.350\sin\theta\right)\left(2\pi - \phi_n^{bf} + \sin\phi_n^{bf}\right)}{8\left(1 - \frac{0.98\left(2\pi - \phi_n^{bf} + \sin\phi_n^{bf}\right)}{2\pi}\right)} \quad \textbf{(5.13)}$$

Finally equating equations (5.2) and (5.12) and substituting S_0 by $\sin\theta$ provides ϕ_n^{bf} as function of θ and f:

$$\frac{\left(0.542\cos\theta + 0.350\sin\theta\right)\left(2\pi - \phi_n^{bf} + \sin\phi_n^{bf}\right)}{\left(1 - \frac{0.98\left(2\pi - \phi_n^{bf} + \sin\phi_n^{bf}\right)}{2\pi}\right)} - \sqrt{\frac{\sin\theta}{2f\phi_n^{bf}}}\left(\phi_n^{bf} - \sin\phi_n^{bf}\right)^{1.5} = 0 \quad \textbf{(5.14)}$$

Knowing θ and f, the above equation needs to be solved iteratively for ϕ_n^{bf}.

5.3.2.3. Open Channel Flow

As discussed in Section 2.3.5, in downward-inclined pipes (steep channels) the free fall does not have any impact on the flow depth. Therefore, far away from the pipe inlet, the flow remains uniform with the liquid depth being equal to the normal depth along the pipe. Figure 5.3 presents a downward-inclined pipe with open channel flow along the pipe.

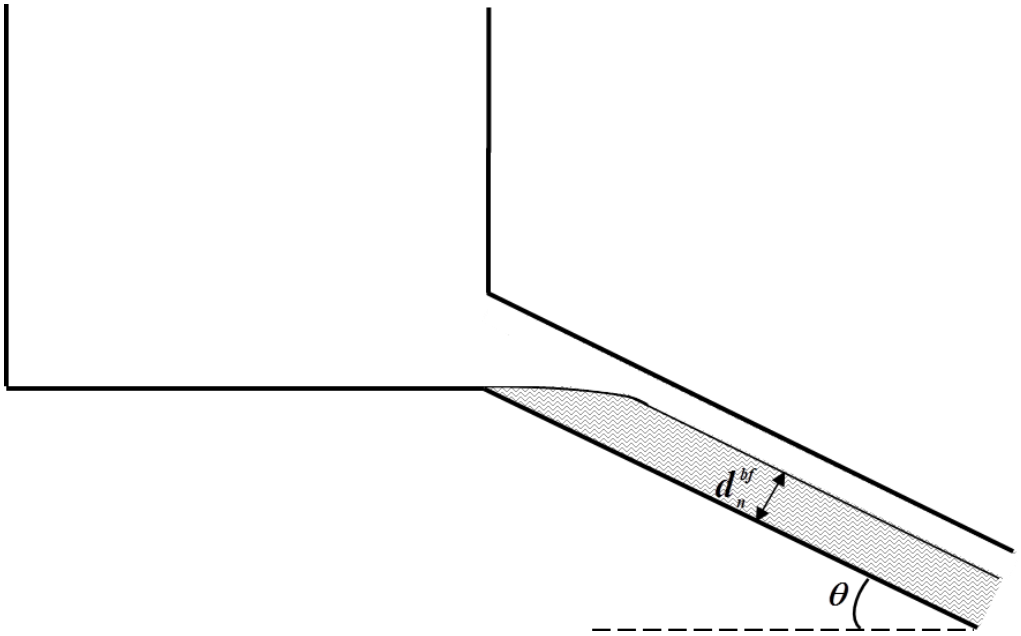

Figure 5.3: Open channel flow in a downward-inclined pipe fed from an upstream storage tank

Following the same approach as for the case of a horizontal pipeline, a transient flow mass balance representing the rate of mass loss from the storage tank (Equation (3.2)) is employed here. But instead of the critical discharge velocity equation, it is combined with the Darcy-Weisbach equation (Equation (3.45)):

$$\frac{dM}{dt} = -\rho \frac{D^{2.5}}{8} \sqrt{\frac{g \sin\theta}{2 f \phi_n}} \left(\phi_n - \sin\phi_n\right)^{1.5} \qquad \textbf{(5.15)}$$

where S_0 is substituted by $\sin\theta$. Here ϕ_n reduces with time from its initial value ϕ_n^{bf} at the start of open channel flow. In this model, it is assumed that the tank drains dry before the bubble formation starts. Therefore, only the mass inside the pipe needs to be considered. As such, replacing M by $A_{wet} L \rho$ into the above equation produces:

$$\frac{d\left(LA_{wet}\rho\right)}{dt} = -\rho \frac{D^{2.5}}{8} \sqrt{\frac{g \sin\theta}{2 f \phi_n}} \left(\phi_n - \sin\phi_n\right)^{1.5} \qquad \textbf{(5.16)}$$

or

$$\frac{dA_{wet}}{\frac{D^{2.5}}{8}\rho\sqrt{\frac{g\sin\theta}{2f\phi_n}}\left(\phi_n-\sin\phi_n\right)^{1.5}}=-\frac{dt}{\rho L} \qquad \textbf{(5.17)}$$

At the initial time t_0 = 0 at the onset of open channel flow, $A_{wet} = A_{wet}^{bf}$ which is calculated from Equation (5.6). Based on this, integrating the above equation between t = 0 and an arbitrary time t produces:

$$\int_{A_{wet}^{bf}}^{A_{wet}}\frac{dA_{wet}}{\frac{D^{2.5}}{8}\rho\sqrt{\frac{g\sin\theta}{2f\phi_n}}\left(\phi_n-\sin\phi_n\right)^{1.5}}=-\frac{t}{\rho L} \qquad \textbf{(5.18)}$$

Similar to the horizontal pipe, trapezoidal rule, presented in Figure 4.5, is used to estimate the above integral (I_i) numerically except that here $\phi_1 = \phi_n^{bf}$ instead of 216^o and $\dot{m}_{d,i}$ is calculated from Equation (3.45). Once I_i is determined, the corresponding time t_i is calculated via Equation (4.59):

$$t_i = I_i \rho L \qquad \textbf{(4.59)}$$

5.3.3. Parametric Studies

In the previous section, the formulation of the flow equations to calculate the transient discharge rate from downward-inclined pipelines following full-bore rupture was presented. The model included successive regimes of full-pipe flow, bubble formation and propagation, and open channel flow. Two patterns for bubble propagation were modelled based on the assumption of two bubble and single bubble propagation along the pipe.

This section first focuses on the verification and testing of the models developed for the two patterns through a sensitivity analysis. For a range of pipeline characteristics including pipeline length, inner diameter and inclination angle, the calculated drift

velocity, u_{drift}, is compared against the liquid velocity in the full section of the pipe, u. For pipes with $u < u_{drift}$ the first pattern is applicable where the upstream and downstream bubbles propagate towards each other. The second pattern is dominant in pipes with $u \geq u_{drift}$.

For downward-inclined pipelines, in addition to pipeline length and inner diameter, the impact of pipe inclination angle (θ) on the discharge velocity u_d, the wetted area A_{wet}, and the cumulative discharged mass is also studied. Finally, an approximate relation between θ and ϕ_n^{bf} in downward-inclined pipes connected to an upstream tank is established based on the results from the parametric studies.

Table 5.1 presents the base case test conditions employed in the investigations. The cylindrical storage tank is assumed to have a cross sectional area of $5m^2$ and is connected to a 100m long, 0.406m diameter pipe. The pipe is declined by $\theta=30^o$ relative to a horizontal level. The tank is filled with water up to a depth of 5m prior to pipe failure. A pipe roughness of 0.05mm is assumed during full pipe flow, bubble formation and propagation, and open channel flow. Unless otherwise specified, the characteristics given in the table are assumed to apply throughout the investigations.

Tank cross sectional area, A_{tank} (m^2)	5
Initial liquid head in the tank, H_o (m)	5
Inventory	Water
Pipeline inner diameter, D (m)	0.406
Pipeline length, L (m)	100
Pipe roughness, ε (mm)	0.05
Pipeline inclination angle, θ (^{o})	30

Table 5.1: Outflow simulations test conditions for full-bore rupture scenario in a downward-inclined pipe fed from an upstream tank

5.3.3.1. Comparison of the Two Models for Bubble Propagation

As described in Section 3.3.1, a stagnant cavity/bubble forms at the pipe outlet only if the liquid velocity in the full section of the pipe (u) is higher or equal to the drift velocity defined via Equation (3.21) (Bendiksen, 1984):

$$u_{drift} = 0.542\sqrt{gD}\cos\theta + 0.35\sqrt{gD}\sin\theta \quad \textbf{(3.21)}$$

If u falls below u_{drift}, the bubble starts propagating towards the pipe upstream. This theory is used to determine the prevailing pattern in downward-inclined pipes.

Table 5.2 shows the calculated liquid velocity (u) for a range of pipeline length, inner diameter and inclination angle from both models, along with the corresponding drift velocity.

Scenario			**Liquid velocity (m/s)**		**Drift velocity (m/s)**
Length (m)	Diameter (m)	θ (^{o})	Bubble at both ends	Bubble only at Pipe inlet	
100	0.152	30	3.100	2.149	0.788
100	0.254	30	4.097	2.863	1.017
100	0.356	30	4.964	3.422	1.204
100	0.406	30	5.302	3.702	1.285
10	0.406	30	5.302	3.702	1.285
50	0.406	30	5.302	3.702	1.285
200	0.406	30	5.302	3.702	1.285
100	**0.406**	**0.1**	**0.850**	**0.695**	**1.082**
100	0.406	1	1.874	1.413	1.094
100	0.406	6	3.286	2.369	1.148

Table 5.2: Comparison of the predicted liquid velocity in the full section of the pipe (u) by two models: 1. bubble propagation from both ends, 2. bubble propagation only from the pipe inlet

As it may be observed from the table, the predicted u by the model for the pattern with bubble propagation from both ends is always higher than that of the pattern with only upstream bubble propagation. This is expected as the propagation of two bubbles increases the liquid discharge rate and consequently the liquid velocity in the full section of the pipe. However, comparing the predicted velocities with the drift velocity, it is clear that except for nearly horizontal pipe (θ=0.1^o), u is always higher than u_{drift}. This finding confirms that the assumption of bubble propagation from both ends is only valid for as long as the pipe is nearly horizontal. For other values of θ, regardless of pipeline characteristics, the bubble only propagates from the pipe upstream while a stagnant cavity is formed at the pipe outlet .Based on this

finding, the next section is concerned with the parametric studies for the model for the second pattern, i.e. bubble propagation only from pipe inlet. The impact of pipeline length, inner diameter and θ on the discharge velocity and wetted area is investigated.

5.3.3.2. Discharge Velocity and Wetted Area

This section presents the results from the parametric studies for the impact of pipeline characteristics on the discharge velocity and wetted area (A_{wet}). In addition to pipeline length and inner diameter, the sensitivity analysis is also conducted for the pipe inclination angle (θ).

As described in the previous section, except for nearly horizontal pipes, the bubble only propagates from the pipe inlet. Therefore, the second model presented in Section 5.3.2.2.2 is employed to calculate the discharge velocity and wetted area. The pipeline length, inner diameter and pipe inclination angle vary in the ranges 50-200m, 0.356-0.457m and 5-50° respectively.

Figure 5.4-5.5, Figure 5.6-5.7 and Figure 5.8-5.9 respectively show the variation of normalised wetted area and discharge velocity with time for various pipeline length, inner diameter and pipe inclination angle. Here the normalised wetted area is defined as A_{wet}/A, i.e. the fraction of the wetted area relative to the overall pipe cross sectional area.

The trend for the graphs is similar to those for horizontal pipe, presented in Section 4.3.3.1. Following the rapid linear drop corresponding to the discharge during full pipe flow, the rapid recovery in the discharge velocity is only present for certain scenarios. It may be observed from the figures that the recovery only occurs for the shortest pipe, i.e. L = 50m. This recovery degenerates with the pipeline length up to a point that the discharge velocity drops at the transition from full-pipe to bubble-formation regime.

This can be explained by the fact that in downward-inclined pipes, pipeline length acts as an additional liquid head. For long pipelines, due to the presence of large

additional liquid head, $Lsin\theta$, the impact of entry loss present during full pipe flow is negligible. Thus, the discharge velocity at the end of full pipe flow will be higher than that of bubble formation and propagation regime.

On the other hand, the magnitude of the recovery in the discharge velocity at the transition from full pipe to bubble formation regime increases with pipe inner diameter. This can be explained by the inverse proportionality of liquid/wall loss with the pipe inner diameter. Consequently, for small diameter pipes the pipe entry loss is negligible comparing to fluid/wall loss, resulting in a higher discharge velocity at the end of full pipe flow due to the presence of additional liquid head.

Finally, comparing equations (4.3) and (5.2) for the discharge velocity during bubble formation and full pipe flow, it may be observed that for both regimes, the discharge velocity increases with pipe inclination angle (θ):

$$u_d = \sqrt{\frac{g\left(H + L\sin\theta\right)}{0.75 + \frac{2fL}{D}}} \qquad \textbf{(4.3)}$$

$$u_d = \sqrt{\frac{g\sin\theta}{\frac{2f}{D}}\left(\frac{\phi_n^{bf} - \sin\phi_n^{bf}}{\phi_n^{bf}}\right)} \qquad \textbf{(5.2)}$$

However, the rate of increase in the discharge velocity is higher in full pipe flow due to the presence of L in the nominator. The recovery in the discharge velocity decreases with θ due to presence of larger liquid head, to a point that the discharge velocity drops at the transition to bubble propagation regime.

The variation of A_{wet} for full pipe flow in downward-inclined pipe is similar to horizontal pipe, producing normalised A_{wet} = 1. During bubble formation and propagation regime, as it may be observed from the figures, normalised A_{wet} is the same for all pipeline lengths and diameters and equal to 0.248. This is because of all pipeline characterises considered here, ϕ_n^{bf} is only a function of θ (see Equation

(5.14)). Consequently, as it can be seen from Figure 5.8 and Figure 5.9, normalised A_{wet} reduces with θ, as a result of reduction in ϕ_n^{bf}. The variation of ϕ_n^{bf} with θ is discussed in detail in Section 5.3.3.4.

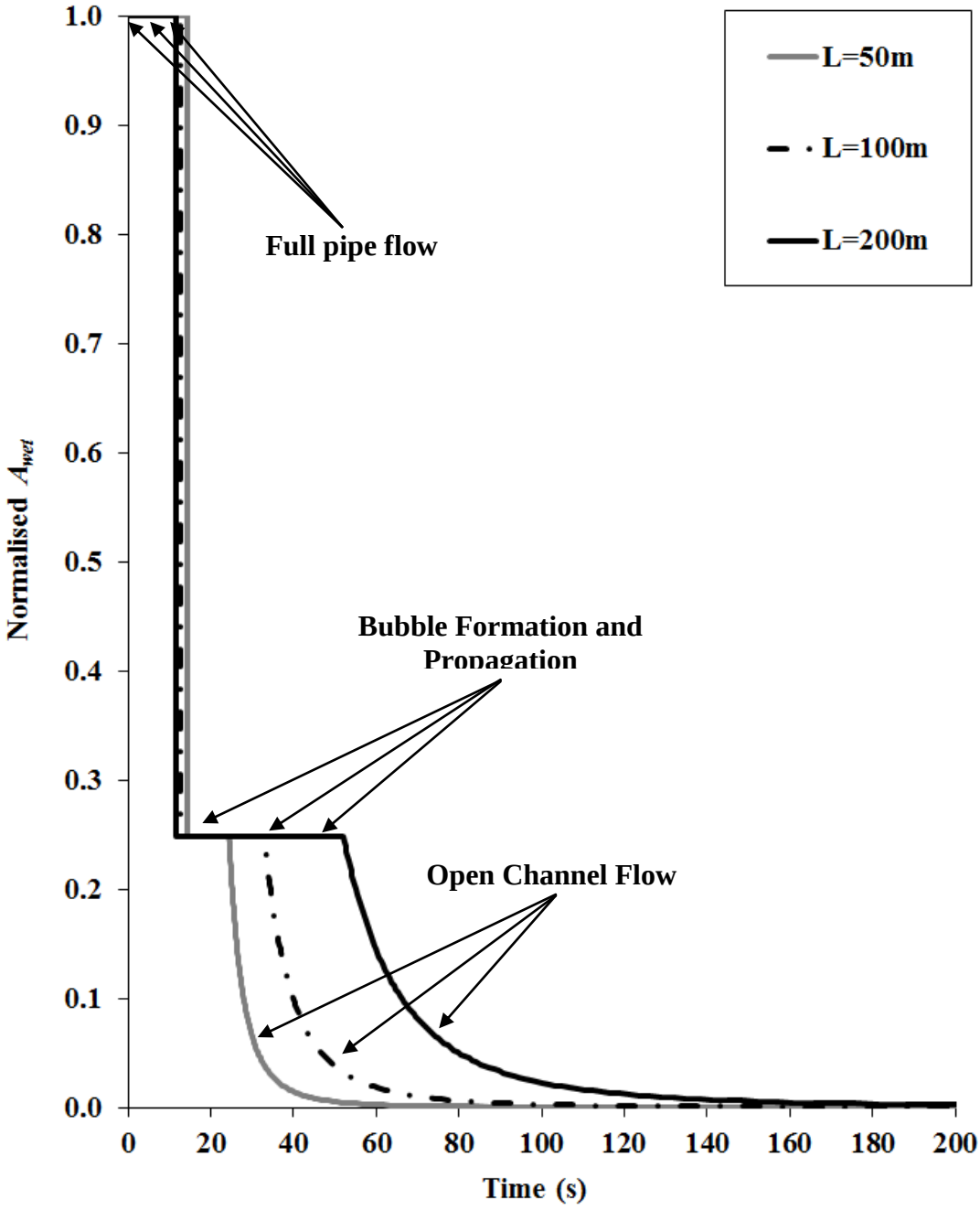

Figure 5.4: Impact of pipeline length on the variation of normalised A_{wet} with time following full-bore rupture in a 0.406m diameter, 30^o downward-inclined pipe fed from an upstream tank

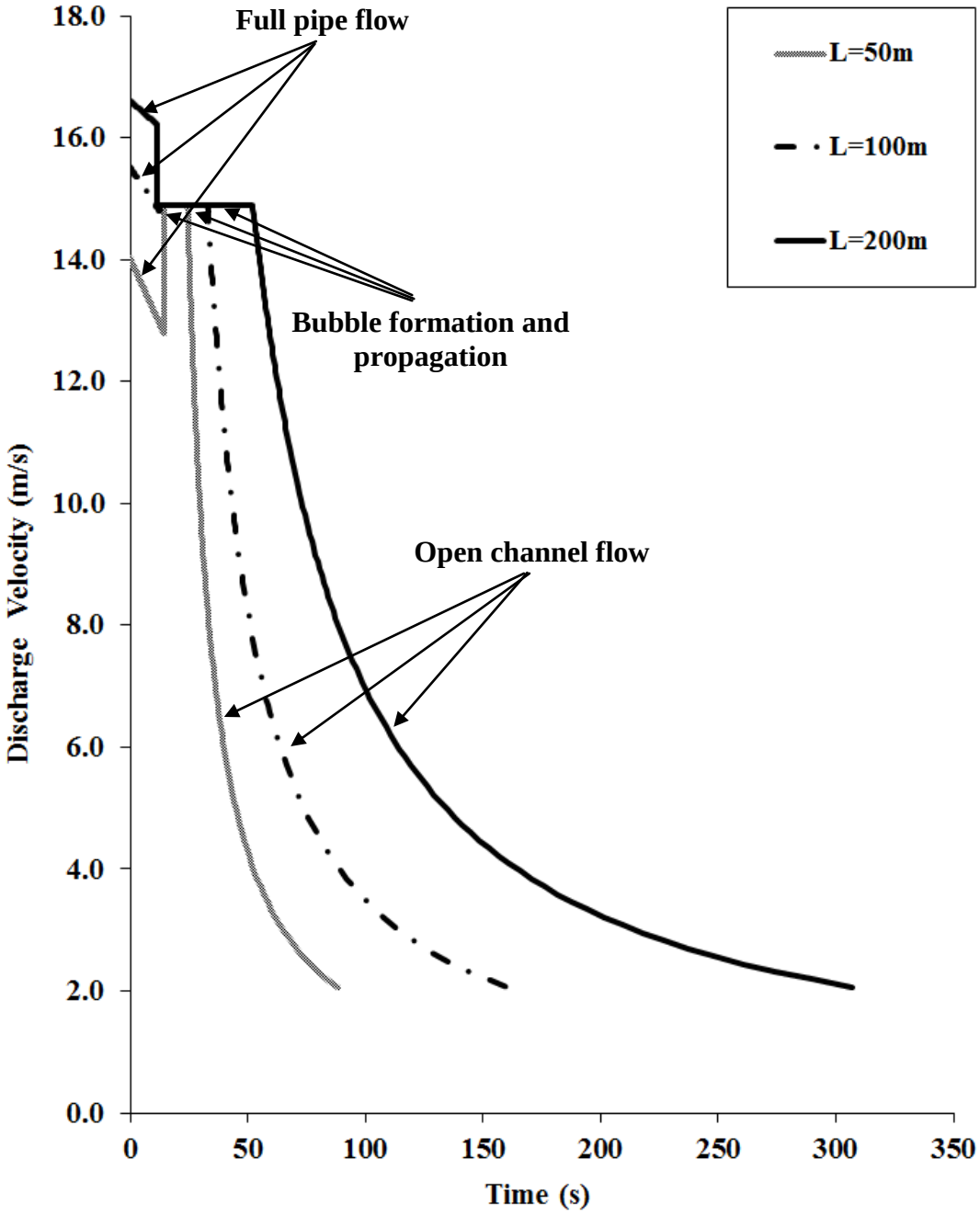

Figure 5.5: Impact of pipeline length on the variation of discharge velocity following full-bore rupture in a 0.406m diameter, 30^{o} downward-inclined pipe fed from an upstream tank

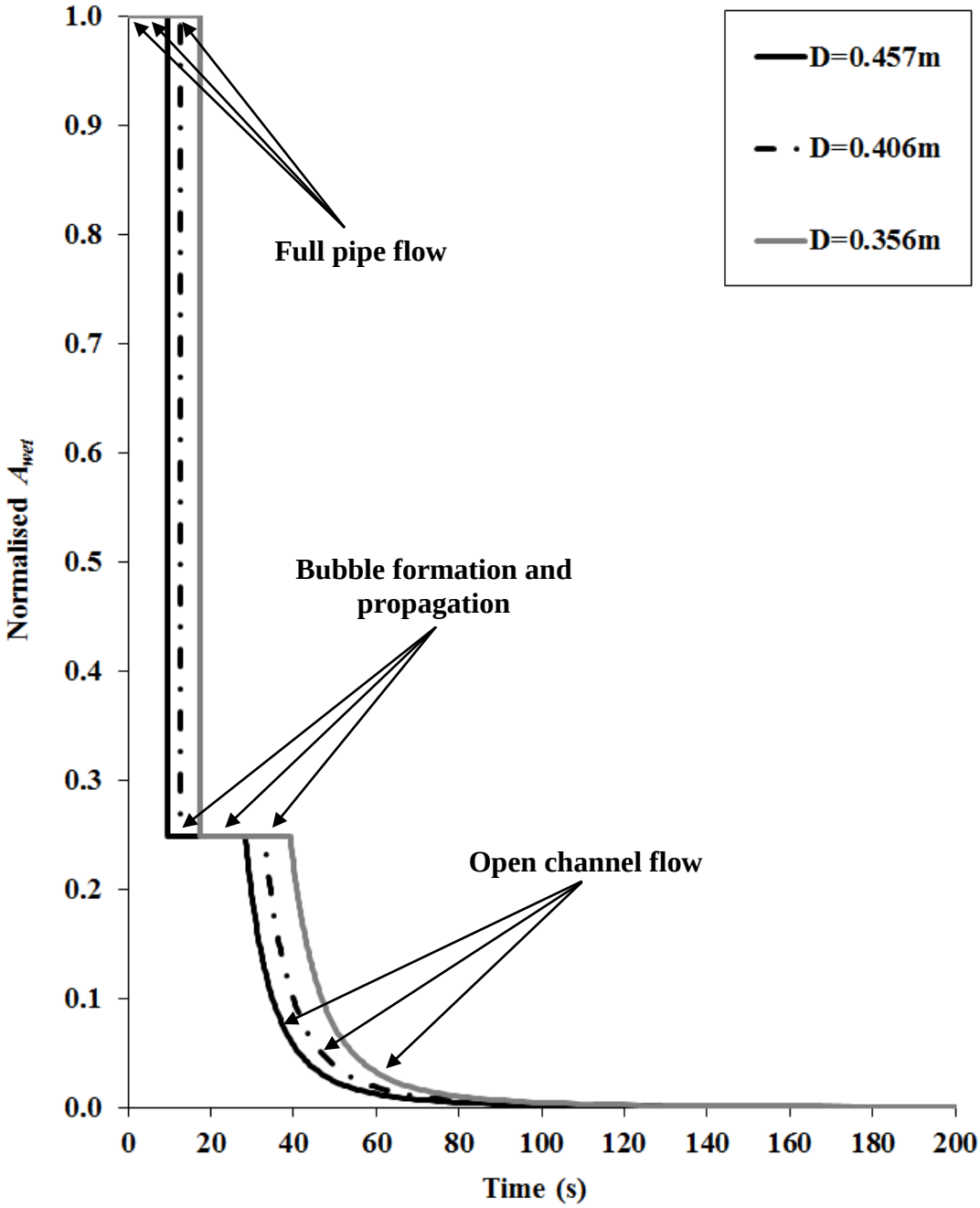

Figure 5.6: Impact of pipeline inner diameter on the variation of normalised A_{wet} following full-bore rupture in a 100m long, 30^o downward-inclined pipe fed from an upstream tank

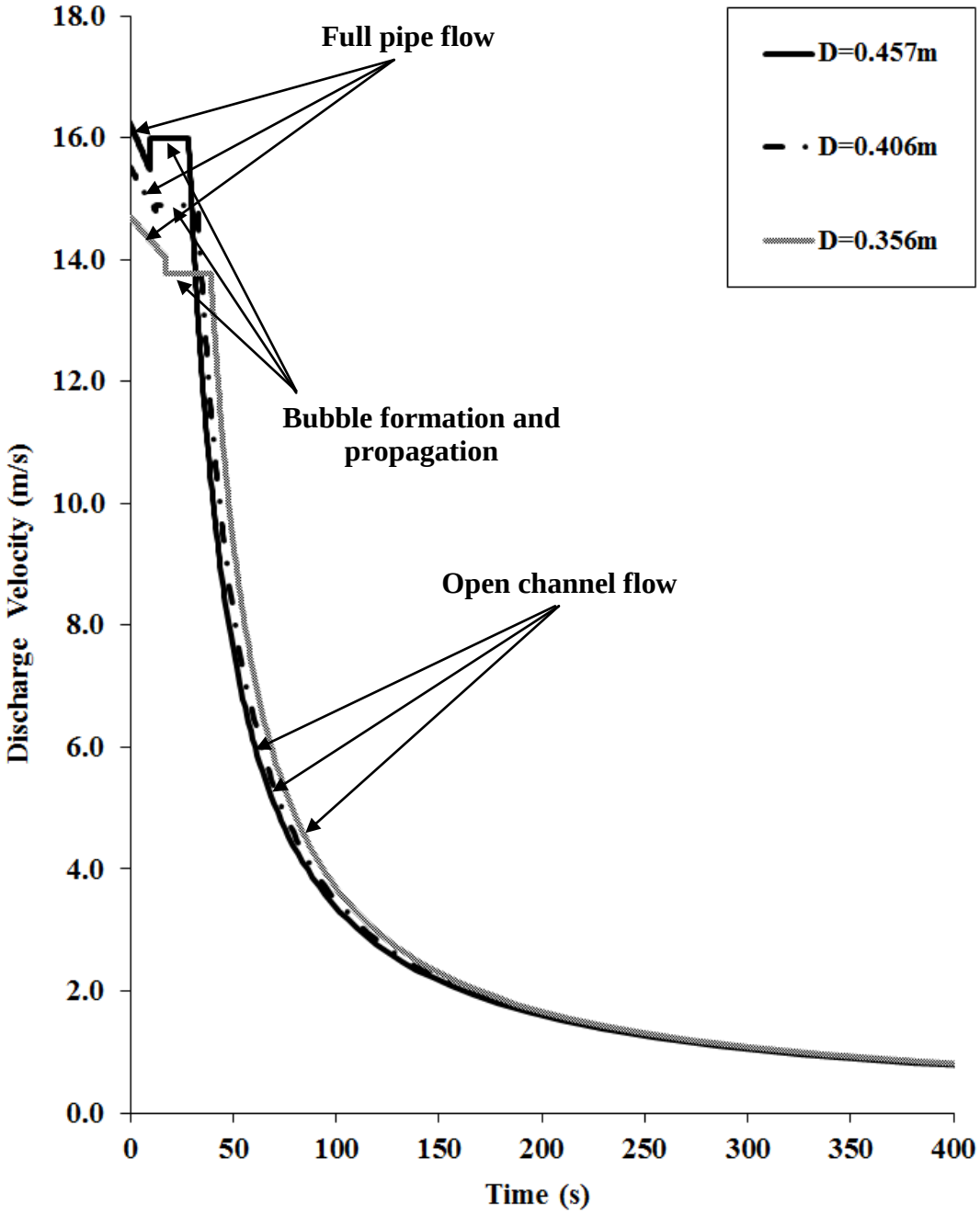

Figure 5.7: Impact of pipeline inner diameter on the variation of discharge velocity following full-bore rupture in a 100m long, 30^{o} downward-inclined pipe fed from an upstream tank

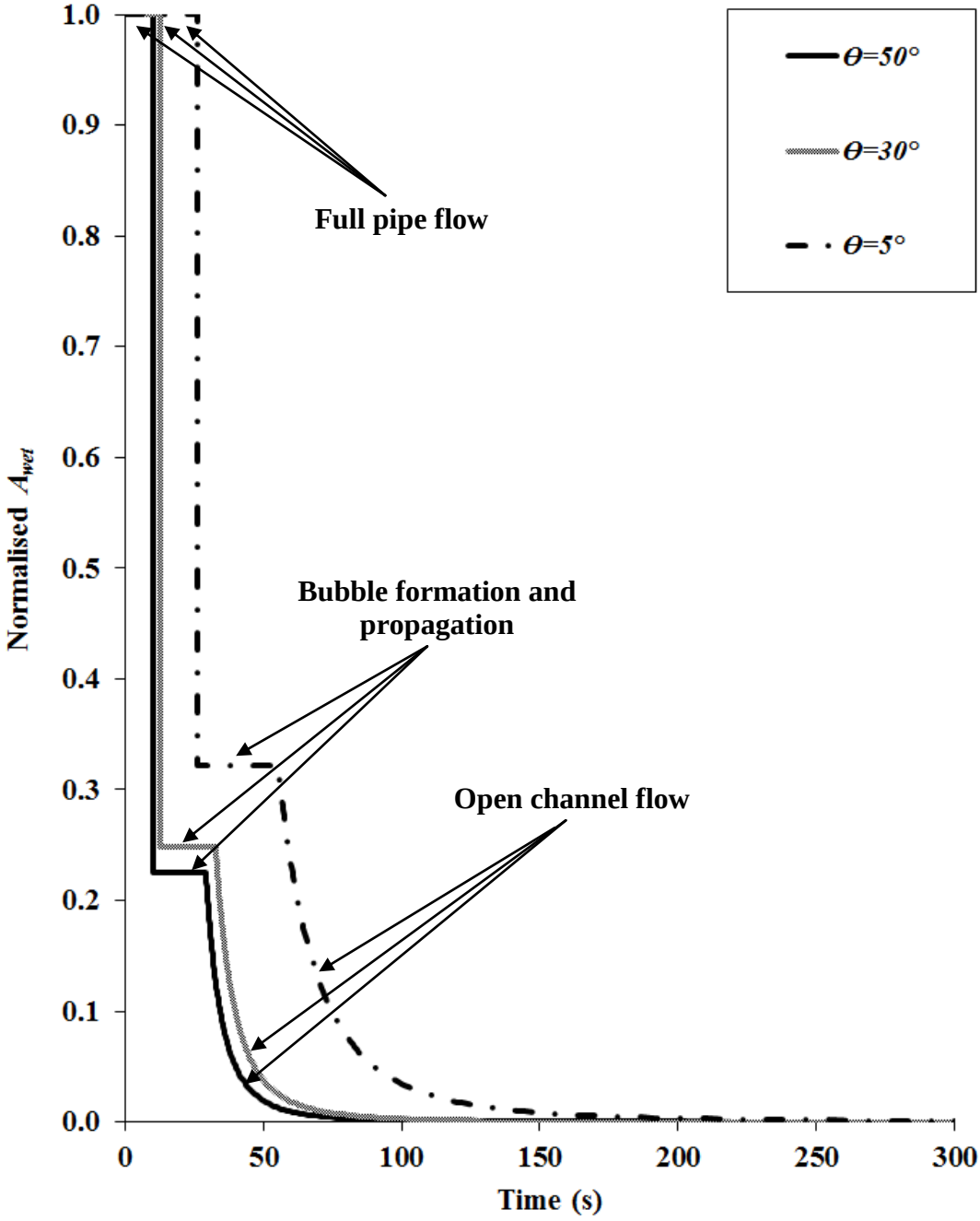

Figure 5.8: Impact of pipeline inclination angle on the variation of normalised A_{wet} following full-bore rupture in a 100m long, 0.406m diameter pipe fed from an upstream tank

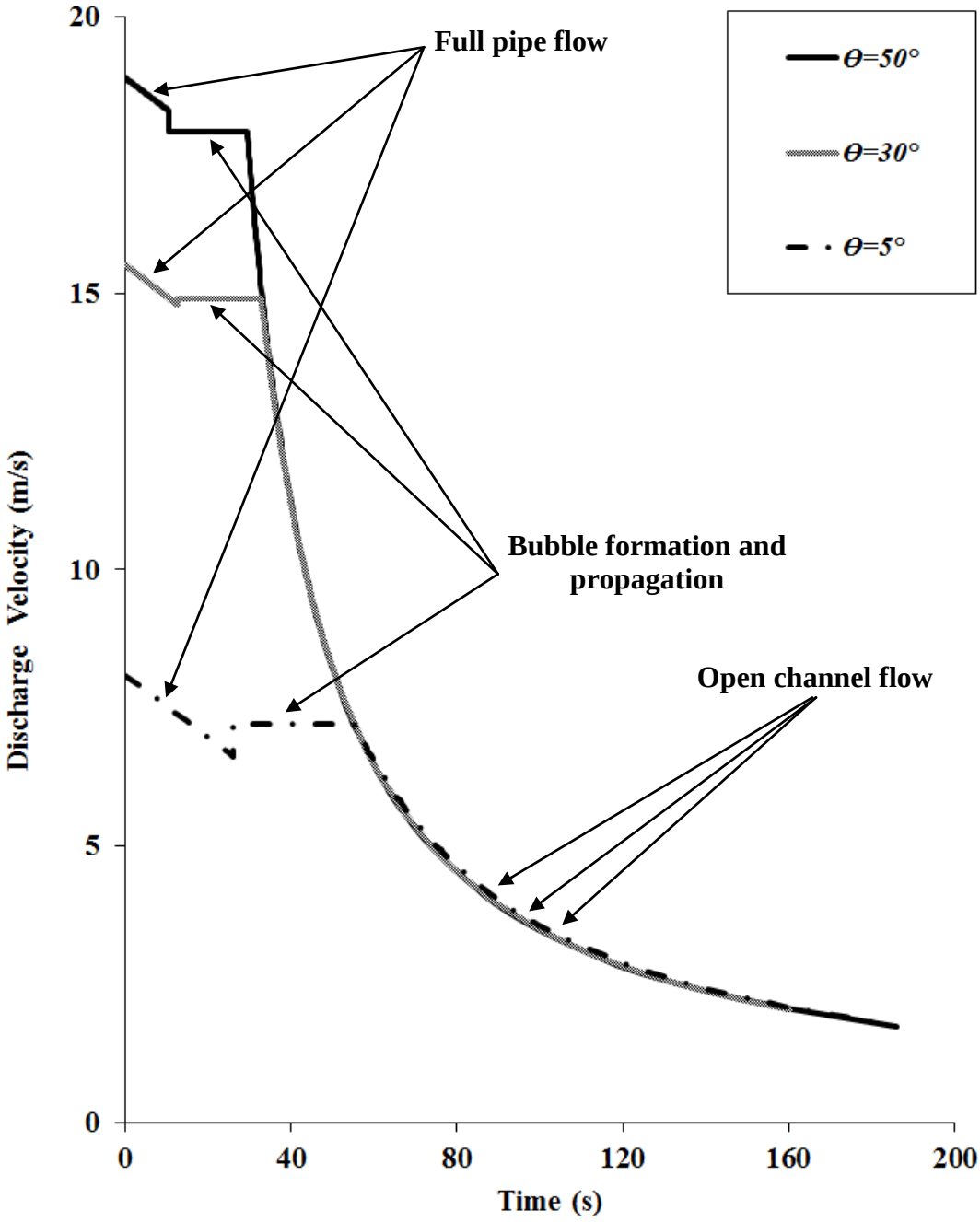

Figure 5.9: Impact of pipeline inclination angle on the variation of discharge velocity following full-bore rupture in a 100m long, 0.406m diameter pipe fed from an upstream tank

5.3.3.3. Normalised Cumulative Discharged Mass

Figure 5.10, Figure 5.11 and Figure 5.12 respectively show the impact of pipeline length, inner diameter and inclination angle in the ranges 100-300m, 0.305-0.508m and 5-50° on the normalised cumulative discharged mass (ratio between cumulative discharged mass and initial fluid mass in the system). On the graphs, the transition from full pipe to bubble propagation, and from bubble propagation to open channel flow are marked by black circular and triangular dots respectively. It may be observed from Figure 5.10 that similar to horizontal pipelines, the released mass during post-full pipe flow increases with pipeline length. For the longest pipeline (L = 300m), less than 40% of the mass is released during full pipe flow, whereas this figure increases to 66% for L = 100m.

The same trend can be seen in Figure 5.11 for the impact of pipeline inner diameter. For the pipe with the largest inner diameter (D = 0.508m) almost half of the inventory is released during bubble formation and open channel flow. On the other hand, the cumulative discharged mass during the each regime marginally varies with θ. For all the cases, majority of the mass is released during full pipe flow due to short length of the pipe (L = 100m).

As such, similar to horizontal pipelines, ignoring post-full pipe flow for long or large-diameter pipelines may lead to significant underestimation of released mass upon rupture.

Table 5.3 presents the comparison between the predicted and theoretical discharged mass during each regime. The calculation of the theoretical released mass during each regime is similar to what described in Section 4.3.3.2 for horizontal pipe except that here the tank is assumed to drain completely before the onset of bubble propagation. As such, L_{eq} of the remaining mass in the tank at the end of full pipe flow is not applicable.

- Full pipe flow

  It is assumed that the tank drains dry during this regime. Therefore, the theoretical mass to be released here is the initial inventory in the tank:

$$M_{full\ pipe\ flow} = \rho H_0 A_{\tan k} \quad \textbf{(5.19)}$$

- Bubble formation and propagation

$$M_{bubble\ propagation} = \rho\left(A - A_{wet}^{bf}\right)L = \rho L \frac{D^2}{8}\left(2\pi - \phi_n^{bf} + \sin\phi_n^{bf}\right) \quad \textbf{(5.20)}$$

- Open channel flow

$$M_{open\ channel\ flow} = \rho A_{wet}^{bf} L = \rho L \frac{D^2}{8}\left(\phi_n^{bf} - \sin\phi_n^{bf}\right) \quad \textbf{(5.21)}$$

where A_{wet}^{bf} is substituted from Equation (5.6).

Scenario			Full pipe flow		Bubble propagation		Open channel flow	
Length (m)	Diameter (m)	Angle (°)	Theoretical (kg)	Predicted (kg)	Theoretical (kg)	Predicted (kg)	Theoretical (kg)	Predicted (kg)
100	0.305	30	24850	24850	5457	5405	1802	1837
100	0.406	30	24850	24850	9670	9600	3192	3199
100	0.508	30	24850	24850	15231	15112	4905	5008
200	0.406	30	24850	24850	19339	19201	6385	6397
300	0.406	30	24850	24850	29009	28801	9577	9596
100	0.406	50	24850	24850	9962	9914	2900	2906
100	0.406	20	24850	24850	9489	9424	3373	3441
100	0.406	5	24850	24850	8662	8656	4134	4200

Table 5.3: Comparison of the theoretical and predicted discharged mass during individual regimes following full-bore rupture in a downward-inclined pipe fed from an upstream tank

It may be observed from the table that for all scenarios during each regime, the predicted released mass is very close to the corresponding theoretical values, with maximum deviation of 2%.

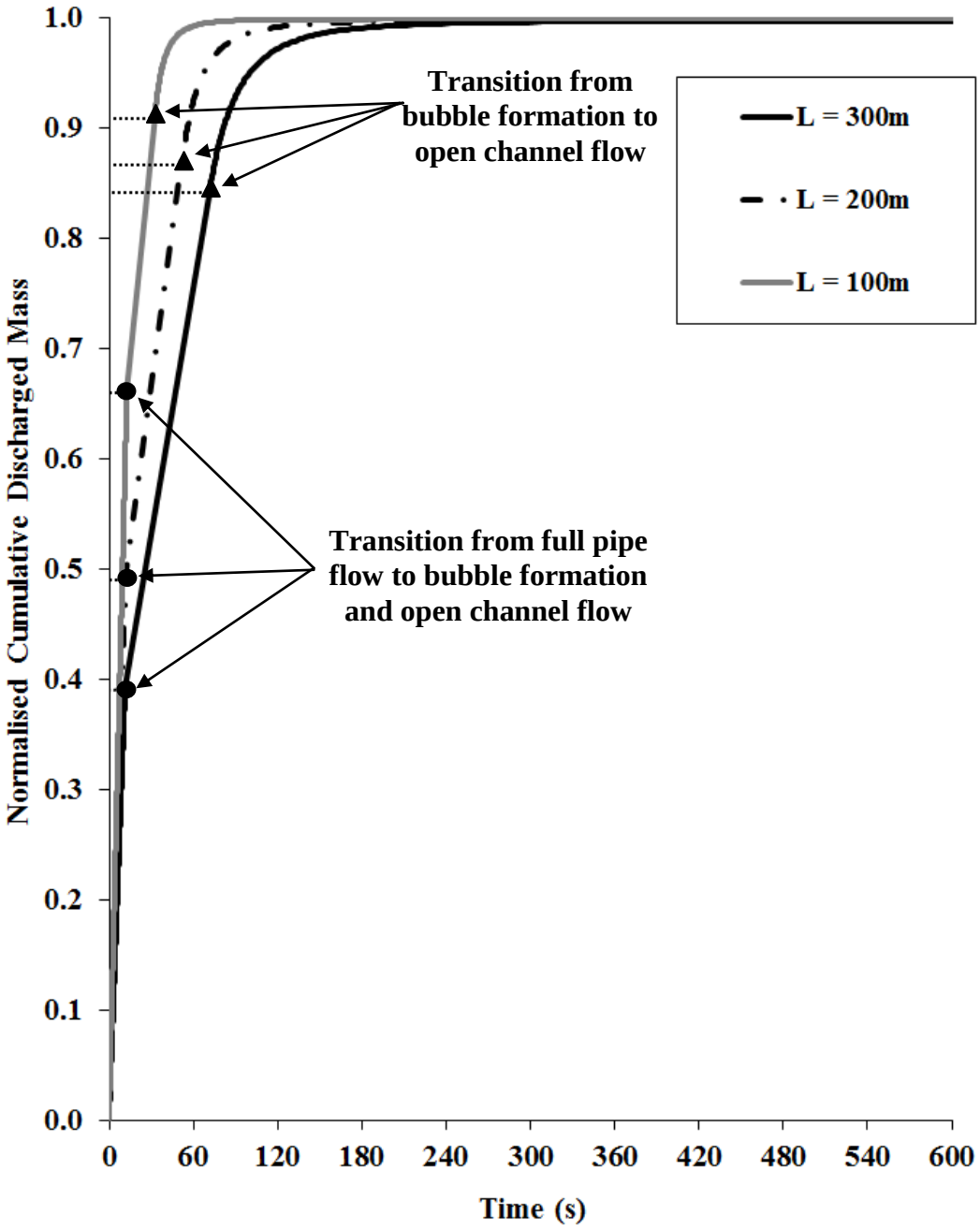

Figure 5.10: Impact of pipeline length on the cumulative discharged mass following full-bore rupture in a 0.406m diameter, 30° downward-inclined pipe fed from an upstream tank

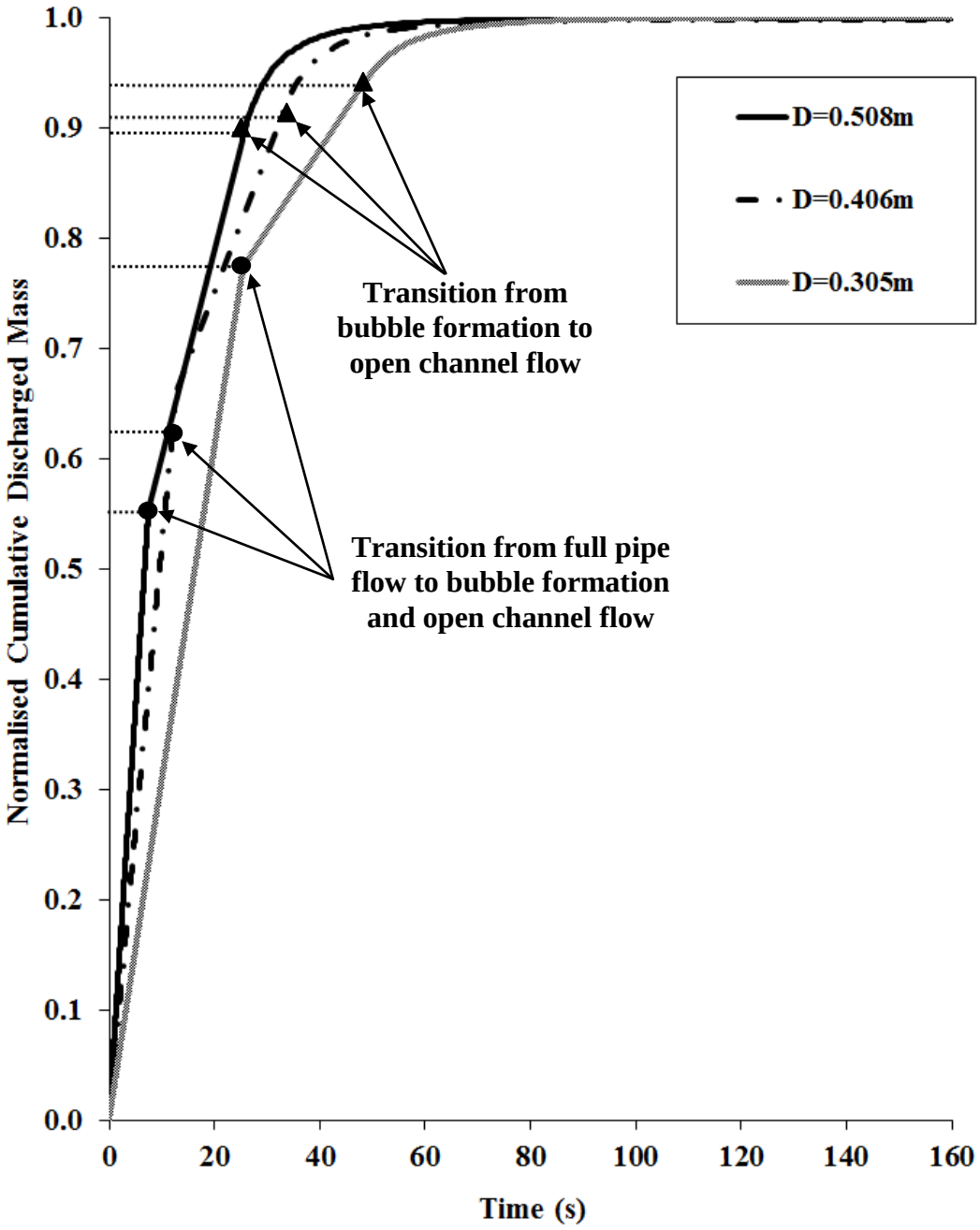

Figure 5.11: Impact of pipeline inner diameter on the cumulative discharged mass following full-bore rupture in a 100m long, 30^{o} downward-inclined pipe fed from an upstream tank

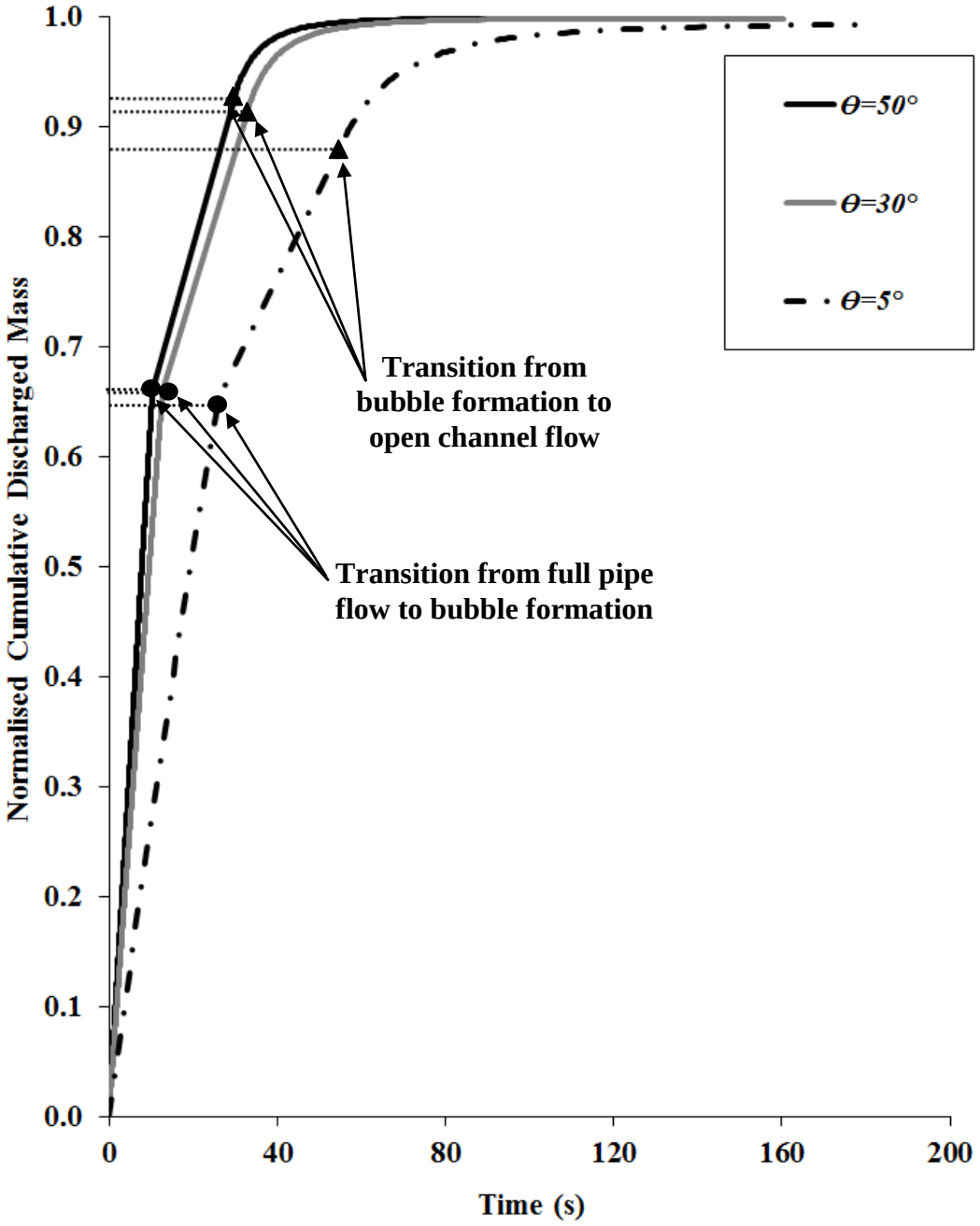

Figure 5.12: Impact of pipeline inclination angle on the cumulative discharged mass following full-bore rupture in a 100m long, 0.406m diameter pipe fed from an upstream tank

5.3.3.4. Variation of Liquid Depth Angle (ϕ_n^{bf}) with θ

Equation (5.14) derived in Section 5.3.2.2.2 shows the variation of ϕ_n^{bf} with θ and pipeline characteristics through f (case of bubble propagation from the upstream end only):

$$\frac{\left(0.542\cos\theta+0.350\sin\theta\right)\left(2\pi-\phi_n^{bf}+\sin\phi_n^{bf}\right)}{\left(1-\frac{0.98\left(2\pi-\phi_n^{bf}+\sin\phi_n^{bf}\right)}{2\pi}\right)} - \sqrt{\frac{\sin\theta}{2f\phi_n^{bf}}}\left(\phi_n^{bf}-\sin\phi_n^{bf}\right)^{1.5}=0 \qquad \textbf{(5.14)}$$

However, the above equation can only be solved iteratively by trial and error. Apart from θ, the above equation is also dependent on D and ε through $f \approx \frac{\varepsilon}{D}$. In this study the default value for ε is 0.05mm for commercial steel (Perry, 1997) which is widely used for crude oil pipelines and thus assumed to remain unchanged. As such, in order to establish a simpler equation to describe the dependency of ϕ_n^{bf} on θ, the calculated values of ϕ_n^{bf} are plotted against θ in the range 6-80^o for pipeline inner diameter in the range 0.102-0.457m. These results are presented in Figure 5.13. As it may be observed from the figure, the variation of ϕ_n^{bf} with pipeline inner diameter is negligible. Therefore, taking the average of the calculated ϕ_n^{bf} for each θ and applying a power-form trendline to the resulting curve, the following equation is obtained with $R^2 = 0.997$:

$$\phi_n^{bf} = 169.08\theta^{-0.074} \qquad \textbf{(5.22)}$$

where the unit for θ is degree (°). Figure 5.14 shows the variation of average ϕ_n^{bf} with θ as well as the power-form trendline. At θ = 0.05^o where the pipeline is nearly horizontal, the above equation produces a value of 211^o for ϕ_n^{bf}, very close to the calculated value of 216^o for ϕ_n^{bf} horizontal pipe in Section 4.3.2.2 . However, at θ =

6^o the calculated ϕ_n^{bf} is 148^o, significantly smaller than 216^o. In addition, the above equation is undefined at $\theta = 0$ due to zero discharge velocity calculated from Darcy-Weisbach equation (Equation (5.2)).

For all other values of θ, the maximum deviation of the predicted ϕ_n^{bf} by Equation (5.22) from those obtained from the model, i.e. Equation (5.14) , is ±3%.

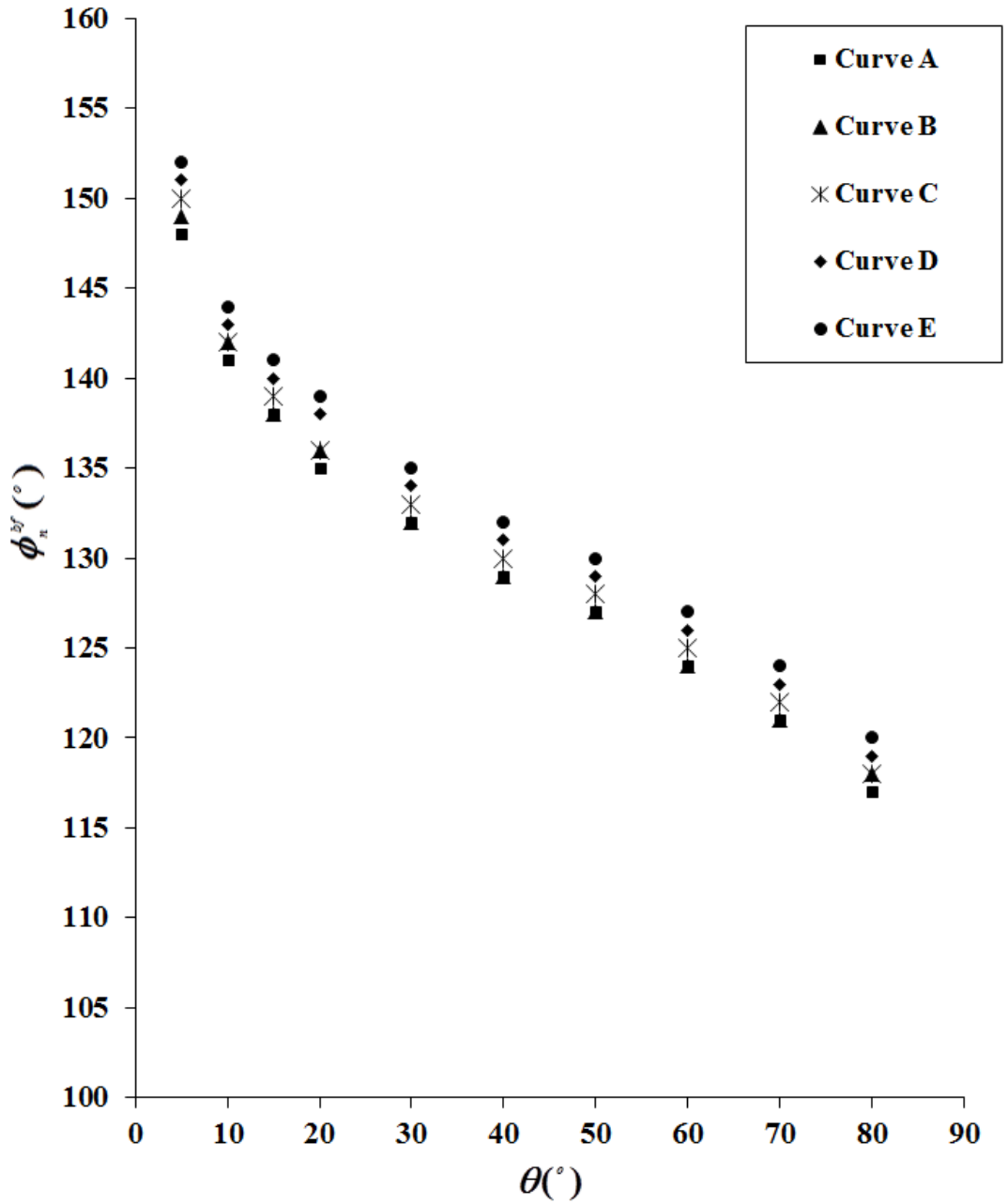

Figure 5.13: Variation of ϕ_n^{bf} with θ for a range of pipeline diameters following full-bore rupture in a downward-inclined pipe fed from an upstream storage tank

Curve A: D = 0.457m
Curve B: D = 0.356m
Curve C: D = 0.254m
Curve D: D = 0.152m
Curve E: D = 0.102m

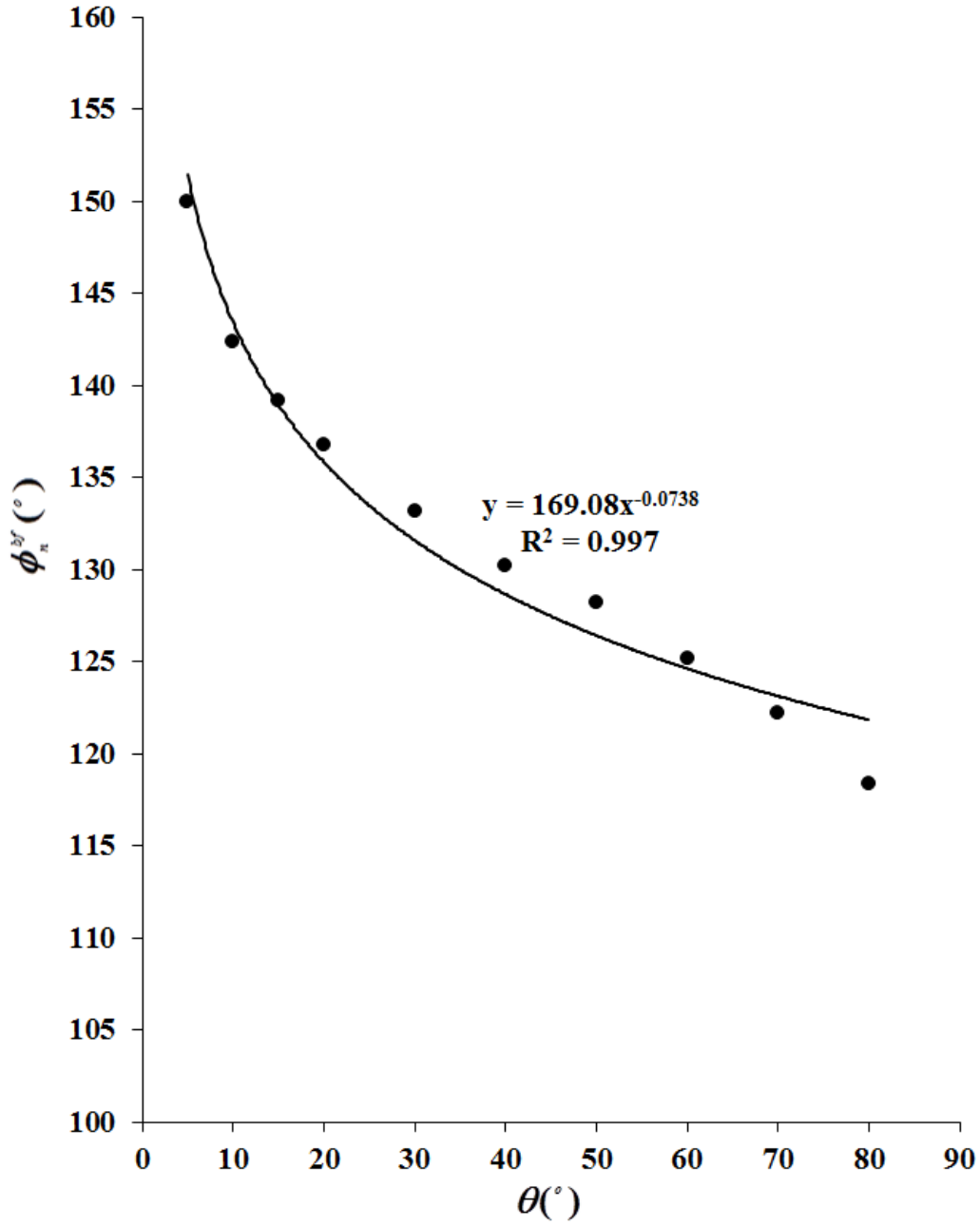

Figure 5.14: Variation of average ϕ_n^{bf} with θ following full-bore rupture in a downward-inclined pipe fed from an upstream storage tank

5.3.4. Experiments

In the current section, the results of a series of experiments conducted to assess the accuracy of the developed outflow flow equations for downward-inclined pipes are presented. First, the validity of the proposed equation for ϕ_n^{bf} corresponding to the liquid depth below the bubble (Equation (5.14)) is tested. In addition, the applicability of the proposed empirical coefficient C_0= 0.98 by Bendiksen (1984) to the system with upstream tank is investigated. This is then followed by investigating the accuracy of the model in predicting the discharge rate through measuring the cumulative discharged mass. The discharge rate is calculated based on the measured cumulative discharged mass. The measured values are compared against those obtained from the model.

5.3.4.1. Upstream Bubble Propagation Velocity u_{ub} and Liquid Depth d_n^{bf}

Figure 5.15 presents the experimental setup used to measure the bubble propagation velocity and the liquid depth below the bubble (d_n^{bf}) in a downward-inclined pipe. As it may be observed, the configuration is similar to Figure 4.12 or horizontal pipe, except that the acrylic pipe is declined by approximately 12°.

Here following the removal of the capping clamp, the bubble location inside the acrylic pipe is recorded by Kodak Ektapro high speed motion analyser, model 4540 at the speed of 1125frame/s. Figure 5.16 presents a selection of photographs from the motion analyser. During the experiment it was observed that the bubble propagated only from the pipe upstream, while the cavity at the pipe downstream remained stagnant. This is consistent with the results obtained through the presented parametric studies in Section 5.3.3.1 where the occurrence of this phenomenon was confirmed based on the drift velocity method.

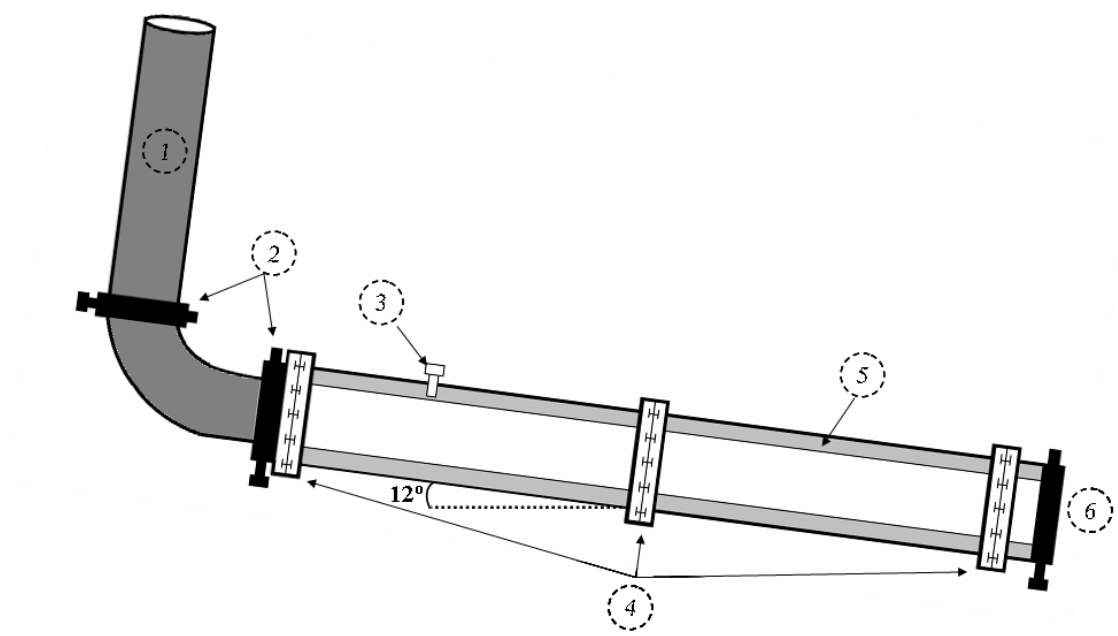

Figure 5.15: Experimental setup to measure the bubble propagation velocity (u_{ub}) and liquid depth below the bubble (d_n^{bf}) following full-bore rupture in a downward-inclined pipe:

1) Stainless steel pipe
2) Connecting clamps
3) Deaerating orifice
4) Connecting flanges
5) Acrylic pipe
6) Plug with a screw

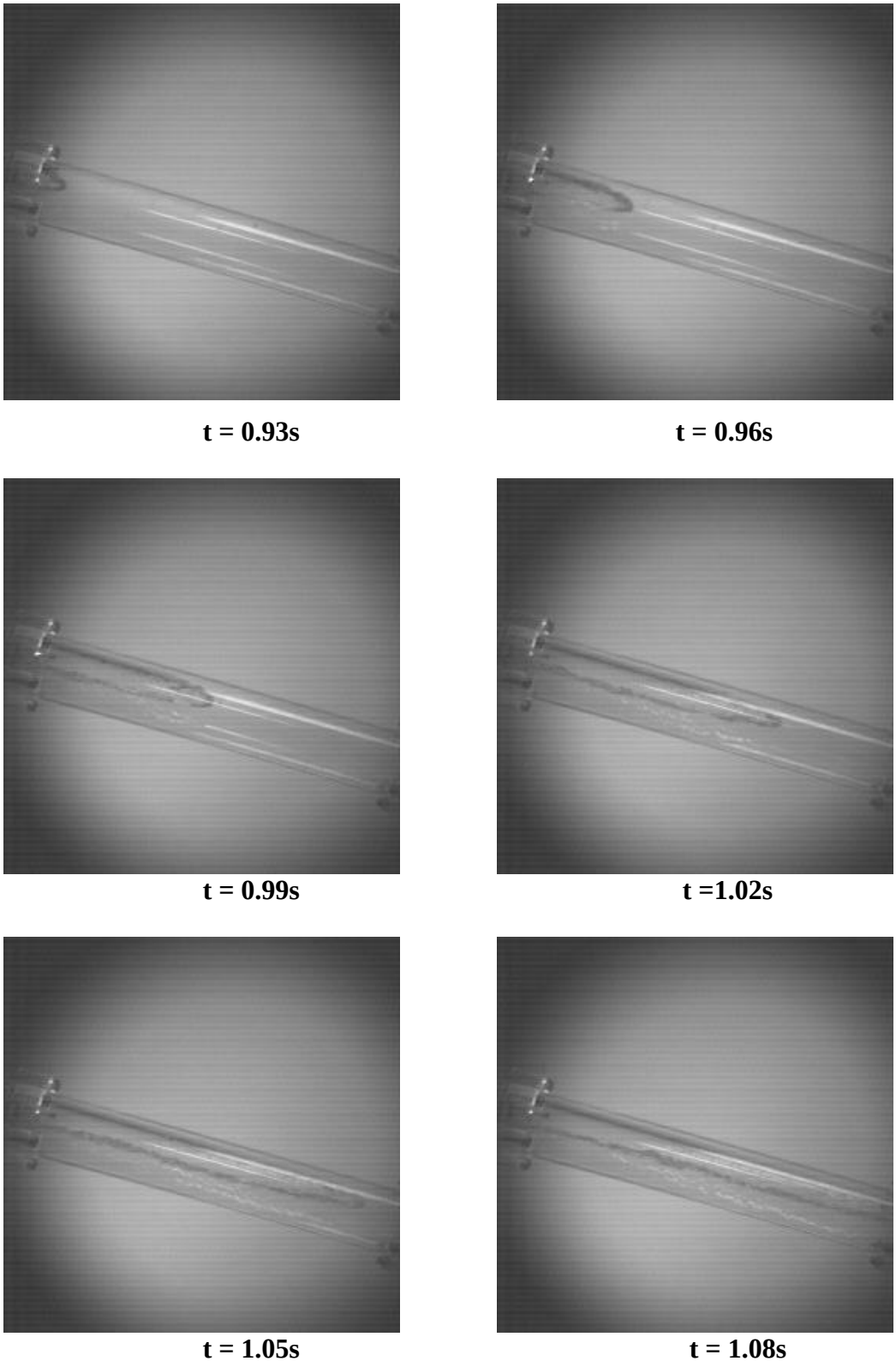

Figure 5.16: Snapshots taken at the speed of 1125frame/s from bubble propagation following full-bore rupture in 0.013m inner diameter, 2.5m long, 12^{o} downward-inclined pipe

Solving equations (5.7) and (5.14) respectively for u_{ub} and ϕ_n^{bf} for a 0.038m inner diameter, 2.5m long, 12^o downward-inclined pipe produces:

$$u_{ub} = 1.269 \ m/s \quad \textbf{(5.23)}$$

$$\phi_n^{bf} = 138^o \quad \textbf{(5.24)}$$

In addition, the obtained approximate value for ϕ_n^{bf} from Equation (5.22) proposed in Section 5.3.3.4 based on the results from the parametric studies is 141°, only 2% larger than $\phi_n^{bf} = 138^o$.

Based on the distance travelled by the bubble, Δx_{actual}, u_{ub} is calculated from Equation (4.48) used for horizontal pipe:

$$u_{ub} = \frac{\Delta x_{actual}}{\Delta t} \quad \textbf{(4.48)}$$

The approach adopted to calculate Δx_{actual} is similar to the one presented in Section 4.3.4.1.

The snapshots taken by the Motion Analyser are presented in Figure 5.16. Figure 5.17 shows the results for u_{ub} in the form of a ratio between the measured and predicted values. As it may be observed from the figure, the obtained u_{ub} from the experiment is significantly larger than the predicted u_{ub} from the model (>50%). In addition, from the snapshots, the average ϕ_n^{bf} is 168^o, which is 22% higher than the calculated value from the model, Equation (5.24).

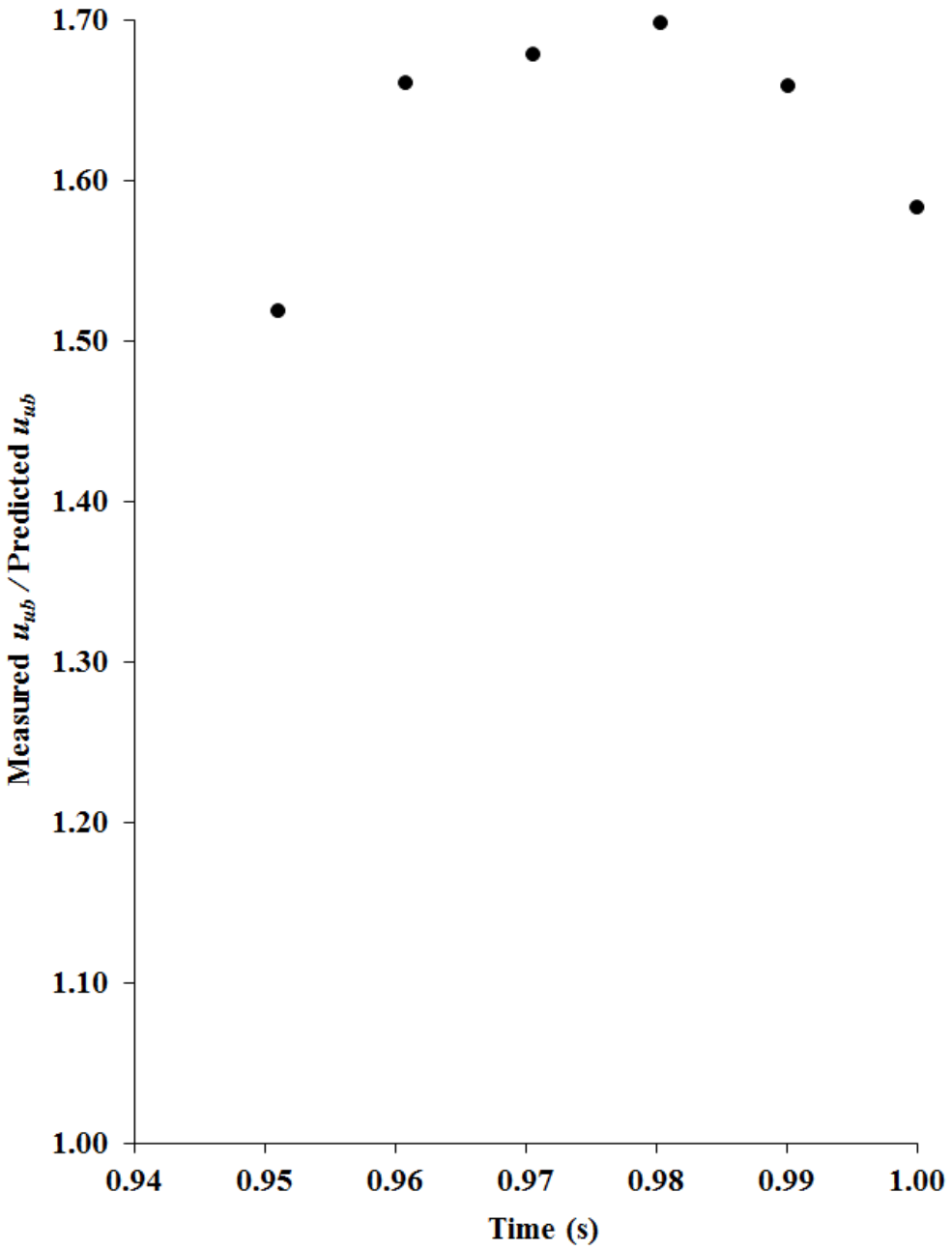

Figure 5.17: Variation of (measured u_{ub} / predicted u_{ub}) with time following full-bore rupture in a 0.038m inner diameter, 2.5m long, 12^{o} downward-inclined pipe

It is postulated that the suggested value of 0.98 for C_0 by Bendiksen (1984) may not applicable here to describe the upstream bubble propagation velocity because:

1) Bendiksen (1984) introduced the bubble to the system from the base of the pipe, while there was a continuous liquid flow entering the pipe upstream. This could potentially cause the bubble to form a slug, rather than an elongated bubble with continuous air ingress.

2) In Bendiksen's experimental rig there was no upstream tank, thus no liquid head. Consequently, the momentum resulting from the liquid head just before the commencement of bubble formation and propagation was not considered.

Considering the above, it is expected that the experimental upstream bubble propagation velocity is higher than the calculated value from the model based on $C_0 = 0.98$. In order to find a new value for C_0 applicable to the system with upstream tank with continuous air ingress from the pipe upstream, u_{ub} and ϕ_n^{bf} are calculated for C_0 in the range 0.98-1.8. The results are presented in Figure 5.18 and Figure 5.19 in the form of (measured u_{ub} / predicted u_{ub}) and (measure ϕ_n^{bf} / predicted ϕ_n^{bf}) respectively.

As it may be observed from the figures, the accuracy of the model in predicting u_{ub} and ϕ_n^{bf} relative to the experimental results increases with C_0. The best fit to both curves is obtained by adding a power-form trendline with $R^2 = 1$, producing the following equations:

$$\text{Measured } \phi_n^{bf} \text{ / Predicted } \phi_n^{bf} = 1.2138 C_0^{-0.447} \quad \textbf{(5.25)}$$

and

$$\text{Measured } u_{ub} \text{ / Predicted } u_{ub} = 2.2818\ C_0^{-1.8729} \quad \textbf{(5.26)}$$

Equating the above equations to 1 gives $C_0 \approx 1.55$. Based on this finding, Equation (5.14) developed to describe the relation between ϕ_n^{bf} and θ in Section 5.3.2.2.2 is modified by replacing $C_0 = 0.98$ with 1.55:

$$\frac{(0.542\cos\theta + 0.350\sin\theta)(2\pi - \phi_n + \sin\phi_n)}{\left(1 - \frac{1.55(2\pi - \phi_n + \sin\phi_n)}{2\pi}\right)} - \sqrt{\frac{\sin\theta}{2f\phi_n}}(\phi_n - \sin\phi_n)^{1.5} = 0 \qquad \textbf{(5.27)}$$

On the other hand, Equation (5.22) proposed in Section 5.3.3.4 by adding a power-form trendline to the results from parametric studies is based on $C_0 = 0.98$. Following the same procedure, this equation is also modified for $C_0 = 1.55$ which gives:

$$\phi_n^{bf} = 191.9\theta^{-0.044} \qquad \textbf{(5.28)}$$

with $R^2 = 0.977$. Once again for nearly horizontal pipe ($\theta = 0.05^o$) the calculated ϕ_n^{bf} from the equation is 219°, less than 2% higher than the predicted value of 216° from horizontal pipe model. The above equation also predicts a value of 177° for ϕ_n^{bf} at $\theta = 6^o$, significantly smaller than 216°, similar to Equation (5.22). For all other values of θ, the maximum deviation of the predicted ϕ_n^{bf} by Equation (5.28) from those obtained from the model, i.e. Equation (5.27) is ±5%.

Systematic and Experimental Errors

Most of the systematic and experimental errors presented for the case of horizontal pipe are also applicable here. Only the last item of the experimental errors is not relevant as the liquid level in the downward-inclined pipe is assumed to be zero at the onset of bubble formation, instead of critical depth.

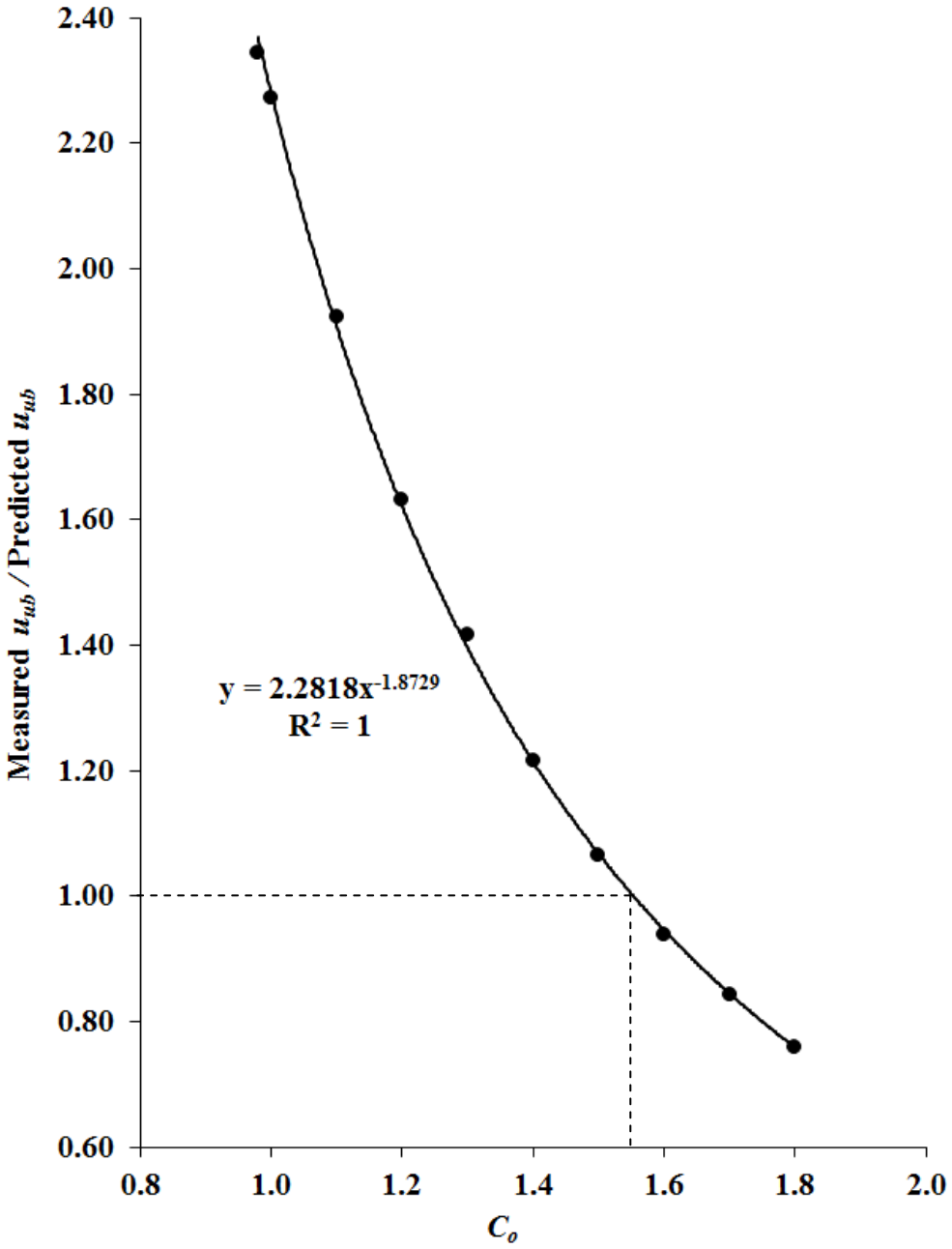

Figure 5.18: Variation of (measured u_{ub} / predicted u_{ub}) with C_0 following full-bore rupture in a 0.038m inner diameter, 2.5m long, 12° downward-inclined pipe

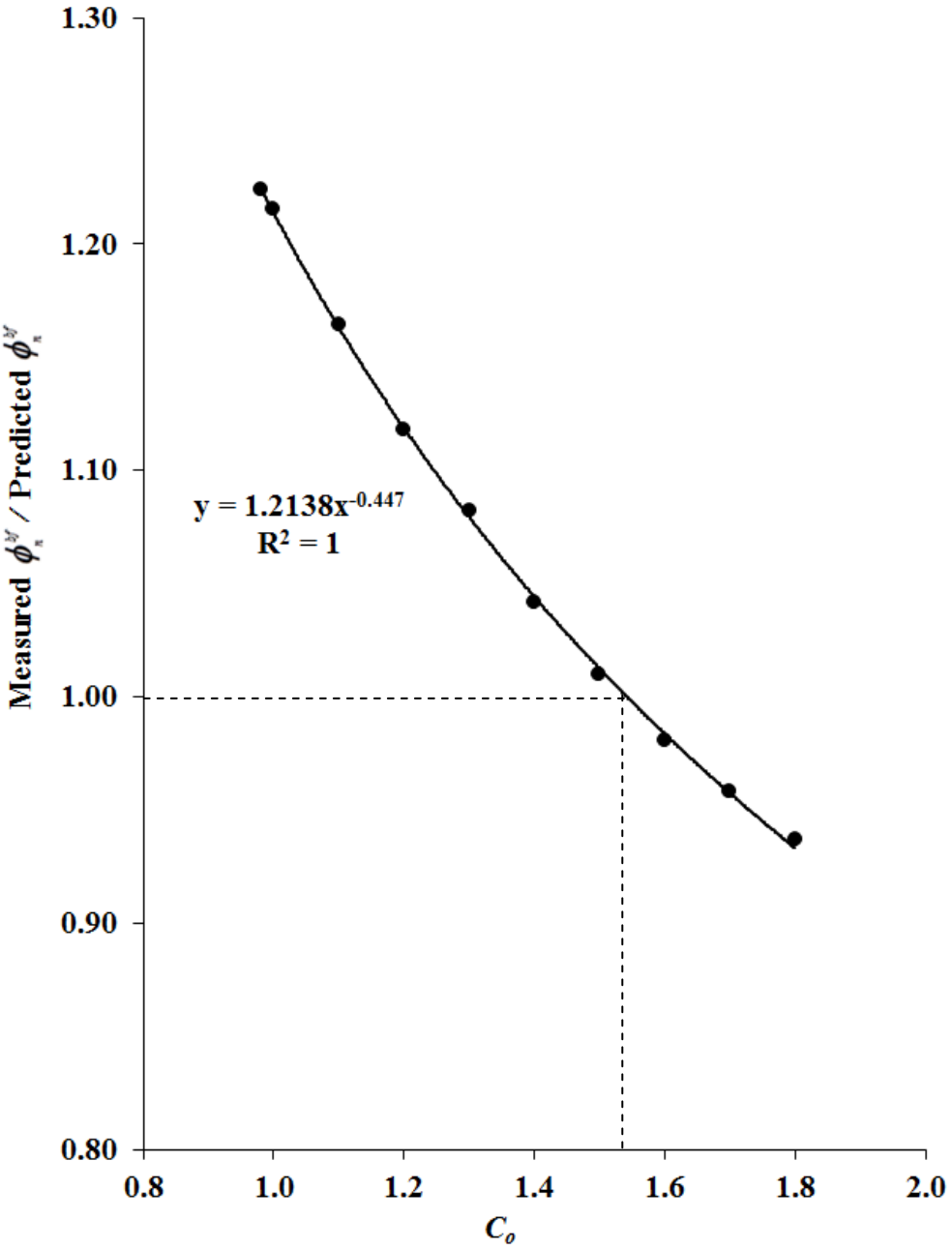

Figure 5.19: Variation of (measured ϕ_n^{bf} / predicted ϕ_n^{bf}) with C_0 following full-bore rupture in a 0.038m inner diameter, 2.5m long, 12^o downward-inclined pipe

5.3.4.2. Normalised Cumulative Discharged Mass and Discharge Rate

Figure 5.20 presents the experimental setup used to determine the accuracy of the outflow model developed in Section 5.3.2 for predicting the discharge rate by measuring the cumulative discharge mass. The experimental setup is similar to the setup used for the horizontal pipe (see Figure 4.15) except that the 0.034m inner diameter, 3m long acrylic pipe is declined by approximately 6°. Following the removal of the rubber bung to simulate the full-bore rupture, the discharged water is collected in a plastic container placed on top of a Mettler PM30K industrial balance. The cumulative discharged mass is measured and recorded by using the Mettler PM30K industrial balance and a LabView – based software (National Instruments Company, 2011). The discharge rate is then calculated based on the measured discharged mass. The approach taken to calculate the discharge rate is similar to what described for horizontal pipe in Section 4.3.4.2.

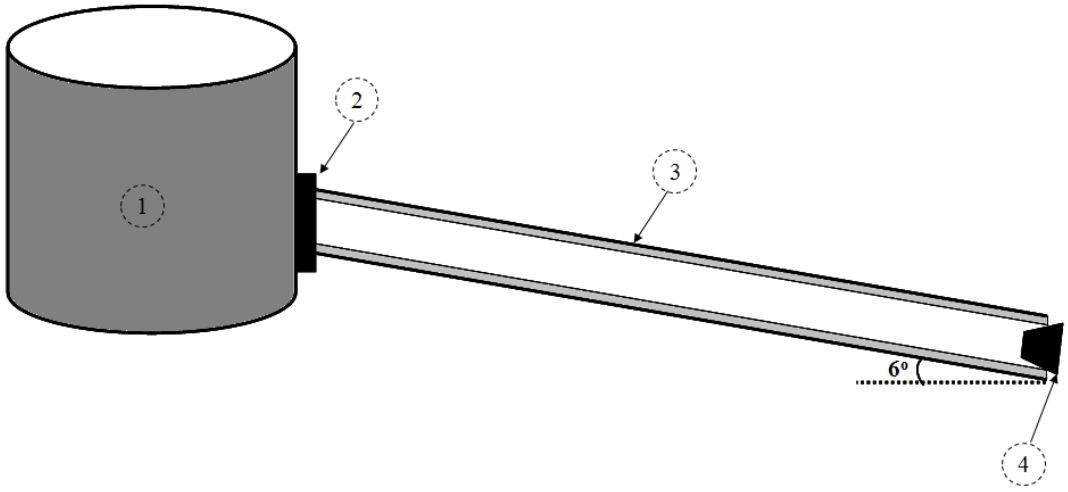

Figure 5.20: Experimental setup to measure the cumulative discharged mass following full-bore rupture in a downward-inclined pipe fed from a plastic container

1) Plastic container
2) Cable gland
3) Acrylic pipe
4) Rubber bung

Figure 5.21 presents the variation of normalised cumulative discharged mass with time. The graph consists of 4 curves. Curve A corresponds to the discharge based on the original values of C_0 and K, 0.98 (Bendiksen, 1984) and 0.5 respectively. Curve

B presents the cumulative discharged mass for the modified value of K = 2.5, proposed in Section 4.3.4.2 to account for the additional entry loss due to silicon sealant at the pipe entrance. C_0 remains the same as in Curve A, i.e. 0.98. To produce Curve C, the modified values for both K and C_0 are used. Therefore, K = 2.5 and C_0= 1.55 from Section 5.3.4.1. Finally Curve D shows the measured normalised cumulative discharged mass from the experiments.

As it may be observed from the figure, the original value of K = 0.5 results in overestimation of cumulative discharged mass during full pipe flow due to presence of additional entry loss from the silicone sealant (see Curve A). Employing the suggested value of 2.5 for K in Section 4.3.4.2 will reduce the deviation of the predicted results by the model from those obtained from the experiments significantly (see Curve B).

On the other hand, for K = 2.5 the predicted results based on C_0 = 0.98 are closer to the measured values than those obtained for the suggested value of 1.55 in Section 5.3.4.1 (compare Curve B and C). In other words, while C_0 = 1.55 provides the closest bubble propagation velocity to the experimental data (see Figure 5.18), it produces more deviated results for cumulative discharged mass during bubble formation and propagation, and open channel flow.

The same trend may also be seen from Figure 5.22 where the variation of discharge rate with time is presented for K = 0.5 and 2.5 and C_0 = 0.98 and 1.55.

The two sets of experiments conducted for measuring the bubble propagation velocity (Section 5.3.4.1) and cumulative discharged mass are conducted for pipes with different characteristics. Therefore, one possible explanation for the above phenomenon might be that in downward-inclined pipes fed from an upstream tank, the value of C_0 may not be independent of pipeline characteristics.

In addition, the pipe inclination angle in the experiments for measuring the cumulative discharged mass is very close to horizontal ($\theta = 6^o$), whereas the one used in measuring the bubble velocity is relatively steep ($\theta = 12^o$). Therefore, the

impact of momentum imposed on the flow at the beginning of bubble propagation for the first case is negligible comparing to the later. Consequently, the value of 0.98 proposed by Bendiksen (1984) for C_0 in the absence of upstream liquid head produces more accurate results for cumulative discharged mass with maximum deviation of 9%.

Systematic and Experimental Errors

The systematic and experimental errors here are every similar to those presented for the horizontal pipe. However, here the impact of manually removing the bung is more significant. Due to the inclination of pipe, the liquid velocity here is much higher compared to the case of horizontal pipe, resulting in larger amount of mass released before FBR.

The high liquid velocity here also imposes stronger vibrations to the container placed on the scale, producing more scattered results for the released mass. The high liquid velocity also causes more water to bounce back after hitting the base of the container, resulting in more deviation of the total released mass from the system initial mass.

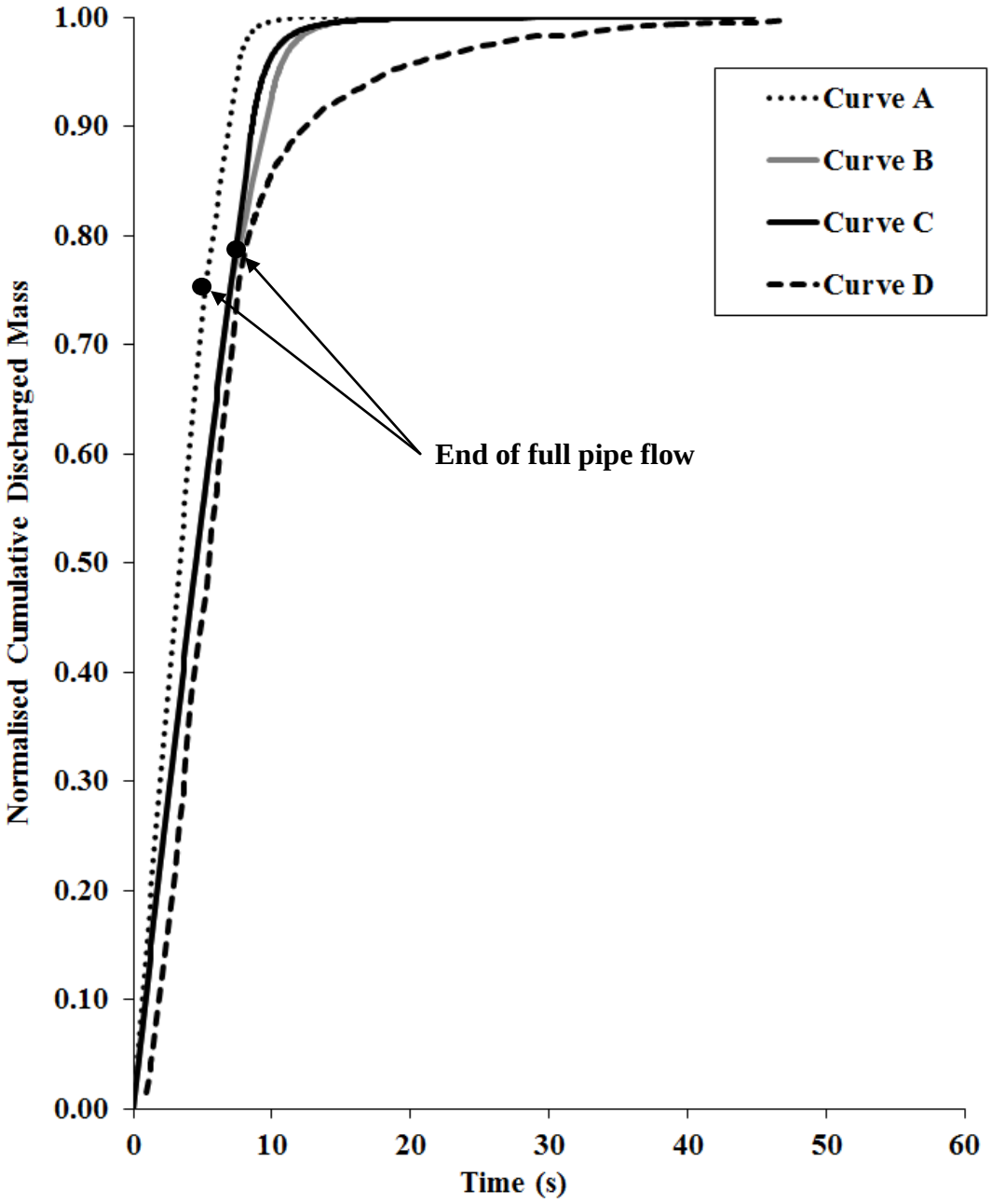

Figure 5.21: Variation of normalised cumulative discharged mass following full-bore rupture in a 0.034m diameter, 3m long, 6° downward-inclined pipe fed from a plastic container

Curve A: K = 0.5 and C_0 = 0.98
Curve B: K = 2.5 and C_0 = 0.98
Curve C: K = 2.5 and C_0 = 1.55
Curve D: Experiments

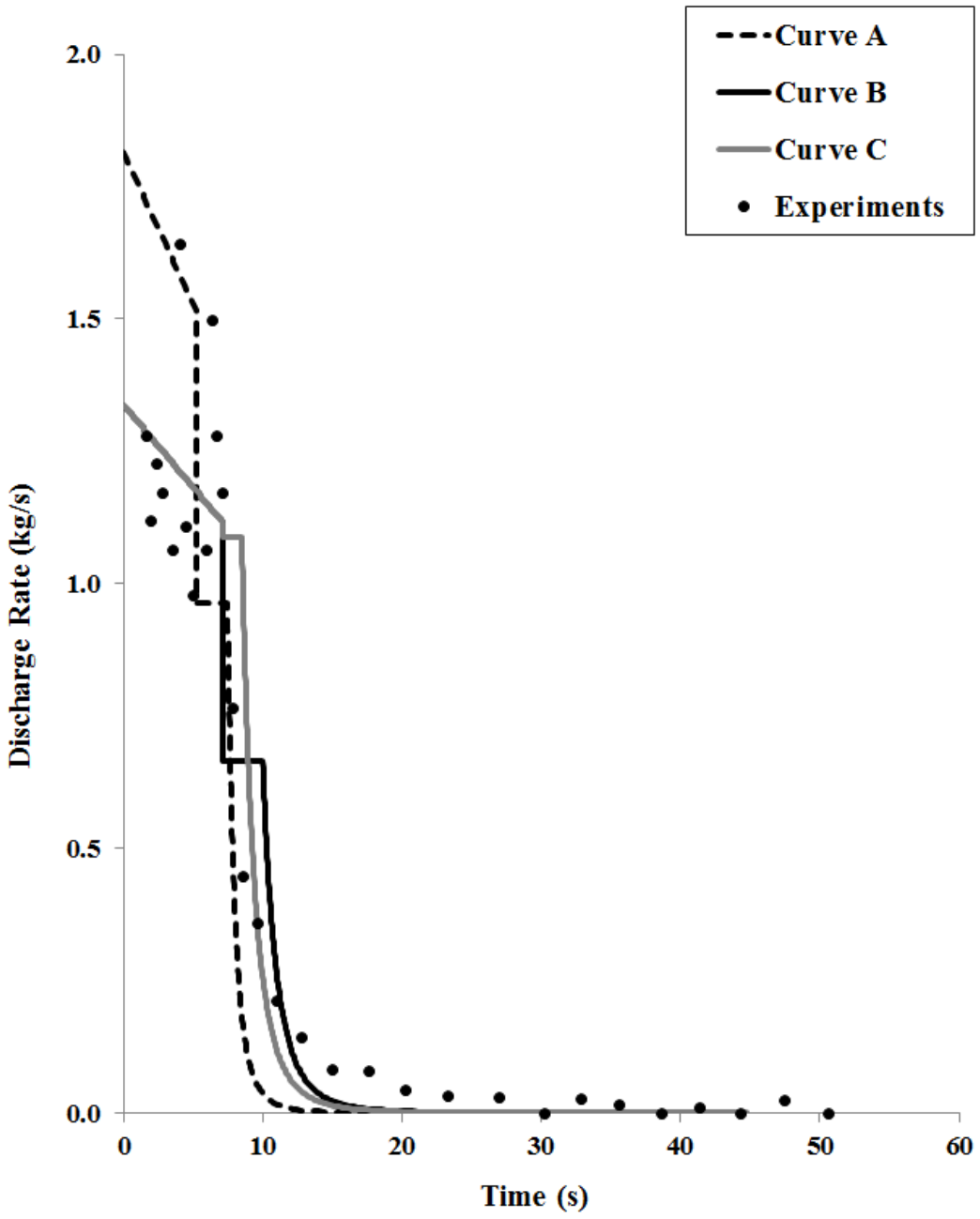

Figure 5.22: Comparison of the measured discharge rate with the predicted values following full-bore rupture in a 0.034m diameter, 3m long, 6° downward-inclined pipe fed from a plastic container

Curve A: K = 0.5 and C_0 = 0.98
Curve B: K = 2.5 and C_0 = 0.98
Curve C: K = 2.5 and C_0 = 1.55
Curve D: Experiments

5.4. Transient Hydraulic Flow Modelling Following Full-bore Rupture of an Isolated Downward-inclined Pipeline

5.4.1. Introduction

In this section the model developed for an isolated horizontal pipeline is extended to account for gravity impacts and frictional losses in downward-inclined pipes. The efficacy of the proposed model is then tested through sensitivity analysis. Here, in addition to the impact of pipeline inner diameter and length, the impact of pipe inclination angle is also studied on the discharge velocity, wetted area and the released mass during individual regimes. An approximate relationship between the liquid depth angle, ϕ_n^{bf}, and the inclination angle, θ, is established based on the results from the parametric studies. Finally, the accuracy of the developed model is assessed through a series of experiments.

5.4.2. Model Theory

5.4.2.1. Bubble Formation and Propagation

Similar to the case of a horizontal pipe with a closed-end, following rupture in a downward-inclined pipe a bubble forms at the pipe downstream and propagates along the pipe. The arrival of the bubble at the closed-end marks the termination of the bubble formation and propagation regime. Figure 5.23 presents the bubble propagation in a downward-inclined pipe with one closed-end.

As described in Section 5.3.2.2, the liquid depth along a downward-inclined pipe is uniform and equal to the normal depth. Therefore, the discharge velocity can be calculated from the Darcy-Weisbach equation (Equation (5.2)):

$$u_d = \sqrt{\frac{gD\sin\theta}{2f}\left(\frac{\phi_n^{bf} - \sin\phi_n^{bf}}{\phi_n^{bf}}\right)} \qquad \textbf{(5.2)}$$

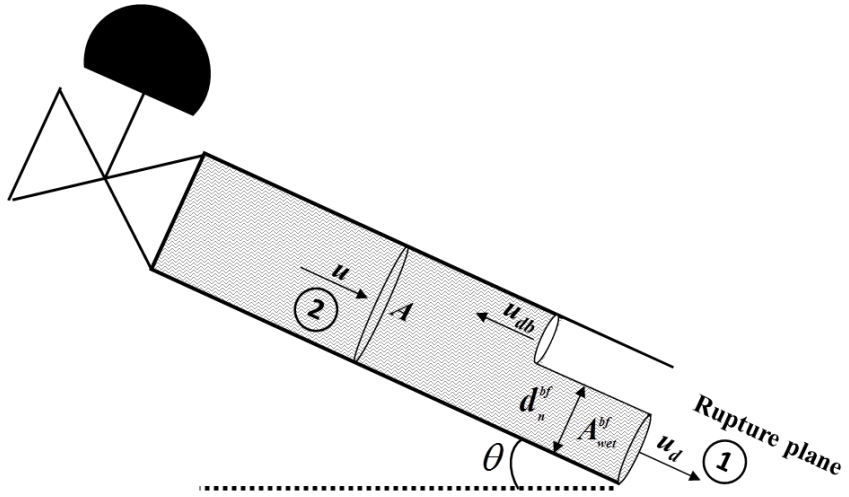

Figure 5.23: Bubble propagation in an isolated downward-inclined pipe

On the other hand, recalling Equation (4.51) resulting from the application of mass conservation to the liquid inside an isolated horizontal pipe, the discharge velocity may also be expressed as:

$$u_d = \frac{u_{db}\left(A - A_{wet}^{bf}\right)}{A_{wet}^{bf}} \qquad \textbf{(4.51)}$$

where A_{wet}^{bf} may be calculated from Equation (5.6) with ϕ_n^{bf} representing the time-invariant value of ϕ at the normal depth.

The bubble propagation velocity (u_{db}) is also calculated from Equation (3.21) (Bendiksen, 1984):

$$u_{db} = 0.542\sqrt{gD}\cos\theta + 0.350\sqrt{gD}\sin\theta \qquad \textbf{(3.21)}$$

Replacing u_{db} and A_{wet}^{bf} from equations (3.21) and (5.6) into Equation (4.51) produces the following equation for the discharge velocity:

$$u_d = \frac{2\pi - \phi_n^{bf} + \sin\phi_n^{bf}}{\phi_n^{bf} - \sin\phi_n^{bf}}\left(0.542\sqrt{gD}\cos\theta + 0.350\sqrt{gD}\sin\theta\right) \quad \textbf{(5.29)}$$

Equating the above equation to Equation (5.2) provides ϕ_n^{bf} as function of θ:

$$\left(2\pi - \phi_n^{bf} + \sin\phi_n^{bf}\right)\left(0.542\cos\theta + 0.350\sin\theta\right) - \sqrt{\frac{\sin\theta}{2f\phi_n^{bf}}}\left(\phi_n^{bf} - \sin\phi_n^{bf}\right)^{1.5} = 0 \quad \textbf{(5.30)}$$

The above equation needs to be solved iteratively to calculate ϕ_n^{bf}. Furthermore, the time required for the bubble to reach the closed-end is calculated from the following equation:

$$t_{bubble} = \frac{L}{u_{db}} = \frac{L}{0.542\sqrt{gD}\cos\theta + 0.350\sqrt{gD}\sin\theta} \quad \textbf{(5.31)}$$

5.4.2.2. Open Channel Flow

As soon as the elongated bubble reaches the closed-end of the pipe open channel flow becomes the dominant regime. Figure 5.24 shows a downward-inclined pipe with one closed-end with open channel flow.

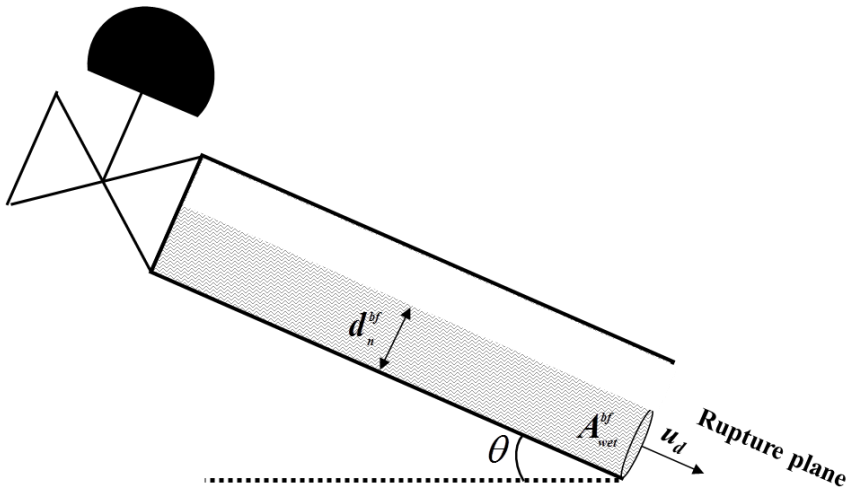

Figure 5.24: Open channel flow in an isolated downward-inclined pipe

Similar to the model developed in Section 5.3.2.3 for the pipeline fed from an upstream tank, the transient flow mass balance is coupled with the Darcy-Weisbach equation for discharge rate (Equation (5.4)). The resulting equation is then integrated between $t_0 = 0$ and t. Therefore, recalling Equation (5.18) from the model for the pipeline fed from an upstream tank:

$$\int_{A_{wet}^{bf}}^{A_{wet}} \frac{dA_{wet}}{\frac{D^{2.5}}{8}\rho\sqrt{\frac{g\sin\theta}{2f\phi_n}}\left(\phi_n - \sin\phi_n\right)^{1.5}} = -\frac{t}{\rho L} \qquad \textbf{(5.18)}$$

Similar to the horizontal pipe, trapezoidal rule, presented in Figure 4.5, is used to estimate the above integral (I_i) numerically except that here $\phi_1 = \phi_n^{bf}$ instead of 175^o and $\dot{m}_{d,i}$ is calculated from Equation (3.45). Once I_i is determined, the corresponding time t_i is calculated via Equation (4.59):

$$t_i = I_i \rho L \qquad \textbf{(4.59)}$$

5.4.3. Parametric Studies

In the previous section a detailed description of a mathematical model was given to simulate the outflow upon full-bore rupture in isolated downward-inclined pipelines. The model included successive regimes of bubble propagation and open channel flow. The gravity impact as well as frictional loss was accounted for through employing the Darcy-Weisbach equation.

This section focuses on the verification of the proposed model through parametric studies to study the impact of pipeline length, inner diameter and inclination angle on the discharge velocity, wetted area and released mass during individual regimes. Then, an alternative equation is proposed based on the results of the parametric studies to calculate ϕ_n^{bf} for a given θ. The accuracy of the proposed equation is

tested by comparing the predicted ϕ_n^{bf} at small values of θ to the value of $\phi_n^{bf} = 175°$ predicted for horizontal pipe presented in Section (4.4.2.1).

The base case input data provided in Table 5.1 for the case of the model for pipeline fed from a storage tank are also applicable here except the initial liquid head.

5.4.3.1. Discharge Velocity and Wetted Area

Figure 5.25, Figure 5.26 and Figure 5.27 present the results of the parametric studies for the impact of pipeline length, inner diameter and pipe inclination angle on the discharge velocity in the ranges 50-200m, 0.305-0.406m and 20-50° respectively. On the other hand, the impact of the above parameters on the normalised wetted area can be seen in Figure 5.28, Figure 5.29 and Figure 5.30. The characteristics given in Table 5.1 are also applicable here except that there is no upstream storage tank.

From the graphs it may be observed that the trend is similar to those presented for isolated horizontal pipes in Section 4.4.3.1. The initial horizontal line corresponds to the discharge during bubble formation and propagation regime while the slow non-linear decline in the discharge velocity corresponds to open channel flow.

It can be seen from Figure 5.25 that for all pipe lengths, the discharge velocity during bubble formation and propagation is the same. This is expected as the bubble propagation velocity is not dependent on pipe length (see Equation (3.21)). As expected, the duration of the drainage process increases with pipeline length. The variation of discharge velocity with pipe inner diameter and pipe inclination angle also follow the expected trend (see Figure 5.26 and Figure 5.27). The discharge velocity increases with pipe inner diameter and θ, while the duration for the complete drainage of the pipe decreases.

On the other hand, similar to the horizontal pipe, the normalised wetted area remains constant and for $\theta = 30^o$ it is equal to 0.102. However, similar to the configuration with upstream tank it reduces with θ. The relation between θ and A_{wet} is discussed in Section 5.4.3.2.

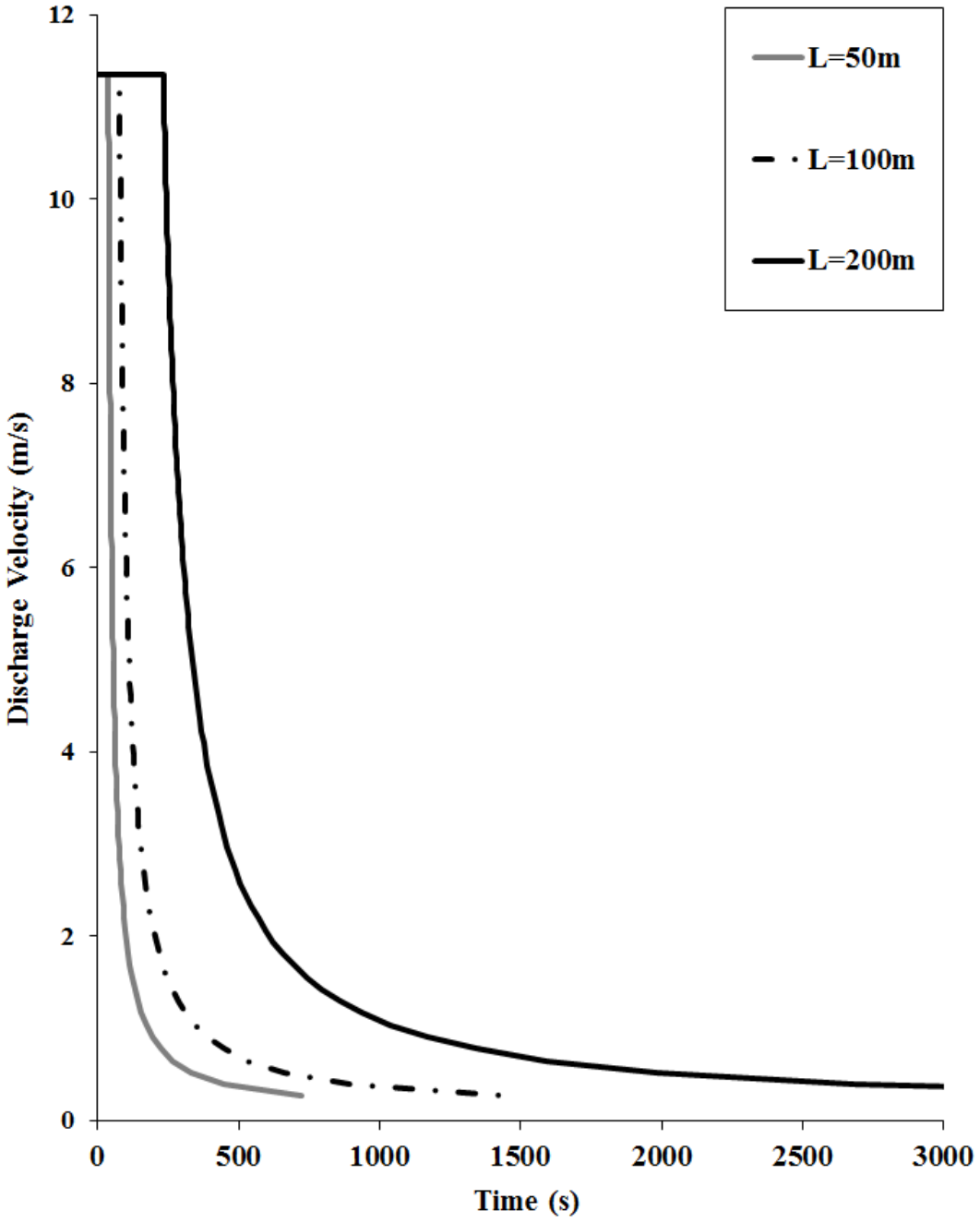

Figure 5.25: Impact of pipeline length on the variation of discharge velocity with time following full-bore rupture in a 0.406m diameter, isolated, 30^{o} downward-inclined pipe

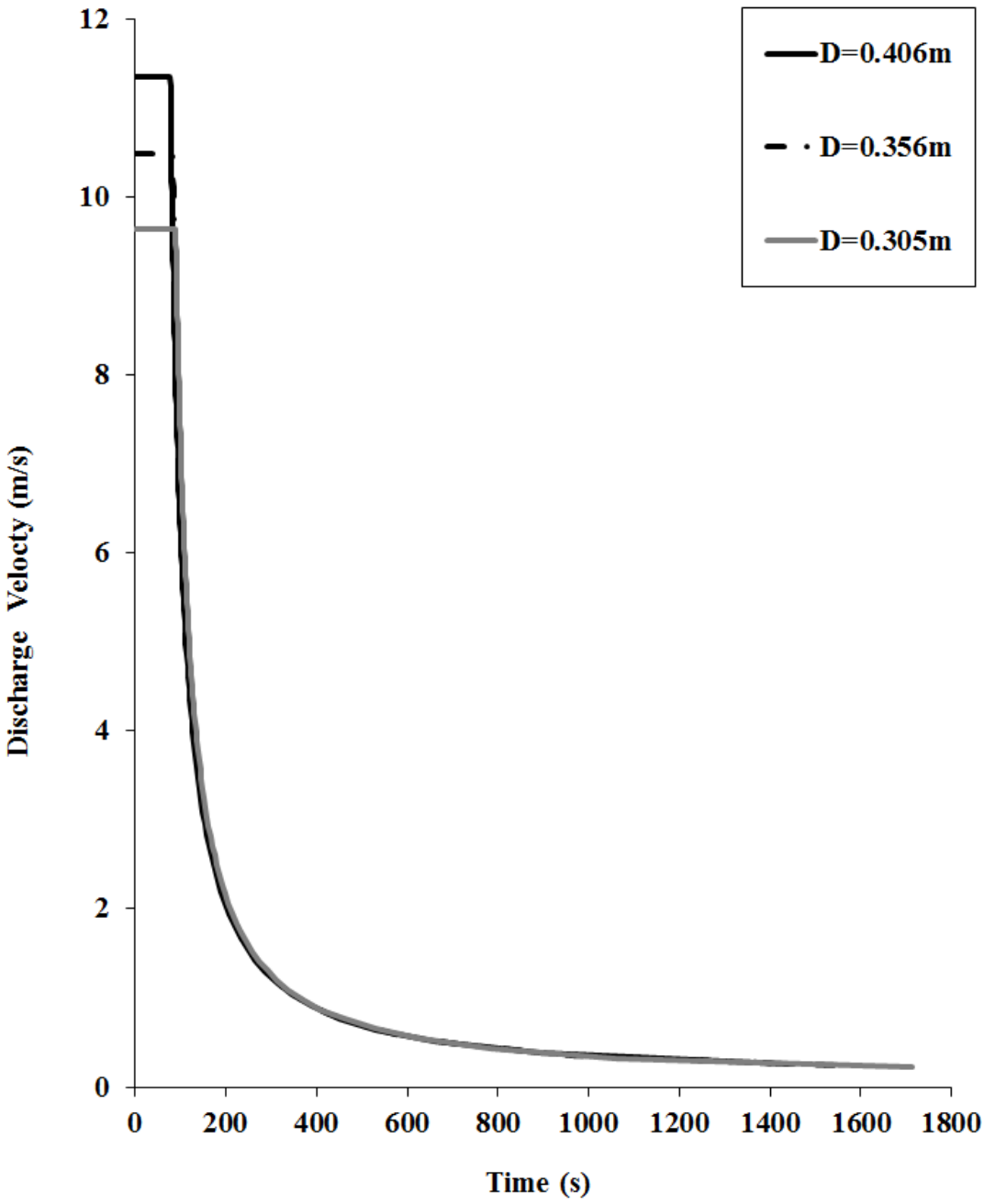

Figure 5.26: Impact of pipeline inner diameter on the variation of discharge velocity with time following full-bore rupture in a 100m long, isolated, 30^{o} downward-inclined pipe

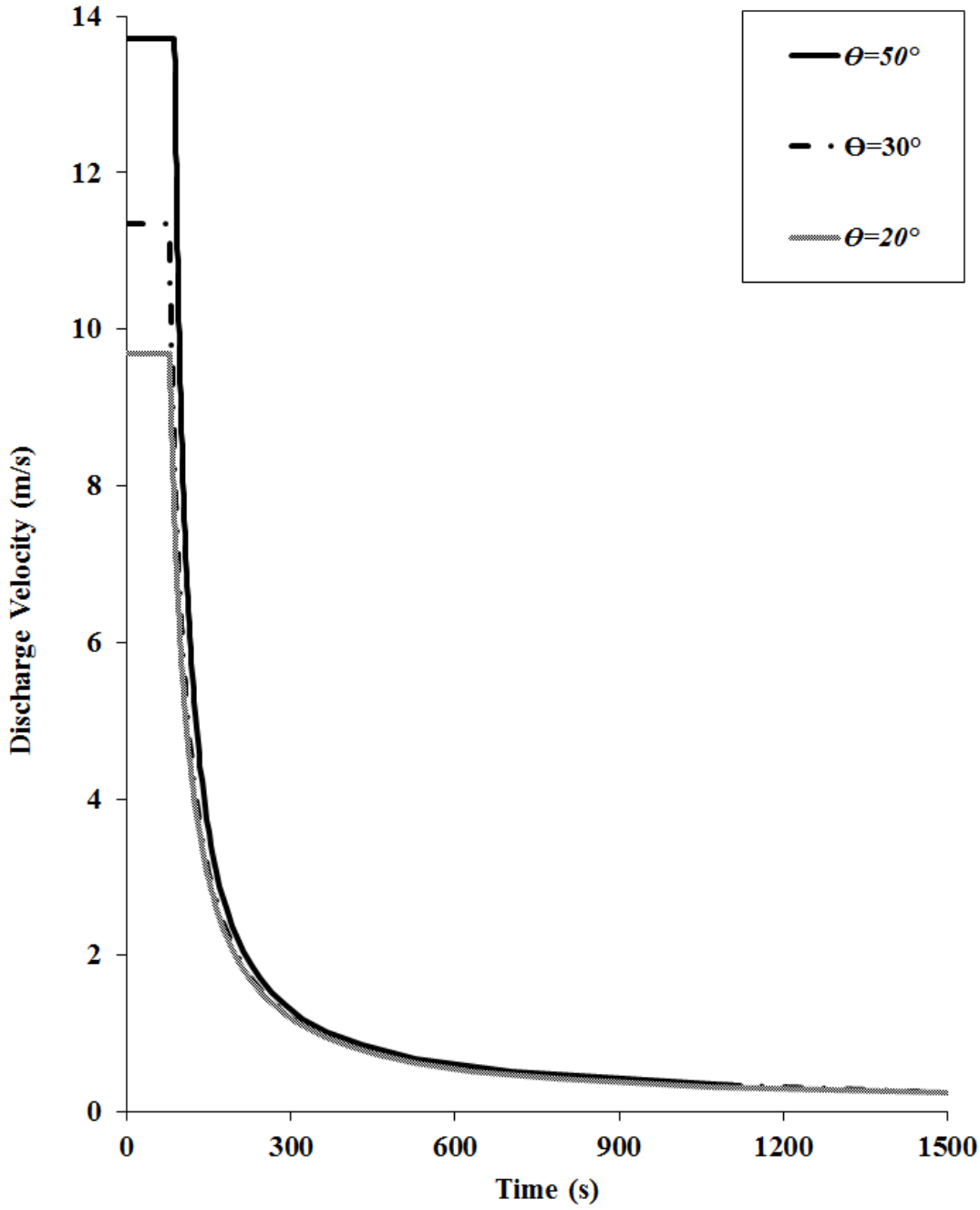

Figure 5.27: Impact of pipeline inclination angle on the variation of discharge velocity with time following full-bore rupture in a 0.406m diameter, 100m long, isolated downward-inclined pipe

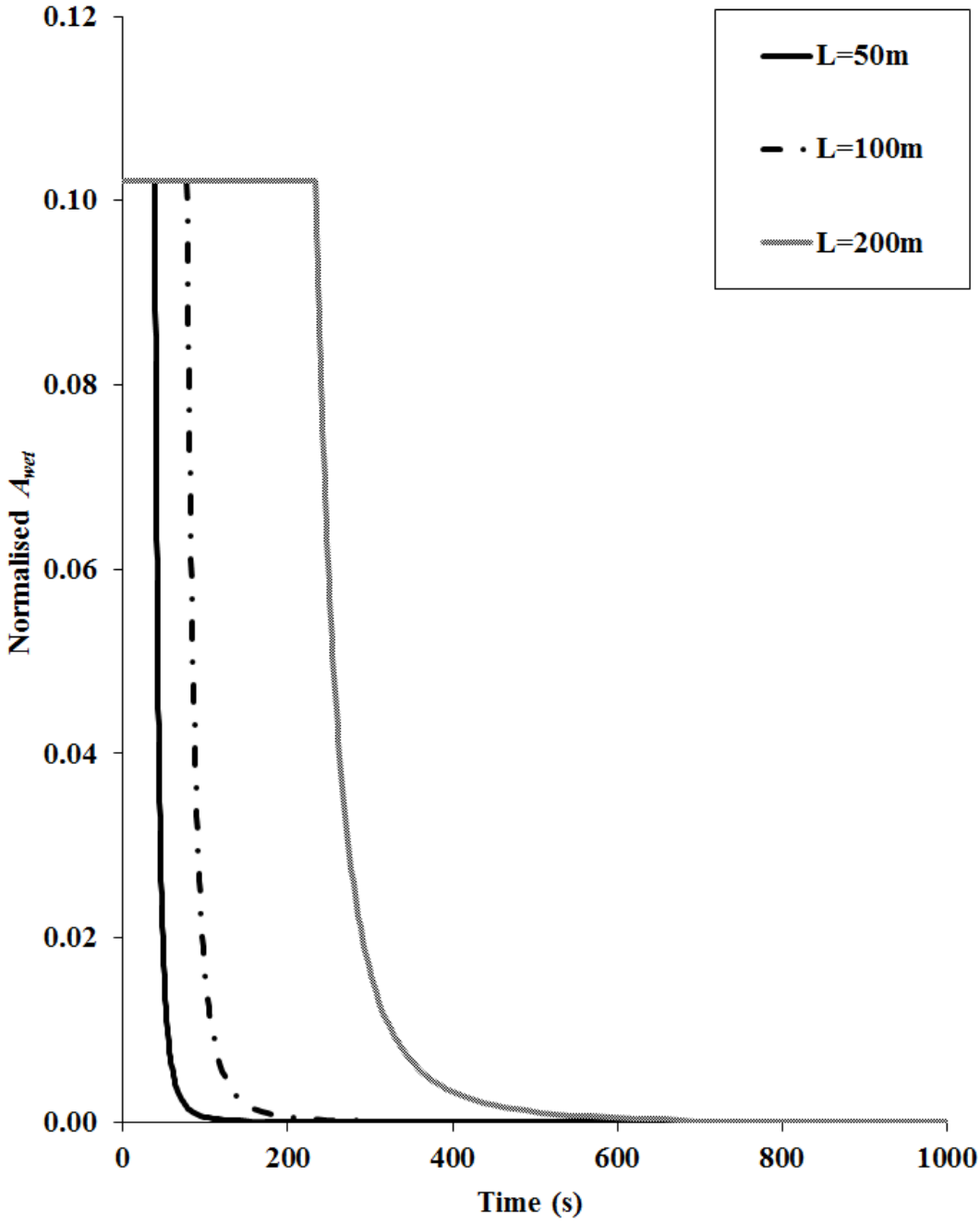

Figure 5.28: Impact of pipeline length on the variation of normalised A_{wet} with time following full-bore rupture in a 0.406m diameter, isolated, 30^o downward-inclined pipe

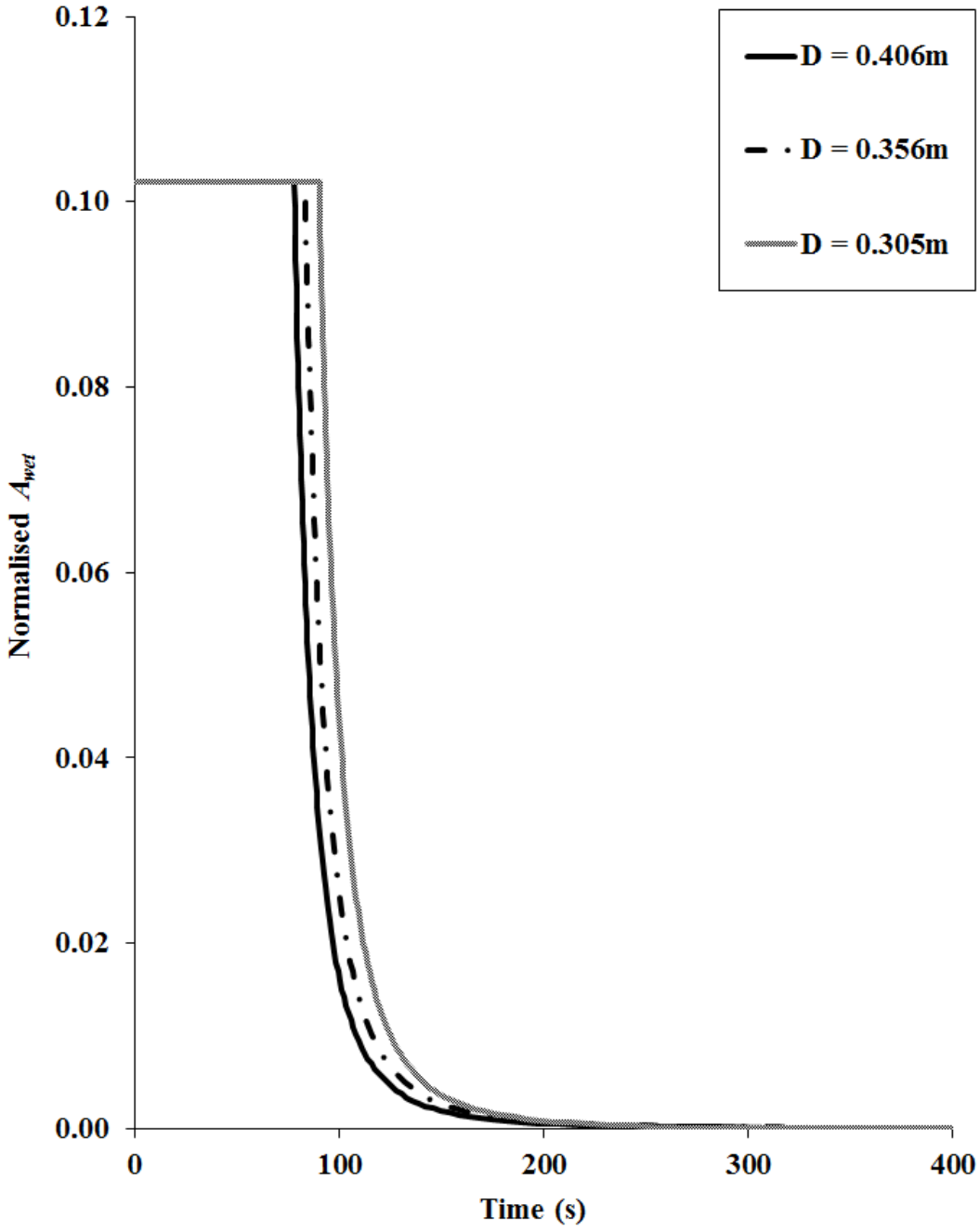

Figure 5.29: Impact of pipeline inner diameter on the variation of normalised A_{wet} with time following full-bore rupture in a 100m long, isolated, 30^o downward-inclined pipe

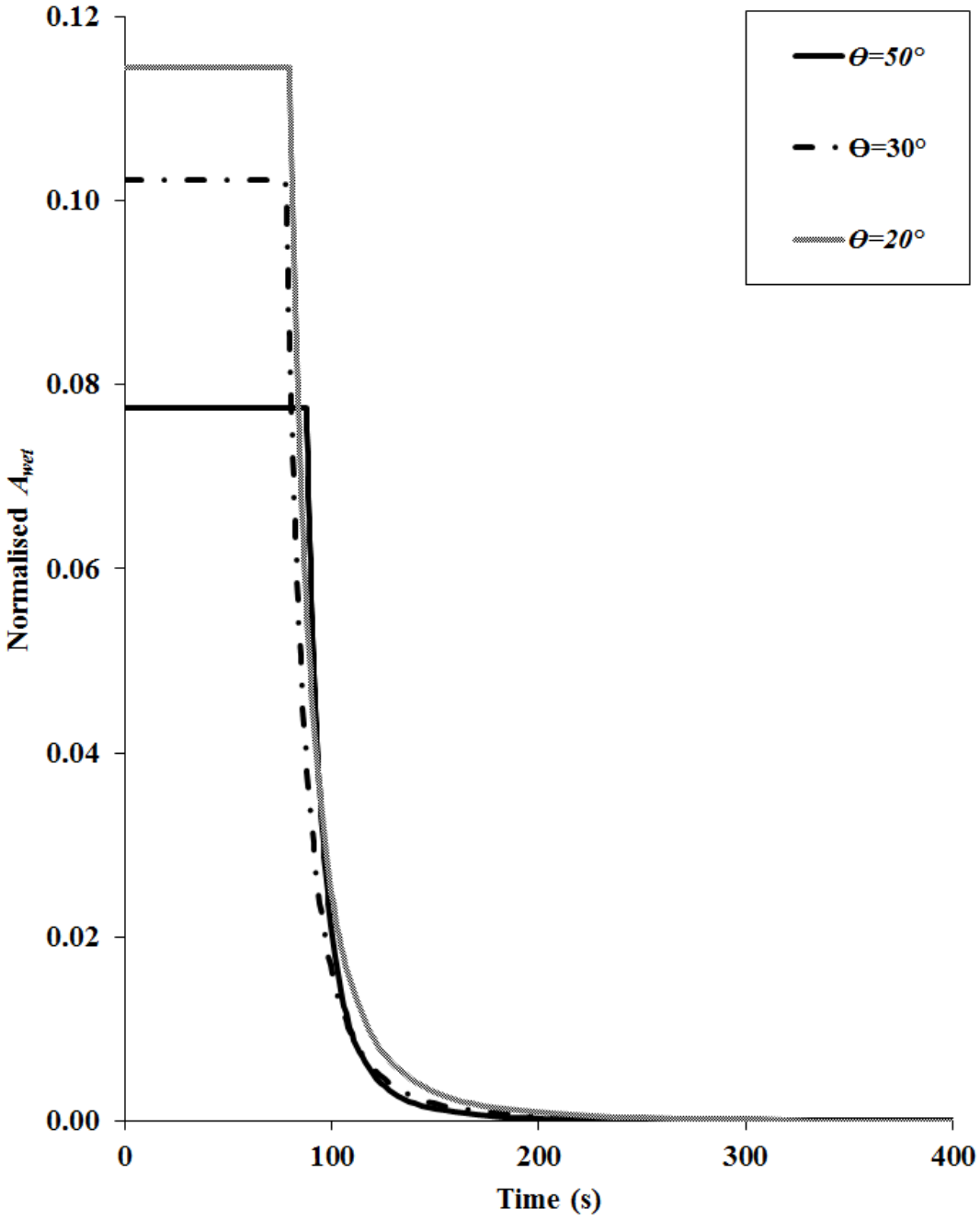

Figure 5.30: Impact of pipeline inclination angle on the variation of normalised A_{wet} with time following full-bore rupture in a 0.406m diameter, 100m long, isolated downward-inclined pipe

5.4.3.2. Variation of Liquid Depth Angle (ϕ_n^{bf}) with θ

Equation (5.30) derived to describe the relationship between ϕ_n^{bf} and θ needs to be solved iteratively:

$$\left(2\pi - \phi_n^{bf} + \sin\phi_n^{bf}\right)\left(0.542\cos\theta + 0.350\sin\theta\right) - \sqrt{\frac{\sin\theta}{2f\phi_n^{bf}}}\left(\phi_n^{bf} - \sin\phi_n^{bf}\right)^{1.5} = 0 \quad \textbf{(5.30)}$$

Similar to the model with upstream tank described in Section 5.3.3.4, in this section an alternative equation is developed based on the results from the parametric studies. Once again, Equation (5.30) is dependent on pipe inner diameter and surface roughness (ε) as well as θ. Employing the commonly used value of 0.05mm for ε, ϕ_n^{bf} is calculated for a range of pipe inner diameters and inclination angles. The results are presented in Figure 5.31.

As it can be seen from the figure, the variation of ϕ_n^{bf} with pipe diameter is marginal. Therefore, taking the average of the calculated ϕ_n^{bf} for each θ and applying a power-form trendline to the resulting curve, the following equation is obtained with $R^2 = 0.995$:

$$\phi_n^{bf} = 137.7\theta^{-0.113} \quad \textbf{(5.32)}$$

The above equation is undefined for θ=0. However, at θ =0.05° the average value of ϕ_n^{bf} is 193°. This equates to a deviation of 10% from the calculated value of 175° for horizontal pipe (see Section 4.4.2.1). For all other values of θ, the average values of ϕ_n^{bf} from Equation (5.32) are in close proximity to those obtained from Equation (5.30), with maximum deviation of $\pm 6\%$.

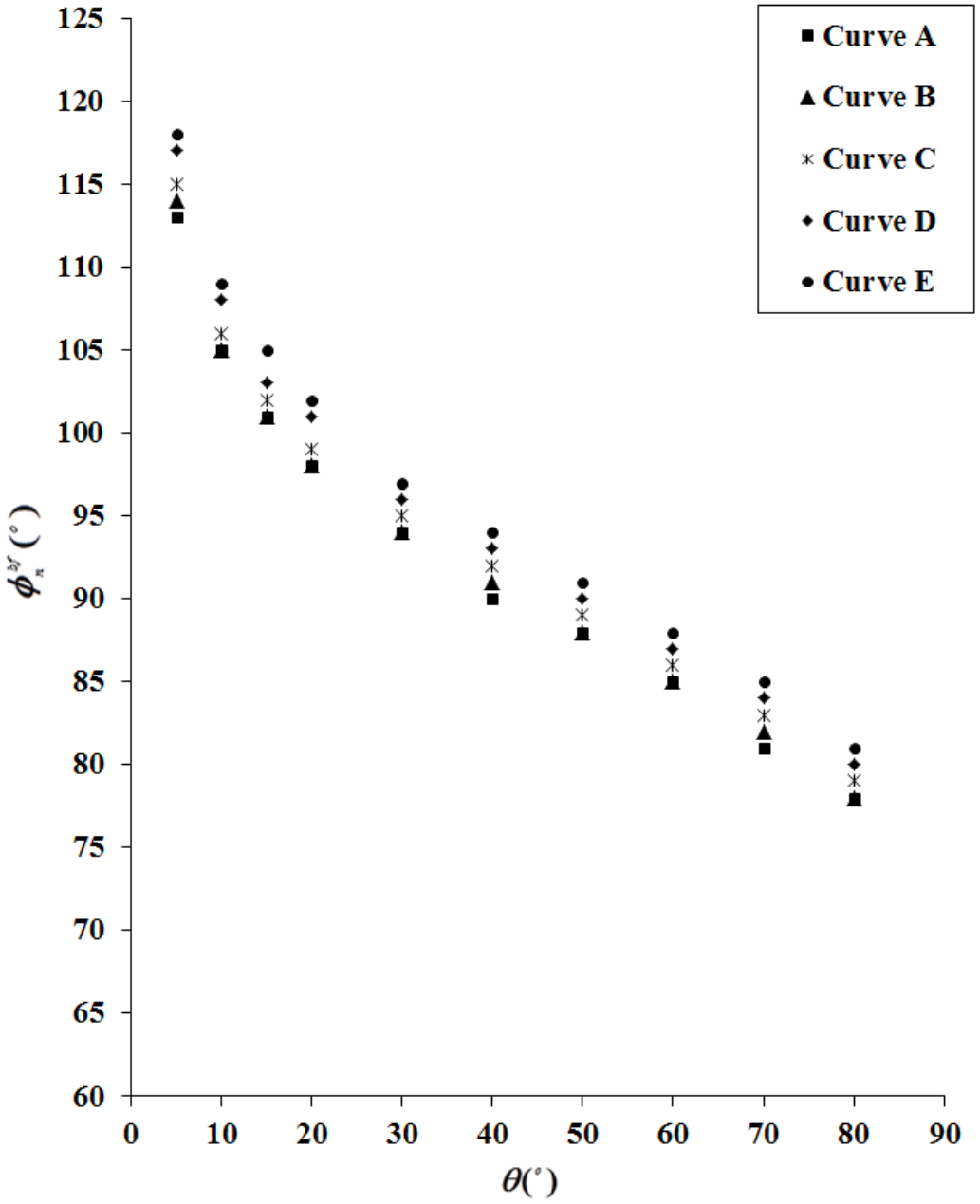

Figure 5.31: Variation of ϕ_n^{bf} with θ for a range of pipeline diameters following full-bore rupture in an isolated downward-inclined pipe

Curve A: D = 0.457
Curve B: D = 0.356m
Curve C: D = 0.254m
Curve D: D = 0.152m
Curve D: E = 0.102m

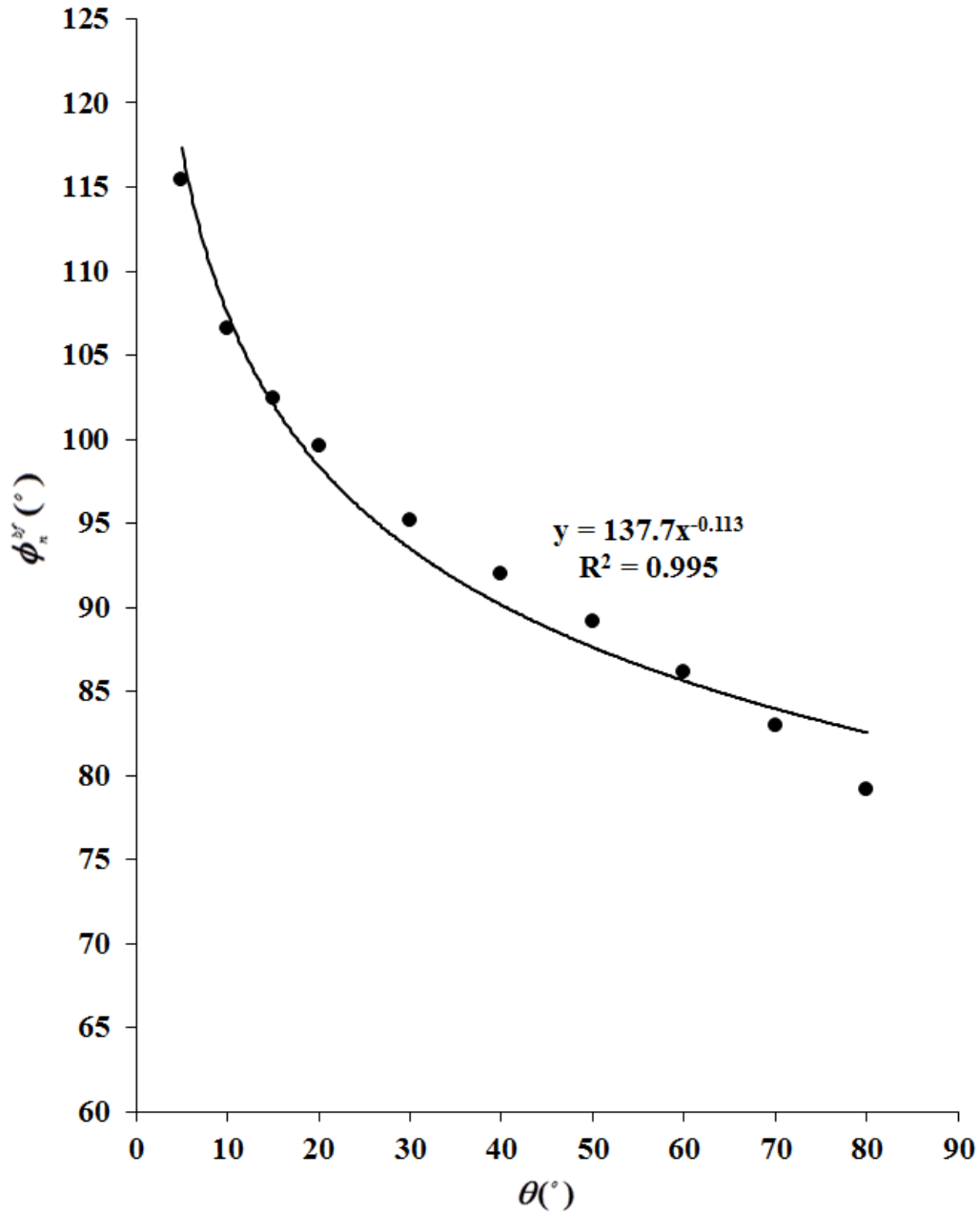

Figure 5.32: Variation of average ϕ_n^{bf} with θ following full-bore rupture in an isolated downward-inclined pipe

5.4.3.3. Released Mass during Individual Regimes

Table 5.4 presents the comparison between the predicted and theoretical discharged mass during each regime for pipeline length, diameter and inclination angle in the ranges 100-300m, 0.305-0.508m and 5-50° respectively. The calculation for the theoretical released mass during each regime is similar to what described in Section 5.3.3.3 except that only bubble propagation and open channel flow are relevant here.

- Bubble formation and propagation

$$M_{bubble\ propagation} = \rho\left(A - A_{wet}^{bf}\right)L = \rho L\frac{D^2}{8}\left(2\pi - \phi_n^{bf} + \sin\phi_n^{bf}\right) \quad \textbf{(5.20)}$$

- Open channel flow

$$M_{open\ channel\ flow} = \rho A_{wet}^{bf} L = \rho L\frac{D^2}{8}\left(\phi_n^{bf} - \sin\phi_n^{bf}\right) \quad \textbf{(5.21)}$$

Scenario			Bubble propagation		Open channel flow	
Length (m)	Diameter (m)	Angle (°)	Theoretical (kg)	Predicted (kg)	Theoretical (kg)	Predicted (kg)
100	0.305	30	6486	6519	763	744
100	0.406	30	11547	11589	1315	1281
100	0.508	30	18077	18144	2059	2006
200	0.406	30	23094	23178	2630	2563
300	0.406	30	34640	34768	3946	3843
100	0.406	50	11865	11902	997	979
100	0.406	20	11389	11434	1473	1436
100	0.406	5	10661	10696	2201	2174

Table 5.4: Comparison of the theoretical and predicted discharged mass during individual regimes following full-bore in an isolated, downward-inclined pipe

Once again it is clear from the table that the predicted and the theoretical discharged mass are very close for all scenarios, with maximum deviation of 3%.

5.4.4. Error Analysis and Dependence of Convergence on $\Delta\phi_n$

This section presents the error analysis for the drainage process including bubble formation and open channel flow in a downward-inclined pipe. Similar to the horizontal pipe presented in Section 4.4.4, the impact of the increment $\Delta\phi_n$ on the convergence in trapezoidal rule used to estimate Equation (5.18) is investigated.

Figure 5.33 shows the discharge rate versus time for various values of $\Delta\phi_n$. The pipe length, diameter and pipe inclination angle are 100m, 0.406m and 30^o respectively. As it may be observed from the graph, similar to the horizontal pipe the convergence in the trapezoidal method used to estimate Equation (5.18) is not affected by the increment. However, the predicted discharge rate during bubble formation and propagation is not the same for all values of $\Delta\phi_n$. For $\Delta\phi_n$ = 3 the model underestimated the discharge rate, while $\Delta\phi_n$ = 5 results in a higher discharge rate compared the other values of $\Delta\phi_n$. All other values of $\Delta\phi_n$ produce the same discharge rate during bubble formation and propagation regime.

On the other hand the impact of the increment $\Delta\phi_n$ on the accuracy of the developed model in calculating the total expelled mass is presented in Figure 5.34. Similar to the horizontal pipe, the deviation between the predicted and theoretical expelled mass, presented in the form of Δ total expelled mass, increases with $\Delta\phi_n$. The theoretical expelled mass is calculated based on the approach described in 5.4.3.3.

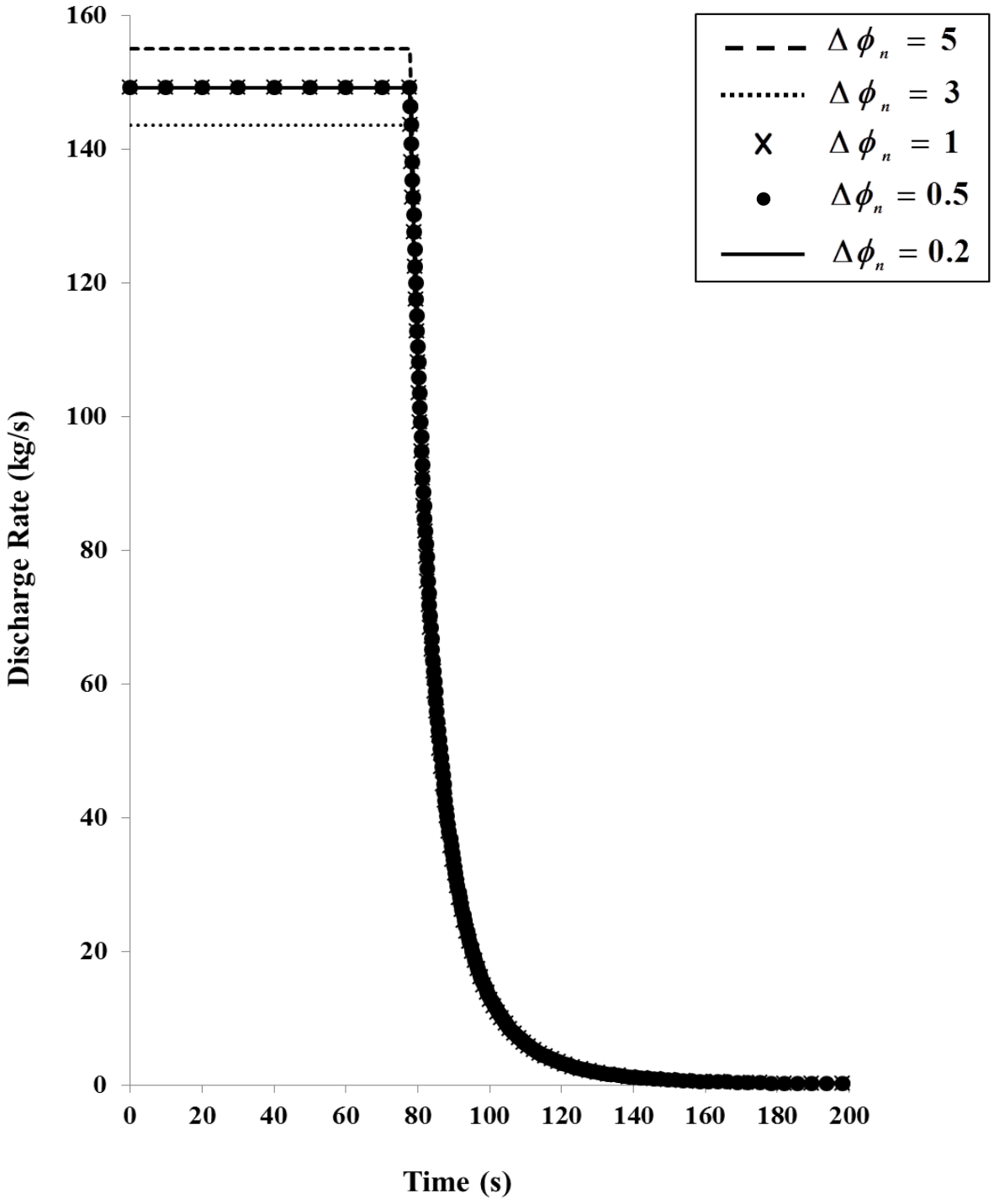

Figure 5.33: Impact of $\Delta\phi_n$ on the convergence in trapezoidal method in a 100m long, 0.406m diameter, 30^o downward-inclined pipe

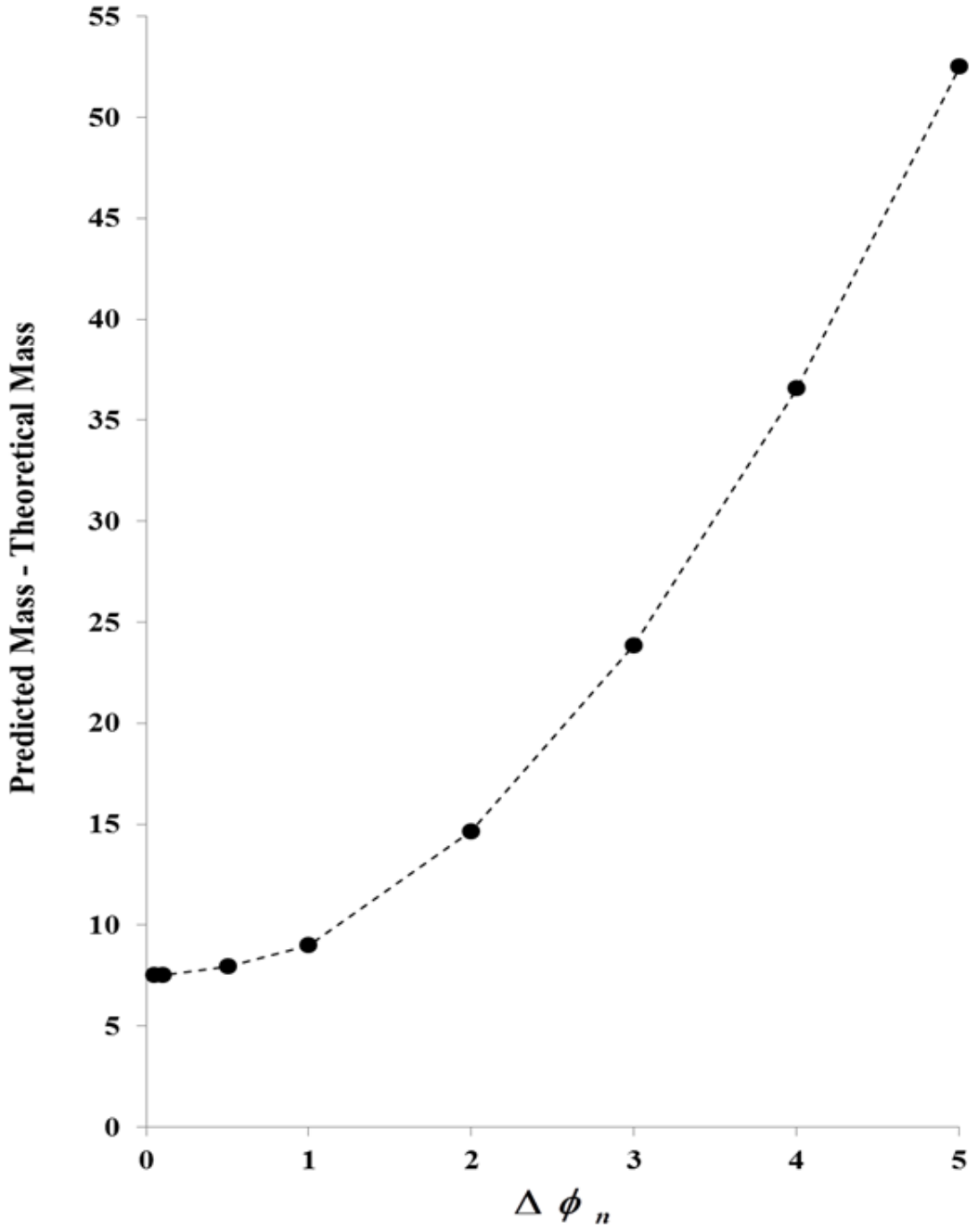

Figure 5.34: Impact of $\Delta\phi_n$ on the accuracy of the developed model for a 100m long, 0.406m diameter, 30^o downward-inclined pipe in predicting the total expelled mass

5.4.5. Experiments

This section presents the results from a series of experiments conducted to assess the accuracy of the proposed model for isolated downward-inclined pipe in calculating the discharge rate. Similar to the isolated horizontal pipes, the investigations are carried out by measuring the cumulative discharged mass.

Figure 5.35 shows the experimental setup used to measure the cumulative discharged mass for an isolated downward-inclined pipe. The setup is the same as that used for measuring the cumulative discharged mass in the isolated horizontal pipe, except that here the 0.034m inner diameter, 3m long, acrylic pipe (2) is declined by approximately 6°.

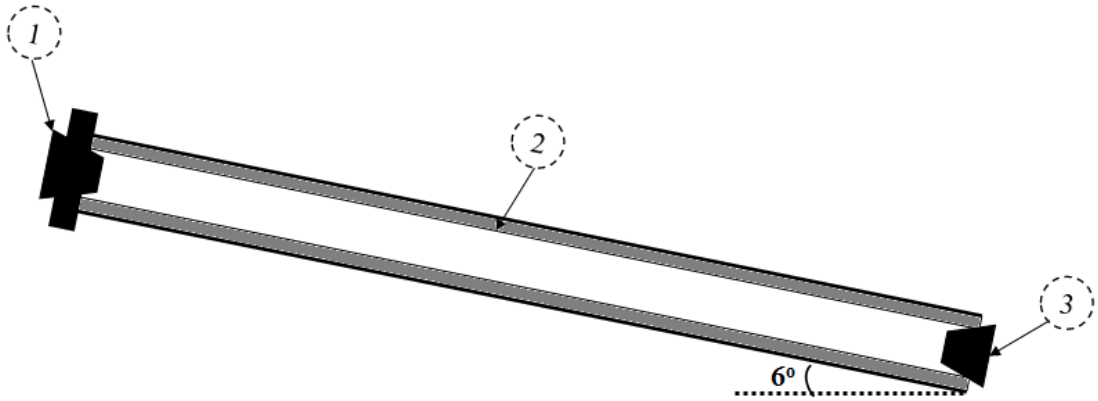

Figure 5.35: Experimental setup to measure the cumulative discharged mass from an isolated downward-inclined pipe

1 & 3) Rubber bung
2) Acrylic pipe

Figure 5.36, Figure 5.37 and Figure 5.38 respectively show the comparison between the predicted and measured discharge rate in linear and logarithmic scale, and measured normalised cumulative discharged mass respectively.

It may be observed from the figures that unlike the horizontal pipe case, the measured discharge rate does not remain constant during bubble propagation regime. In fact it increases significantly towards the end of this regime, which is believed to

be as a result of the decrease in the wall/pipe friction loss. Although in the model for the downward-inclined pipe the frictional loss is considered, it is assumed to be constant for the duration of bubble propagation regime. However, based on the results it is clear that the reduction in frictional loss can have a significant impact on the discharge rate. Further work is recommended to account for the variation of frictional loss with time.

It is worth noting that due to the small scale of the experiment (L = 3m) and the pipe being declined, the duration of the released is very short, less than 20s. Therefore, it is difficult to obtain reliable results specifically during the later stage of drainage, i.e. open channel flow. Conducting further experiments for longer pipes can explain the observed trends with greater confidence.

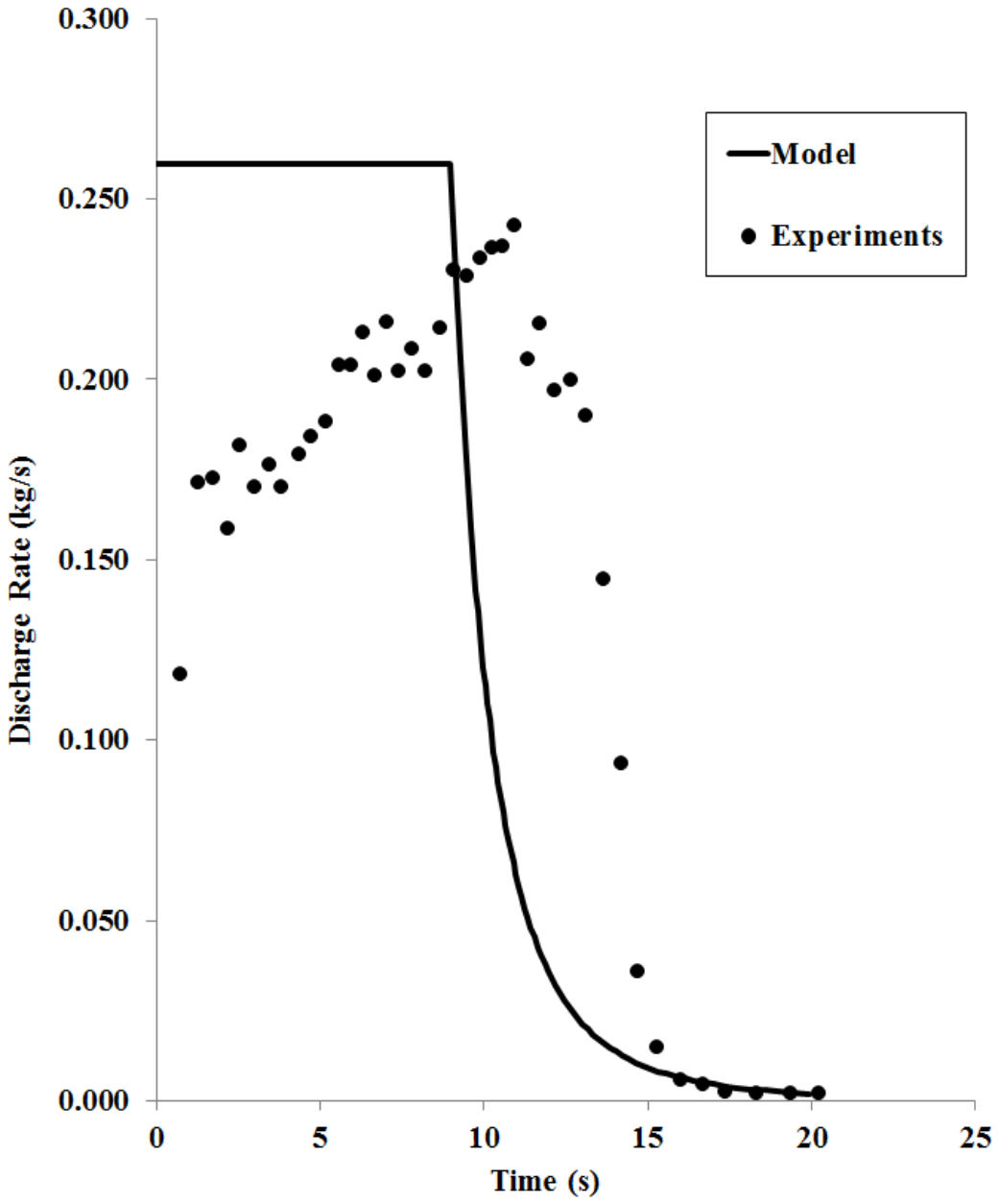

Figure 5.36: Comparison of the measured discharge rate with the predicted values from the model following full-bore rupture in an isolated downward pipe in linear scale

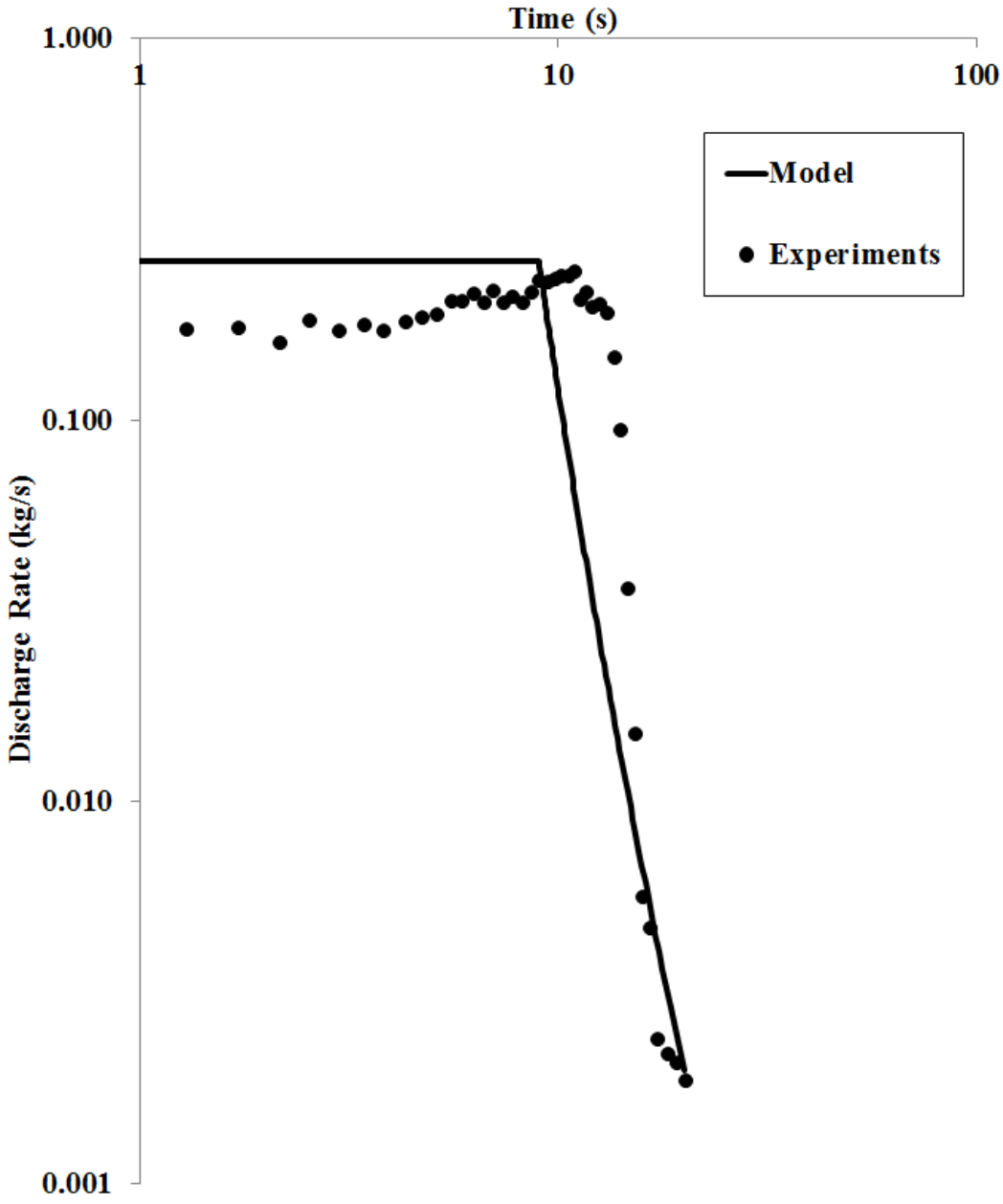

Figure 5.37: Comparison of the measured discharge rate with the predicted values from the model following full-bore rupture in an isolated downward pipe in logarithmic scale

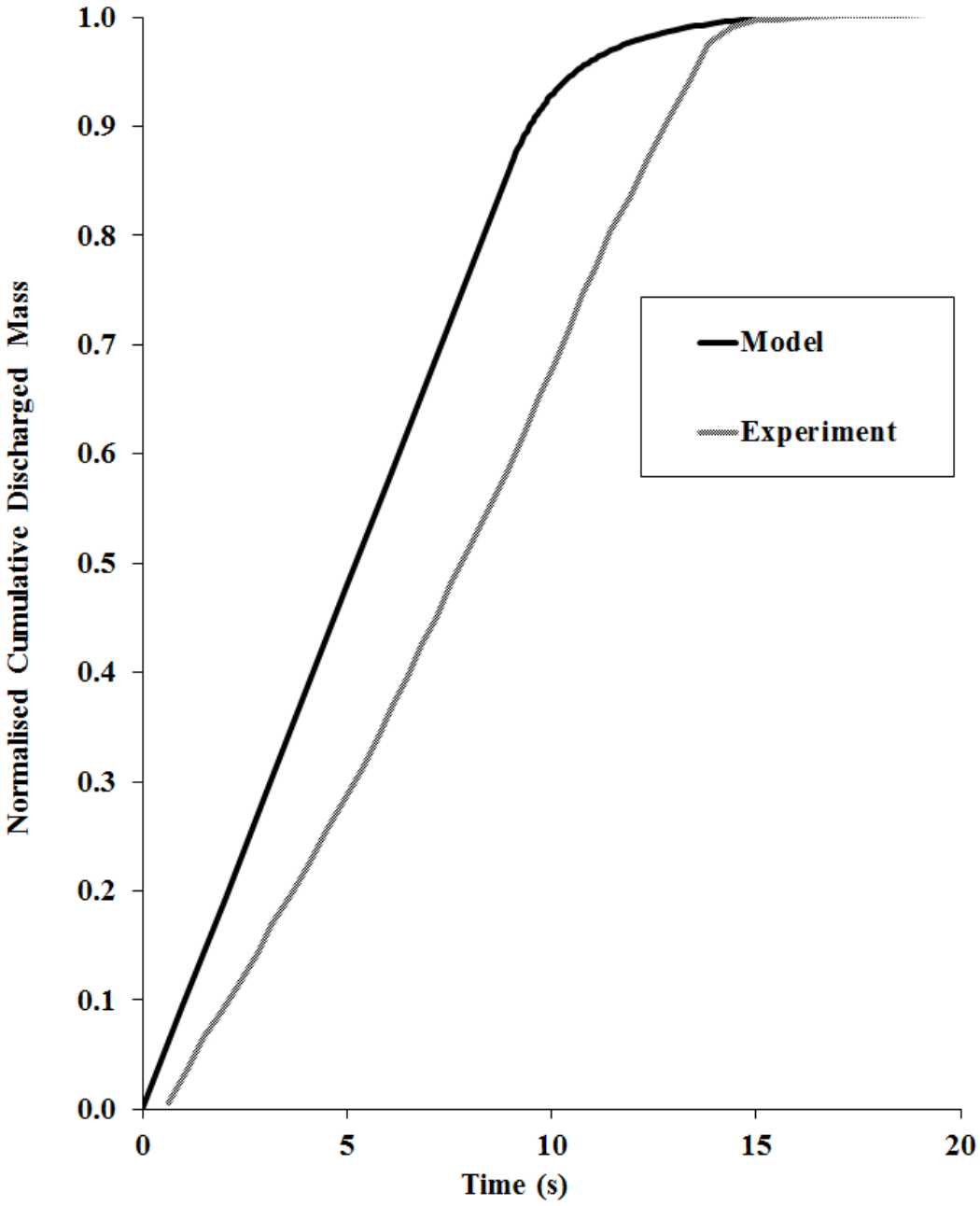

Figure 5.38: Comparison of the measured normalised cumulative discharged mass with the predicted values from the model for the outflow from the isolated downward-inclined pipe

5.5. Conclusion

In this chapter the development, verification and validation of mathematical models to simulate the outflow upon full-bore rupture in downward-inclined pipelines were presented. Similar to the horizontal pipe, two upstream boundary conditions including upstream storage tank and isolated pipe following Emergency Shut Down Valve (ESDV) closure were considered.

In order to formulate the model for the pipe fed from an upstream tank, first the previously developed model for the horizontal pipe was modified by introducing the pipe inclination angle. The critical discharge theory was also replaced by the Darcy-Weisbach equation to calculate the discharge during bubble propagation and open channel flow.

Two patterns for bubble propagation along the pipe were considered:

- Bubbles propagation from both ends
- Bubble propagation only from the pipe inlet (upstream)

Similar to the case of a horizontal pipe, the first pattern was modelled based on the application of continuity and mass balance between the propagating bubbles and discharging liquid. This model was then simplified by assuming $u_{db} = 0$ allowing only the propagation of the upstream bubble for the second pattern. The drift velocity method was then used to determine the dominant pattern in the pipe for a range of pipeline characteristics including length, inner diameter and inclination angle. It was found that except for nearly horizontal pipelines, the liquid velocity u was always higher than u_{drift}, confirming the occurrence of the second flow pattern in the pipe.

Based on this finding, the efficacy of the developed model for the second pattern was then verified through studying the impact of pipeline characteristics on the discharge velocity, wetted area and cumulative discharged mass. It was observed that the rapid recovery in the discharge velocity was only present for short or large diameter pipes. This discontinuity was due to the negligible impact of pipe entry loss present only in full pipe flow compared to fluid/wall frictional loss in long or small

diameter pipelines. Consequently, the predicted discharge velocity at the end of full pipe flow was higher due to presence of larger liquid head in the form of $Lsin\theta$.

This was in contrast to the observation for horizontal pipes where the magnitude of the recovery was more significant in long or small diameter pipes. Furthermore, similar to horizontal pipes, it was shown that for long or large diameter pipelines, the majority of the mass was released during post-full pipe flow. The cumulative discharged mass during the individual regimes marginally varied with θ.

Based on the results from the parametric studies, a simplified equation was proposed to describe ϕ_n^{bf} as a function of θ only. This was done by taking the average of the calculated ϕ_n^{bf} from the model and applying a power-form trendline to the resulting curve. ε was assumed to be 0.05mm, a widely-used value for carbon steel. For all values of $\theta > 6°$ the average values of ϕ_n^{bf} calculated from the proposed equation and the model were in good agreement, with maximum deviation of $\pm 3\%$.

Through series of experiments the applicability of the proposed value of 0.98 for the empirical coefficient C_0 suggested by Bendiksen (1984) for calculating the upstream bubble propagation velocity was investigated. It was observed that compared to the experimental results, the model underestimated the bubble propagation velocity, u_{ub}. The same behaviour was observed for ϕ_n^{bf}, with the predicted value from the model being 22% less than the measured data. A possible explanation of this trend was the impact of additional momentum imposed on the flow due to the presence of the upstream liquid head in the tank. In addition, Bendiksen (1984) introduced the bubble from the base of the pipe, instead of bubble propagation from the pipe inlet. Based on these explanations, a new value for C_0 was proposed by applying power-form trendlines to the resulting curves showing (measured ϕ_n^{bf} / predicted ϕ_n^{bf}) and (measured u_{ub} / predicted u_{ub}) for a range of C_0. Equalling the resulting equations to 1 produced 1.55 for C_0.

In addition, the accuracy of the model in predicting the discharge rate was tested by measuring the cumulative discharged mass and calculating the discharge rate based on the measured values. It was observed that similar to the horizontal pipe, K = 2.5 proposed in Chapter 4 to account for the additional entry loss due to silicon sealant produced closer results to the experimental data. However, the suggested value of 1.55 for C_0 instead of original value of 0.98 (Bendiksen, 1984) resulted in larger deviation of calculated cumulative discharge mass and discharge rate from the experimental data.

It was postulated that unlike the case of co-current bubble propagation in a downward-inclined pipe without the upstream tank, here C_0 was dependent on pipe characteristics such as pipeline length and inner diameter. In addition, the pipe used for measuring the cumulative discharged mass was mildly declined ($\theta = 6^o$), whereas θ was 12^o in the experiment for bubble propagation velocity. Therefore, the impact of upstream liquid head on the bubble propagation velocity was not significant. Further investigations can determine a unique value for C_0 which would produce minimum discrepancy for both u_{ub} and cumulative discharged mass.

The second part of this chapter focused on a pipe with upstream closed-end where the bubble could only propagate from the opening at the downstream end of the pipe. For this configuration, the developed model for the pipe fed from the upstream tank was used without full pipe flow. Similar to the configuration with upstream tank, a relationship between ϕ_n^{bf} and θ was established based on the results from the parametric studies. The calculated ϕ_n^{bf} from the resulting equation and the predicted values by the model for all values of $\theta > 6°$ were in good agreement, with maximum deviation of $\pm 6\%$.

Finally, through series of experiments the accuracy of the model in predicting the discharge rate was assessed through measuring the cumulative discharged mass. From the results it was observed that unlike the horizontal pipe case, the discharge rate during bubble propagation increased with time possibly as a result of reduction in fluid/pipe wall loss, which was assumed to remain constant in the model. Further

experiments are recommended to be carried out in larger scale to confirm the above trend.

CHAPTER 6: CONCLUSION AND FUTURE WORK

6.1. Conclusion

This thesis described the development and application of mathematical models for simulating the transient outflow following full-bore rupture of pressurised pipelines containing incompressible liquids. Two configurations were considered for the pipeline:

- Pipeline fed from an upstream storage tank
- Isolated pipeline where the pipe was closed at one end following emergency shut down

The models for the configurations with upstream tank accounted for full pipe flow, bubble formation and propagation, and open channel flow. For the isolated pipe models only the last two regimes were applicable. Full pipe flow for full-bore rupture case was modelled by employing the published model by Joye & Barrett (2003). Effort was particularly concentrated on developing flow equations for the bubble propagation regime based on Benjamin's bubble theory (1968) and Bendiksen's findings (1984) for bubble velocity in various pipeline configurations. For open channel flow, depending on the pipe inclination angle, the flow was assumed as either critical (horizontal pipe) or normal (downward-inclined pipe).

Chapter 2 presented the theoretical basis for the pipeline outflow model with its assumptions and justifications. The basic equations governing the flow of incompressible liquids in pipes, including the conservation equation for mass and the Bernoulli equation were explained and discussed.

In Chapter 3 a thorough review of the available mathematical models for simulating failures of pipelines containing incompressible (non-flashing) liquids were presented. This included models for full pipe flow, bubble formation and propagation, and open channel flow.

Chapter 4 described the development, verification and validation of hydraulic transient models to simulate the outflow following full-bore rupture in horizontal pipes. The impact of fluid/wall pipe frictional loss was ignored during post-full pipe flow. For the configuration with an upstream storage tank, it was assumed that the bubble formation from both ends of the pipe started once the liquid head reached the critical depth, which in turn remained constant throughout the bubble propagation regime. In the absence of frictional loss, the corresponding liquid depth angle was calculated as 216^{o}. Through experiments for short pipes, it was observed that this liquid depth below the bubble indeed remained unchanged, with close proximity to the calculated value from the model. The results from the proposed equation by Bendiksen (1984) for single, co-current bubble propagation velocity were very close to those obtained from the model for co-current bubble propagation in the presence of downstream bubble and upstream liquid head.

In addition, the original full pipe model developed by Joye & Barrett (2003) underestimated the discharge velocity compared to the measured values which was believed to be due to an additional entry loss from silicone sealant at the pipe entrance. A new entry loss coefficient of 2.5 was suggested which produced significantly closer results to the measured value for all three regimes.

Similarly for isolated pipe, the variation of liquid depth with time during bubble propagation regime was ignored, while the downstream bubble approached the closed-end. Based on the experimental results, the assumption of constant discharge rate during this regime was valid for the isolated pipe. The slight increase in the discharge rate towards the end of the regime was believed to be due to ignoring fluid/pipe wall loss.

Based on the results from the parametric studies, it was observed that the majority of the inventory (>50%) for long or large-diameter pipelines was released during the regimes of bubble propagation and open channel flow, i.e. after full pipe flow. Therefore, ignoring these two regimes could potentially result in significant underestimation of mass upon full-bore rupture. Comparing the theoretical and

predicted released mass during individual regimes proved the model's efficacy in predicting the released mass, with maximum deviation of 1%.

In addition, there was a recovery in the predicted discharge velocity at the end of full pipe flow which increased with pipeline length, but decreased with pipe inner diameter. This trend, which was believed to be a discontinuity in the model, stemmed out from the assumption of negligible frictional loss during post-full pipe flow.

Chapter 5 focused on the extension of the developed models in Chapter 4 to account for the pipe inclination angle for both isolated pipes and those fed from an upstream tank. Here the impact of frictional loss was accounted for during all three regimes. However, its reduction with time during bubble propagation regime was assumed to be negligible. Two patterns were assumed for the bubble propagation regime in this case. The first pattern was similar to that in horizontal pipe, i.e. bubble propagation from both ends of the pipe. In the second pattern it was assumed that the bubble only propagated from the pipe upstream, while there was a stagnant cavity at the pipe downstream. Based on the drift velocity method, it was showed that except for horizontal pipes the dominant pattern in downward-inclined pipes was the second pattern, regardless of pipeline characteristics.

In addition, the experimental results showed that the proposed equation by Bendiksen (1984) for single, co-current bubble propagation velocity could not be applied to the case of upstream bubble propagation in the presence of a downstream bubble and upstream liquid head in a downward-inclined pipe. A new coefficient was then suggested to modify Bendiksen's equation (1984). However, using the new coefficient did not produce the closest results for the predicted discharge rate against the measured values. Since the new coefficient was obtained for a pipe with different characteristics, it was postulated that unlike horizontal pipe, here the empirical coefficient for bubble propagation velocity was not independent of pipeline characteristics.

On the other hand, it was interesting to see that unlike horizontal pipe, the assumption of constant discharge rate during bubble propagation in isolated downward-inclined pipes was not valid. A significant increase was observed in the discharge velocity, specifically towards the end of the bubble propagation regime. This phenomenon was also explained by the impact of reduction in frictional loss during bubble propagation regime which was not considered in the model. It was concluded that while for horizontal pipes this assumption may be valid, further work would be required to account for the variation of fluid/pipe wall loss with time.

The parametric studies results showed that unlike pipe length and diameter, the angle of inclination did not have a major impact on the amount of mass released during individual regime. In addition, based on the results from the parametric studies for both configurations, simplified equations were proposed to describe the relation between the constant liquid depths below the bubbles during bubble propagation with pipe inclination angle. The proposed equations were valid for $\theta > 6^o$ with $\pm 3\%$ and $\pm 6\%$ deviation from the original equations developed in the models for a pipe connected to an upstream tank and an isolated pipe respectively.

The discontinuity in the model for the discharge velocity at the end of full pipe flow indicated a different behaviour for downward-inclined pipes comparing to horizontal pipes. Here the recovery in the discharge velocity increased with pipe diameter, but decreased with pipeline length. This was explained by the negligible impact of entry loss during full pipe flow due to presence of significant fluid/pipe wall loss for small diameter or long pipelines and the presence of additional liquid head, $Lsin\theta$.

In conclusion, the work presented in this study provides the mathematical basis for the accurate assessment of the consequences associated with the rupture of pressurised pipelines containing incompressible liquids. It goes beyond the current state of the art by allowing the analysis of the post-full pipe flow which was ignored by numerous authors who studied the outflow upon failure of liquid pipelines. This development addresses pipelines with various inclination angles, isolated or fed from storage tanks. Furthermore, this work illustrates the importance of accounting for

post-full pipe flow on the total amount of inventory discharged when modelling such types of failures.

Since the discharge rates act as the source terms for subsequent dispersion, fire and explosion, the results of this work will help to define the hazardous effects with greater certainty. Not only will this help to identify physical effects but will also yield cost benefits in terms of targeted control, protection and mitigation systems designed to combat these effects.

6.2. Suggested Future Work

Variation of fluid/pipe wall loss with time during bubble propagation regime

In the models developed in the present work, the variation of frictional loss with time during bubble propagation regime has been ignored. Based on the experimental results, there is obvious need to extend the models to account for this variation. Validation of the extended model with further experiments for pipes with various surface roughness values is highly desirable.

Variation of liquid depth and bubble propagation velocity with time during bubble propagation regime

The basic assumption for modelling bubble propagation upon full-bore rupture in this study was constant liquid depth below the bubbles and bubble propagation velocity throughout this regime. While based on the experimental results this assumption proved to be relatively valid for short pipes, it might not produce accurate results for long pipelines where the impact of frictional loss will also be more significant. Conducting further experiments for various pipeline lengths can confirm the applicability of the above assumption. Depending on the findings from the experiments, detailed CFD modelling for bubble propagation velocity will provide further knowledge on this matter.

Model discontinuity in predicting the discharge velocity at the end of full pipe flow

Based on the results from the parametric studies, there were discontinuities in discharge velocity at the transition from full pipe to bubble propagation regime. Although this is believed to be the models artefacts, further investigations along with more experiments can clarify this matter.

Initiation of downstream bubble propagation during full pipe flow in horizontal pipes connected to upstream storage tanks

In this study it was conservatively assumed that the upstream and downstream bubbles propagation started simultaneously once the liquid level in the tank reached d_c^{bf} . However, for long distance pipelines, the downstream bubble propagation might initiate earlier during full pipe flow. Further investigations including modelling and experiments are highly recommended to account for this phenomenon.

Modelling outflow for pipelines containing highly viscose fluids

The findings from this study were based on low/negligible viscosity fluid. The proposed equation for bubble propagation velocity by Bendiksen (1984) was applicable to the fluids with negligible viscosity. In addition, the experiments were conducted for water with low viscosity. Further experiments for fluids with high viscosity are strongly recommended to compare with the developed model in this work. Based on the results, possible extension of the bubble propagation model will allow the use of the overall outflow model for broader range of viscosities.

Modelling outflow upon leakage in a pipe

The focus of this work has been on the full-bore rupture, representing the worst case scenario. Extension of the developed models is highly recommended to account for the leakage in the pipe.

NOMENCLATURE

A : pipe cross sectional area

A_b : bubble cross sectional area

A_{tank} : tank cross sectional area

A_{wet} : wetted area

C_{chezy} : Chezy coefficient

C_v : velocity coefficient

C_0 : bubble velocity coefficient

D : pipe inner diameter

d : liquid depth

D_h : hydraulic diameter

D_{tank} : tank diameter

d_c : critical depth

d_e : brink depth

d_n : normal depth

e: total energy of the unit mass

$E_{specific}$: specific energy

F : mechanical energy converted to heat

f : Fanning friction factor

F_c : frictional loss due to sudden contraction

F_e : frictional loss due to sudden expansion

F_f : fluid/pipe wall frictional loss

F_{ft} : frictional loss due to fittings and bends

Fr : Froude number

g: gravitational acceleration

H : liquid head in the tank

h : specific enthalpy

h_l : head loss

i: internal energy

K : velocity head coefficient

L : pipe length

L_e : equivalent length for loss calculation

L_{eq} : equivalent length for the tank remaining mass

M : fluid mass

$\dot{m}_d$: mass discharge rate

n: roughness parameter

P : pressure

P_{wet} : wetted perimeter

Q : volumetric flow rate

q : net heat absorbed from surroundings

R_h : hydraulic radius

Re : Reynolds number

S_e: energy slope

S_0 : channel slope

T : Flow top width

t : time

u: axial liquid velocity in the full section of the pipe

u_d : discharge velocity

u_{db} : downstream bubble propagation velocity

u_{drift} : drift velocity

u_{moving} : bubble rise velocity in a moving liquid

u_{ub} : upstream bubble propagation velocity

$\dot{u}$: velocity of a finite element of the fluid

W_s : work done by the surroundings

x : distance

Z : liquid level height

z : elevation of channel base

α : correction factor

ε : surface roughness

μ: dynamic viscosity

v : volume per unit mass

ρ : density

θ : inclination angle

ϕ : liquid depth angle

ϕ_c^{bf} : critical liquid depth angle during bubble formation and propagation regime

ϕ_n^{bf} : normal liquid depth angle during bubble formation and propagation regime

REFERENCES

Akan, A., "Open Channel Hydraulics," (2006).

Atkinson, K.E., "An introduction to numerical analysis," (1989).

Bendiksen, K.H., "An experimental investigation of the motion of long bubbles in inclined tubes," J. Multiphase Flow, 10 (4), 467 (1984).

Bendiksen, K.H., D. Malnes, R. Moe, and S. Nuland, "The dynamic two-fluid model OLGA: theory and applications," SPE Production Eng., 6, 171 (1991).

Benjamin, R., "Gravity currents and related phenomena," J. Fluid Mech, 31(2), 209 (1968).

Bird, R.B., W.E. Stewart, and E.N. Lightfoot., "Transport Phenomena," John Wiley & Sons (2007).

Chanson, H., "The Hydraulics of Open Channel Flow: An Introduction," Elsevier (2004).

Chow, V.T., "Open-Channel Hydraulics," (1959).

Churchill, S.W., "Friction-factor Equation Spans All Fluid-flow Regimes," Chem. Eng. - New York, 84 (24), 91 (1977).

Coulson, J.M., J.F. Richardson, "Chemical Engineering," Volume 1, Pergamon, Oxford (1999).

Dey, S., "EDR in cicular channels," J. Irrig. Drain. E-ASCE, 127 (2), 110 (2001).

Dumitrescu, D.T., "Strömung an einer Luftblase im senkrechten Rohr," Z. Angew, Math. Mech (1943).

DISC Theory, DNV Software (Unpublished).

Evett, J. B. and C. Liu , "2500 Solved Problems in Fluid Mechanics and Hydraulics," McGraw Hill (1989).

Falvey, H.T., "Air-water Flow in Hydraulic Systems," Bureau of Reclamation, Engineering Monograph No.14 (1980).

Flow of Fluids through Valves, Fittings, and Pipe, Crane Co. Engineering Division (1957).

French, R., "Open-Channel Hydraulics," Civil Engineering Series, McGraw-Hill (1994).

Hager, W.H., "Cavity Outflow from a Nearly Horizontal Pipe," Int. J. Multiphas Flow, 25, 349 (1999).

Inogamov, N.A., and A.M. Oparin, "Bubble motion in inclined pipes," J. Exp. Theor. Phys+, 97 (6), 1168 (2003).

Jones, G.M., R.L. Sanks, G. Tchobanoglous and II, B.E. Bosserman , " Pumping Station Design", Elsevier (2008).

Joye, D.D., and B.C. Barrett, "The tank drainage problem revisited : do these equations actually work ? ," Can. J. Chem. Eng., 81, 1052 (2003).

Kalinske, A.A. and P.H. Bliss, "Removal of air from pipe lines by flowing water", P Am Soc Civil Eng (ASCE), 13(10), 3 (1943).

Kandasamy, J.K., "Discussion on 'Transition to a Free-surface Flow at End of a Horizontal Conduit' by Montes," J. Hydraul Res. 37 (1), 136 (1999).

Kent, J.C., “The Entrainment of Air by Water Flowing in Circular Conduits and with Downgrade Slope,” PhD Thesis, University of Berkeley (1952).

Kossik, J., “Draining time for unpumped tanks,” Chem. Eng. - New York, 107, 115 (2000).

Lauchlan, C.S., M. Escarameia, R.W.P. May, R. Burrows, and C. Gahan, “Air in Pipelines,” Review Literature And Arts Of The Americas (2005).

Little, M.J., “Air Transport in Water and Effluent Pipelines,” 2nd International Conference on Marine Waste Discharge,Istanbul, Turkey (2002).

Loiacono, N., “Time to drain a tank with piping,” Chem. Eng. - New York, 94 (11), 164 (1987).

Mahgerefteh, H.,P. Saha, and I. G. Economou, “A study of the dynamic response of emergency shutdown valves following full-bore rupture of gas pipelines,” Trans. Inst. Chem. Eng., Part B, 75, 201 (1997).

Mahgerefteh, H.,P. Saha, and I. G. Economou, “Fast numerical simulation for full-bore rupture of pressurized pipelines,” AIChE J., 45 (6), 1191 (1999).

Mahgerefteh, H.,P. Saha, and I. G. Economou, “Modelling fluid phase transition effects on dynamic behaviour of ESDV,” AIChE J., 46, (5), 997 (2000).

Mannan, S., “Lees' Loss Prevention in the Process: Hazard Identification, Assessment and Control,” (2005).

McCabe, W., J. Smith, and P. Harriott, “Unit Operations of Chemical Engineering,” (1956).

Montes, J.S., “Transition to a Free-surface Flow at End of a Horizontal Conduit,” J. Hydraul Res , 35 (2) (1997).

Mosvell, G., “Luft I utslippsledninger (Air in outfalls),” Prosjektkomiteén for rensing av avløpsfann (project committee on sewage), Oslo, Norwegian Water Institute (NIVA) (1976).

Nicklin, D.J., J.O. Wilkes, and J.F. Davidson, “Two Phase Flow in Vertical Tubes,” Trans.Inst.Chem.Engr., 40, 61 (1962).

Offshore Installations (Safety Case) Regulations 2005, Offshore Information Sheet No. 2/2006, Health and Safety Executive (2006).

Offshore Technology Report, OTO 98 162, Subsea hydrocarbon pipeline failure: survey of available prediction schemes, HSE (1998).

Perry, R.H., and D.W. Green, Perry's chemical engineers’ handbook, 7th Ed., McGraw Hill, London (1997).

Pipeline Accident Report, “Rupture of Enbridge Pipeline and Release of Crude Oil near Cohasset,” Minnesota National Transportation Safety Board (2002).

Pothof, I.W.M., “Co-current air-water flow in downward sloping pipes,” PhD Thesis, Delft University of Technology (2011).

Richardson, S.M., and G. Saville, “Blowdown of pipelines,” Society of Petroleum Engineers Europe 91, Paper SPE 23070, Aberdeen, UK, 369 (1991).

Richardson, S.M., and G. Saville, “Isle of Grain pipeline depressurisation tests,” HSE OTH 94441, HSE Books, HSE, Bootle, U.K. (1996a).

Richardson, S.M., and G. Saville, “Blowdown of LPG pipelines,” Trans. IChemE, 74B, 236 (1996b).

Rohsenow, W.M., J.P. Hartnett, and Y.I. Cho, “Handbook of heat transfer,” McGraw-Hill, New York (1998).

Schwarzhoff, J.A., and J.T. Sommerfeld, “How Fast Do Spheres Drain?” Chem. Eng. - New York , 95 (9), 158 (1988).

Shoaei, M. and J.T. Sommerfeld, “Draining Tanks: How Long Does it ReallyTake?” Chem. Eng. - New York, 96 (1), 154 (1989).

Smith, C., “Brink depth for a circular channel,” J. Hydraul Eng. - ASCE, 88 (6), 125 (1962).

Sommerfeld, J.T., and M.P. Stallybrass, “Elliptic integral solutions for drainage of horizontal cylindrical vessels with piping friction,” Ind. Eng. Chem. Res., 31 (3), 743 (1992).

Sterling, M., and D,W. Knight, “The free overfall as a flow measuring device in circular channel,” P. I. Civil Eng. - Water, 235-243 (2001).

Sturm, T.W., “Open Channel Hydraulics,” McGraw Hill (2001).

Tiğrek, S., C.E. Firat, and A.M. Ger, “Use of Brink Depth in Discharge Measurement,” J. Irrig. Drain. E-ASCE, 134 (1), 89 (2008).

Uchida, H., and H. Nariai, “Discharge of Saturated Water through Pipes and Orifices,” Chem. Eng. Prog., 62 (8), 88 (1966).

U.S. Department of Transport, Code of Federation Regulations (CFR) Title 49D, Part 195, “Transportation of hazardous liquids by pipeline, ” Accident Report Data Base.3 (1982 – 1997).

Wallis, G.B., C.J. Crowley, and Y. Hagi, “Conditions for a pipe to run full when discharging liquid into a space filled with gas, J. Fluid Eng. – T. ASME, 99 (6), 405–413 (1977).

Water Measurement Manual, U.S. Department of the Interior Bureau of Reclamation (2001).

White, F.M., “Fluid Mechanics,” McGraw Hill (1999).

Wisner, P.E., F.N. Mohsen, and N. Kouwen, “Removal of Air from Water Lines by Hydraulic Means,” J. Hydraul Eng. – ASCE , 101, HY2, 243 (1975).

Yen, B.C., and N. Pansic, “Surcharge of Sewer Systems.Department of Civil Engineering,” University of Illinoise at Urbana-Champaign (1980).

Zukoski, E.E., “Influence of viscosity, surface tension, and inclination angle on motion of long bubbles in closed tubes,” J. Fluid Mech., 25 (4), 821 (1966).

WEB REFERENCES

CBC News, “Alta oil pipeline leaked 28,000 barrels” (May, 2011).
http://www.cbc.ca/news/canada/edmonton/story/2011/05/03/edmonton-pipeline-leak-alberta.html

Energy Global, “Demand for pipeline rising worldwide” (2010).
http://www.energyglobal.com/sectors/pipelines/articles/Tube_2010_report.aspx

Green Technology , “Kalamazoo River Oil Spill: Clean-up Efforts Underway In Michigan” (July, 2010).
http://www.huffingtonpost.com/2010/07/28/kalamazoo-river-oil-spill_n_662829.html#s120171&title=Michigan_River_Oil

International Business Times, “Nigerian Pipeline Blast Spurs UN Call for Fuel Management Review” (29 December 2006).
http://www.ibtimes.com/articles/20061229/nigeria-oil-explosion-un.htm

Klug, F, “Enbridge's estimated cost of Kalamazoo River oil spill clean-up exceeds its $650 million insurance policy” (September, 2011).
http://www.mlive.com/news/kalamazoo/index.ssf/2011/09/enbridges_estimated_cost_to_cl.html

Mitch, M. Engauge Digitiser, Version 4.1 (July 2007).
http://www.softpedia.com/developer/Mark-Mitch-21698.html

National Instruments Company, LabVIEW (2011).
http://www.ni.com/labview/

The Economic Times, 04.01PM IST, AFP (9 November 2011).
http://economictimes.indiatimes.com/news/news-by-industry/energy/oil-gas/global-oil-demand-to-rise-14-by-2035-iea/articleshow/10667201.cms

The Seattle Times, “Nigerian Pipeline Fire Kills As Many As 100” (16 May 2008). http://seattletimes.nwsource.com/html/nationworld/2004418253_nigeria16.html

US Department of Transportation Pipeline and Hazardous Materials Safety Administration (2011). http://primis.phmsa.dot.gov/comm/reports/safety/AllPSI.html?nocache=9408#_liquid